

Insights into Asphaltene Stability, Aggregation, Deposition and Molecular Structure

Edris Joonaki

Submitted for the degree of Doctor of Philosophy

Institute of Petroleum Engineering

School of Energy, Geoscience, Infrastructure and Society

Heriot-Watt University

Edinburgh, UK

April 2019

The copyright in this thesis is owned by the author. Any quotation from the thesis or use of any of the information contained in it must acknowledge this thesis as the source of the quotation or information.

PREFACE

The following work is prepared as a part of my PhD studies at Heriot-Watt University under the supervision of Professor Bahman Tohidi and Dr Rod Burgass. This PhD study was funded by the “James-Watt” PhD scholarship of Institute of Petroleum Engineering of Heriot-Watt University, which is greatly acknowledged. A major part of the materials provided here have been presented or published by the candidate elsewhere, previously. A list of publications concerning these materials in this thesis is presented in the “LIST OF PUBLICATIONS BY THE CANDIDATE” section.

Abstract

Asphaltenes are the heaviest, most polar, and most surface-active species of crude oils which are fairly stable in the oil; however, a small variation in the pressure, composition, and temperature can cause asphaltene phase instability and alteration in their solubility parameter and can precipitate and aggregate out of the crude oil, leading to expensive deposition problems in pipelines, well, valves, and porous media. The overarching aim of this body of work is to depict the fundamental structure and behaviour of asphaltenes for ultimate application in different operating conditions. In this treatise, asphaltenes are studied over a wide range length scale, ranging from the macro to the molecular scale.

Following a literature review, the dissertation begins by reporting the results of a study on the destabilization and deposition of asphaltenes using various experimental techniques. Asphaltenes were destabilised owing to addition of a normal alkane (*n-alkane*) to the crude oil, and the influence of amphiphilic molecules on asphaltene stabilisation was also illustrated. It is shown that the current techniques that are employed to select the most appropriate asphaltene inhibitor based on their efficiency should be revisited to provide a better methodology for choosing the most suitable strategy for inhibitor/solvent injection.

In the study of asphaltene deposition, a new High Pressure-High Temperature Quartz Crystal Microbalance (HPHT-QCM) rig was designed and developed to determine the rates of asphaltene deposition onto the solid surfaces. Also, a reliable procedure is proposed for selection of chemical additives for remediation/prevention strategies to handle gas-induced asphaltene deposition problems. The factors that can play a role in controlling the effect of chemistries on asphaltenes at various conditions are also investigated in this thesis. Furthermore, the differences between the molecular structures of *n*-alkane and gas induced asphaltenes is explored. Based on the results, it was denoted that the gas induced asphaltenes are structurally, morphologically, and compositionally different from *n*-alkane precipitated asphaltenes which lead to have different interactions between the asphaltene and inhibitor molecules and diverse rankings of chemistries based on the utilised evaluation techniques. In this thesis, a new two-dimensional dynamic model was

developed and validated to simulate asphaltene precipitation, aggregation, and deposition at isothermal and non-isothermal conditions. The effect of the aggregate size on the rate of aggregation and deposition was studied through this simulation study, and it was inferred that the rate of asphaltene deposition increases as a function of concentration of nanoaggregates in the well column. The tendency of smaller aggregates to deposit onto the surfaces could be explained because of the increase in the diffusion coefficient of asphaltene aggregates.

For the first time, experimental results of the effect of water with different salinities on gas induced asphaltene aggregation and deposition at elevated pressure and temperature conditions were attained. The roles of ion type on formation of asphaltene stabilised water in oil micro-emulsions, asphaltene deposition, and respective water wettability alteration of solid surface at micro scale were also investigated. Finally, the effects of oil composition changes owing to different gas injection scenarios and addition of paraffin waxes on asphaltene destabilisation and deposition under real field conditions were thoroughly illustrated.

To my parents Sima & Morad, and my wonderful wife

who have been constant source of inspiration and encouragement to me and without their endless support, patience, dedication and love this work has never been accomplished.

ACKNOWLEDGEMENTS

First and foremost, all praises go to the God; the worthiest of appreciation, the beneficent and the merciful, for all his blessings throughout my life and his helps to overcome the obstacles and hardships of this work.

I want to extend my profound and deep gratitude to my first supervisor, Professor Bahman Tohidi, for providing me with the opportunity to be a member of the prestigious “Hydrate and Phase Equilibria Research Group” of Institute of Petroleum Engineering of Heriot-Watt University. His office was always open to me when I had any question or concern. It was really a great pleasure working under his supervision. I would like to express my sincere appreciation to my second supervisor, Dr Rod Burgass who has always been ready to support in the Lab whenever needed. I was greatly privileged to work under his supervision. My very special thanks go to one of my best friends/colleagues Dr Aliakbar Hassanpouryouzband for his insightful suggestions, discussions and comments which have been the priceless source of knowledge for me. Special thanks to Dr. Jim Buckman for providing fantastic unique ESEM experimental facility during my PhD studies. The James-Watt scholarship of Heriot-Watt University provided during my PhD research studies is greatly appreciated. Many thanks to my examiners, Dr Jingsheng ma (internal), Dr Alfred Hase and Dr Hamid Reza Nasriani (Both externals) for their valuable comments and suggestions which really improve the overall quality of the thesis.

I am extremely thankful to my parents and my parents-in-law for their constant love and prayers, helping me to complete this work. Countless thanks go to all my friends in Edinburgh, especially Benyamin Ghorbanzadeh, Mehrdad Vasheghani Farahani, Amir Jahanbakhsh, Mohammad Reza Mahabadian, Jalal Foroozesh, Rasoul Nazari Moghaddam, Khosro Jarrahan, and Vahid Azari for the joyful moments we had together and their great sense of humour.

Last but not the least, I cannot put into words my appreciation for the supports of my beloved wife, Shima. She was always there for me to share my problems and gracefully endured every single concern I had during this work. I whole heartedly and profoundly thank her unyielding devotion and love.

E. Joonaki

LIST OF PUBLICATIONS BY THE CANDIDATE

1. **Joonaki, E.**, Buckman, J., Burgass, R., Tohidi, B., “Water versus Asphaltenes; Liquid–Liquid and Solid–Liquid Molecular Interactions Unravel the Mechanisms behind an Improved Oil Recovery Methodology”, *Nature Scientific Reports*, (2019) 9:11369.
2. **Joonaki, E.**, Buckman, J., Burgass, R., Tohidi, B., “Exploration of the Difference in Molecular Structure of n-C7 and CO₂ Induced Asphaltenes”, *Industrial & Engineering Chemistry Research*, 2018, 57 (26), pp 8810–8818.
3. **Joonaki, E.**, Burgass, R., Hassanpouryouzband, A., Tohidi, B., “Comparison of Experimental Techniques for Evaluation of Chemistries against Asphaltene Aggregation and Deposition: New Application of High Pressure and High Temperature Quartz Crystal Microbalance”, *Energy & Fuels*, 2018, 32 (3), pp 2712–2721.
4. Hassanpouryouzband, A., **Joonaki, E.**, Taghikhani, V., Bozorgmehry, R., Chapoy, A., Tohidi, B., “New Two-Dimensional Particle-Scale Model to Simulate Asphaltene Deposition in Wellbores and Pipelines”, *Energy & Fuels*, 2018, 32 (3), pp 2661–2672.
5. **Joonaki, E.**, Burgass, R., Tohidi, B., “Experimental and Modelling Study on Application of New Class of Asphaltene Inhibitors for Enhanced Oil Recovery Purposes: Adsorption and Wettability Alteration”, Abu Dhabi International Petroleum Exhibition & Conference, November 2016, SPE183328-MS.
6. **Joonaki, E.**, Hassanpouryouzband, A., Burgass, R., Tohidi, B., “Effect of Water Chemistry on Asphaltene Stabilised Water in Oil Emulsions-A New Search for Low Salinity Water Injection Mechanism”, 79th EAGE Conference and Exhibition 2017, Paris, France.
7. **Joonaki, E.**, “A Comprehensive Study on Asphaltene Characterisation Using NMR, FTIR, ESEM, EDX, QCM Techniques: from Reservoir to Ambient Conditions”, 18th International Conference on Petroleum Phase Behavior and Fouling (PetroPhase-2017), Le Havre, France.
8. **Joonaki, E.**, Burgass, R. W., Tohidi, B., “A Novel Multi-Disciplinary Approach for Asphaltene Associated Flow Assurance Problems Handling Inspired by Cholesterol Deposition in Blood Vessels”, 17th International Conference on Petroleum Phase Behaviour and Fouling (PetroPhase2016), Elsinore, Denmark.

LIST OF AWARDS AND ACHIEVEMENTS BY THE CANDIDATE (*Out of PhD Studies*)

1. SPE Bursary Award, 2016.
2. Adrian Todd Golden Key Fund, 2016.
3. UK Newton Award, 2017.
4. First (1st) Place in SPE-OMC Student Paper Contest in PhD Category, and winner of best presentation award provided by Eni, TOTAL and Schlumberger, 2017.
5. Winner of Prestigious Heriot-Watt University Annual Fund, 2017.
6. EAGE Travel Grant, 2017.
7. First (1st) Place/Best Presentation Award in EGIS Symposium, Heriot-Watt University, 2018.
8. Top 5 in UK Doctoral Research Award, Engineering Category, UCL, London, 2019.

DECLARATION STATEMENT

(Research Thesis Submission Form should be placed here)

Table of Contents

List of Figures	i
List of Tables	viii
List of Symbols	xi
Chapter 1- Introduction	1
1.1 References	4
Chapter 2- Literature Review	6
2.1 Introduction	6
2.2 Effects of Different Conditions on Asphaltene Precipitation & Deposition	9
2.2.1 Effect of Pressure Changes on Asphaltene Precipitation.....	9
2.2.2 Effects of Temperature Changes on Asphaltene Precipitation	9
2.2.3 Effect of Composition Changes on Asphaltene Precipitation.....	11
2.2.4 Effects of Fluid flow on Asphaltene Precipitation and Deposition.....	11
2.2.5 Effects of Rock Types and Their Wettability States on Asphaltene Deposition	12
2.2.6 Effect of Water Salinity on Asphaltene Deposition	12
2.3 Interaction between Asphaltenes and Other Flow Assurance Problems	13
2.4 A Complete Flow Chart for Solving an Asphaltene Problem in Industry.....	13
2.4.1 Sampling	14
2.4.1.1 Bottom Hole Sampling	14
2.4.1.2 Single Phase Sampling.....	15
2.4.1.3 New Technologies for Sampling, Testing, Monitoring and Warning Applications	15
2.4.2 Experimental Reservoir Fluid & Asphaltene Characterization Studies	16
2.4.3 Modelling Studies of Asphaltene Precipitation	24
2.4.3.1 Solubility Models.....	24
2.4.3.2 Solid Models	26
2.4.3.3 Thermodynamic Micellization Model	27
2.4.3.4 New Techniques: ADEPT and ASIST Models.....	27
2.4.3.4.1 ADEPT	27
2.4.3.4.2 Asphaltene Instability Trend Tool (ASIST)	28

2.4.3.5 Application of de Boer Plot: A Risk Assessment Technique	29
2.4.4 Asphaltene Inhibition and Remediation Techniques	29
2.4.4.1 New and Under Development Inhibition Techniques.....	32
2.4.4.2 Related Case Studies of Inhibition & Remediation techniques	33
2.5 Case Studies Analysis Based on Proposed Work Flow Chart.....	33
2.5.1 Case. 1, An Oilfield in Gulf of Mexico	34
2.5.2 Case. 2, Oilfield from South Kuwait	35
2.6 A Short Explanation about the Enhanced Oil Recovery (EOR) Approaches	36
2.6.1 The Effects of EOR Processes on Asphaltene Deposition in Porous Media	37
2.7 Why are some asphaltenes projects being failed?	39
2.8 Conclusions	40
2.9 References	41
Chapter 3- New Insights into Determination of Asphaltene Appearance Point and Evaluation of Asphaltene Inhibitors Based on n-Alkane Titration.....	48
3.1 Introduction	48
3.2 Experimental Section	50
3.2.1 Materials.....	50
3.2.2 Hybrid Technique.....	51
3.2.3 Refractive Index (RI) Measurements	52
3.2.4 Near Infrared (NIR) Spectroscopy and Optical Microscopy	53
3.3 RESULTS AND DISCUSSION	54
3.3.1 Asphaltene Appearance Point (AAP) Detection by the Hybrid Technique...54	
3.3.2 Hybrid Technique vs. Refractive Index (RI) and Optical Microscopy Measurements	58
3.3.3 Evaluation of Asphaltene Inhibitors and Proposed Mechanisms.....	61
3.4 Conclusions	67
3.5 References	69
Chapter 4- Comparison of Experimental Techniques at Ambient and High-Pressure Conditions for Evaluation of Chemistries against Asphaltene Aggregation and Deposition: New Application of HPHT-QCM.....	72
4.1 Introduction	72
4.2 Experimental Section	73

4.2.1	Materials.....	73
4.2.2	Asphaltene Inhibitor Screening Test (AIST)	74
4.2.3	Detection of asphaltene appearance point using UV-vis-NIR Spectrophotometer	75
4.2.4	Quartz Crystal Microbalance (QCM).....	76
4.3	RESULTS AND DISCUSSION	77
4.3.1	Asphaltene Inhibitor Screening Test (AIST)	77
4.3.2	Evaluation of Asphaltene Inhibitors Using UV-vis-NIR Spectrophotometer	80
4.3.3	Evaluation of Asphaltene Inhibitors Using HPHT-QCM	86
4.4	Conclusions	91
4.5	References	92
Chapter 5- Exploration of the Difference in Molecular Structure of n-C₇ and CO₂ Induced Asphaltenes		95
5.1	Introduction	95
5.2	Experimental Section	96
5.2.1	Chemicals.....	96
5.2.2	n-C ₇ Induced Asphaltenes and HPHT-QCM Deposits.....	97
5.2.3	ESEM/EDX Analysis.....	98
5.2.4	Characterisation by FTIR Spectroscopy	98
5.2.5	¹ H and ¹³ C NMR Experiments	99
5.2.5.1	NMR Analysis procedure	99
5.3	Results and Discussion.....	99
5.3.1	HPHT-QCM Results	99
5.3.2	Characterisation of CO ₂ and n-C ₇ Asphaltenes.....	100
5.3.2.1	ESEM/EDX analysis.....	101
5.3.2.2	FTIR Spectroscopy	104
5.3.2.3	¹ H and ¹³ C NMR Analysis	106
5.4	Conclusions	113
5.5	References	114
Chapter 6- Effects of Waxes and Respective Chemistries on Asphaltene Aggregation and Deposition Phenomena: Experimental and Modelling Studies		118
6.1	Introduction	118

6.2	Experimental Section	120
6.2.1	Materials.....	120
6.2.2	Determination Rheological Properties, WAT and Wax Pour Point.....	121
6.2.3	QCM Tests	122
6.2.4	PC-SAFT Equation of State	123
6.3	Results and Discussion.....	124
6.3.1	Performance of Different Wax Inhibitors: WAT and Pour Point Determination	124
6.3.2	Effect of Wax and Related Inhibitors on Asphaltene Instability	128
6.3.3	Thermodynamic Modelling.....	132
6.4	Conclusions	135
6.5	References	136
Chapter 7-A New 2-D Particle Scale Model to Simulate Asphaltene Deposition in Wellbores and Pipelines.....		140
7.1	Introduction	140
7.2	Model Development	142
7.2.1	Thermodynamic Modelling.....	142
7.2.2	Viscosity.....	145
7.2.3	Kinetics of Asphaltene Precipitation.....	145
7.2.4	Aggregation of Precipitated Asphaltenes.....	146
7.2.5	Kinetics of Asphaltene Deposition	147
7.2.6	Modelling the Mass and Heat Transfer Process.....	147
7.2.7	Size Classification of Precipitated Asphaltene Particles.....	150
7.2.8	Change in Pressure and Fluid Velocity along the Flow	152
7.3	Results and Discussion.....	155
7.3.1	Example of an Asphaltene deposition Simulation	155
7.3.2	Capillary Tube Experiments	165
7.4	Conclusions	167
7.5	References	168
Chapter 8-Effect of Different Gas Injection Scenarios on Asphaltene Precipitation and Deposition Using Quartz Crystal Microbalance.....		172
8.1	Introduction	172
8.2	Experimental Sections.....	173

8.2.1	Materials.....	173
8.2.2	High Pressure-High Temperature Quartz Crystal Microbalance (HPHT-QCM)	176
8.3	Results and Discussion.....	178
8.4	Conclusions	185
8.5	References	185
Chapter 9- Water versus Asphaltenes; Liquid–Liquid and Solid–Liquid Molecular Interactions Unravel the Mechanisms behind an Improved Oil Recovery		
Methodology		188
9.1	Introduction	188
9.2	Materials and Methods	191
9.3	Results and Discussion.....	193
9.3.1	Characterisation of asphaltene and the parent oil	193
9.3.2	Formation of water in oil micro-emulsions: the roles of asphaltenic compounds at water/oil interface, ionic strength, and ion valency.....	195
9.3.3	The effect of water with/out various ionic strengths on asphaltene aggregation.....	198
9.3.4	The role of brine solutions with different salinities on asphaltene deposition and respective micro-scale wettability transition of solid surface	200
9.4	References	209
Chapter 10- Conclusions and Recommendations		214
10.1	Major Contributions	214
10.2	Key Findings	215
10.3	Recommendations and Prospects	217
Appendix 1		220
Appendix 2		224
	Numerical Method.....	224
Appendix 3		226
	References	226

List of Figures

Figure 2. 1. Two-step process of asphaltene aggregation	7
Figure 2. 2. Phase diagram and change in crude oil/asphaltene properties owing to pressure variation through an isotherm condition	9
Figure 2. 3. Proposed work flow chart for mitigation of asphaltene related flow assurance problems in oil & gas industry	14
Figure 2. 4. Schematic of new developed small volume multi-tasking flow assurance tool [45]	19
Figure 2. 5. The determination of asphaltene onset pressure (AOP) in a live oil during the gas injection with and without presence of an asphaltene inhibitor [45]	20
Figure 2. 6. Showing of dispersants inhibition principle which acts as resin molecules related to the asphaltene molecules	30
Figure 3. 1. ESEM micrographs of asphaltene precipitates	51
Figure 3. 2. Procedure of Hybrid Technique.....	52
Figure 3. 3. FTIR spectra of supernatant fluids in various crude oil/n-heptane mixtures....	55
Figure 3. 4. AAP detection by hybrid technique for the real crude oil titrated with n-heptane for different ageing times of 1hr, 1day, and 1week	56
Figure 3. 5. AAP detection by hybrid technique for the real crude oil titrated with n-heptane after removing the effect of ageing time.....	58
Figure 3. 6. AAP detection by refractive index measurements with ageing time of 1 hr. ...	59
Figure 3. 7. The micrographs of crude oil diluted with different concentrations of n-heptane; a) 0 vol% of n-C ₇ , b) 35 vol% of n-C ₇ , c) 39 vol% of n-C ₇ , d) 41 vol% of n-C ₇ , e)	





45 vol% of n-C ₇ , and f) 55 vol% of n-C ₇ aged for 1 hr for the detection of asphaltene appearance point. The white scale bar in pictures is 100 μm.	60
Figure 3. 8. a) Effect of two commercial inhibitors AI. 3 and 4 with concentration of 200 ppm on AAP obtained by hybrid technique. Effect of nonylphenol, Dodecylbenzene sulfonic acid (DDBSA), and phthalic acid all with concentration of 200 ppm on AAP using b) Hybrid technique, and c) NIR spectroscopy.....	62
Figure 3. 9. Determination of AAP using refractive index measurements for different crude oil/inhibitors mixtures, a) blank oil, b) DDBSA, c) AI. 3, and d) AI. 4 all with inhibitor concentration of 200 ppm for ageing time of 1hr.	63
Figure 3. 10.. FTIR spectra of supernatant fluid of crude oil/n-heptane system in presence of different inhibitors- Possible interactions between Asphaltene and one of the commercial inhibitor molecules (AI. 4).....	65
Figure 4. 1. AIST results for crude oil “P” treated with inhibitors 6, 10 and 12 at 100, 300 and 600 ppm for different ageing times of 0 hr, 1 hr, 6 hr and 24 hr.....	78
Figure 4. 2. Results of the UV-vis-NIR spectrophotometer technique for the crude oil “P” with, (a) inhibitor 10, (b) inhibitor 12, and (c) inhibitor 6 at 100, 300 and 600 ppm, after mixing with n-heptane and ageing time of 24 hr at 25 °C.	81
Figure 4. 3. Effect of asphaltene inhibitor on asphaltene particle size obtained by ESEM micrographs: a) with AI. 6, b) without inhibitor. All pictures are analysed using ImageJ. This figure also presents schematic diagram of possible inhibitors interaction with asphaltenes which curbs the asphaltene-asphaltene nanoaggregate interactions to form larger particles. (): asphaltene monomer, (): asphaltene aggregates, (): heteroatoms, (): inhibitor.....	84
Figure 4. 4. Effect of temperature on performance asphaltene inhibitors for crude oil “P”, a) crude oil “P” with and without inhibitors 6 and 12 at 600 ppm at 25 °C, b) Crude oil “P” with and without inhibitors 6 and 12 at 600 ppm at 60 °C, after blending with n-heptane for 24 hr ageing time.....	86

Figure 4. 5. Results of the HPHT-QCM technique for the crude oil “P” with, (a) inhibitor 10, (b) inhibitor 12, and (c) inhibitor 6 at various concentrations, after injecting natural gas at 60 °C.....	88
Figure 4. 6. AOP/GOR versus concentration of three inhibitors 6, 10 and 12.	89
Figure 4. 7. Results of the effect of asphaltene inhibitors on deposition rate at various concentrations, a) AI. 12, b) AI. 10 and c) AI. 6.	90
Figure 5. 1. HPHT-QCM results at 60 °C for a) measurement of AOP and respective GOR and b) determination of asphaltene deposition rate, due to natural gas and CO ₂ injection.	100
Figure 5. 2. ESEM/EDX elemental mapping of n-C ₇ -asphaltenes by ESEM: (a) micrograph of asphaltene, (b) elemental analysis, (c) S <i>k</i> mapping, (d) C <i>k</i> mapping, (e) O <i>k</i> mapping	102
Figure 5. 3. ESEM/EDX elemental mapping of CO ₂ -asphaltenes by ESEM: (a) micrograph of asphaltene, (b) elemental analysis, (c) S <i>k</i> mapping, (d) C <i>k</i> mapping, (e) O <i>k</i> mapping	103
Figure 5. 4. a) Full FTIR spectra of n-C ₇ and CO ₂ -asphaltenes. b) Zoomed in plot of the aromatic C–H region. Sulfoxide can be observed for both asphaltenes. Presence of C–S and long alkyl chains are intense for n-C ₇ and CO ₂ -asphaltene, respectively. c) Comparison of spectra of two studied asphaltenes in the range of 1500-1800 cm ⁻¹ . It is found that the n-C ₇ asphaltene is dominated thoroughly by aromatic C=C stretch vibrations at ~1600 cm ⁻¹ . (R-COOH) functional group can be detected in CO ₂ induced asphaltene. d) The spectra of free and hydrogen bonded O–H group. The CO ₂ -asphaltenes shows a distinct content of O–H at ~3440 cm ⁻¹ which cannot be observed as an accountable moiety in the n-C ₇ asphaltene. e) The C–H stretch region for CH ₂ /CH ₃ in alkyl features. The C–H vibrations in methyl groups attached to aromatic cores is seen in n-C ₇ asphaltene structure.....	105
Figure 5. 5. Representative proton 400.1 MHz NMR spectrum of a) n-C ₇ asphaltene, b) CO ₂ -asphaltene.....	106

Figure 5. 6. Representative carbon 100.6 MHz NMR spectrum for a) n-C ₇ asphaltene, b) aliphatic domain of CO ₂ -asphaltene, and c) aromatic domain of CO ₂ -asphaltene.	108
Figure 5. 7. The determined C _p /C _{ar} ratio as a function of total number of aromatic rings in n-C ₇ and CO ₂ -asphaltenes molecular structures.	111
Figure 5. 8. Proposed aromatic structures for studied n-C ₇ asphaltenes based on integrated ¹ H and ¹³ C NMR results.....	112
Figure 5. 9. Proposed aromatic structures for studied CO ₂ -asphaltenes based on integrated ¹ H and ¹³ C NMR results.....	113
Figure 6. 1. The viscosity changes due to temperature reduction for the blank crude oil and in presence of various inhibitors at specified concentrations.....	125
Figure 6. 2. The effect of wax inhibitors on pour point reduction for the modified crude oil sample.	127
Figure 6. 3. Results of the HPHT-QCM experiments for the examined crude oil with wax inhibitors: a) INH-3, b) INH-4, c) INH-6, and d) INH-9 at different concentrations.	129
Figure 6. 4. AOP/GOR versus concentration of four wax inhibitors; INH-3, 4, 6, and 9.	130
Figure 6. 5. Results of the effect of different wax inhibitors: a) INH-3, b) INH-4, c) INH-6, d) INH-9 on the asphaltene deposition rate at various concentrations.....	131
Figure 6. 6. The effect of addition of wax at various concentrations to the crude oil on a) AOP/GOR, b) representative asphaltene deposition rate.....	132
Figure 6. 7. PC-SAFT modelling results of the effect of wax addition to the crude oil on asphaltene stability at various concentrations of 1.5wt%, 3wt%, 5wt%, and 7wt%: a) modelling results, b) zoomed-in plot of modelling results with experimental data, c) relative error of PC-SAFT predictions compared to experimental data.	134

Figure 7. 1. Flow chart of the flash algorithm used to study the stability of asphaltene- oil mixtures.....	144
Figure 7. 2. Schematic of precipitation, aggregation, and deposition of asphaltene during the production from the reservoir to well head.	151
Figure 7. 3. Typical simulation loop; each step begins with thermodynamic calculation part, continues with mass and heat transfer calculations, geometry section, data recording and ends with time update.....	154
Figure 7. 4. Asphaltene phase behaviour at different pressure and temperature for the crude oil investigated in this study.....	156
Figure 7. 5. Well temperature and pressure profiles along the true vertical depth in two asphaltene stable and asphaltene unstable regions.....	158
Figure 7. 6. Viscosity variation with the true vertical depth in two asphaltene stable and asphaltene unstable regions.....	159
Figure 7. 7. Asphaltene deposit layer thickness distribution along the depth of the well bore for different production times.	160
Figure 7. 8. Asphaltene concentration change along the depth of the well bore for different production times.....	161
Figure 7. 9. Asphaltene particles size classification along the depth of the well bore at the initial flow of the production.	162
Figure 7. 10. Asphaltene particles size classification along the depth of the well bore after 9 months of production.	164
Figure 7. 11. Average asphaltene particles size distribution along the depth of the well bore for different production times.	165
Figure 7. 12. The comparison of the results obtained from the model with the asphaltene deposition experimental data in a capillary tube for a) Test#1 and b) Test#2.	166

Figure 8. 1. Picture and schematic diagram of HPHT-QCM set up	178
Figure 8. 2. Results of the HPHT-QCM method for the crude oil mixed with natural gas at 60 °C.....	179
Figure 8. 3. Results of 3 repetitions for the crude oil mixed with natural gas at 60 °C	180
Figure 8. 4. The effect of injected gas type on asphaltene onset pressure obtained by HPHT-QCM technique	181
Figure 8. 5. Plot showing changes in RF vs. time represents asphaltene deposition rate affected by different injected gas types.....	184
Figure 9. 1. Characterisation of asphaltene isolated from crude oil BR, (a) representative ¹³ C 100.6 MHz NMR spectra, (b) representative ¹ H 400.1 MHz NMR spectra, (c) FTIR spectra of asphaltene with representative structures assigned to related spectra range, (d) Determined C _p /C _{ar} ratio as a function of total number of aromatic rings in studied asphaltene molecular structure, (e) ESEM micrograph of asphaltene with white scale bar of 20 μm, EDX elemental mapping of (f) C <i>k</i> mapping, (g) S <i>k</i> mapping, and (h) O <i>k</i> mapping, (i) hypothetical asphaltene molecular structure derived based on the attained advanced spectroscopy data. No effort was accomplished to fit the structure to the molecular weight, solubility, or further physical circumscriptions.....	194
Figure 9. 2. Formation of spontaneous asphaltene stabilised water in oil micro-emulsions and its effect on the fluid viscosity. (a) FTIR spectra of blank petroleum fluid and after contact with DI water, 1M HS and 0.1M LS brines, and CaCl ₂ and NaCl brines with ionic strength of 0.1M. (b) Water in oil (W/O) micro-emulsions contents for blank oil and after contact with DI water and various brines with different ionic strengths and respective viscosity data. Microscopic images of the W/O micro-emulsions for (c) blank crude oil BR, (d) large 1M HS brine droplets, (e) smaller 0.1M LS brine droplets compared to HS brine, and (f) tiny DI water droplets. The white scale bar in microscopic images is 100 μm.	197
Figure 9. 3. Images of asphaltene aggregates for (a) blank oil, and in presence of (b) DI water, (c) 0.1M LS brine, (d) 1M HS brine. Here the white scale bar in micrographs is 10	

µm. The particle size distribution of asphaltene aggregates for (e) blank oil BR, and with (f) DI water, (g) LS brine, and (h) HS brine. The particle sizes are counted with ImageJ.199

Figure 9. 4. Amplitude and acceleration decay at the quartz crystal-oil interface.....201

Figure 9. 5. The effect of water with/out various ionic strengths and ion types on (a) AOP shifting and related GOR changes, and (b) asphaltene deposition rate onto the QCM surface. ESEM micrographs of micro-droplets of water on gold plate of QCM surface in presence of (c) DI water, (d) 0.1M LS brine, (e) no water, plain surface, and (f) 1M HS brine illustrating water contact angle variability owing to ionic strength changes. The white scale bar depicted in images is 20 µm. (g) the average contact angle values of water micro-droplets on the surface with/out presence of brines with different salinities and ion types and respective elemental analysis of trapped brine sandwiched between asphaltene deposits and the QCM surface.203

Figure 9. 6. Model representation of the molecular scale phenomena that elucidate the effect of ionic strength on asphaltene aggregation, deposition, formation and stability of W/O micro-emulsions, asphaltene interactions at water-oil interface and microscopic wettability transition for (a) high ionic strength, and (b) low ionic strength brines with respective Debye length (κ^{-1}). Ions can alter the electrostatic potential (ψ). Micro-brine droplets and thin water film sandwiched between oil-asphaltene deposits and the QCM solid surface, owing to cations (mainly multivalent ones) induced rupture of protective water films the asphaltene aggregates are allowed to adhere and trapped patches of brine are left on the surface. The ions water shielding and anions (in (a) & (b)) are not depicted for the sake of lucidity.....208

Figure A1. 1 More ESEM micrographs of n-C₇-asphaltenes with different magnifications220

Figure A1. 2 More ESEM micrographs of CO₂-asphaltenes with different magnifications220

List of Tables

Table 2. 1. The effect of Rock type and wettability state on asphaltene deposition.....	12
Table 2. 2. Introduction of asphaltene precipitation onset determination techniques and their advantages and disadvantages	16
Table 2. 3. Advantages and disadvantages of techniques for determination of asphaltene aggregation onset	18
Table 2. 4. Summary of published research studies of using QCM in application of asphaltene precipitation and deposition investigations	20
Table 2. 5. Summary of different models with their assumptions and advantages and disadvantages	25
Table 2. 6. Summary of most recent published research works on investigation of enhanced oil recovery processes on asphaltene precipitation and deposition.....	37
Table 3. 1. Properties of Crude Oil “AC” utilised in this study.....	50
Table 3. 2. Properties of non-commercial asphaltene inhibitors used in this study.....	50
Table 4. 1. Properties of Crude Oil “P” Used in This Study.....	74
Table 4. 2. Natural gas composition.....	76
Table 4. 3. AIST results for crude oil “P” treated with inhibitors 6, 10 and 12 at 100, 300 and 600 ppm for various ageing times	79
Table 4. 4. Detection of asphaltene appearance point of crude oil “P” with 100, 300 and 600 ppm dosage of different asphaltene inhibitors, after mixing with n-heptane and aging for 24 hr at 25 °C.....	82
Table 4. 5. Ranking of asphaltene inhibitors obtained from different techniques	91
Table 5. 1. Chemical Composition of Asphaltenes (w/w%).....	100
Table 5. 2. Average molecular parameters of n-C ₇ and CO ₂ -asphaltene molecules derived from the integrated ¹ H and ¹³ C NMR analysis.....	109

Table 6. 1. Properties of crude oil used in this study at 1 atm and 20 °C	120
Table 6. 2. The composition suggested optimum dosage by supplier and application of each wax inhibitor	120
Table 6. 3. The experiment conditions and results of rheometer tests with atmospheric geometry, using blank crude oil and blended with various wax inhibitors.....	126
Table 6. 4. The test conditions and results of rheometer experiments on oscillation mode, using blank crude oil and dosed with different wax inhibitors	127
Table 7. 1. Classification of asphaltene based on sizes of the aggregates	150
Table 7. 2. Parameters used in the modeling of asphaltene deposition.....	155
Table 8. 1. Oil Composition at atmospheric and reservoir conditions and respective Thermodynamic Data *	173
Table 8. 2. Injected Mix.A gas composition	175
Table 8. 3. Injected natural gas composition.....	176
Table 8. 4. Injected flue gas composition	176
Table 8. 5. Experimental conditions and asphaltene phase behaviour for different gas injection scenarios.....	181
Table 9. 1. Material properties of the petroleum fluid, BR: oil density ρ_o , viscosity μ_o , asphaltene content f , asphaltene density ρ_a , water content (ppm)	193
Table 9. 2. Elemental contents of the asphaltenes isolated from petroleum fluid BR (w/w%)	193
Table A1. 1 SARA analysis of the crude oil used in chapter 5.....	221
Table A1. 2 Infrared spectral range assignments of the main bands observed in n-C ₇ and CO ₂ asphaltenes characterised in this study	221
Table A1. 3 Proton chemical shift correlation chart for studied asphaltenes.....	222
Table A1. 4 Carbon chemical shift correlation chart for studied asphaltenes	223
Table A2. 1 Definition of parameters used in equation 3	224

Table A3. 1 Bare ion radii, hydrated ion radii, ion size parameter \AA , and the individual ion activity coefficient parameters in eq. 4 for various cations used in this study226

List of Symbols

\tilde{a}	Helmholtz free energy
\tilde{a}^{hc}	Hard-Chain reference contribution to Helmholtz free energy
\tilde{a}^{disp}	Dispersion contribution to Helmholtz free energy
\tilde{a}^{res}	Residual Helmholtz free energy
<i>AAP</i>	Asphaltene appearance point
<i>AOP</i>	Asphaltene onset pressure
<i>ASTM</i>	American society for testing and materials
<i>C</i>	Concentration of asphaltene
C_{BH}	Concentration of asphaltene at bottom hole
C_k	Concentration of particle size k
C_f	Concentration of asphaltene in oil phase
C_{eq}	Concentration of asphaltene at equilibrium condition
<i>Cm</i>	Centimetre
<i>cP</i>	Centipoise
<i>CPM</i>	Cross-polarized microscopy
<i>DSC</i>	Differential scanning calorimetry
D_{wo}	Asphaltene diffusivity Coefficient in oil phase
<i>ESEM</i>	Environmental Scanning Electron Microscopy
f_d	Diffusivity coefficient tuning parameter
f_F	Friction factor
<i>FTIR</i>	Fourier transform infrared
<i>GOR</i>	Gas-oil ratio
<i>gr</i>	Gram
<i>g</i>	Acceleration due to gravity

h_c	Convective heat transfer coefficient of casing material
h_{As}	Convective heat transfer coefficient of asphaltene
<i>HPLC</i>	High Performance Liquid Chromatography
<i>Hrs</i>	Hours
<i>Hz</i>	Hertz
<i>INH</i>	Inhibitor
k	Asphaltene size group number
k_B	Boltzmann constant
k_d	Asphaltene deposition rate constant
k_p	Precipitation rate constant
k_0	Precipitation rate constant tuning parameter
k_{ho}	Thermal conductivity of oil
L	Length of capillary/wellbore
<i>LT</i>	Light transmittance
<i>MW</i>	Molecular weight
<i>NIR</i>	Near infrared
N_{Re}	Reynolds Number
<i>ppm</i>	Part per million
P	Pressure
P_{res}	Reservoir pressure
P_{WH}	Wellhead pressure
<i>QCM</i>	Quartz crystal microbalance
<i>rad</i>	Radian
<i>RF</i>	Resonance frequency
<i>rpm</i>	Round per minute
<i>SARA</i>	saturates, aromatics, resins, and asphaltenes

r	Radius
r_w	Wellbore/Capillary Radius
r_k	Radius of particle size k
R	Universal gas constant
R_{per}	Rate of asphaltene precipitating out of oleic phase
R_d	Rate of asphaltene deposition
t	Time
T	Temperature
T_{res}	Reservoir temperature
T_{WH}	Wellhead temperature
T_o	Oil temperature
UV	Ultraviolet
V_r	Radial Velocity
V_z	Axial velocity
V_θ	Angle Velocity
WAT	Wax appearance temperature
WDT	Wax disappearance temperature
x_i	Composition of species i
z	Axial length
Z	Compressibility factor
ΔP	Differential pressure
ΔRF	Differential resonant frequency

Greek Letters

α_p	Precipitation rate constant tuning parameter
------------	--

α_T	Thermal diffusivity
β	Collision efficiency
ε	Relative roughness
ε_h	Turbulent heat diffusivity
ε_m	Turbulent mass diffusivity
η	Viscosity
η^*	Viscosity of dilute gas
η_p	Packing fraction
θ	Angle
μ_k^{res}	Residual chemical potential
v	Mean friction velocity
ν_μ	Kinematic viscosity
ν_v	Molar volume
ξ	Viscosity reducing parameter
ρ	Density
ρ_r	Reduced density
ρ_n	Total number density of molecules
φ_k	Fugacity Coefficient
ϕ	Volume fraction of asphaltene particles

Chapter 1- Introduction

Despite the enormous amount of modern research, the process of defining asphaltenes is still under debate. Asphaltenes are referred to as functional molecules and the heaviest and most polar fraction of crude oil. These polydisperse molecules have a polyaromatic hydrocarbon core with aliphatic chains in their structure. They also contain different heteroatoms (e.g. N, O, and S) on the periphery which make acidic and basic moieties in asphaltenes and contribute to the asphaltene self-association and asphaltene interactions with other polar surface active species in oleic phase[1]–[5]. Additionally, asphaltenes contain trace amount of metals (e.g. Va, Ni, and Fe) on porphyrin like structures[6]–[8]. Asphaltenes are soluble in aromatics (e.g. toluene and xylene) and insoluble in aliphatics (e.g. n-heptane, n-pentane)[9]. Asphaltenes are recognised to be precipitated and aggregated typically as the fluid pressure is reduced due to reservoir pressure depletion towards the bubble point pressure and mixing with other crude streams and addition of gas or gas and liquids (e.g. for EOR purposes) which cause asphaltene deposition and restricted flow[10]–[12]. Restricted flow through porous media and subsea infrastructure caused by asphaltene deposition restricts the oil flow to the surface leading to deferred production[1], [13] and this could result in expensive and severe problems for oil companies worldwide. Asphaltene related research works have become more intensive in recent years because of growth in the production of high asphaltenic heavy oils[12], [14]. The principles and mechanisms beyond the asphaltene precipitation, aggregation and deposition phenomena and their inhibition processes have not yet been fully understood.

In the risky multibillion-dollar oil and gas industry, making the correct decision on using the most appropriate strategy to handle the asphaltene deposition problem is inevitably crucial. Asphaltene flow assurance challenges can be caused by (i) lack of accurate technique for determination of asphaltene precipitation and deposition onsets and evaluation of chemistries against asphaltene deposition, (ii) using inappropriate asphaltene inhibitors, and (iii) lack of a reliable asphaltene deposition simulator for accurate prediction of asphaltene deposits amount along the wellbore/pipeline.

The main aim of the investigations presented is to unravel the main drivers of asphaltene destabilization and aggregation in oil-heptane, oil-gas, and oil-gas-water mixtures and to reveal the mechanisms by which asphaltenes deposit on surfaces and the role additives play against those drivers. The findings of this research are presented in nine chapters and a brief description of the content of each chapter can be found below.

Chapter 2. The aim of this chapter is to critically review the new developed technologies in asphaltene precipitation and deposition areas. An extensive work flow chart with the aim of solving asphaltene problems in oil and gas industry was also proposed. Then different successful case studies are analysed based on the proposed flow chart. One of our findings reveals that most of optical based techniques for asphaltene precipitation onset determination might not be reliable and accurate, since they just detect asphaltene aggregation onset indeed not the precipitation onset. This may cause asphaltene problems remaining unsolved in the industry.

Chapter 3. Many of previous studies were conducted in conditions where asphaltene precipitates are already aggregated, and very few have targeted asphaltene particles before or near precipitation state. In this chapter, an experimental technique called the “Hybrid Technique” is validated for detection of asphaltene appearance point and evaluation of different amphiphilic asphaltene inhibitors. The effect of ageing time on asphaltene precipitation onset has also been removed by a new approach, and in different ageing times, the same asphaltene appearance points (AAP) have been obtained. The hybrid technique can also detect the possible interactions between asphaltene and inhibitor molecules and propose the related mechanisms. In this study, the effect of various non-commercial inhibitors including phthalic acid, two amphiphiles of nonylphenol (NP), and Dodecylbenzene sulfonic acid (DDBSA) and two commercial inhibitors on the behaviour of asphaltenes and their interactions with asphaltene nanoaggregates have been investigated by using the hybrid technique.

Chapter 4. In previous chapters it has been inferred that the current techniques which are employed to select the most appropriate asphaltene inhibitor based on their efficiency should be revisited to provide a better methodology for choosing the most suitable strategy for inhibitor/solvent injection at elevated pressure and temperature conditions. This chapter

addresses this asphaltene challenge using a Quartz Crystal Microbalance (QCM) based technique, with emphasis on selection of chemical additives for remediation/prevention strategies to handle gas induced asphaltene deposition problems. The proposed technique can work at high pressure conditions, simulating the effect of pressure and dissolved gas on asphaltene phase behaviour and deposition tendencies with and without inhibitors. It can also assess the deposition rate onto the quartz crystal surface due to asphaltene deposition under real reservoir conditions. In this study, the ability of different asphaltene inhibitors to shift asphaltene onset points (AOPs) and reduce the amount of deposited asphaltenes in dead crude oils is investigated.

Chapter 5. This chapter presents the first compositional and structural research study on the QCM asphaltene deposits under gas injection conditions and compare it to n-C₇ asphaltenes from the same crude oil precipitated in the laboratory. This study combines the use of Fourier transform infrared (FTIR) spectroscopy, nuclear magnetic resonance (NMR), environmental scanning electron microscopy (ESEM) and energy dispersive X-ray (EDX) analysis. Furthermore, deposits collected from chemically treated fluids were also studied. The aim of this chapter is to probe the main reasons (at molecular level) of different rankings of asphaltene inhibitors which were obtained in Chapter 4 based on the operating conditions.

Chapter 6. Following the effect of crude oil streams mixing on asphaltenes, the objective of this chapter is to shed some light on the interaction of asphaltenes and waxes and address the condition where an asphaltenic oil is commingled with a wax/paraffin inhibitor containing oil during combination of different oil streams. It is a crucial building block for development of a suitable and cost-effective strategy for handling of wax/asphaltene associated flow assurance problems. In this work, for the first time the quartz crystal microbalance (QCM) technique has been used to investigate the effect of waxes and related chemicals, which are used to mitigate wax deposition, on asphaltene aggregation and deposition phenomena. Asphaltene onset pressure and asphaltene deposition rate have been monitored using QCM at elevated pressure and temperature conditions.

Chapter 7. In order to address the third asphaltene associated flow assurance challenge, lack of a reliable asphaltene deposition simulator for accurate prediction of asphaltene

deposits amount on the solid surface, in this chapter a new two-dimensional dynamic model was developed to simulate asphaltene precipitation, aggregation, and deposition at isothermal and non-isothermal conditions. The PC-SAFT equation of state was used to model the asphaltene precipitation. Additionally, novel kinetic models were used to account for the aggregation and deposition of asphaltene particles. The effect of aggregate size on the rate of aggregation and deposition was studied. The results obtained from the new model for the rate and the amount of asphaltene deposition were compared with the experimental data reported in the literature.

Chapter 8. In this chapter several experiments have been conducted to discover how the phase behaviour of crude oil is influenced by injection of gas, particularly its effect on asphaltene precipitation and deposition rate. Tests are conducted on reservoir fluid to gather PVT and flow assurance data for injection of N₂, CO₂, CH₄, natural gas, flue gas and mixture of N₂ (20.05 mole%), CH₄ (41.30 mole%) and CO₂ (38.65 mole%) (named Mix.A) at high pressure and temperature condition. Measurements include asphaltene onset pressure (AOP) for various gases and comparisons of asphaltene deposition rate.

Chapter 9. In this chapter it has been denoted that following asphaltene aggregation phenomenon through π -stacking and hydrogen bonding interactions, asphaltene aggregates can form a thin layer at the crude oil-brine interface through noncovalent interactions such as -O-H...O hydrogen bonds and/or alter the wettability state of the solid surface from initially water-wet into mixed-oil wetting. In this study the impacts of water with variety of salinities and ion types on formation of water in oil micro-emulsions, asphaltene deposition, and induced water wettability transition at micro scale were depicted.

Chapter 10. The conclusions of the research discussed in Chapters 3 through 9, the implication of these findings in the flow assurance research area, and some recommendations for the future works are finally presented in this chapter.

1.1 References

- [1] J. L. Amundaraín Hurtado, M. Chodakowski, B. Long, and J. M. Shaw, "Characterization of Physically and Chemically Separated Athabasca Asphaltenes

- Using Small-Angle X-ray Scattering,” *Energy & Fuels*, vol. 25, no. 11, pp. 5100–5112, Nov. 2011.
- [2] S. I. Andersen and J. G. Speight, “PETROLEUM RESINS: SEPARATION, CHARACTER, AND ROLE IN PETROLEUM,” *Pet. Sci. Technol.*, vol. 19, no. 1–2, pp. 1–34, 2001.
- [3] O. León, E. Rogel, J. Espidel, and G. Torres, “Asphaltenes: Structural characterization, self-association, and stability behavior,” *Energy and Fuels*, vol. 14, no. 1, pp. 6–10, 2000.
- [4] O. C. Mullins, “The Modified Yen Model,” *Energy & Fuels*, vol. 24, no. 4, pp. 2179–2207, Apr. 2010.
- [5] E. Joonaki, A. H. Youzband, R. Burgass, and B. Tohidi, “Effect of Water Chemistry on Asphaltene Stabilised Water in Oil Emulsions-A New Search for Low Salinity Water Injection Mechanism,” in *79th EAGE Conference and Exhibition 2017*, 2017.
- [6] O. C. Mullins, “The asphaltenes,” *Annu. Rev. Anal. Chem.*, vol. 4, pp. 393–418, 2011.
- [7] J. G. Speight, “Petroleum Asphaltenes-Part 1: Asphaltenes, resins and the structure of petroleum,” *Oil gas Sci. Technol.*, vol. 59, no. 5, pp. 467–477, 2004.
- [8] S. I. Andersen, J. O. Jensen, and J. G. Speight, “X-ray diffraction of subfractions of petroleum asphaltenes,” *Energy and Fuels*, vol. 19, no. 6, pp. 2371–2377, 2005.
- [9] O. C. Mullins, E. Y. Sheu, A. Hammami, and A. G. Marshall, *Asphaltenes, heavy oils, and petroleomics*. Springer Science & Business Media, 2007.
- [10] F. M. Vargas, J. L. Creek, and W. G. Chapman, “On the Development of an Asphaltene Deposition Simulator,” *Energy & Fuels*, vol. 24, no. 4, pp. 2294–2299, Apr. 2010.
- [11] P. Juyal, V. Ho, A. Yen, and S. J. Allenson, “Reversibility of Asphaltene Flocculation with Chemicals,” *Energy & Fuels*, vol. 26, no. 5, pp. 2631–2640, May 2012.
- [12] E. Joonaki, H. R. Erfani Gahrooei, and S. Ghanaatian, “Experimental study on adsorption and wettability alteration aspects of a new chemical using for enhanced oil recovery in carbonate oil reservoirs,” *J. Unconv. Oil Gas Resour.*, vol. 15, 2016.
- [13] L. C. R. Junior, M. S. Ferreira, and A. C. da Silva Ramos, “Inhibition of asphaltene precipitation in Brazilian crude oils using new oil soluble amphiphiles,” *J. Pet. Sci. Eng.*, vol. 51, no. 1, pp. 26–36, 2006.
- [14] A. Ayyaswami, “Innovative In-Situ Remedial Technologies for Petroleum Hydrocarbon Remediation,” in *SPE Middle East Health, Safety, Environment & Sustainable Development Conference and Exhibition*, 2014.

Chapter 2- Literature Review

2.1 Introduction

Flow assurance is a major challenge in offshore and deep-water developments. Hydrate, wax, asphaltene and other solid phases could cause serious challenges. Changes in fluid conditions (e.g., temperature, pressure and/or composition) during oil production, transportation, and processing, can cause precipitation and deposition of organic solids inside wellbores, pipelines and porous media. These could result in expensive and serious problems for oil companies worldwide.

Asphaltenes are the heaviest, most polar and most surface active species of crude oils which are insoluble in n-alkanes (e.g. n-hexane, n-heptane) and soluble in light aromatics (e.g. toluene, xylene)[1]. Asphaltene molecules contain large polycyclic aromatic hydrocarbons with peripheral aliphatic chains which are embedded with a small amount of heteroatoms such as sulfur, oxygen and nitrogen[2]. They also consist of trace moieties of metals (in ppm) such as iron, nickel, and vanadium which can be appeared in porphyrin or non-porphyrin structures[3]. Based on asphaltene concentrations in crude oils, the asphaltene molecules are dispersed in the oleic phase with a size range of ~1.5 to ~5 nm in width[4]. It is widely believed that the asphaltene nano-aggregates will either flocculate to form larger particles[5] which can flow through a channel (e.g. pipeline, porous media) or deposit on the surfaces. In many oil reservoirs, asphaltenes are fairly stable in the oil, however a small variation in pressure, composition, and temperature can cause asphaltene phase instability and alteration in their solubility parameter[6], [7], and they can precipitate and aggregate out of the crude oil, leading to expensive deposition problems in pipelines, well, valves and porous media. Although various experimental approaches like neutron scattering and small angle X-ray scattering, molecular diffusion, size exclusion chromatography, Vapour Pressure Osmometry (VPO), mass spectroscopy and fluorescence depolarization have generally been employed for quantifying the molecular weight of asphaltenes[8], most of the reported values in the literature are the molecular weight of the aggregates of asphaltenes not the individual molecules. This is mainly because of intense tendency of asphaltene molecules for self-association. Utilizing novel techniques of Time-

Resolved Fluorescence Depolarization (TRFD)[9], Fluorescence Correlation Spectroscopy (FCS) [10] and Laser Desorption Ionization (LDI) Mass Spectroscopy[11] gives much more precisely estimation of asphaltene molecular weight (500-1000 Da). In reservoir conditions (high pressure), asphaltenes are stable and thought to maintain in equilibrium, either as individual molecules or stable nano-aggregates suspended in the oil named micelles. Asphaltene aggregates formation in crude oils is a two-step process: phase separation and asphaltene aggregation (Figure 2.1).

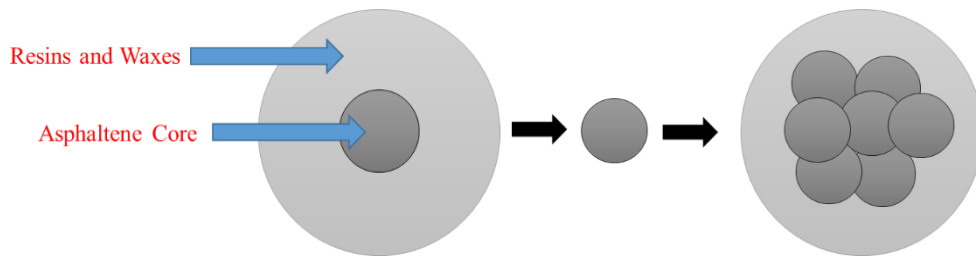


Figure 2. 1. Two-step process of asphaltene aggregation

Wax and gas hydrate deposits are more usual than asphaltene deposits especially in offshore environments, but unlike wax and gas hydrates, asphaltene related flow assurance problems can cause a significant challenge because of the difficulty and expensive inhibition and remediation processes which are required for these problems, and besides that asphaltenes are not well characterized by the researchers. Asphaltene related researches have become more intensive in recent years because of a growth in the production of high asphaltenic heavy oils[12] and gas injection based enhanced oil recovery (EOR) techniques. However, it is interesting to mention that there are many reports that mention light oils which are easy to flow with very low asphaltene content have more asphaltene deposition problems than crude oils with high asphaltene contents [7]. Hence in order to set a suitable plan for removing asphaltene related flow assurance issues, finding the source of these problems and the capability to estimate the thermodynamical behaviour and fluid flow characteristics of crude oils including asphaltene molecules are so crucial. The principles behind the asphaltene precipitation, aggregation and deposition phenomena have not yet been completely figured out. Asphaltene deposition through the porous media is a complicated issue. For accurate investigations of influences of asphaltene deposition, it is crucial to count on various developed models for adsorption and deposition of asphaltenes. Reliable models and

simulators of asphaltene deposition are hard to be developed because of the absence of knowledge. In fact, no suitable models and simulator are valid for deposition of asphaltenes in oil formations during the preliminary crude oil production and different EOR processes.

Adsorption and mechanical entrapment are the main and important discovered asphaltene deposition mechanisms. Hence asphaltene precipitation and deposition in the wellbores and reservoirs are dynamic processes, and parameters such as oil velocity, pressure, temperature, and composition variations effect the trend of these processes. So, the efficiency of an asphaltene remediation & prevention in the oil reservoirs relies on many factors and requires dynamic asphaltene modelling.

The objective of this chapter is to provide a comprehensive review of the knowledge and experience of new developed techniques for asphaltene studies. This literature review carefully concentrates on the history and development of different modelling studies of asphaltene precipitation and deposition, asphaltene remediation and inhibition techniques, different techniques for asphaltene precipitation and aggregation onset determination and measuring the amount of asphaltene deposition all with the explanation of their advantages and disadvantages. The fundamentals of different successful case studies are explained based on our proposed work flow chart for asphaltene problem solving. The effect of different factors: oil composition, temperature, pressure, fluid flow, water salinity and reservoir rock wettability on asphaltene aggregation and deposition are reviewed precisely. There are many unanswered questions related to asphaltene flow assurance problems: Why are some asphaltenes projects being failed? Desirable sampling for investigating asphaltene problems, is downhole sample the only way forward? How is modelling approaches ability in predicting asphaltene stability zone? How about amount of asphaltene? Are new techniques like Asphaltene-Instability-Trend (ASIST) and Asphaltene Deposition Tool (ADEPT) reliable? Are optical based techniques for asphaltene precipitation onset determination accurate and reliable? This chapter presents appropriate answers for these questions which can also be developed and considered in the future studies.

2.2 Effects of Different Conditions on Asphaltene Precipitation & Deposition

2.2.1 Effect of Pressure Changes on Asphaltene Precipitation

Asphaltene precipitation is occurred through a range above and below the bubble point, during the pressure depletion at a constant temperature. In-situ density of crude oil and the asphaltene solubility in crude oil decrease due to pressure reduction during the oil production from an undersaturated reservoir, and as a result asphaltene may precipitate. The maximum quantity of asphaltene precipitation occur at or around the bubble point pressure [7]. Coming out of the light gases from the oil solution causes an increase in the density and a reduction in amount of asphaltene precipitation accordingly, which occurs at below the bubble point (Figure 2.2).

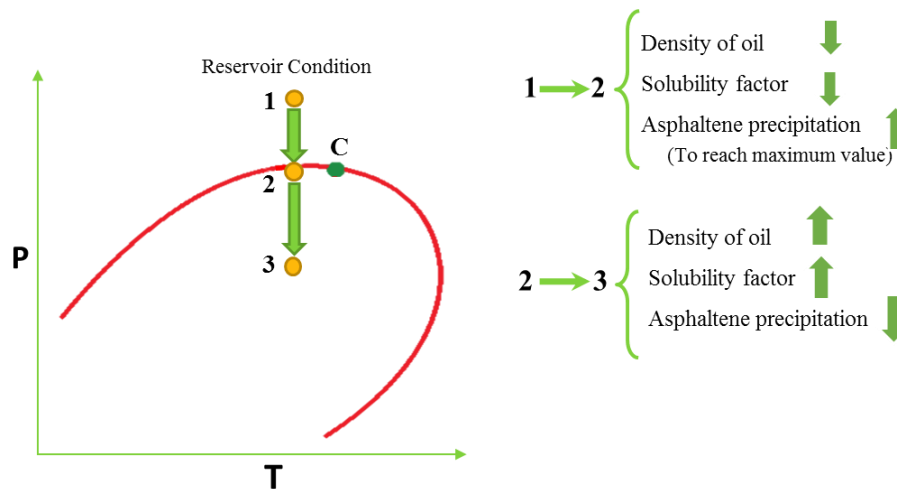


Figure 2. 2. Phase diagram and change in crude oil/asphaltene properties owing to pressure variation through an isotherm condition

2.2.2 Effects of Temperature Changes on Asphaltene Precipitation

The influence of temperature changes on asphaltene precipitation is more complex than pressure variations. First, we briefly explain about the enthalpy changes of the reactions in one system. The enthalpy changes can be described as follows in terms of formation or breaking of bonds:

$$\Delta H = (\text{energy gained in bond breaking}) - (\text{energy released in bond making})$$

There are different experimental techniques for determination of enthalpy changes in asphaltene studies which are: Titration Calorimetry, Differential scanning calorimetry (DSC), Enthalpy of Mixing and Microcalorimetry. The heat of mixing of Asphaltenes/Crude oils and different solvents has been studied and obtained by many researchers. Andersen & Christensen[13] employed calorimetric measurements of heat of dilution of asphaltene solutions to depict the presence of an apparent critical micelle concentration (CMC) of asphaltenes due to the change in heat signal as a function of asphaltene concentration. Zhang et al.[14] utilized enthalpy of mixing, DSC and microcalorimetry techniques to figure out that mixing of asphaltenes and aromatics is an exothermic process. Mahmoud et al.[15] investigated the heat of mixing of Asphaltenes and n-alkanes by using enthalpy of mixing technique. They concluded that this reaction is exothermic. Stachowiak et al.[16] changes the system and considered the mixing of crude oil and n-alkanes. They used titration calorimetry technique for their study. They concurred that this process is exothermic, but for (C₆) n-hexane the process is endothermic. Ekulu et al.[17] employed the mixing of crude oil and heptol solution for their studies and inferred that it is an endothermic process. They used DSC technique with the temperature range of 300-400K for their investigations. Stachowiak et al.[18] conducted experiments for illustration of enthalpy changes of asphaltene precipitation due to pressure depletion, which is the main process during the primary oil production. They concluded that this process is exothermic.

Generally considering the definition of the Gibbs energy $\Delta G = \Delta H - T\Delta S$ [19] is a simple way to find out the influence of temperature changes on asphaltene precipitation. Asphaltenes are unstable with $\Delta G < 0$. There are three main conditions: 1- If the reaction is exothermic and entropy of reaction is decreased and $\Delta G > 0$, so the asphaltene precipitation and aggregation happen by heating of the system. 2- If the reaction is endothermic and entropy of reaction is increased and $\Delta G > 0$, so the asphaltene precipitation and aggregation happen by cooling of the system. 3- If the reaction is endothermic and entropy of reaction is reducing, so ΔG is maintain positive and consequently there is no precipitation and aggregation at all.

2.2.3 Effect of Composition Changes on Asphaltene Precipitation

During different oil production scenarios such as artificial gas lifting or gas injection processes such as miscible flooding with CO₂, N₂, and natural gas, can cause oil composition changes and then serious asphaltene related problems accordingly. Injected gas reduces the density of crude oil which makes a reduction in the asphaltene solubility. Oil composition changes, which cause asphaltene precipitation problems, may also be raised due to oil-based muds and/or acid contamination due to stimulation processes. A further research study would be needed to illustrate the effect of more gas compositions on asphaltene precipitation and deposition and the impact of gas impurities on asphaltene behaviour for EOR purposes (In chapter 8, we will investigate this topic further).

2.2.4 Effects of Fluid flow on Asphaltene Precipitation and Deposition

Sometimes production scheme changes are utilized to control the asphaltene precipitation and deposition [20]. Fluid flow through pipeline with high shear rate causes asphaltene deposition. So, by decreasing the shear stress the problem can be mitigated. Incompatible miscible fluids flow within pipelines and separation of heavy ends in the form of colloids, flocs and attachment to the walls of conduits cases serious flow assurance problem. Therefore, as a solution for this problem we should remove incompatible materials from asphaltenic oil flow and minimize the blending of thin feed stock fluids within asphaltenic oils flows. Separation of phases from a miscible phase to oil, gas and heavy organics phase is occurred by minimization of pressure reduction into the petroleum production lines and systems [20]. Lack of neutralization of electrostatic forces may lead to break up of asphaltene steric colloids and release of sticky asphaltene particles which are attached to the walls causes pipelines plugged consequently. Hence to remove this barrier neutralization of electrostatic forces should be done. Mohammad Tavakkoli et al.[21] utilized Quartz Crystal Microbalance (QCM) technique for investigation of effects of different flow rates on asphaltene deposition. Various flow rates illustrated that the rate of asphaltene deposition is not related to the flow rate at initial time scale. But, for long terms, the influence of the flow rate is undeniable. They concluded that at very long times and high enough flow rates, the rate of asphaltene deposition is independent of the flow rate.

The asphaltene deposition has no dependency upon the flow rate and overlap for all times at very high flow rate conditions.

2.2.5 Effects of Rock Types and Their Wettability States on Asphaltene Deposition

Based on experimental work by Mousavi Dehghani et al.[22], it was found that rock type cause an undeniable influence on the asphaltene deposition on matrix surface. The results for two types of limestone and sandstone are presented in Table 2.1.

Table 2. 1. The effect of Rock type and wettability state on asphaltene deposition

Water wet State		
Sandstone Rock	>	limestone Rock
Amount of deposited asphaltene		
Sandstone Rock	<	Limestone Rock (Because on existence of more water films on sandstone rock surface)
Asphaltene deposition rate		
Sandstone Rock	<	Limestone Rock

2.2.6 Effect of Water Salinity on Asphaltene Deposition

Hematfar et al.[23] investigated the Impact of Asphaltene adsorption on two phase flow in porous media. The objectives of this work were studying the effect of brine salinity and asphaltene concentration on adsorption of asphaltene on pore surfaces, and also evaluation of the effect of asphaltene adsorption on water flooding performance and oil-water relative permeability. From their experimental results it can be concluded that when the asphaltene adsorption increased, the oil relative permeability and consequently recovery factor decreased. On the other hand, when the brine salinity decreased, asphaltene adsorption on rock surfaces increased. Therefore, higher brine salinity will give a higher oil recovery and lower asphaltene precipitation and lower porosity & permeability reduction accordingly.

2.3 Interaction between Asphaltenes and Other Flow Assurance Problems

One of the most recent research work in this area is the investigation of the influence of asphaltene molecules on wax crystallization in crude oils by Kriz and Andersen[24]. They figured out that very low concentrations of dispersed asphaltenes make a reaction with the paraffin molecules and completely incorporate in the structure of waxes. This causes a delay in wax crystallization and dispersed asphaltenes act as polymeric wax inhibitors. Besides asphaltene molecules flocculate together and co-precipitate with waxes, which leads to form an unorganized asphaltene-paraffin composite rather than a proper wax network. They also concluded that this influence strongly relies on the degree of asphaltene dispersion or aggregation more than on the asphaltene type or origin. Further studies on this interesting topic could help industry to mitigate some flow assurance problems related to waxes and asphaltenes (In chapter 6 we will shed light on possible interaction between paraffin waxes/respective chemicals and asphaltenes).

2.4 A Complete Flow Chart for Solving an Asphaltene Problem in Industry

Here an extensive work flow chart for mitigating an asphaltene flow assurance problem is proposed for the industry (Figure 2.3). Each step is explained in detail in following sections. Then different successful case studies are analysed based on this proposed flow chart.

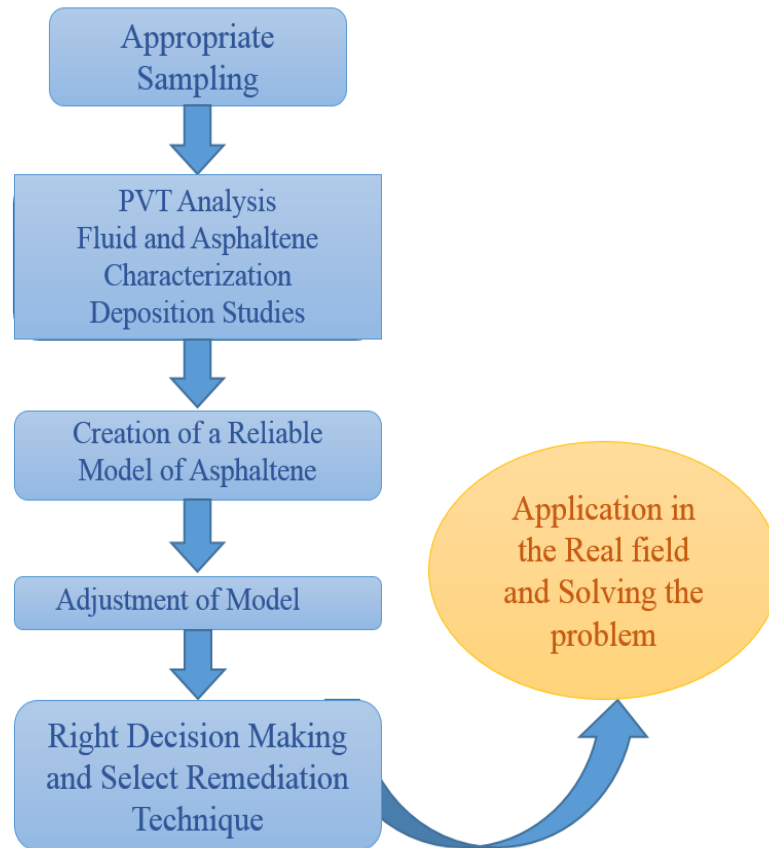


Figure 2. 3. Proposed work flow chart for mitigation of asphaltene related flow assurance problems in oil & gas industry

2.4.1 Sampling

It should be mentioned that a very important requirement in acquiring a precise assessment of asphaltene precipitation and deposition in crude oils is the existence of high modality of the reservoir fluid sample. A desirable sample is the one which is being representative of reservoir fluid, being maintained at reservoir conditions during the transportation to the laboratory and being free of contamination like oil-based muds, acid and etc.

2.4.1.1 Bottom Hole Sampling

There are mainly two types of bottom hole sampling: First, collecting the reservoir fluid during the drilling phase, and second collecting the fluid from the oil well tubing of a quite equipped well. The target for the first type of sampling is surveying the reservoir fluid and determining pressure. The aim for the second one is for investigation of the reservoir fluid

thermodynamic behavior [25], [26]. One of the greatest advantages of bottom hole sampling is having “real” asphaltenes rather than “dead” asphaltenes for the research as well as for the inhibitor selection process. also has some disadvantages which are: this approach is much costlier than surface sampling, and it should be done at constant temperature and pressure condition.

2.4.1.2 Single Phase Sampling

Single-phase samples can be obtained by utilizing various approaches at variety period of times in the life of the oilfield: 1- Single-phase reservoir sampler (SRS) during drillstem testing, 2- The wireline-conveyed MDT Modular Formation Dynamics deployed tester run with a single-phase multisample chamber in open hole[27], 3- The Cased Hole Dynamics Tester (CHDT) in cased hole.

2.4.1.3 New Technologies for Sampling, Testing, Monitoring and Warning Applications

Nowadays sampling and testing tools contain an array of instruments that can do downhole fluid analysis (DFA). DFA tools can do real time fluid properties measurements at reservoir conditions, which allow engineers to analyse before sample collection[28].

Sampling from separators or extracting live oil near perforations and performing flow assurance tests in the laboratory is an expensive monitoring approach in offshore and Deepwater fields. Recently intelligent completions were widely used for monitoring and warning purposes. This technique utilized sensors which transmit downhole temperature, pressure and flow rates in real time and remotely control pumps and valves. This technology give the facility of remotely production monitoring and flow assurance barriers handling. As an example of this technology, we can mention the use of chemical sensors. These chemical sensors are installed at strategic locations in the well completion and along a pipeline[29], [30][31]. By employing this technology, real time data for monitoring of deposition solids, corrosion rates and fluid rheological properties are obtained, and therefore the interventions for sampling or remediation will be performed when it is necessary.

2.4.2 Experimental Reservoir Fluid & Asphaltene Characterization Studies

Dead oils, or crude oils which have lost their gaseous fractions are separated into saturates, aromatics, resins and asphaltenes relying on their solubility and aromaticity by using SARA analysis[32]. It is a simple procedure, but it also has some disadvantages: - The SARA analysis outcomes are not comparable with the live oil in real conditions of oil reservoirs, - Depending on the type of precipitant used, the SARA results are not repeatable for one single oil, - It provides insufficient characterization where live oil properties are needed. Many different techniques have been used for asphaltene onsets determination such as: Filtration technique, UV-vis spectrophotometry, acoustic resonance, NMR, refractive index, light scattering, light reflexion and light transmittance, etc. These commercial techniques can only detect asphaltene particles that are at least 0.5 μm in diameter, for asphaltene onset determination. In other words, asphaltene precipitation onset measurements by these conventional techniques can obtain after asphaltene molecules start to aggregate to reach the detection range. In addition, they cannot measure the amount of precipitated asphaltenes. Hence, these methods determine asphaltene aggregation onset indeed not the asphaltene precipitation onset. Therefore, in this chapter we categorised the techniques into two groups of techniques for determination asphaltene precipitation onsets and techniques for determination of asphaltene aggregation onset. The first group of approaches for determination of asphaltene precipitation onset with all their advantages and disadvantages are presented in Table 2.2. The second group of methodologies for determination of asphaltene aggregation onset are: Light transmittance[33], light scattering[34], refractive index[35], light reflexion[36], microscopy[37], acoustic resonance[38] and UV-vis spectrophotometry[39]. Some of their advantages and disadvantages are given in Table 2.3.

Table 2. 2. Introduction of asphaltene precipitation onset determination techniques and their advantages and disadvantages

Techniques	Advantages	Disadvantages	References
Filtration technique	<ul style="list-style-type: none"> ✓ It quantifies the amount of precipitated asphaltene ✓ The upper and lower asphaltene phase boundaries 	<ul style="list-style-type: none"> ✓ Results depend on filter size ✓ Need more time than measuring 	[40]

	<p>can be defined</p> <ul style="list-style-type: none"> ✓ The asphaltenes are physically extracted from the oil, and so may be further characterized through mass spectrometry, molecular-diffusion studies or SARA analysis ✓ Reliable 	acoustic resonance or light scattering	
Density technique	<ul style="list-style-type: none"> ✓ It is Easy to be extended and checked 	<ul style="list-style-type: none"> ✓ Applicable in just restricted conditions 	[41]
Viscosity technique	<ul style="list-style-type: none"> ✓ The results are obtained promptly 	<ul style="list-style-type: none"> ✓ It has very limited working conditions ✓ It is not examined with crude oils (Just tested in Asphaltene Solutions) ✓ It is extremely high time dependant 	[42]
Electrical Conductivity technique	<ul style="list-style-type: none"> ✓ It is reliable ✓ It has the capability of wide working conditions 		[43]
Heat Transfer technique		<ul style="list-style-type: none"> ✓ Significant amount of precipitate is required to detect an alteration 	[44]

Table 2. 3. Advantages and disadvantages of techniques for determination of asphaltene aggregation onset

Techniques	Advantages	Disadvantages	References
Acoustic resonance	<ul style="list-style-type: none"> ✓ It is less time consuming than the gravimetric methods 	<ul style="list-style-type: none"> ✓ The presence of other solids could cause similar changes in acoustic properties ✓ The technique does not allow the fluid to be mixed, giving rise to potentially inaccurate onset measurements due to heterogeneous distribution of asphaltenes ✓ The method does not detect the lower boundary of the asphaltene-precipitation envelope. 	[38]
Light-scattering technique	<ul style="list-style-type: none"> ✓ High speed of testing ✓ The low volume of single-phase reservoir fluid required 		[34]
High pressure microscope technique	<ul style="list-style-type: none"> ✓ This technique allows microscopic visualization of the appearance of asphaltene particles as pressure decreases ✓ It can be implemented by particle size analysis 	<ul style="list-style-type: none"> ✓ It provides only a qualitative indication of particle size and number ✓ To quantify these parameters, proprietary particle-size analysis (PSA) imaging software has been used 	[37]

	imaging software		
--	------------------	--	--

2.4.2.1 Application of Quartz Crystal Microbalance (QCM)

The quartz crystal microbalance is an extremely high sensitive equipment for measuring and detecting the adsorption of very small amounts (nanogram range) of solids to the surface of piezoelectric quartz crystal by monitoring the alterations in resonance frequency[45]. This device is mainly utilized for biological studies. Researchers at Heriot-Watt University have started the using of QCM in petroleum industry since 1992, covering various applications like saturation point and hydrate dissociation point determinations, evaluation of anti-depositional paint coatings, choosing the best chemical treatment for cleaning solids adhering to the pipeline surfaces and determination of asphaltene onset and the effect of variety of inhibitors on asphaltene deposition[45], [46]. QCM technique can be utilized to determine the asphaltene stability by n-C₇ titration which is used in ASTM D7157. The advantage of QCM rather than ASTM D7157 is that there is no need to use an optical device in QCM technique.[45] developed a new prototype small volume multi-tasking QCM rig for their studies. Figure 2.4 show the schematic of this new developed apparatus.

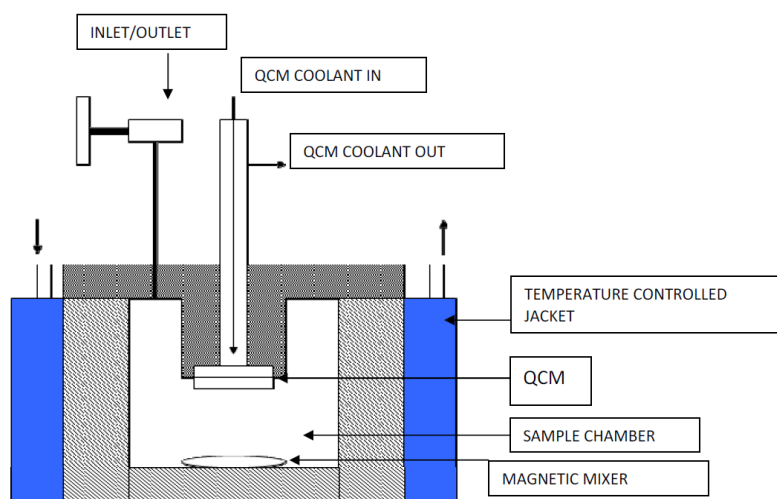


Figure 2. 4. Schematic of new developed small volume multi-tasking flow assurance tool [45]

In this research work, the asphaltene onset pressures in real fluids with and without presence of asphaltene inhibitor were obtained by using new developed QCM rig. The results proved that the QCM technology can be used for accurate determination of asphaltene onsets without using a visual tool and for evaluation of asphaltene inhibitor performance at realistic conditions. Figure 2.5 presents the difference between the asphaltene onset pressures with and without inhibitor and the amount of asphaltene deposition during the gas injection into a real fluid by seeing the reduction in resonance frequency (RF).

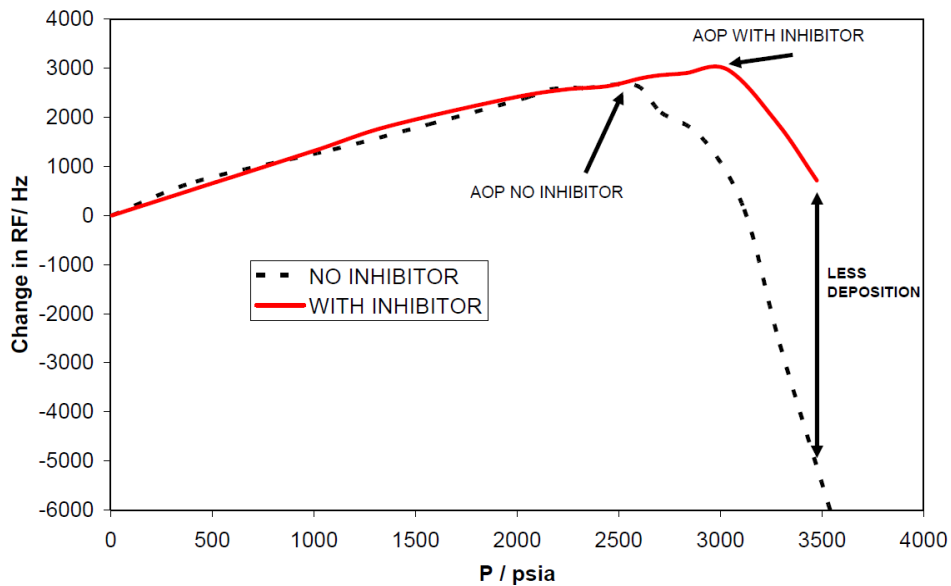


Figure 2. 5. The determination of asphaltene onset pressure (AOP) in a live oil during the gas injection with and without presence of an asphaltene inhibitor [45]

Few researchers have also used quartz crystal microbalance for asphaltene studies. Table 2.4 presents a summary of published research works of using QCM for asphaltene studies.

Table 2. 4. Summary of published research studies of using QCM in application of asphaltene precipitation and deposition investigations

Objectives	Results	Reference
Investigation of the adsorption of asphaltene and resins	<ul style="list-style-type: none"> ✓ Generally, there is no tendency of resin to adhere to the surface. ✓ The adsorption of resins reduces with 	[47]

<p>on gold surface</p>	<p>increasing toluene content in the solvent</p> <ul style="list-style-type: none"> ✓ Unlike resins, asphaltenes were irreversibly adsorbed in multilayers from toluene and 50-50% n-heptane in toluene solutions. 	
<p>The kinetics and thermodynamics of asphaltene adsorption from toluene-heptane and toluene-pentane solutions on gold surface was studied</p>	<ul style="list-style-type: none"> ✓ An initial adsorption process was controlled by the diffusion of asphaltene from bulk solution to the surface ✓ It was predicted that asphaltene would adsorb preferentially in the order of gold > stainless steel > aluminium surfaces by using the thermodynamic free energy predictions 	<p>[48]</p>
<p>A combined quartz crystal microbalance and X-ray photoelectron spectroscopy was employed to illustrate the interactions of asphaltene-metal</p>	<ul style="list-style-type: none"> ✓ The fractional coverage data calculated from combined QCM and XPS measurements for Cold Lake asphaltene on gold surface followed Langmuir (type-I) isotherm ✓ The free energy of asphaltene adsorption estimated from QCM and XPS data was compared well with each other and was calculated to be in the range of -27 kJ/mol to -32 kJ/mol for assumption of asphaltene molecular mass ranging 750-5000 g/gmol. The thickness of adsorbed asphaltene film range from 6–8 nm. 	<p>[49]</p>

<p>The adsorption and desorption of asphaltene into low saline aqueous solutions from a saturated silica surface were investigated</p>	<ul style="list-style-type: none"> ✓ The basic crude oil had larger affinity toward a silica surface than the acidic crude oil ✓ The water wettability of silica surfaces coated with components from the basic crude oil increased significantly because of high salinity aqueous solutions, however slight alterations were observed for silica surfaces coated with components from the acidic crude oil ✓ It was concluded that the presence of acidic components was disadvantageous for low salinity desorption of the acidic crude oil, on the other hand the presence of basic components was more important for low salinity desorption of the basic crude oil 	<p>[50]</p>
<p>Development and validation of new small volume multi-tasking flow assurance tool</p>	<ul style="list-style-type: none"> ✓ Asphaltene stability, asphaltene onset pressure (AOP) and asphaltene inhibitor screening and evaluation all can be done precisely by QCM technology 	<p>[45]</p>
<p>Investigation of the Asphaltene deposition in different depositing environments and various conditions</p>	<ul style="list-style-type: none"> ✓ The rate constant of adsorption was reduced when the temperature increased, which correspond to a lower amount of mass adsorbed at higher temperatures for the initial 	<p>[21]</p>

	<p>time scale However, for long times, the diffusion coefficient was increased with the temperature, which results in more amount of adsorbed mass at higher temperatures in the long run</p> <ul style="list-style-type: none"> ✓ Viscosity of the adsorbed layer was decreased with an increase in the temperature. The viscosity value was small because the adsorbed mass included asphaltene molecules and not bulk asphaltene ✓ Viscosity of the n-C₇ induced asphaltene deposit was higher than the viscosity of the n-C₅ asphaltene deposit because of the heavier nature of n-C₇ asphaltene compared to n-C₅ asphaltene ✓ Polydispersity of asphaltene had a significant role in the deposition of asphaltene onto a gold surface. n-C₇ induced asphaltene mass adsorbed reached equilibrium much sooner than n-C₅ induced asphaltene, and the maximum amount of mass adsorbed at equilibrium for n-C₅ asphaltene was much higher than n-C₇ induced asphaltene ✓ Illustration of different surface types proved that, the asphaltene mass 	
--	--	--

	<p>adsorbed during initial time was increased when steel was rusted, but, in a long run, there was a reduction</p> <ul style="list-style-type: none"> ✓ Different flow rates showed that at initial time scale the effect of flow rate on the rate of adsorption was eligible. But, for long times, the influence of the flow rate was undeniable ✓ The asphaltene adsorption curve reached equilibrium sooner at higher flow rates, and at very long times and high flow rates, the rate of adsorption was not affected by flow rate 	
--	---	--

2.4.3 Modelling Studies of Asphaltene Precipitation

There are variety of approaches for asphaltene precipitation modelling. The asphaltene precipitation models are divided into different categories: Solubility models, Solid models, Thermodynamic micellization and Colloidal models. Each one with its assumptions, advantages and disadvantages is explained in detail in following sub sections.

2.4.3.1 Solubility Models

The base of solubility models is the Flory-Huggins theory[51]. Asphaltene stability is described in terms of reversible solution equilibrium. According to the Flory-Huggins, the chemical equilibrium condition between the asphaltene-rich phase A and solvent-rich phase B is $\mu_i^A = \mu_i^B$, where μ_i is the chemical potential of component i. There are various solubility models such as Nor-azlan model[52], Cimino model[53], Hirschenberg model[37] CPA EoS and PC-SAFT EoS. These models and their assumptions, advantages and disadvantages are presented in Table 2.5.

Table 2. 5. Summary of different models with their assumptions and advantages and disadvantages

Models	Assumptions	Advantages	Disadvantages
Hirschenberg [37]	<p>Asphaltene precipitation is a reversible process</p> <p>Composition of liquid phase is calculated by Soave Equation-of-State with assumption of no asphaltene precipitation</p> <p>Asphaltene precipitation does not alter the vapor-liquid equilibrium calculations</p>	<p>✓ The model results are consistent with experiments of asphaltene precipitation</p> <p>✓ It is easy to implement</p>	<p>✓ The prediction of this model is poor to reproduce the experimental data.</p>
Nor-azlan model [52]	<p>The precipitated asphaltene does not influence the vapour-liquid equilibrium calculation</p>	<p>✓ A suitable tool for screening aims</p>	<p>✓ Does not match the experimental data quantitatively</p>
Cimino model [53]	<p>An asphaltene nucleus includes both asphaltene class components and the solvent</p>	<p>✓ It represents the behaviour of asphaltene very well</p>	<p>✓ It requires several experimental data to determine the model parameters</p> <p>✓ It is not applicable when the composition of fluid changes for</p>

			example during gas injection
Perturbed Chain Statistical Association Fluid Theory (PC-SAFT) Equation-of-State[54]	Asphaltene precipitation is a reversible process Asphaltene associates to form pre-aggregates Asphaltene rich phase contains some amount of the other crude oil components	<ul style="list-style-type: none"> ✓ Able to handle asymmetric mixtures and associating molecules such as asphaltenes that most of the Equation-of-States could not handle ✓ The PC-SAFT can represent the behaviour of asphaltene properly 	

2.4.3.2 Solid Models

In these models, oil and gas are modelled with a cubic Equation-of State, while asphaltene is treated as a single component existing in the solid phase. Ngeim model[55] considered asphaltene as heaviest oil component which consists non-precipitating and precipitating components. The precipitating component has a larger interaction coefficient with light components in comparison with non-precipitating component. Hence, we have more incompatibility of the precipitating component with the lighter components, which causes the transfer of the precipitating component into the solid phase.

2.4.3.3 Thermodynamic Micellization Model

This model was developed by Pan and Firoozabadi [56]. There are two main assumptions for this model. 1- Asphaltene molecules form a micelle core and the resin molecules adsorb on the surface of this core. 2- Gibbs free energy minimization principle is used to determine the structure and concentration of the micelle. The only advantage of this model is that the calculated size of the asphaltene micelles in crude oils predicted by this model matched the experimental data. However, the results for the amount of precipitation have not been presented.

Generally the statistical thermodynamics and colloidal science are used for colloidal models[57]. At first these models assume the existence of asphaltenes as solid particles in colloidal suspension stabilized in the crude oil by adsorption of resin molecules on their surfaces. The vapour-liquid equilibrium is also calculated by utilizing an equation of state (EoS) which establishes the composition of the liquid phase from which asphaltene aggregation may occur.

Another approach that is used for asphaltene precipitation modelling, is named association equation of state models[58]. The assumptions for this model are: - Asphaltene molecules exist mainly as monomers in the bulk crude oil and as aggregates in an associated state in the precipitation phase, - Asphaltene association leads to asphaltene precipitation, - The asphaltene precipitation process is thermodynamically reversible, - The asphaltene precipitation phase is a pseudo-liquid phase. Four main factors of composition, molecular weight, molecular size and interaction energy of each component are used as inputs for this model in order to obtain suitable result of asphaltene precipitation prediction.

2.4.3.4 New Techniques: ADEPT and ASIST Models

2.4.3.4.1 ADEPT

A new deposition model which has been under progression is the Rice University asphaltene deposition tool (ADEPT)[59]. This tool can have two thermodynamic and deposition modules. PC-SAFT is used for the thermodynamic module and a mathematical

model is employed for deposition module, which represents a mass balance of aggregates in a controlled volume.

Thermodynamic Module has 4 inputs which are live oil composition, density of live oil/stock tank oil, bubble pressure at various temperature and asphaltene onset pressures at various temperatures. As a result, this module presents asphaltene solubility along the axial length of a wellbore and/or pipelines as a function of pressure and temperature. Besides that, the phase behaviour of asphaltenes in crude oil is also obtained.

ADEPT Deposition Module has 3 inputs of asphaltene solubility as a function of pressure, temperature and composition, operating variables (e.g. oil flow rate, length & diameter of the pipeline), constants which are describing the kinetics of asphaltene precipitation, aggregation and deposition. This module gives the oil industry describing of the transport of precipitated asphaltenes and also prediction of asphaltene deposition and its magnitude through a pipeline and/or a wellbore. Unfortunately, uncertainties are existed about the accurate kinetics of asphaltene precipitation and aggregation when utilized to estimate kinetics in the real field turbulent flow conditions. It should also be mentioned that the most appropriate way for measuring the precipitation and aggregation rates has not yet been reported.

Application of ADEPT in Industry

The thickness of solid asphaltene deposits at various depths in a well in the Marrat reservoir in southern Kuwait was determined by ADEPT. The simulator predictions, while not an exact match, were very close to the deposit profile reported in the field[59].

2.4.3.4.2 Asphaltene Instability Trend Tool (ASIST)

One model which was found to be used within the industry is the asphaltene instability trend (ASIST) tool. Asphaltene instability is a sign of oncoming precipitation and deposition[60].

The onset solubility parameter vs the square root of the partial molar volume of a precipitant for a series of n-paraffins and the extrapolation for the onset solubility parameter are the inputs of the ASIST. This tool provides the estimation of condition for instability in a reservoir, the prediction of asphaltene onset pressures during oil production,

the interpretation of refractive index tests performed before and after start-up and the characterization of kinetics of asphaltene precipitation as the refractive index tests are performed periodically.

Application of ASIST in Industry

An example of the ASIST's application is the Blind Faith platform in the US Gulf of Mexico, one of the deepest producing platforms in the world and contains four subsea wells producing from two reservoirs, Pink and Peach[61]. It was found that the risk of facing asphaltene problem for Pink reservoir fluid is less than the risk of Peach reservoir fluid. By utilizing the ASIST in their studies, they proposed the mixing of the Peach and Pink fluid together as the best way for handling the problem. They figured out that the mixtures with higher Pink fluid content were likely to have more stable asphaltene content than mixtures with higher Peach fluid content. Prediction was confirmed after 2 years of production and the related flow assurance problem was removed.

2.4.3.5 Application of de Boer Plot: A Risk Assessment Technique

The De Boer plot[62] as a risk assessment tool is used to propose the lighter oils and farther from the bubble point, have more intensive and serious asphaltene issues. For the input of this tool, density at a given pressure and temperature vs the difference between reservoir pressure and boiling point pressure is utilized. It is pessimist and assumes that the whole reservoir is saturated in asphaltenes[63], and in addition it is not appropriate to make operative and really reliable decisions. These are which we can name as its disadvantages. In the previous case study (US Gulf of Mexico) this technique showed that asphaltene precipitation could be problematic during the primary depletion process in both reservoirs. However, Montesi et al.[61] noted that this estimation is doubtable because of its assumption of asphaltene saturation at reservoir conditions.

2.4.4 Asphaltene Inhibition and Remediation Techniques

There are three main categories for asphaltene remediation and inhibition techniques: Mechanical, Chemical and Thermal techniques. In the following sub-sections all the

categories are explained in detail, and the inhibition mechanisms behalf of each one are also presented.

Chemical Techniques: They contain addition of dispersants, flocculants, antifoulants, coagulants, and polar co-solvents which can be employed to handle asphaltene deposition in its different conditions and situations[63]. Dispersants work by surrounding the asphaltene molecules forming steric colloids, they act as resin molecules related to asphaltene molecules (Figure 2.6).

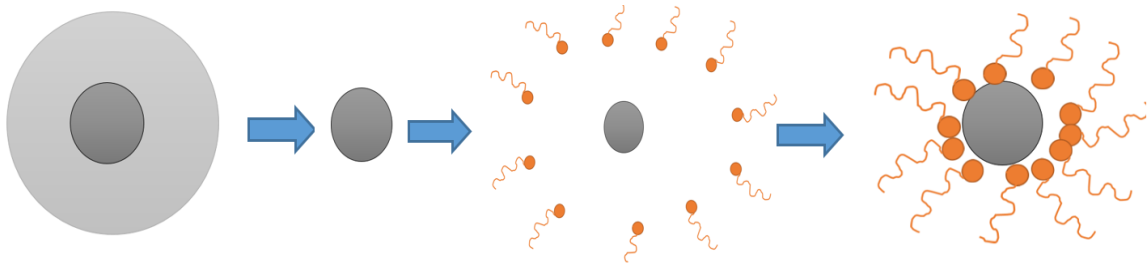


Figure 2. 6. Showing of dispersants inhibition principle which acts as resin molecules related to the asphaltene molecules

Ionic Liquids: The popularly utilized ionic compounds for heavy oil and bitumen recovery are the ones which consist $[\text{PF}_6]^-$ and $[\text{BF}_4]^-$; but, these chemical ionic compounds generate hydrogen fluoride (HF) gas emissions when they are employed. The applications of using these compounds are became limited since they are not inert into different organic compounds in heavy crude oils, which might limit. Hence, these ionic compounds should be utilized in an inert atmosphere and are not appropriate to be employed under the high pressure and high temperature conditions where it is hard to handle the moisture in the oil reservoir[64]. The influence of new ionic compound on heavy oil recovery utilizing spontaneous imbibition tests was investigated by Joonaki et al.[64]. It was shown that when the new ionic compound was mixed with heavy oil recovery, the recovery factor was increased from 41% to 74% by using free imbibition tests. It was shown that the new created ionic liquid can be utilized to upgrade heavy oil by decreasing the asphaltene content, crude oil viscosity, and average molecular weight of heavy oil. It can also be used as a dispersant agent and acted as resin molecules in crude oils. Adeniyi S. Ogunlaja et al.[65] investigated the effect of different imidazolium based ionic liquids on dispersion of asphaltene molecules. They found that a strong interaction between asphaltene molecules

and ionic liquids happened through π - π interaction between cation and asphaltenes through hydrogen bonding. It was also observed that the order of reactivity of 1-butyl-3-methylimidazolium chloride was higher than 1-butyl-3-methylimidazolium nitrate and 1-methyl-1H-imidazolium-2-carboxybenzoate, and the reactivity of 1-butyl-3-methylimidazolium nitrate is higher than 1-methyl-1H-imidazolium-2-carboxybenzoate accordingly.

Antifoulants are utilized to inhibit the attachment and growth of deposits on the surfaces and walls of the oil production pipelines. Tributyltin Oxide (TBTO) and Teflon are two compounds which are used as Antifoulants[66]. As an advantage of using TBTO, we can mention that it gradually leaches from the hull eliminating the fouling organisms in the surrounding area. But causing health and environmental problems is a disadvantage of using this compound. Injection of Coagulant is another approach in chemical based treatment techniques[67]. Coagulants are mainly polymers, have a role similar to resins which form steric colloids and then aggregation of colloids in the form of asphaltene flocs. Polar co-solvents, such as aromatic hydrocarbons, can re-dissolve the asphaltene deposits and to be an effective approach they should have a high level of aromaticity.

Mechanical Techniques: These techniques are mainly divided into three approaches: Pigging, Mechanical/Manual Striping and Mechanical Vibration. The treatment principle behind the mechanical/manual striping technique is that this technique is done by mechanically scraping the oil well tubing (Yarranton, 2000). Also the treatment principle beyond the pigging technique is that the soluble or insoluble pigs are injected into the oil pipelines, the pigs would remove huge amount of the asphaltene deposit build up as they travel through the crude oil pipelines[68], [69]. It should be mentioned that generally there are two advantages and three disadvantages related to mechanical treatment techniques. For their advantages it could be expected that they are so effective and appropriate for cleaning the oil tubing and pipelines. Besides that, the smart pigs may make the facility of remote visualization, control, local heating, etc. Low efficiency of the pigging technology in removing the heavy organic deposits in the oil reservoirs could be mentioned as their disadvantages. In addition, the mechanical removal of asphaltene deposits may be an

expensive and also time-consuming treatment technique, and the disposal of the asphaltene deposits sometimes leads to cause serious problems.

Thermal Techniques: There are various treatment techniques based on heating of the crude oil for mitigation of asphaltene deposition problems such as steam injection, hot water injection, hot gas injection, hot chemical injection, microwave technique, in-situ combustion and exothermic chemical reactions. Hot fluids are circulated within the well and also injected through the oil formation and areas that are plugged by asphaltenes in order to remove the asphaltene deposits[70]. The treatment principle of this method is melting of the asphaltene deposits. Most of these thermal techniques are not cost effective because of their operational costs, and also some of them, such as microwave technique, are mostly applicable in the laboratory scale and not suitable for the real field applications.

2.4.4.1 New and Under Development Inhibition Techniques

External Force Field Techniques: These new and novel techniques contain different methodologies to produce the external force field for asphaltene deposition removal, which are using electrostatic force field, electrodynamic force field, magnetic field, ultrasonic technique and microwave technique[71], [72]. Unfortunately, up to now all these techniques are usable in laboratory studies and small scales.

Biological Methods: These treatment techniques work by using bio-process which might reduce asphaltenes into lighter molecules. This bio-process is named biodegradation. The asphaltene deposits are metabolized as a source of carbon and energy (by the proper species of bacteria, fungi, etc) during this biodegradation process[20], [73]. Microorganisms need couple of months to years to degrade a significant quantity of asphaltenes, and this problem makes the biodegradation as a fairly slow process. Using the biodegradation process as an approach for asphaltene deposition remediation has not been investigated frequently. If this method would be practical, it could be an important mechanism for addressing asphaltene related flow assurance problems.

2.4.4.2 Related Case Studies of Inhibition & Remediation techniques

An oilfield from eastern Venezuela had intense asphaltene flow assurance problems which cause the plugging of well production within seven months[74]. Different treatment techniques were employed to handle the problem such as physically scraping the wellbore and injection of xylene into the tubing. Each treatment process contained the cost of about US \$50,000 and shutting the oil production for two days. After the applying of the treatment techniques the oil production rate was increased dramatically and also the frequency of the treatments was decreased to every eight months. Hence as a consequence of having more oil production and less frequent treatment an annualized benefit of 60,882 barrels and return on investment of more than 3,000% were obtained.

Another case study of using remediation techniques is an oilfield in the Adriatic Sea which contains two deep-water subsea wells. It had thick asphaltene deposits along a 3,300 ft length of the oil tubing which was started at a depth of 6,500 ft under the seafloor. After studying on asphaltene characteristics of the oil sample from this oilfield a continuous downhole injection of appropriate asphaltene dispersant was advised. After the treatment process the oil production level was increased to 98%-100% of effectiveness. The oil production was continued for several years without any pipeline and oil tubing blockage.

Another case, which is related to the mechanical treatment, is an oilfield in the northern Monagas province of eastern Venezuela[74]. Completely plugging of two pipeline sections with the length of 30,513 was determined by using fluid flow testing. An inclined injector head frame was utilized and authorized for the injection of the Coiled Tubing (CT) into the horizontally positioned pipeline. Water-based gel was also pumped to move the dislodged solids. As a result, by using the CT instead of other treatment options to remove the asphaltene deposits, the profit of saving 1 million USD was obtained and also this treatment process allowed the normal operations to be returned faster.

2.5 Case Studies Analysis Based on Proposed Work Flow Chart

In this section different case studies are analysed based on the proposed work flow chart in Section 4, which indicates the potential use of this flow chart for solving the asphaltene flow assurance problems. The presented flow chart contains 6 steps, and the case studies are explained step by step based on the presented flow chart.

2.5.1 Case. 1, An Oilfield in Gulf of Mexico

In the Gulf of Mexico, Hydro Gulf of Mexico LLC had potential asphaltene precipitation problems in a deepwater development[75].

1st Step- Sampling: The blending of two different fluids of oil and condensate was occurred by two wells which were penetrating the formation at different depths. Appropriate samples were collected from these wells for the experimental studies.

2nd Step- Experimental Studies: First, SARA analysis was employed for determining the asphaltene content. It was found that the sample contained 61.7% saturates, 26.0% aromatics, 11.4% resins and 0.9% asphaltenes. In addition, the Near Infra-Red (NIR) light-scattering and High-Pressure Microscopic (HPM) were utilized for Asphaltene Onset Pressure (AOP) determination. It is obtained that the asphaltene onset pressures were 7,000 psi \pm 100 psi and 10,700 psi with 20% OBM contamination and without contamination respectively.

3th Step- Creation of a Reliable Model: A molecular equation of state (EoS) was developed for the evaluation of reservoir fluid at pressure, and temperature and composition conditions along the 28,000 ft length of the oil pipeline and also for the prediction of conditions at key locations through the first five years of the production.

4th Step- Adjustment of the Model: By applying the model for the current study it was found that decreasing the pressure from its initial value asphaltene precipitation would be increased, and also by decreasing the pressure from 16,988 to 10,000 psi 10% of the fluid asphaltene content would be precipitated. It was also concluded that by mixing the black oil and gas condensate the asphaltene onset pressure (AOP) would be increased, and if the pressure would be reduced to 10,000 psi and a quantity of gas condensate would be added to the fluid, 60% of the fluid asphaltene content would be precipitated.

5th Step- Decision Making and Selection of the Most Appropriate Solution: Based on modelling and experimental studies in the previous steps the injection of suitable asphaltene precipitation inhibitors was recommended. It was also suggested that the oil production from the layers should be consecutive, first production from the oil layer, then the gas condensate layer without any blending.

6th Step- Application in the Real field: The recommended inhibition techniques were applied in the real oilfield. At last the project was successful and the oil production from this oilfield was continued without facing any asphaltene problems.

2.5.2 Case. 2, Oilfield from South Kuwait

Very serious and undeniable problems for reservoir management and production operations of Greater Burgan oilfield of South Kuwait were faced by asphaltene deposition on tubulars and pipelines[27]. Toluene was successfully employed at first, but because of some restrictions the use of solvents which are more environmentally friendly is mandatory.

1st Step- Sampling: For fluid and asphaltene characterization, four single-phase samples were gathered from four wells in the Marrat carbonate reservoir interval.

2nd Step- Experimental Studies: SARA analysis for the live oil from Well MG-OF4 was utilized and the results of 68.3% saturates, 11.2% aromatics, 18.4% resins and 2.1% asphaltenes were obtained. This technique was used again for the deasphalted oil (DAO) and the results of 59.5% saturates, 25% aromatics, 15.3% resins and 0.2% asphaltenes were gained. Hence there is a reduction in asphaltene content of 90% compared with the live oil. Gravimetric measurement was also employed for the reservoir fluid from well MG-OF4. The pressures of 6,200 psi and 3,235 psi were obtained as asphaltene onset pressure and bubble point pressure respectively. For more studies of the asphaltene onset pressures at different conditions the acoustic resonance technique was used. It was found that the solution with 40% DAO was more effective than one with 40% toluene in decreasing of the Asphaltene onset pressure. The solvating power of the deasphalted oil was improved more drastically by the addition of 1% asphaltene dispersant.

3th Step- Creation of a Reliable Model: A thermodynamic model was developed for the asphaltene studies of this case with an assumption of asphaltene as a solid phase in equilibrium with the reservoir fluid.

4th Step- Adjustment of the Model: Simulation results of the fluid behaviour over the range of conditions argued that during the oil production, the asphaltene precipitation from the Marrat oils was undeniable and significant. It was concluded that for minimizing the

asphaltene deposition, a cost-effective solvent injection for batch treatment or periodic injection on pipelines was needed.

5th Step- Decision Making and Selection of the Most Appropriate Solution: As one of the most suitable approach to handle the problem the injection of deasphalted oil as an asphaltene solvent was proposed. This was suggested because the removal of asphaltenes by precipitation is a reversible process for various kind of oils. The deasphalted oil, which is made by removing the precipitated asphaltenes, could be able to dissolve the asphaltenes much higher than the original live oil.

6th Step- Application in the Real field: After applying the injection of deasphalted oil, a huge amount of asphaltene was dissolved from the borehole wall within 24 hours. It can be mentioned that the employed technique is more environmentally friendly than other methods and its cost approximately 50% less than utilizing toluene.

2.6 A Short Explanation about the Enhanced Oil Recovery (EOR) Approaches

Nowadays it becomes a hot research topic for the petroleum research groups worldwide to develop an approach with high efficiency for increasing oil recovery from the existing oil reservoirs. The EOR methods generally divided into three different groups: Thermal, Chemical and Gas Injection techniques. The first thing that is crucial to do, when the oil reservoir pressure is depleted through primary and secondary oil production, is to restore the pressure within the reservoir to one appropriate for oil production as a tertiary recovery or enhanced oil recovery (EOR) technique[64]. In this regard, the CO₂ injection, water injection, water alternating gas injection and Carbonated water injection can be ideal EOR approaches in many cases. Since the late 70's, the gas injection (especially CO₂ injection) is the only approach which has been gained the most attention and success worldwide. The trapped oil can also be recovered by employing chemical/surfactant flooding and decreasing the capillary forces which prevent the oil from flowing through the porous media into the wellbores. Thermal flooding is generally limited to heavy oil fields only. Besides additional economic benefit through different EOR processes, environmentally safe and employing at least part of the existing infrastructure in injection methodologies (CO₂/Water/WAG/CWI), some of them might have some disadvantages such as asphaltene

precipitation and deposition in heavy oil reservoirs which may cause permeability reduction and wettability alterations.

2.6.1 The Effects of EOR Processes on Asphaltene Deposition in Porous Media

Although a significant amount of research projects focused on different injection scenarios, the interactions between the injected fluid and residual oil and the actual mechanisms by which residual oil might move through porous media during the injection and its serious effect on asphaltene deposition and pore plugging have not yet been fully understood. A summary of selected and most recent published studies on the effect of enhanced oil recovery processes on asphaltene deposition is presented in Table 2.6.

Table 2. 6. Summary of most recent published research works on investigation of enhanced oil recovery processes on asphaltene precipitation and deposition

Objectives of Study	Experimental Techniques and Devices	Results	Reference
Visual study of asphaltene deposition due to CO ₂ injection and pressure depletion	High Pressure Cell & Image Processing Technique	Asphaltene depositions at different pressures and temperatures and CO ₂ mol% for two different crude oils were obtained. By increasing the mole percent of CO ₂ from 5 to 20%, the area of deposited asphaltene was increased at pressure range of 30 to 140 bar. By increasing the temperature, asphaltene particles tend to flocculate and make larger particles.	[76]
Investigation of the	X-ray CT Images	In all injection scenarios there	[77]

<p>effects of immiscible CO₂ injection process on asphaltene deposition and permeability reduction</p>		<p>were oil effective permeability reductions and the CO₂ dry or secondary flooding process had a much smaller oil effective permeability reduction compared to tertiary recovery</p>	
<p>Investigation of the oil recovery mechanisms and asphaltene precipitation problem in immiscible and miscible CO₂ flooding processes</p>	<p>IFT Measurements and Conventional Core flooding</p>	<p>The linear regression equation of the measured equilibrium IFT versus equilibrium pressure data for the first pressure range gave zero equilibrium IFT at the equilibrium pressure of $P_{eq} = 10.6$ MPa, as the minimum miscibility pressure (MMP) The oil recovery factor (RF) became higher at a higher pressure during the immiscible CO₂ flooding. Once the pressure exceeded the MMP, the oil RF increased slightly and eventually reached a nearly constant maximum value in the miscible CO₂ flooding The measured asphaltene content of the produced oil was decreased with the pore volume (PV) of injected CO₂ in each coreflood test due to CO₂-induced asphaltene</p>	<p>[78]</p>

		precipitation. A higher average asphaltene content of the produced oil was found under the immiscible conditions Total oil recovery factor was much higher at the higher temperature under the miscible conditions	
Asphaltene precipitation, aggregation and deposition were for the first time investigated during solvent injection at elevated temperatures for heavy oil recovery	PVT Cell, Focused Ion Beam (FIB) and Scanning Electron Microscope (SEM)	The influence of various types of light hydrocarbons as a solvent on asphaltene agglomeration was illustrated, and it was concluded that the thickness of asphaltene deposition was increased with decreasing carbon number of the solvent	[79]

2.7 Why are some asphaltenes projects being failed?

Recently many oil companies spent a lot of money on asphaltene precipitation & deposition remediation projects. Because of the lack of a clear and consistent process for deciding on how & when to employ the appropriate remediation approaches (Mechanical, Chemical, Thermal and etc.), some of these projects were not completely successful in their objectives.

The amount of inhibitor, type of inhibitor, soaking time, number of treatment jobs and the time period between two treatment jobs affect the outcome of an asphaltene treatment plan. Accurate prediction of asphaltene precipitation, aggregation, and deposition in the porous media and wellbore significantly decreases high expenses related to the reservoir remediation, well intervention approaches, and oilfield production suspension.

2.8 Conclusions

There are some points which can be safely concluded from the sections above which have been tried to be addressed in the following chapters:

1. Up to now, most of the mentioned asphaltene precipitation models in previous sections have been examined just on confined sets of experimental data. Many of the researchers assert that their models could give appropriate estimations, nevertheless none of them could be employed for systematically asphaltene precipitation prediction since the modelling results of real field application in industry show the limitation of most state-of-art approaches for the prediction of asphaltene precipitation and deposition.
2. Researchers try to generate new reliable models that can incorporate the most recent experimental findings (e.g. asphaltene molecular size and structures). This important topic can be considered to have more accurate asphaltene deposition simulator.
3. It is proved that the proposed work flow chart for mitigation of the asphaltene related flow assurance problems can be used as a general rule for the oil companies to remove the asphaltene barriers.
4. Most of the current experimental techniques for asphaltene precipitation onset determination do not have an accurate performance in this regard. Further research studies can be conducted in this regard.
5. Each group of chemical compounds can be used for some crude oils with specific characteristics and they have certain roles in inhibition and remediation processes. This topic can be demonstrated in more details.
6. A suitable dynamic modelling of asphaltene precipitation for an accurate prediction should consist the effect of pressure, temperature, composition variation, oil velocity and the amount of asphaltene aggregates in a grid block.
7. It can be concluded that water films on reservoir rock surfaces may prevent the deposition of asphaltene on the rock surfaces. It needs to be investigated further for different water chemistries.

8. During the gas injection process which is one of the most important EOR approaches, the amount of asphaltene precipitation extremely high relies on the amount of gas which is combined with oil. This can be illustrated further.
9. It is proved that Quartz Crystal Microbalance (QCM) technology can also be used as a flow assurance tool besides its use in biological studies. It can be a reliable technique for investigation of asphaltene deposition during pressure depletion or gas injection processes.

2.9 References

- [1] J. J. Adams, "Asphaltene adsorption, a literature review," *Energy and Fuels*, vol. 28, no. 5, pp. 2831–2856, 2014.
- [2] O. C. Mullins, *In Structure and dynamics of asphaltenes*. Plenum Press, 1998.
- [3] J. G. Speight and S. E. Moschopedis, "On the molecular nature of petroleum asphaltenes," ACS Publications, 1981.
- [4] E. Joonaki, A. H. Youzband, R. Burgass, and B. Tohidi, "Effect of Water Chemistry on Asphaltene Stabilised Water in Oil Emulsions-A New Search for Low Salinity Water Injection Mechanism," in *79th EAGE Conference and Exhibition 2017*, 2017.
- [5] M. Wang, Y. Hao, M. R. Islam, and C. C. Chen, "Aggregation thermodynamics for asphaltene precipitation," *AIChE J.*, vol. 62, no. 4, pp. 1254–1264, 2016.
- [6] H. W. Yarranton and J. H. Masliyah, "Molar mass distribution and solubility modeling of asphaltenes," *AIChE J.*, vol. 42, no. 12, pp. 3533–3543, 1996.
- [7] A. H. Youzband, P. Kor, E. Joonaki, V. Taghikhani, R. B. Boozarjomehry, and A. Chapoy, "Development of a New Model for Quantifying of Asphaltene Deposition-Role of Precipitation, Aggregation and Radial Transport," in *79th EAGE Conference and Exhibition 2017*, 2017.
- [8] et al. Buenrostro-Gonzalez, Eduardo, "The overriding chemical principles that define asphaltenes.," *Energy Fuels* 15.4 972-978.
- [9] and O. C. M. Groenzin, Henning, "Asphaltene molecular size and weight by time-resolved fluorescence depolarization.," *Asph. heavy oils, Pet. Springer, New York, NY, 2007. 17-62*.
- [10] A. B. Andrews, R. E. Guerra, O. C. Mullins, and P. N. Sen, "Diffusivity of Asphaltene Molecules by Fluorescence Correlation Spectroscopy," *J. Phys. Chem. A*, vol. 110, no. 26, pp. 8093–8097, Jul. 2006.

- [11] O. C. Mullins, B. Martínez-Haya, and A. G. Marshall, “Contrasting Perspective on Asphaltene Molecular Weight. This Comment vs the Overview of A. A. Herod, K. D. Bartle, and R. Kandiyoti,” *Energy & Fuels*, vol. 22, no. 3, pp. 1765–1773, May 2008.
- [12] J.-A. Östlund, P. Wattana, M. Nydén, and H. S. Fogler, “Characterization of fractionated asphaltenes by UV–vis and NMR self-diffusion spectroscopy,” *J. Colloid Interface Sci.*, vol. 271, no. 2, pp. 372–380, 2004.
- [13] S. I. Andersen and S. D. Christensen, “The Critical Micelle Concentration of Asphaltenes As Measured by Calorimetry,” *Energy & Fuels*, vol. 14, no. 1, pp. 38–42, Jan. 2000.
- [14] Y. Zhang, T. Takanohashi, T. Shishido, S. Sato, I. Saito, and R. Tanaka, “Estimating the Interaction Energy of Asphaltene Aggregates with Aromatic Solvents,” *Energy & Fuels*, vol. 19, no. 3, pp. 1023–1028, May 2005.
- [15] R. Mahmoud, P. Gierycz, R. Solimando, and M. Rogalski, “Calorimetric Probing of n-Alkane–Petroleum Asphaltene Interactions,” *Energy & Fuels*, vol. 19, no. 6, pp. 2474–2479, Nov. 2005.
- [16] C. Stachowiak, J.-R. Vigué, J.-P. E. Grolier, and M. Rogalski, “Effect of n-Alkanes on Asphaltene Structuring in Petroleum Oils,” *Langmuir*, vol. 21, no. 11, pp. 4824–4829, May 2005.
- [17] G. Ekulu, C. Nicolas, C. Achard, and M. Rogalski, “Characterization of Aggregation Processes in Crude Oils Using Differential Scanning Calorimetry,” *Energy & Fuels*, vol. 19, no. 4, pp. 1297–1302, Jul. 2005.
- [18] C. Stachowiak, J.-P. E. Grolier, and S. L. Randzio, “Transitiometric Investigation of Asphaltenic Fluids Under In-Well Pressure and Temperature Conditions,” *Energy & Fuels*, vol. 15, no. 5, pp. 1033–1037, Sep. 2001.
- [19] D. H. Napper, “Steric stabilization,” *J. Colloid Interface Sci.*, vol. 58, no. 2, pp. 390–407, 1977.
- [20] and A. E. Mansoori, G. Ali, “Remediation of asphaltene and other heavy organic deposits in oil wells and in pipelines.” S,” *Socar Proc.* 4 12-23.
- [21] M. Tavakkoli, S. R. Panuganti, F. M. Vargas, V. Taghikhani, M. R. Pishvaie, and W. G. Chapman, “Asphaltene Deposition in Different Depositing Environments: Part 1. Model Oil,” *Energy & Fuels*, vol. 28, no. 3, pp. 1617–1628, Mar. 2014.
- [22] et al. Mousavi Dehghani, Sayed Ali, “Experimental investigation on asphaltene deposition in porous media during miscible gas injection,” *Iran. J. Chem. Chem. Eng.* 26.4 39-48.

- [23] V. Hematfar, B. B. Maini, and Z. Chen, “Experimental Investigation of the Impact of Asphaltene Adsorption on Two Phase Flow in Porous Media,” *SPE European Formation Damage Conference & Exhibition*. Society of Petroleum Engineers, Noordwijk, The Netherlands, p. 10, 2013.
- [24] P. Kriz and S. I. Andersen, “Effect of Asphaltenes on Crude Oil Wax Crystallization,” *Energy & Fuels*, vol. 19, no. 3, pp. 948–953, May 2005.
- [25] J. Bon, H. K. Sarma, J. T. Rodrigues, and J. G. Bon, “Reservoir-fluid sampling revisited-A practical perspective,” *SPE Reserv. Eval. Eng.*, vol. 10, no. 06, pp. 589–596, 2007.
- [26] F. Conti and R. Kumar, “Hydrocarbon Sampling in Tight Chalk,” *SPWLA 54th Annual Logging Symposium*. Society of Petrophysicists and Well-Log Analysts, New Orleans, Louisiana, p. 12, 2013.
- [27] A. K. M. Jamaluddin, B. Ross, D. Ross, and M. Hashem, “Single-Phase Bottomhole Sampling Technology,” *J. Can. Pet. Technol.*, vol. 41, no. 07, p. 6, 2002.
- [28] O. C. Mullins, G. Fujisawa, C. Dong, S. Betancourt, T. Terabayashi, M. Hashem, and H. Elshahawi, “Compartment Identification by Downhole Fluid Analysis,” *Petrophysics*, vol. 46, no. 04, p. 11, 2005.
- [29] N. R. Nagarajan, L. Leal, V. K. Mishra, J. Y. Zuo, and K. Indo, “Downhole Fluid Analysis Tools and Methods: Laboratory Measurements vs. Downhole Fluid Analysis,” *International Petroleum Technology Conference*. International Petroleum Technology Conference, Kuala Lumpur, Malaysia, p. 13, 2014.
- [30] J. A. Canas, S. Colacelli, E. G. Freitas, and B. Andrews, “New Downhole Fluid Analysis (DFA) Technologies Supporting Improved Reservoir Management,” *Latin American & Caribbean Petroleum Engineering Conference*. Society of Petroleum Engineers, Buenos Aires, Argentina, p. 9, 2007.
- [31] G. Fujisawa, R. Jackson, S. Vannuffelen, T. Terabayashi, T. Yamate, C. Dong, and M. O’Keefe, “Reservoir Fluid Characterization With A New-Generation Downhole Fluid Analysis Tool,” *SPWLA 49th Annual Logging Symposium*. Society of Petrophysicists and Well-Log Analysts, Austin, Texas, p. 7, 2008.
- [32] T. Fan, J. Wang, and J. S. Buckley, “Evaluating Crude Oils by SARA Analysis,” *SPE/DOE Improved Oil Recovery Symposium*. Society of Petroleum Engineers, Tulsa, Oklahoma, p. 7, 2002.
- [33] A. Hammami, C. H. Phelps, T. Monger-McClure, and T. M. Little, “Asphaltene Precipitation from Live Oils: An Experimental Investigation of Onset Conditions and Reversibility,” *Energy & Fuels*, vol. 14, no. 1, pp. 14–18, Jan. 2000.

- [34] Y.-F. Hu and T.-M. Guo, "Effect of temperature and molecular weight of n-alkane precipitants on asphaltene precipitation," *Fluid Phase Equilib.*, vol. 192, no. 1–2, pp. 13–25, 2001.
- [35] J. S. Buckley, "Predicting the onset of asphaltene precipitation from refractive index measurements," *Energy and Fuels*, vol. 13, no. 2, pp. 328–332, 1999.
- [36] J.-L. D. J. Castillo, S. Acevedo, Carlos Canelon, Hervé Carrier, "No Title High pressure and high temperature investigations of asphaltene stability using an extrinsic refractometer.," *6th Int. Conf. Pet. Phase Behav. Fouling, Jun 2005, Amsterdam, Netherlands. pp.1, 2005.*
- [37] A. Hirschberg, L. N. J. deJong, B. A. Schipper, and J. G. Meijer, "Influence of Temperature and Pressure on Asphaltene Flocculation," *Soc. Pet. Eng. J.*, vol. 24, no. 03, pp. 283–293, 1984.
- [38] A. Sivaraman, Y. Hu, F. B. Thomas, D. B. Bennion, and A. K. M. Jamaluddin, "Acoustic Resonance: An Emerging Technology to Identify Wax And Asphaltene Precipitation Onset Conditions In Reservoir Fluids," in *Annual Technical Meeting*, 1997.
- [39] S. I. Andersen, "Flocculation onset titration of petroleum asphaltenes," *Energy & Fuels*, vol. 13, no. 2, pp. 315–322, 1999.
- [40] S. Negahban, J. N. M. Bahamaish, N. Joshi, J. Nighswander, and A. K. M. Jamaluddin, "An Experimental Study at an Abu Dhabi Reservoir of Asphaltene Precipitation Caused By Gas Injection," *SPE Prod. Facil.*, vol. 20, no. 02, pp. 115–125, 2005.
- [41] G. Ekulu, P. Magri, and M. Rogalski, "Scanning Aggregation Phenomena in Crude Oils with Density Measurements," *J. Dispers. Sci. Technol.*, vol. 25, no. 3, pp. 321–331, Dec. 2004.
- [42] S. EL MOHAMED, F. HARDOUIN, and H. GASPAROUX, "Flocculation des produits lourds du pétrole," *J. Chim. Phys.*, vol. 85, no. 1, pp. 135–144.
- [43] P. Fotland, "PRECIPITATION OF ASPHALTENES AT HIGH PRESSURES; EXPERIMENTAL TECHNIQUE AND RESULTS," *Fuel Sci. Technol. Int.*, vol. 14, no. 1–2, pp. 313–325, Jan. 1996.
- [44] P. F. Clarke and B. B. Pruden, "Asphaltene precipitation: detection using heat transfer analysis, and inhibition using chemical additives," *Fuel*, vol. 76, no. 7, pp. 607–614, 1997.
- [45] B. Burgass, R., & Tohidi, "Development and Validation of Small Volume Multi-Tasking Flow Assurance Tool.," *Soc. Pet. Eng. (2011, January 1).*

- [46] B. Burgass, Rhoderick William; Tohidi Kalorazi, “Reducing the risks of solid deposition by using internal pipeline coating,” *15th Int. Conf. Pipeline Prot. Aachen, Ger.*, 2003.
- [47] P. Ekholm, E. Blomberg, P. Claesson, I. H. Auflem, J. Sjöblom, and A. Kornfeldt, “A Quartz Crystal Microbalance Study of the Adsorption of Asphaltenes and Resins onto a Hydrophilic Surface,” *J. Colloid Interface Sci.*, vol. 247, no. 2, pp. 342–350, 2002.
- [48] K. Xie and K. Karan, “Kinetics and thermodynamics of asphaltene adsorption on metal surfaces: A preliminary study,” *Energy & fuels*, vol. 19, no. 4, pp. 1252–1260, 2005.
- [49] A. Rudrake, K. Karan, and J. H. Horton, “A combined QCM and XPS investigation of asphaltene adsorption on metal surfaces,” *J. Colloid Interface Sci.*, vol. 332, no. 1, pp. 22–31, 2009.
- [50] U. Farooq, J. Sjöblom, and G. Øye, “Desorption of Asphaltenes from Silica-Coated Quartz Crystal Surfaces in Low Saline Aqueous Solutions,” *J. Dispers. Sci. Technol.*, vol. 32, no. 10, pp. 1388–1395, Oct. 2011.
- [51] P. J. Flory, “Thermodynamics of high polymer solutions.,” *J. Chem. Phys.* 10.1 51-61.
- [52] N. Nor-Azlan and M. A. Adewumi, “Development of Asphaltene Phase Equilibria Predictive Model,” *SPE Eastern Regional Meeting*. Society of Petroleum Engineers, Pittsburgh, Pennsylvania, p. 13, 1993.
- [53] R. Cimino, S. Corra, P. A. Sacomani, and C. Carniani, “Thermodynamic Modelling for Prediction of Asphaltene Deposition in Live Oils,” *SPE International Symposium on Oilfield Chemistry*. Society of Petroleum Engineers, San Antonio, Texas, p. 14, 1995.
- [54] D. L. Gonzalez Rodriguez, “Modeling of asphaltene precipitation and deposition tendency using the PC-SAFT equation of state.,” *Diss.* 2008.
- [55] L. X. Nghiem, M. S. Hassam, R. Nutakki, and A. E. D. George, “Efficient Modelling of Asphaltene Precipitation,” *SPE Annual Technical Conference and Exhibition*. Society of Petroleum Engineers, Houston, Texas, p. 10, 1993.
- [56] H. Pan and A. Firoozabadi, “A Thermodynamic Micellization Model for Asphaltene Precipitation: Part I: Micellar Size and Growth,” *SPE Prod. Facil.*, vol. 13, no. 02, pp. 118–127, 1998.
- [57] K. J. Leontaritis and G. A. Mansoori, “Asphaltene flocculation during oil production and processing: A thermodynamic colloidal model,” in *SPE International Symposium on Oilfield Chemistry*, 1987.

- [58] Y.-K. Li, L. X. Nghiem, and R. A. Heidemann, "Investigation of Phase Behavior Predictions With a Chemical-Association Equation of State," *SPE Enhanced Oil Recovery Symposium*. Society of Petroleum Engineers, Tulsa, Oklahoma, p. 12, 1986.
- [59] A. S. Kurup, J. S. Buckley, J. Wang, H. J. Subramani, J. L. Creek, and W. G. Chapman, "Asphaltene Deposition Tool: Field Case Application Protocol," *Offshore Technology Conference*. Offshore Technology Conference, Houston, Texas, USA, p. 14, 2012.
- [60] J. L. Creek, J. Wang, and J. S. Buckley, "Verification of Asphaltene-Instability-Trend (ASIST) Predictions for Low-Molecular-Weight Alkanes," *SPE Prod. Oper.*, vol. 24, no. 02, pp. 360–368, 2009.
- [61] A. Montesi, R. A. Pinnick, S. Subramanian, J. Wang, and J. L. Creek, "Asphaltene Management in GOM DW Subsea Development," *Offshore Technology Conference*. Offshore Technology Conference, Houston, Texas, USA, p. 20, 2011.
- [62] R. B. de Boer, K. Leerlooyer, M. R. P. Eigner, and A. R. D. van Bergen, "Screening of Crude Oils for Asphalt Precipitation: Theory, Practice, and the Selection of Inhibitors," *SPE Prod. Facil.*, vol. 10, no. 01, pp. 55–61, 1995.
- [63] et al. Khanifar, Ahmad, "Study of asphaltene precipitation and deposition phenomenon," *2011 Natl. Postgrad. Conf. IEEE, 2011*.
- [64] E. Joonaki and S. Ghanaatian, "The Application of Nanofluids for Enhanced Oil Recovery: Effects on Interfacial Tension and Coreflooding Process," *Pet. Sci. Technol.*, vol. 32, no. 21, pp. 2599–2607, 2014.
- [65] A. S. Ogunlaja, E. Hosten, and Z. R. Tshentu, "Dispersion of Asphaltenes in Petroleum with Ionic Liquids: Evaluation of Molecular Interactions in the Binary Mixture," *Ind. Eng. Chem. Res.*, vol. 53, no. 48, pp. 18390–18401, 2014.
- [66] C. Spurell, "Measuring Antifoulant and Corrosion Inhibitor Effectiveness in the Lab," in *CORROSION 2001*, 2001.
- [67] K. Okamoto and K. Hotta, "Purification Experiments of Ocean Sludge by Activating Microorganisms and Using Coagulants," in *The Tenth ISOPE Pacific/Asia Offshore Mechanics Symposium*, 2012.
- [68] L. C. Pretorius, "New Application Technology for Internal Pipeline Coatings In-Situ Pipeline Protection using Pigging Techniques," in *CORROSION 2006*, 2006.
- [69] M. G. F. M. Gomes, F. B. Pereira, and A. C. F. Line, "Pigging In Subsea Flexible Flowlines," *Offshore Technology Conference*. Offshore Technology Conference, Houston, Texas, p. 10, 1994.

- [70] A. Shandrygin, O. Dinariev, D. Mikhailov, M. Nukhaev, and A. Lutfullin, “Enhancing efficiency of steam-thermal treatment of formations with high-viscosity oil,” in *SPE Russian Oil and Gas Conference and Exhibition*, 2010.
- [71] A. Y. Zekri, S. A. Shedid, and H. Alkashef, “Use of Laser Technology for the Treatment of Asphaltene Deposition in Carbonate Formations,” *Pet. Sci. Technol.*, vol. 21, no. 9–10, pp. 1409–1426, Jan. 2003.
- [72] U. K. Gollapudi, S. S. Bang, and M. R. Islam, “Ultrasonic Treatment for Removal of Asphaltene Deposits During Petroleum Production,” *SPE Formation Damage Control Symposium*. Society of Petroleum Engineers, Lafayette, Louisiana, p. 8, 1994.
- [73] A. Ayyaswami, “Innovative In-Situ Remedial Technologies for Petroleum Hydrocarbon Remediation,” in *SPE Middle East Health, Safety, Environment & Sustainable Development Conference and Exhibition*, 2014.
- [74] L. Cenegy, “Survey Of Successful World-wide Asphaltene Inhibitor Treatments In Oil Production Fields,” *Proc. SPE Annu. Tech. Conf. Exhib.*, 2001.
- [75] D. L. Gonzalez, G. J. Hirasaki, A. K. M. Jamaluddin, W. G. Chapman, and T. Solbakken, “Impact of Flow Assurance in the Development of a Deepwater Prospect,” *SPE Annual Technical Conference and Exhibition*. Society of Petroleum Engineers, Anaheim, California, U.S.A., p. 10, 2007.
- [76] P. Zanganeh, S. Ayatollahi, A. Alamdari, A. Zolghadr, H. Dashti, and S. Kord, “Asphaltene Deposition during CO₂ Injection and Pressure Depletion: A Visual Study,” *Energy & Fuels*, vol. 26, no. 2, pp. 1412–1419, Feb. 2012.
- [77] T. Wang, Y. Song, Y. zhao, Y. Liu, and N. Zhu, “Measurement of Immiscible CO₂ Flooding Processes and Permeability Reduction due to Asphaltene Precipitation by X-ray CT Imaging,” *Energy Procedia*, vol. 37, pp. 6920–6927, 2013.
- [78] M. Cao and Y. Gu, “Oil recovery mechanisms and asphaltene precipitation phenomenon in immiscible and miscible CO₂ flooding processes,” *Fuel*, vol. 109, pp. 157–166, 2013.
- [79] L. M. Arciniegas and T. Babadagli, “Quantitative and visual characterization of asphaltenic components of heavy-oil after solvent interaction at different temperatures and pressures,” *Fluid Phase Equilib.*, vol. 366, pp. 74–87, 2014.

Chapter 3- New Insights into Determination of Asphaltene Appearance Point and Evaluation of Asphaltene Inhibitors Based on n-Alkane Titration

3.1 Introduction

As discussed in details within chapter 2, many different techniques have been used for asphaltene onset determination such as Filtration technique[1], acoustic resonance[2], [3], refractive index method[4], light scattering[5], [6], density and viscosity measurements[7]–[9], high-pressure microscopy[10], [11], and indirect method[12]. Some of these conventionally used techniques can only detect asphaltene particles that are at least 0.5 μm in diameter, for asphaltene onset determination[5], [13]–[15]. These methods determine asphaltene precipitates aggregation onset which may not be the precipitation onset, and this may cause inaccurate results for use in other studies and/or selection of inappropriate asphaltene inhibitors. Other techniques like indirect method are not particle size dependent, but they need toluene to be added to the system as a diluent before adding to UV-vis spectroscopy, and this adds costs and time. In order to handle the asphaltene problems, amphiphilic dispersants which consist of polar group (s) have been utilised to reduce the size of the asphaltene particles below the precipitation threshold or delay the onset of aggregation and deposition by polar head group interactions between asphaltene and amphiphiles. The structure of the amphiphilic dispersants typically contain an aliphatic tail attached to a benzene ring with one or two functional or head groups ($-\text{OH}$, $-\text{SO}_3\text{H}$, and $-\text{O}-$)[16] which could inhibit the asphaltene nanoaggregates to form the asphaltene precipitates mainly through hydrogen bonding, ion-pairing and π - π interactions with heteroatoms and aromatic rings in asphaltene molecules.

Although amphiphilic asphaltene inhibitors could be considered as a part of the solution, lack of proven techniques for validation and evaluation of the utilised amphiphiles is the other side of the issue. Many of previous studies were conducted in conditions where asphaltene precipitates are already aggregated, and very few have targeted asphaltene particles before or near precipitation and flocculation states. The Inhibition of asphaltenes

in aliphatic solvents employing different oil-soluble amphiphiles containing long-chain alkylbenzene, alkyl alcohol, alkylamine, and *p*-alkylphenol (C_n phol) was investigated by Gonzalez et al[17]. Chang and Fogler studied the capabilities of a various alkylbenzene derived amphiphiles for stabilisation of asphaltenes in apolar alkane solvents[18]. The results from their study reveal that C_n phol and *p*-alkylbenzene sulfonic acid (C_n bsa) are efficient amphiphiles in peptisation of asphaltenes in alkane solvents. Leo'n et al[19] also studied the adsorption behaviour of a set of alkylbenzene derived amphiphiles on asphaltenes surfaces.

In order to formulate and generate a new asphaltene inhibitor chemistry, the optimisation of functional groups in its structure which interacts with asphaltene surface active groups should be considered for different crude oils. One of the main objectives of this study is to provide novel insights into both the mechanism of asphaltene precipitation inhibition in oil/heptane solutions and the influence of different inhibitors/amphiphiles on the stabilisation of asphaltene nanoaggregates. In this regard, an experimental method which is named hybrid technique herein, is employed for evaluation of the chemicals. By employing this approach, the inhibitors used in this study and all other inhibitors in the literature can be evaluated based on their capabilities to delay the precipitation onset.

This chapter presents capability of the hybrid technique for determination of asphaltene precipitation onset and also evaluation of asphaltene inhibitors, which is based on the integration of applying artificial gravimetric force and Fourier Transform Infrared (FTIR) spectroscopy. The effects of different chemicals including phthalic acid, two amphiphiles of nonylphenol (NP), and Dodecylbenzene sulfonic acid (DDBSA) and two commercial inhibitors on asphaltene aggregation have also been studied besides proposing their related interaction mechanisms which lead to asphaltene aggregation and deposition inhibition. It should be mentioned that the amphiphiles and dispersants currently used in this study have been chosen based on their surface active and functional groups to investigate the influence of these groups on asphaltene nanoaggregates stabilisation in crude oils through different asphaltene dispersion mechanisms.

3.2 Experimental Section

3.2.1 Materials

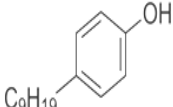
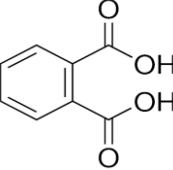
Experiments were conducted at ambient conditions on one type crude oil which is called “AC”. Table 3.1 shows the properties of crude oil AC from the North Sea.

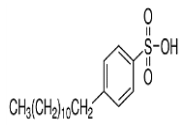
Table 3. 1. Properties of Crude Oil “AC” utilised in this study

Petroleum Fluid	f (g.g ⁻¹) (n-C ₇ asphaltene content)	ρ_o (g.mL ⁻¹)	MW _o (g.mol ⁻¹)	μ_o (cP)
AC	0.0435	0.844	242	15.51

Two commercial inhibitors AI. 3 and 4, nonylphenol ($\geq 99\%$) and HPLC-grade dodecylbenzene sulfonic acid (DDBSA) ($\geq 95\%$ & $\leq 2\%$ H₂SO₄) both as amphiphilic inhibitors, phthalic acid ($\geq 99.5\%$), HPLC-grade anhydrous n-heptane ($> 99\%$), anhydrous toluene ($> 99.8\%$), HPLC grade acetone ($\geq 99.9\%$) and ethanol ($\geq 99.8\%$) all from Sigma-Aldrich were used in this study. Some physical properties of utilised asphaltene inhibitors are presented in Table 3.2.

Table 3. 2. Properties of non-commercial asphaltene inhibitors used in this study

Inhibitor	Molecular Formula	Density (gr/cm ³) @ 25 °C	Molecular Weight (gr/mol)	Solubility in Water (gr/l) @ 25 °C	Chemical Structure
Nonylphenol	C ₁₅ H ₂₄ O	0.952	220.35	5.45E-3	
Phthalic acid	C ₈ H ₆ O ₄	1.592	166.14	5.7	

Dodecylbenzenesulfonic acid (DDBSA)	C ₁₈ H ₃₀ O ₃ S	1.06	326.49	N/A	
--	--	------	--------	-----	---

3.2.2 Hybrid Technique

Firstly, the crude oil samples were heated up to 70 °C before each set of tests. Then the glass centrifuge tubes were filled with solutions comprising various ratios of n-heptane (used as an asphaltene precipitant) and test fluid from 15 to 70 Vol % n-heptane. The centrifuge tubes were shaken by hand to mix the solution well before being left to age for 1 hr, 1 day, and 1 week. After ageing, a small amount of crude oil was added to each test tube to remove the effect of ageing time on asphaltene precipitation state. Then, the prepared solutions were centrifuged by Heraeus Megafuge. In order to obtain appropriate gravitational force which can balance both the buoyancy and drag forces on the asphaltene particles and settle the asphaltenes in the oil/n-heptane solutions, the Stokes' Law is used which is defined as $v_e = d^2 \delta \rho g / 18 \mu$, where v_e is the velocity of the colloidal asphaltene particle in gravitational field of g , d is the average asphaltene particle diameter, $\Delta \rho$ is the discrete to continuous phase density contrast and μ is the liquid viscosity[20]. Stokes' Law was shown to be suitable for different asphaltene precipitates sizes and these results were confirmed with asphaltene particle size determination from ESEM micrographs of the asphaltene precipitates as presented in Figure 3.1. It seems that the precipitated asphaltene has a porous structure with the size range of 100-700 nm depending on the crude oil used which is made by asphaltene nanoaggregates.

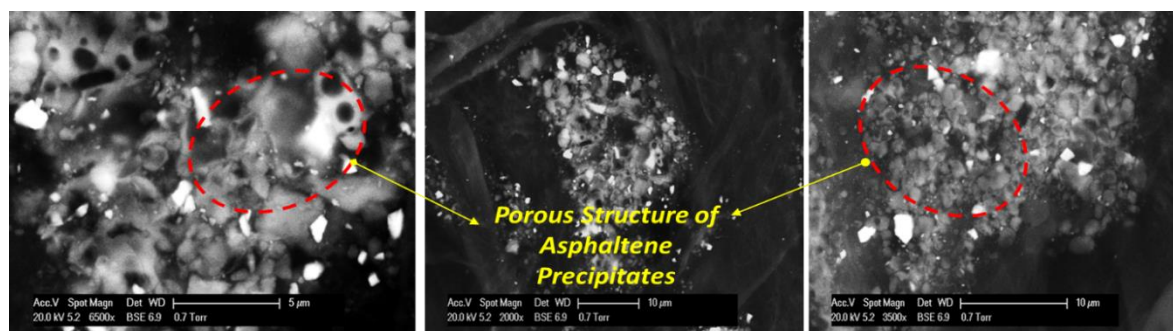


Figure 3. 1. ESEM micrographs of asphaltene precipitates

Based on the ESEM micrographs, the asphaltene nanoaggregates with a size of 100 nm and above (when the asphaltene precipitation state starts) are separated during the centrifugation step of hybrid technique with 4300 RCF and duration of 35 min. Hence only stable asphaltene particles smaller than that particular range remained in the supernatant solution, making the hybrid technique more sensitive than other conventional methods. After this step, one mL of the supernatant fluid was removed by syringe and directly put in Fourier transform infrared (FTIR) spectrometer without adding any diluent. Then, the transmittance number at specific wavelengths range, which represents the functional groups of heteroatoms in asphaltene molecule, was measured by an FTIR-4000 Series (JASCO Edition) spectrometer. The values of transmittance versus different volume percent of n-heptane in the crude oil/h-heptane solution were plotted. A sudden change in transmittance number corresponds to the volume percent of n-heptane at the Asphaltene Appearance Point (AAP). In this work, the AAP for each specific technique represents the minimum amount of n-heptane that should be added to crude oil to cause asphaltene precipitation that is discernible by the utilised technique. Figure 3.2 shows the schematic diagram of the procedure of hybrid technique used in this study.

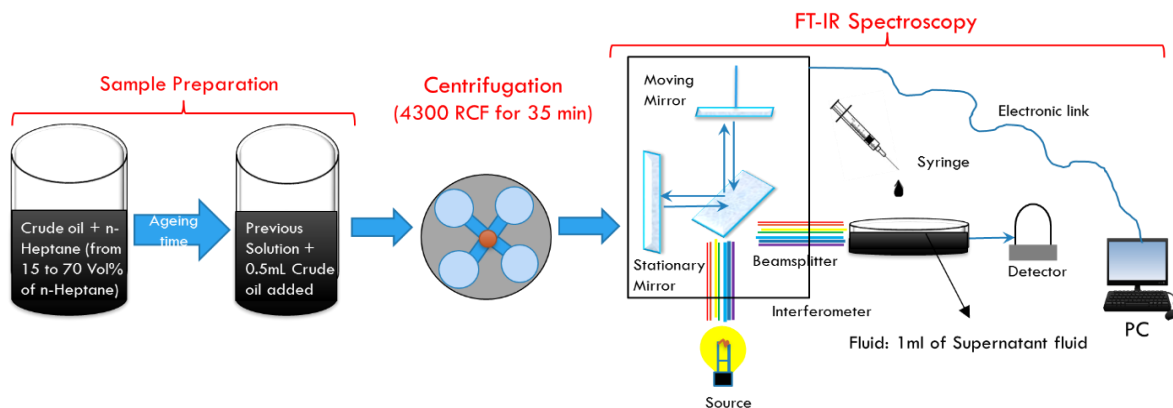


Figure 3. 2. Procedure of Hybrid Technique

3.2.3 Refractive Index (RI) Measurements

Refractive index (RI) measurement by refractometer-model J457 made by Rudolph research was used for asphaltene precipitation investigations in this study. This technique has smart measure™ which improves results with live measurement and sample load well monitoring., dual electronic temperature control from 10 °C to 110 °C or 10 °C to 120 °C,

Refractive Index ± 0.00002 , BRIX ± 0.01 accuracy in the range of refractive index 1.26 – 1.72, BRIX 0 – 100. It was utilised to have a comparative study for asphaltene appearance point (AAP) detection between the hybrid technique and RI measurements. Firstly, the measuring prism should be retained clean. The instrument should also be calibrated against a refractive index standard provided by Rudolph research at 25°C and 589 nm wavelength. The temperature control of the liquid being tested, and the cleanliness of the prism has to be repeatedly checked. The first step for this method is the titration of crude oil with n-heptane. Then different mixtures of crude oil/n-heptane were prepared in the test tubes with various concentrations of n-heptane ranging from 0 to 100 Vol%. The vigorous shaking of the samples inside the test tubes is also needed to inhibit premature asphaltene precipitation because of poor mixing. The n-heptane titration was conducted at ambient condition. After the titration completion and particular ageing time for 1 hr, the refractive index of each one of the samples was determined at 25 °C and 1 atm using mentioned calibrated and temperature-controlled instrument.

3.2.4 Near Infrared (NIR) Spectroscopy and Optical Microscopy

The mixtures of crude oil and n-heptane were prepared following the same procedure that was expressed in section 2.3. Mixtures of different ratios of crude oil and n-heptane were prepared ranging from 0 to 70 vol% of n-heptane. The test tubes were rigorously shaken by hand and the mixtures were transferred to 7 mL UV-vis-NIR spectrophotometer test tube. The prepared samples were left to be undisturbed for the specified 1 hr ageing time. In this case the ageing time is the period of time apportioned between crude oil/n-heptane mixture preparation and the measurement of the NIR transmittance. Then, the NIR transmittance was determined utilising a Hitachi UV-Vis-NIR spectrophotometer Model U-3010. The transmittance numbers were determined for wavelengths ranging between 1000 and 1300 nm. Since the signal is not saturated, it was identified that different wave lengths in this range can be employed to detect the asphaltene appearance point. The transmittance numbers were then normalized utilising the transmittance of the crude oil as the reference. The normalized light intensity/transmittance values were plotted as a function of the volume fraction of n-heptane added to the mixture. Asphaltene appearance points were measured by the reduction in the normalized light intensity due to asphaltene aggregates

formation that disturb the route of light from its source to detector. The first deviation from the linear trend indicated the precipitation of asphaltenes. The samples were also observed under a state-of-the-art petrographic microscope with a 50× magnification lens for determination of asphaltene precipitation.

3.3 RESULTS AND DISCUSSION

3.3.1 Asphaltene Appearance Point (AAP) Detection by the Hybrid Technique

Asphaltene precipitation from crude oil AC was investigated by n-heptane titration with different ageing times of 1 hr, 1d ay, and 1 week using the hybrid technique. By monitoring the changes in transmittance numbers (%) for supernatant fluids of different crude oil/n-heptane mixtures after centrifugation, alterations in stable asphaltene particles concentration can be detected. Since the dispersed asphaltene particles scatter the light through FTIR spectrometer, the transmittance number was increased in samples which were losing asphaltenes and reduced in rest of the samples which were gaining asphaltene particles. Figure 3.3 presents the FTIR spectrum of supernatant fluids of samples with different concentrations of n-heptane added to the crude oil.

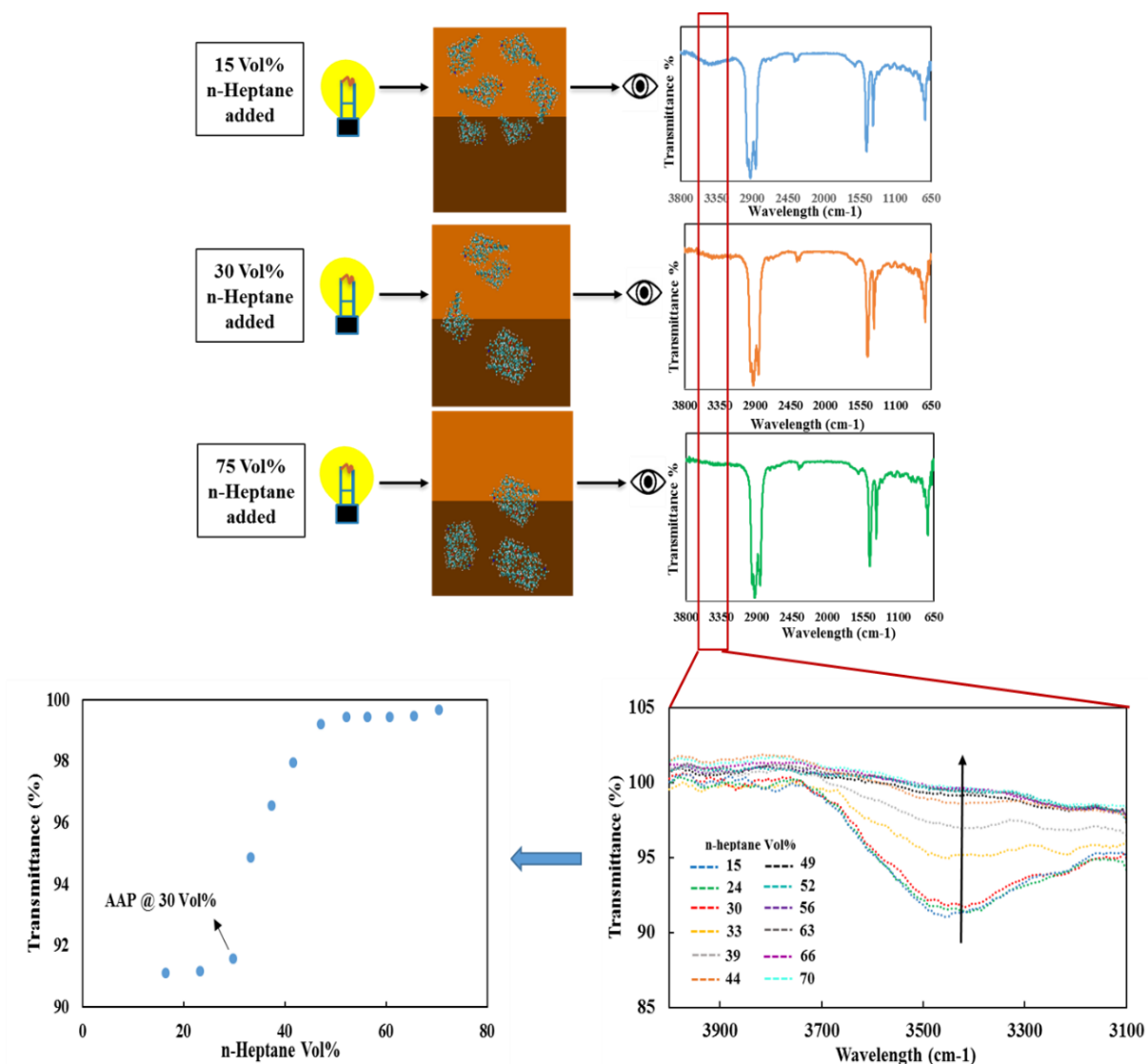


Figure 3. 3. FTIR spectra of supernatant fluids in various crude oil/n-heptane mixtures.

The spectra presented is distributed through different regions which represent each functional group in the crude oil. The intensity of the band at 780 cm^{-1} corresponds to the CH_2 (ethyl group) which was negligibly small in all spectra. Generally, the absorption bands observed between 900 cm^{-1} and 700 cm^{-1} are mainly due to different aromatic C-H bending deformations. The absorption band around the 870 cm^{-1} represents the highly substituted aromatic structure. As can be observed in Figure 3.3, there is a change in intensity of the C=C aromatic stretching vibration at 1614 cm^{-1} and $-\text{CH}_3$ bending vibration at 1377 cm^{-1} . A significant variation in absorption at 1461 cm^{-1} which represents $-\text{CH}_2$ bending vibration was seen with high intensity. A weak shoulder band at around the

1715 cm^{-1} corresponds to the stretching of carbonyl, carboxylic or derivative groups in the solution. The absorption bands in the spectral range of 2955-2850 cm^{-1} represent the stretching vibration of aliphatic $-\text{CH}_3$ and $-\text{CH}_2$ groups. The absorbance band in the spectral range of 3500-3300 cm^{-1} , centred around 3448 cm^{-1} , is assigned to the N-H/O-H groups in the pyrrole and carboxylic/phenol active groups of asphaltene molecule. Thus 3448 cm^{-1} was for monitoring the change in transmittance number due to alteration in asphaltene concentration in the supernatant fluid.

Figure 3.4 shows the measured transmittance numbers (@ 3448 cm^{-1}) of one mL of supernatant fluids of different crude oil/n-heptane mixtures after applying a centrifugal force of 4300 RCF for 35 min versus concentration of n-heptane for various ageing times.

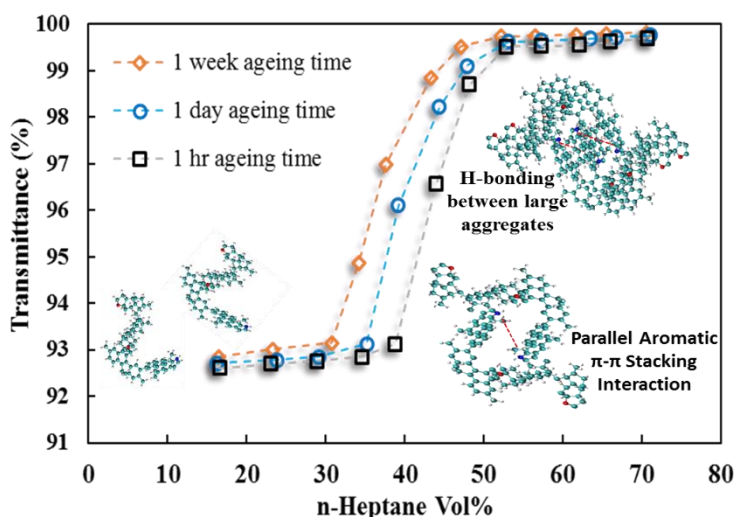


Figure 3. 4. AAP detection by hybrid technique for the real crude oil titrated with n-heptane for different ageing times of 1hr, 1day, and 1week

As can be seen from Figure 3.4, at early stages of the n-heptane injection dimerization of asphaltene molecules happened through π - π stacking interactions between aromatic cores. Due to the appearance of H-bonding from FTIR spectra after asphaltene precipitation onset, it can be proposed that the main mechanism after dimerization is the aggregation of larger asphaltene particles through H-bonding actually when aromatic-aromatic interaction becomes more difficult in larger nanoaggregates.

The last point in the linear trend before a sudden deviation in transmittance number corresponds to the Asphaltene Appearance Point (AAP). For the crude oil/n-heptane

mixture with 1 hr ageing time, the measured transmittance number from 15 to 25 Vol% of n-heptane shows a linear trend, while there is a deviation from the linear trend at around 30 Vol% which represents the asphaltene appearance point. As can be seen from Figure 3.4, the volume percentage of n-heptane that should be added to the crude oil to detect the asphaltene appearance point alters based on the ageing times. As the ageing time is increased from 1 hr to 1 day, the transmittance number deviates at lower n-heptane concentration, and the AAP changes from about 40 to 35 Vol% of n-heptane. The average standard deviation (ASD) for the AAP detection by the hybrid technique is 2.07, 2.31 and 2.75% for 1 hr, 1 day and 1 week ageing times respectively. A similar effect of ageing times on asphaltene precipitation have also been reported in the literature[12], [21]. They investigated the effect of ageing time on n-heptane induced asphaltene precipitation. It has been shown that the necessary time to detect the asphaltene precipitation onset can differ from 1 hr to 1 month based on the concentration of normal alkane. The effect of ageing time on AAP shifting is not related to the centrifugal force in the hybrid technique since it is entirely linked to the thermodynamical equilibrium of asphaltene precipitants in the system. Because of an induced compositional gradient, the thermodynamic equilibrium of the crude oil/n-heptane system is no longer valid, and the compositional gradient should be considered in the determination of asphaltene appearance point accordingly. Therefore, by utilising the hybrid technique and adding a small amount of crude oil to the crude oil/n-heptane mixture after particular ageing time, insignificant asphaltene compositional gradient is reached and the mentioned thermodynamic equilibrium is obtained. As a result, the asphaltene appearance points converge towards the same value, which is the real AAP without the effect of ageing time. Figure 3.5 shows the results after removing this effect on AAP detection by the hybrid technique and accumulated asphaltene aggregates at the bottom of the test tubes after centrifugation for different stages.

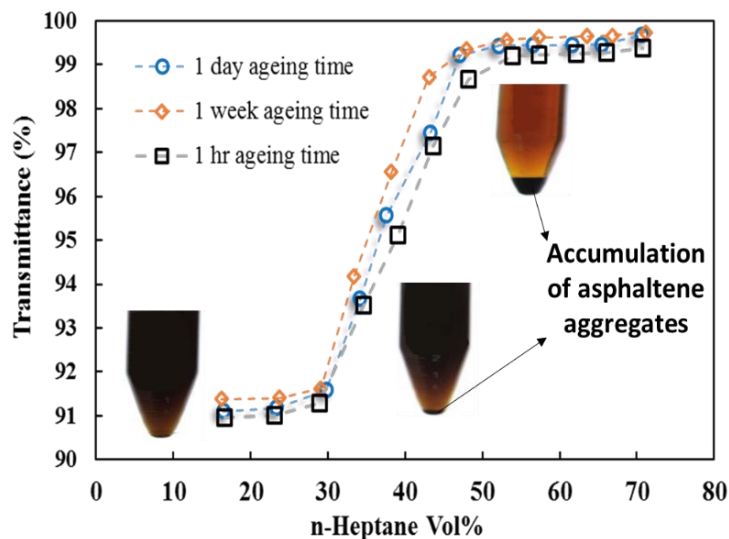


Figure 3. 5. AAP detection by hybrid technique for the real crude oil titrated with n-heptane after removing the effect of ageing time

At low n-heptane concentrations which cause true molecular asphaltene solutions in crude oil (not aggregated asphaltenes), there are no sediments of the precipitated asphaltenes in the solution at the bottom of the tube. At high concentrations of n-heptane, the asphaltene nanoaggregates are accumulated at the bottom of the test tube for different ageing times. Figure 3.5 shows some growth of asphaltene accumulation at 30-40 Vol% n-heptane and a significant increase at 55 Vol% n-heptane. As it can be seen the last points in the linear trend, which represents the AAP, are the same in the value of about 30.67 Vol% for all the 1 hr, 1 day and 1 week ageing times, and the ageing time effect has been removed by the new proposed procedure. The ASD for this set of tests is 2.86, 1.94 and 3.05% for 1 hr, 1 day, and 1week ageing times, respectively.

3.3.2 Hybrid Technique vs. Refractive Index (RI) and Optical Microscopy Measurements

To prove the advantages of the hybrid technique over other techniques, refractive index, near infrared and optical microscopy measurements were used to detect the asphaltene appearance point in crude oil AC/n-heptane system with 1 hr ageing time at ambient condition.

The refractive index function versus concentration of n-heptane was plotted. Refractive index function ($RIfn$) is:

$$RIfn = \frac{(n^2 - 1)}{(n^2 + 2)} \quad (3.1)$$

Where n is refractive index. Figure 3.6 shows the almost linear relationship between the refractive index function and volume percentage of n-heptane from 0 to 40 Vol%.

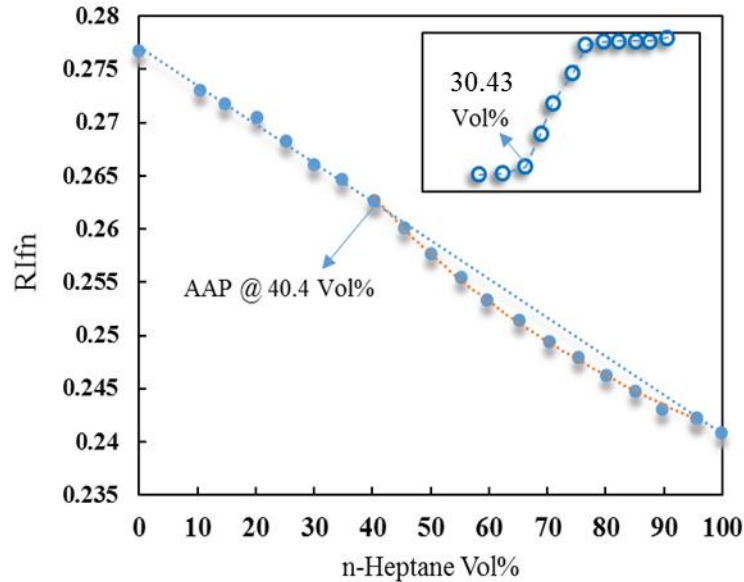


Figure 3. 6. AAP detection by refractive index measurements with ageing time of 1 hr.

When the asphaltene particles start to precipitate out from the solution, which can be detectable by refractometer, the refractive index function no longer follows the linear behaviour and a gradual deviation from the linear relationship is observed as shown in Figure 3.6. This difference in the refractive index function can be illustrated by the fact that as the asphaltene molecules stick together and precipitate out of the solution, so they no longer contribute to the refractive index of the solution. Since the asphaltene precipitates are very refractory substances, lower refractive index of the remaining mixture causes the gradual deviation of the refractive index function. Buckley[4] suggested that at the asphaltene precipitation onset point there is a sharp linear drop in the refractive index function. However, Wattana et al.[21] concluded that the asphaltenes precipitation is a gradual process, as shown in the curvature of the refractive index function after the initial precipitation occurred. If the asphaltenes precipitated together, then a sudden large change

in the refractive index could be observed, and the refractive index function behaviour would again be linear.

In this study, the AAP detected by refractive index measurement is 40.4 Vol% of n-heptane, as shown in Figure 3.6, while the AAP obtained by the hybrid technique is 30.43 Vol% at the same conditions. The ASD is 0.75% for this set of tests by refractometer. A comparison of the hybrid technique and RI measurements illustrates that for the same set of mixtures and the same ageing time, the hybrid technique detects the AAP at a lower volume percentage of n-heptane than the RI measurement. It means that the hybrid technique is more sensitive in detecting asphaltene particles in precipitation state than the traditional approaches. This is due to the lower minimum value of the asphaltene particle sizes which is detectable with hybrid technique than with RI method.

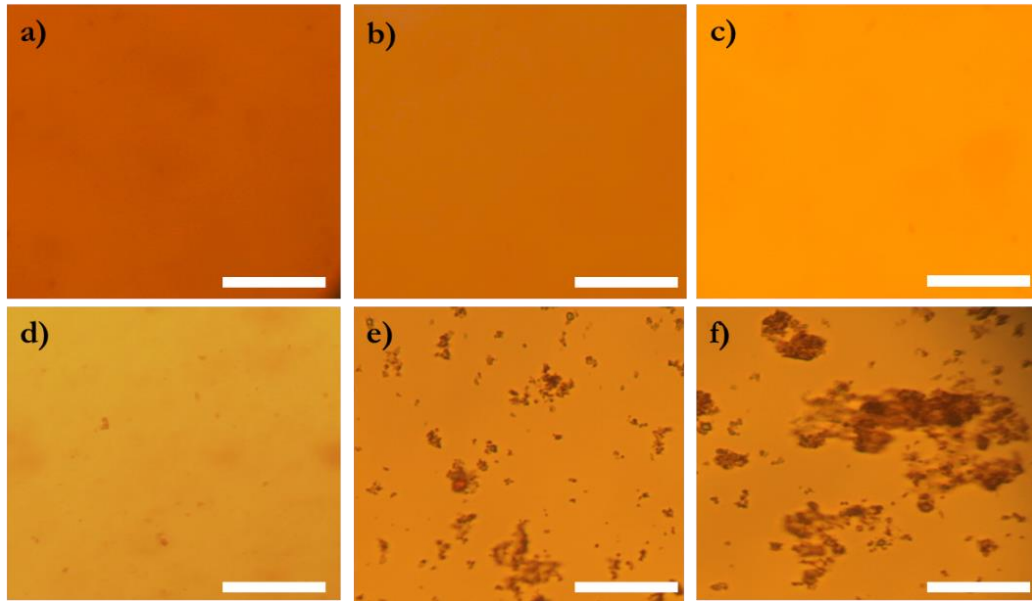


Figure 3. 7. The micrographs of crude oil diluted with different concentrations of n-heptane; a) 0 vol% of n-C₇, b) 35 vol% of n-C₇, c) 39 vol% of n-C₇, d) 41 vol% of n-C₇, e) 45 vol% of n-C₇, and f) 55 vol% of n-C₇ aged for 1 hr for the detection of asphaltene appearance point. The white scale bar in pictures is 100 μ m.

Micrographs of various crude oil/n-heptane mixtures have been presented in Figure 3.7. It depicts that the detection of asphaltene appearance point happens ~41 vol % of n-heptane and the results of RI measurements and direct microscopy technique are in good agreement.

3.3.3 Evaluation of Asphaltene Inhibitors and Proposed Mechanisms

The hybrid technique, NIR spectroscopy, and RI measurements have been used in this work to evaluate the effectiveness of asphaltene inhibitors on asphaltene precipitation at ambient and condition. The blend of crude oil AC and different concentrations of n-heptane were prepared in the centrifuge test tubes following the same procedure that was explained in previous sections. Then the solutions were treated with NP, DDBSA, Phthalic acid, two commercial inhibitors AI. 3 and 4 all with dosage of 200 ppm. It is worth noting that the mentioned dosage rate is based on crude oil and the chemical has been added to the crude oil prior to the addition of n-Heptane. The test tubes were vigorously shaken by hand and left undisturbed for one hour as ageing time. The rest steps of the hybrid technique, NIR and IR based methods and the corresponding results analysis are following the same procedures as mentioned before in previous sections.

The inhibitor effectiveness on asphaltene precipitation inhibition was investigated by monitoring the asphaltene appearance point changes due to presence of different inhibitors. Figure 3.8 presents the AAP shift for all inhibitors using the crude oil AC. The intersection point between the two trend lines which were drawn before and after the detection point represents the volume percentage of n-heptane at the asphaltene precipitation onset.

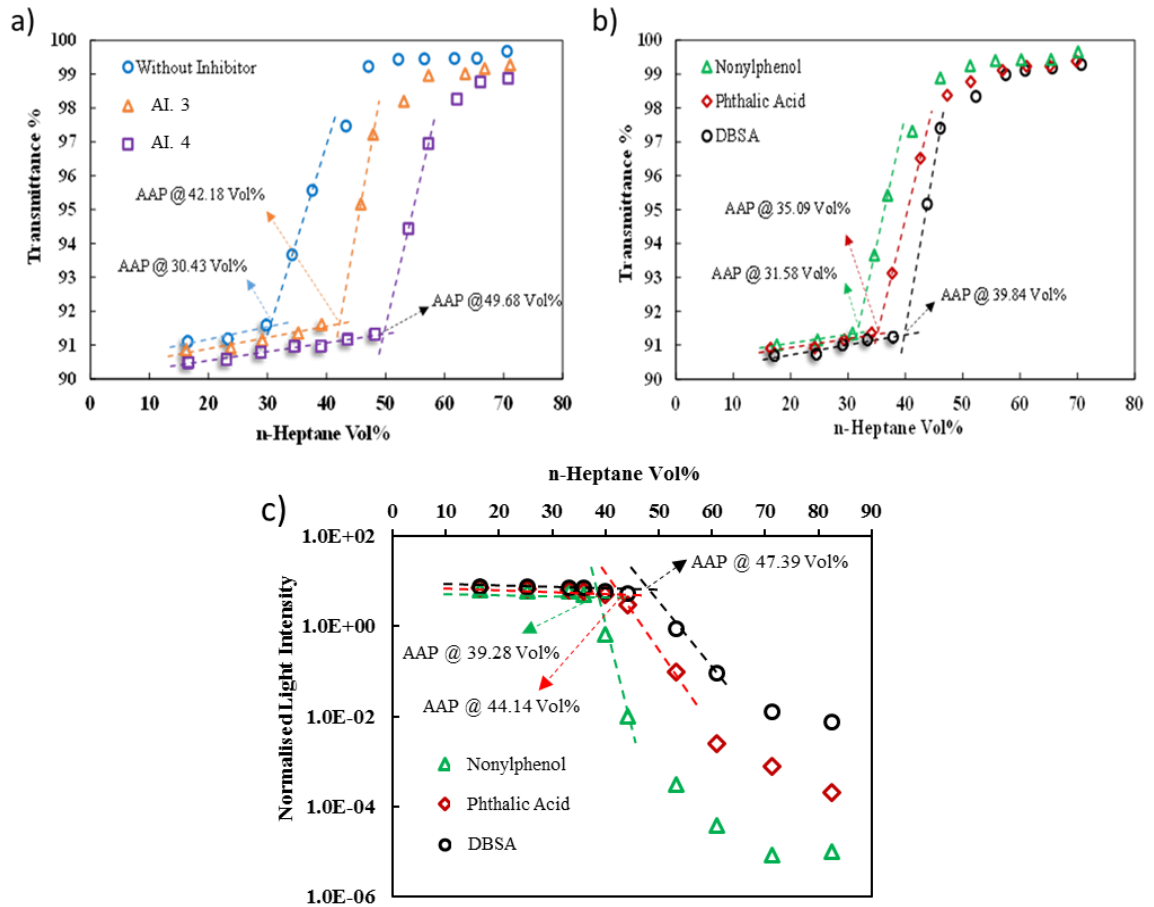


Figure 3. 8. a) Effect of two commercial inhibitors AI. 3 and 4 with concentration of 200 ppm on AAP obtained by hybrid technique. Effect of nonylphenol, Dodecylbenzene sulfonic acid (DDBSA), and phthalic acid all with concentration of 200 ppm on AAP using b) Hybrid technique, and c) NIR spectroscopy.

As can be observed, based upon AAP, the AI. 4 is the best inhibitor and nonylphenol is the weakest inhibitor. Results of these tests show that the AI. 4 shifts the AAP from 30.43 to 49.68 Vol% of n-heptane. Among utilised amphiphilic inhibitors DDBSA, with shifting the AAP to 39.84 Vol%, has the best ability to inhibit asphaltene precipitation followed by phthalic acid and NP. The commercial inhibitor shows better performance than all non-commercial inhibitors with shifting the AAP to 42.18 Vol% of n-heptane. The ASD for detection of asphaltene appearance point obtained by the hybrid technique is 1.63%, 1.57%, 2.05%, 2.24% and 2.51% for the AI. 3, AI. 4, DDBSA, Phthalic acid, and NP, respectively.

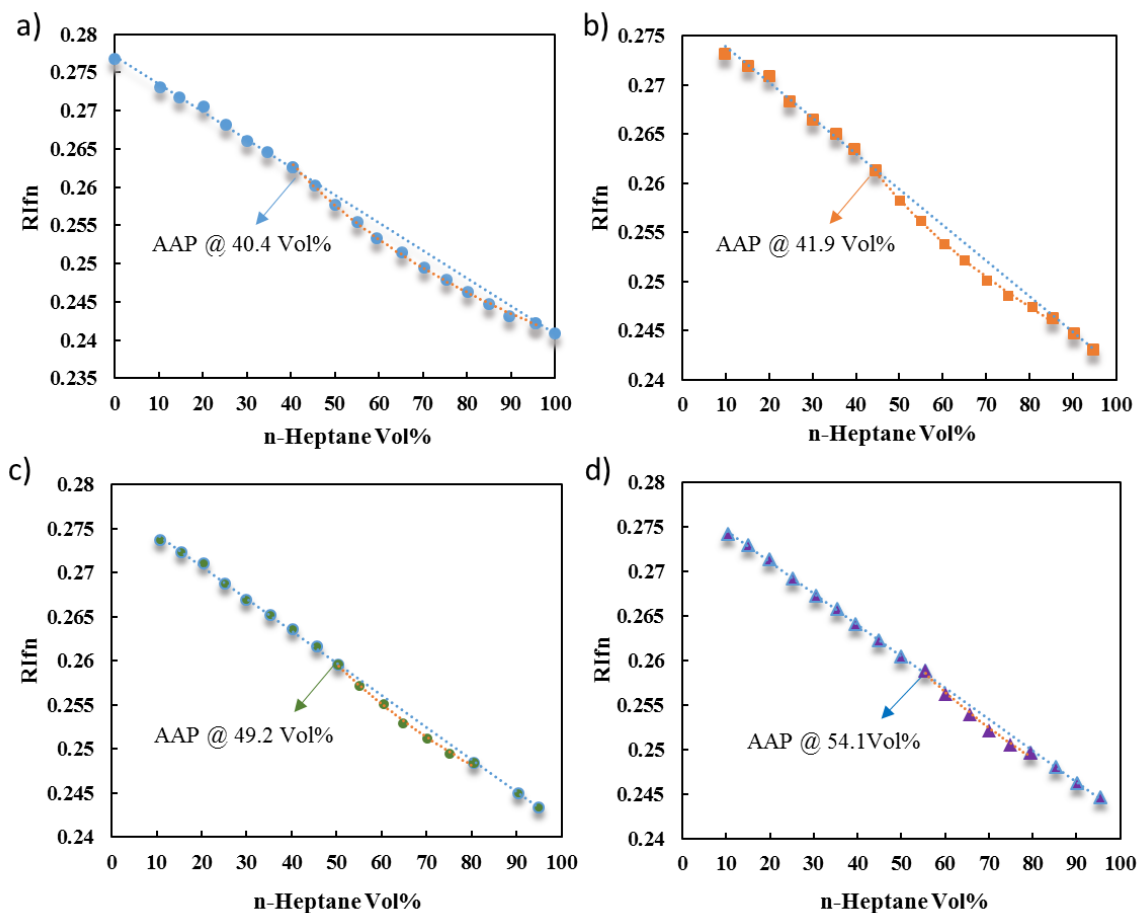


Figure 3. 9. Determination of AAP using refractive index measurements for different crude oil/inhibitors mixtures, a) blank oil, b) DDBSA, c) AI. 3, and d) AI. 4 all with inhibitor concentration of 200 ppm for ageing time of 1hr.

Figure 3.9 shows the results of AAP monitoring using refractive index measurement with/our presence of 200 ppm DDBSA, AI. 3 and 4. The results clearly have a good agreement with hybrid and NIR spectroscopy techniques. The ranking of inhibitors at given concentration based on their impacts on making a delay in AAP is as follows: AI. 4 > AI. 3 > DDBSA. The ASD for detection of asphaltene appearance point attained by RI measurement technique is 1.15%, 1.69%, and 1.98% for the DDBSA, AI. 3, and AI. 4, respectively.

Understanding of the mechanisms behind the inhibition of asphaltene precipitation is required to find out the reasons behind the mentioned trend. As a general point of view on asphaltene precipitation inhibition mechanism, it is believed that there are free inhibitors

monomers after adding to the crude oil solutions which can interact with active sites of asphaltene molecules (e.g. carboxylic, sulfoxide, pyridine, phenol, thiophene and pyrrole) and cause stabilisation and suspension of asphaltene particles in the solution. Previous studies claimed that both hydrogen bonding and π - π interactions could be occurring between asphaltene and the inhibitor molecules. Based on the investigation of how various amphiphiles interact with asphaltene molecules, it has been understood that the stabilisation of the asphaltene particles relies on the head groups of amphiphiles. It has also been found that the amphiphiles which consist of basic head groups (e.g. $-\text{NH}_2$) have the weakest adsorption on the asphaltene surfaces among other utilised compounds [18], [22]–[24].

As mentioned before, one of the advantages of the hybrid technique over other techniques for evaluation of asphaltene inhibitors is that it allows us to find the possible interactions between asphaltene and inhibitors molecules and suggest the proposed mechanism of asphaltene precipitation inhibition. The acid-base interaction between asphaltenes and DDBSA was characterised using FTIR spectroscopy. Typically, the SO-H stretching band from DDBSA molecules causes a remarkable change in transmittance number in its wavelength range. Hence, a change of DDBSA's SO-H stretching band in the presence of asphaltene nanoaggregates could be because of the breakage of DDBSA's SO-H bond by the transition of the proton of its sulfonic acid (SO_3H) group to the corresponding conjugate basic active groups on asphaltene molecules. The FTIR spectrum related to the supernatant solution of crude oil/n-heptane mixture with the presence of different inhibitors is presented in Figure 3.10.

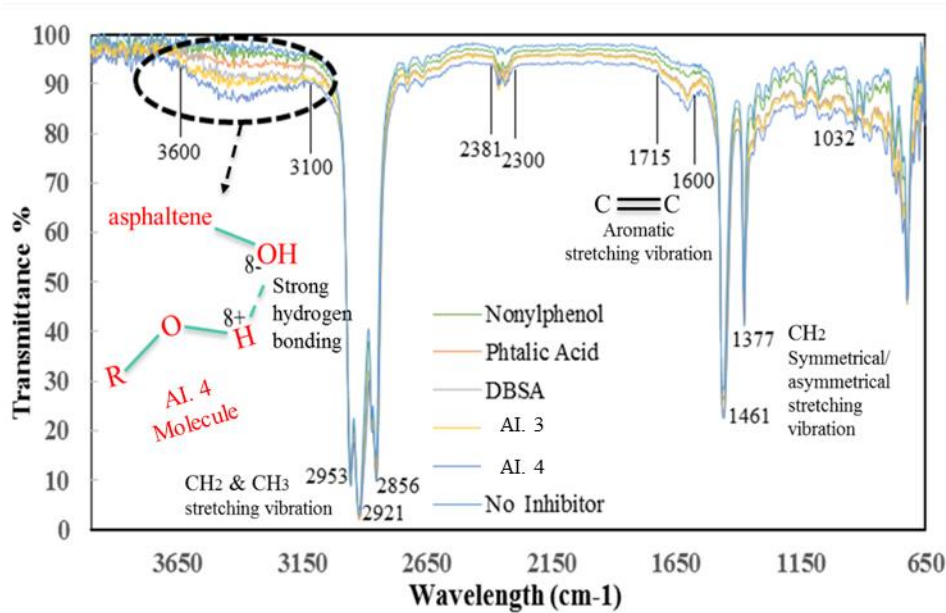
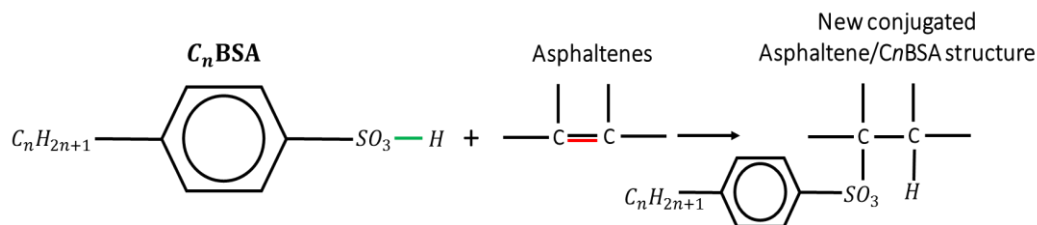


Figure 3. 10.. FTIR spectra of supernatant fluid of crude oil/n-heptane system in presence of different inhibitors- Possible interactions between Asphaltene and one of the commercial inhibitor molecules (AI. 4).

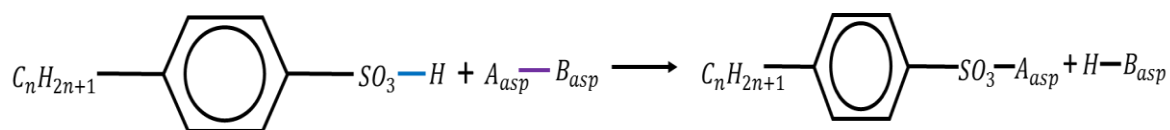
As can be observed the absorbance bands in various spectral ranges represent particular types of groups that are present in the system. The wide broad band centered around 3448 cm^{-1} indicated the presence of the H-bonding creation between asphaltene/DDBSA molecules. The H-bonding between the DDBSA's S=O group and the asphaltene's carboxylic, phenol and pyrrole groups could be considered for the appearance of this band.

The π -electrons exists in the asphaltenes highly electronic conjugated structures, and the electrophilic addition interaction between C_n BSA and the π -electrons of asphaltenes has been proposed[22], [25]. Chang and Fogler[18] proposed two different mechanisms for this electrophilic addition. The first mechanism is:



Based on this mechanism, the C_n BSA molecules could react with the asphaltenes π -electrons (as the Lewis base) started by the C_n BSA's $\text{SO}_3\text{-H}$ bond and enclosed with the

association of the asphaltenes and the *P*-dodecylbenzene sulfonate group to create a larger complex conjugated structure. The other possible *C_n*BSA/asphaltene interaction mechanism is the acid-base exchange interaction of *C_n*BSA with the basic and acidic sides of asphaltene molecules which are defined as *B_{asp}* and *A_{asp}*, respectively. This mechanism is expressed by:



The reaction products that are $C_nH_{2n+1}-\text{C}_6\text{H}_4-\text{SO}_3^-A_{asp}$ and H^+-B_{asp} will associate together in apolar medium through acid-base interactions.

This study suggests novel insights into the mechanism of asphaltene precipitation inhibition caused by DDBSA molecules. We believe that the DDBSA molecules could protonate the heteroatoms in asphaltenes carboxylic, sulfoxide, phenol, pyridine and pyrrole active groups, and its long alkyl chain tail causes significant solvation. A very strong acid-base interaction is established through ion-pair interaction between the protonated asphaltene (AH^+) and sulfonate ion ($DDBS^-$). On the other hand, the wide broad band centred around 3448 cm^{-1} indicated the presence of the H-bonding formation between asphaltene and DDBSA molecules. The H-bonding between the DDBSA's S=O group and the asphaltene's pyridine/pyrrole and phenol/carboxylic groups is formed due to the appearance of this band. Therefore, we have two different interactions of ion-pair and H-bonding between these two molecules which could be occurred simultaneously.

The decrease in the FTIR transmittance number of asphaltenes in the presence of DDBSA and significant performance of DDBSA in asphaltene precipitation inhibition suggest that after the addressed reaction above the asphaltenes and DDBSA molecules can associate into a bigger electronic complex structure than that of asphaltene/DDBSA themselves. Since asphaltenes have a vast range of structures, the proposed complex interaction mechanism herein might be valid only when the $-N/O-H$ groups bonded to a protonated active group in an asphaltene molecule.

The phthalic acid is another chemical that is used as an asphaltene inhibitor in this study. Since it has two $-OH$ functional groups on its benzoic ring, it can interact with asphaltene

nanoaggregates through both active sites. Based on the FTIR and the hybrid technique results, it can be seen that the H-bonding between two –OH groups of phthalic acid and –N/O-H groups (pyridine/phenol in this case) in asphaltenes is its main mechanism of asphaltene precipitation inhibition.

Therefore, phthalic acid can confine the asphaltene nanoaggregates to be clustered. The acid-base interaction is occurred between asphaltenes and NP's amphiphilic molecules through H-bonding of NP's hydroxyl group and pyridine/phenol active sites of the asphaltene. The Phenol's aromatic benzene group can delocalize the electrons bonded between the oxygen and hydrogen of the hydroxyl group to make the nonylphenol more acidic than the usual alcohol. The NP-asphaltene H-bonding interactions was studied through monitoring of the transmittance number of the bonded OH stretching band in the range of 3100-3600 cm^{-1} . It can be observed that NP interacts at the periphery of the asphaltene nanoaggregates through H-bonding with –N/O-H groups of asphaltenes.

At high concentrations of NP, it is expected that NP molecules can saturate all the H-bonding sites of asphaltene nanoaggregates and make them suspend in the solution with the barrier created around the asphaltenes through H-bonding.

The best performance of AI. 4 is because of its high polarity, well designed and condensed aromatic structure, which can act like natural resin molecules around the asphaltene molecules and make them stable in the crude oil. The intensive absorbance at the broad band centred around 3500 cm^{-1} is due to very strong H-bonding firmly stabilised by π - π stacking of AI. 4's benzoic rings with asphaltene's aromatic cores.

3.4 Conclusions

In this study, the hybrid technique has been developed and examined for the determination of asphaltene appearance point and evaluation of asphaltene inhibitors. The effectiveness of two commercial inhibitors, phthalic acid and the alkylbenzene-derived amphiphiles including nonylphenol (NP) and dodecylbenzene sulfonic acid (DDBSA) as asphaltene inhibitors were studied. The effects of the structures of these chemicals on their capabilities to hinder the asphaltene precipitation were also investigated and possible mechanisms of

asphaltene precipitation inhibition were proposed. On the basis of these investigations, the following conclusions can be drawn:

1. It has been found that the hybrid technique has some key benefits over other methods. The hybrid technique is more sensitive and accurate in detection of asphaltene appearance point (AAP) compared to RI measurements, optical microscopy and NIR spectroscopy. It should be mentioned that the hybrid technique can also detect the possible molecular interactions between asphaltene and inhibitor molecules. It can be utilised for various crude oils with different values of asphaltene contents.
2. Based on the results obtained from hybrid technique, the inhibition abilities of the compounds increase in the order of NP (phenol group) < Phthalic acid (double hydroxyl group) < DDBSA (sulfonic acid group) \leq AI. 3 < AI. 4, which indicates that coupled double H-bonding and π - π stacking between asphaltene-inhibitor aromatic cores could be the strongest and the most stable interaction for asphaltene precipitation inhibition that is the AI. 4's inhibition mechanism.
3. Possible mechanisms of asphaltene precipitation inhibition by the phthalic acid and DDBSA are proposed. The mechanism proposed by Fogler and Chang[18] for the peptisation of asphaltenes in apolar alkane solvents also holds for the inhibition of asphaltene precipitation from crude oils by the alkylphenol amphiphiles. The hybrid technique verified that asphaltenes can form acid-base interactions with nonylphenol through H-bonding. We proposed that the NP can saturate the H-bonding acceptor/donor sides of asphaltenes in high NP concentrations. The decrease of the transmittance number of phthalic acid's O-H stretching band and the increase of the stabilisation of the asphaltenes aggregates suggest one of the asphaltene-phthalic acid interactions can involve an additional H-bonding to the conjugated -N/O-H groups of asphaltenes. The DDBSA molecules can stabilise the asphaltene nanoaggregates through a couple ion-pair-H-bonding interaction with asphaltenes when the -N/O-H groups bonded to a protonated active group.

While it is generally realised that asphaltenes are polydisperse fractions of crude oils, this research study denotes a framework for future investigations utilising different kinds of

inhibitors/dispersants and mixtures of real and/or modelled asphaltene molecules. Further feasibility studies on the application of the hybrid technique and newly formulated asphaltene inhibitors in the industry can also be considered. A detailed study on the effect of pressure and temperature on inhibitor screening is necessary as a future work which is presented in the next chapter (Chapter 4)

3.5 References

- [1] S. Negahban, J. N. M. Bahamaish, N. Joshi, J. Nighswander, and A. K. M. Jamaluddin, "An Experimental Study at an Abu Dhabi Reservoir of Asphaltene Precipitation Caused By Gas Injection," *SPE Prod. Facil.*, vol. 20, no. 02, pp. 115–125, 2005.
- [2] A. Sivaraman, Y. Hu, F. B. Thomas, D. B. Bennion, and A. K. M. Jamaluddin, "Acoustic Resonance: An Emerging Technology to Identify Wax And Asphaltene Precipitation Onset Conditions In Reservoir Fluids," in *Annual Technical Meeting*, 1997.
- [3] A. K. M. Jamaluddin, J. Creek, C. S. Kabir, J. D. McFadden, D. D'Arcuz, M. T. Joseph, N. Joshi, and B. Ross, "A Comparison of Various Laboratory Techniques to Measure Thermodynamic Asphaltene Instability." Society of Petroleum Engineers.
- [4] J. S. Buckley, "Predicting the onset of asphaltene precipitation from refractive index measurements," *Energy and Fuels*, vol. 13, no. 2, pp. 328–332, 1999.
- [5] Y.-F. Hu and T.-M. Guo, "Effect of temperature and molecular weight of n-alkane precipitants on asphaltene precipitation," *Fluid Phase Equilib.*, vol. 192, no. 1–2, pp. 13–25, 2001.
- [6] A. Hammami and M. A. Raines, "Paraffin Deposition From Crude Oils: Comparison of Laboratory Results With Field Data," *SPE J.*, vol. 4, no. 1, pp. 9–18, 1999.
- [7] C. Nicolas, C. Achard, M. M. Rogalski, G. Ekulu, C. Nicolas, C. Achard, and M. M. Rogalski, "Characterization of Aggregation Processes in Crude Oils Using Differential Scanning Calorimetry," *Energy Fuels*, vol. 19, no. 4, pp. 1297–1302, 2005.
- [8] G. Ekulu, P. Magri, and M. Rogalski, "Scanning aggregation phenomena in crude oils with density measurements," *J. Dispers. Sci. Technol.*, vol. 25, no. 3, pp. 321–331, 2004.
- [9] S. EL MOHAMED, F. HARDOUIN, and H. GASPAROUX, "Floculation des produits lourds du pétrole," *J. Chim. Phys.*, vol. 85, no. 1, pp. 135–144.

- [10] a. Hirschberg, L. N. J. DeJong, B. a. Schipper, and J. G. Meijer, “Influence of Temperature and Pressure on Asphaltene Flocculation,” *Soc. Pet. Eng. J.*, vol. 24, no. 3, pp. 283–293, 1984.
- [11] a Hammami and J. Ratulowski, “Precipitation and Deposition of Asphaltenes in Production Systems: A Flow Assurance Overview,” *Asph. Heavy Oils, Pet.*, pp. 617–660, 2007.
- [12] M. Tavakkoli, M. R. Grimes, X. Liu, C. K. Garcia, S. C. Correa, Q. J. Cox, and F. M. Vargas, “Indirect Method: A Novel Technique for Experimental Determination of Asphaltene Precipitation,” *Energy & Fuels*, vol. 29, no. 5, pp. 2890–2900, 2015.
- [13] M. P. Hoepfner, “Investigations into Asphaltene Deposition, Stability, and Structure.,” 2013.
- [14] H. W. Yarranton, D. P. Ortiz, D. M. Barrera, E. N. Baydak, L. Barré, D. Frot, J. Eyssautier, H. Zeng, Z. Xu, G. Dechaine, M. Becerra, J. M. Shaw, A. M. McKenna, M. M. Mapolelo, C. Bohne, Z. Yang, and J. Oake, “On the size distribution of self-associated asphaltenes,” *Energy and Fuels*, vol. 27, no. 9, pp. 5083–5106, 2013.
- [15] J. L. Amundara??n Hurtado, M. Chodakowski, B. Long, and J. M. Shaw, “Characterization of physically and chemically separated athabasca asphaltenes using small-angle x-ray scattering,” *Energy and Fuels*, vol. 25, no. 11, pp. 5100–5112, 2011.
- [16] L. Goual, M. Sedghi, X. Wang, and Z. Zhu, “Asphaltene aggregation and impact of alkylphenols,” *Langmuir*, vol. 30, no. 19, pp. 5394–5403, 2014.
- [17] G. González and A. Middea, “Peptization of asphaltene by various oil soluble amphiphiles,” *Colloids and Surfaces*, vol. 52, pp. 207–217, 1991.
- [18] C.-L. Chang and H. S. Fogler, “Stabilization of Asphaltenes in Aliphatic Solvents Using Alkylbenzene-Derived Amphiphiles. 1. Effect of the Chemical Structure of Amphiphiles on Asphaltene Stabilization,” *Langmuir*, vol. 10, no. 6, pp. 1749–1757, 1994.
- [19] O. León, E. Rogel, A. Urbina, A. Andújar, and A. Lucas, “Study of the adsorption of alkyl benzene-derived amphiphiles on asphaltene particles,” *Langmuir*, vol. 15, no. 22, pp. 7653–7657, 1999.
- [20] L. Goual, M. Sedghi, H. Zeng, F. Mostowfi, R. McFarlane, and O. C. Mullins, “On the formation and properties of asphaltene nanoaggregates and clusters by DC-conductivity and centrifugation,” *Fuel*, vol. 90, no. 7, pp. 2480–2490, 2011.
- [21] P. Wattana, D. J. Wojciechowski, G. Bolaños, and H. S. Fogler, “Study of Asphaltene Precipitation Using Refractive Index Measurement,” *Pet. Sci. Technol.*, vol. 21, no. 3–4, pp. 591–613, 2003.

- [22] C.-L. Chang and H. S. Fogler, “Stabilization of Asphaltenes in Aliphatic Solvents Using Alkylbenzene-Derived Amphiphiles. 1. Effect of the Chemical Structure of Amphiphiles on Asphaltene Stabilization,” *Langmuir*, vol. 10, no. 6, pp. 1749–1757, 1994.
- [23] Malcolm A. Kelland, *Production Chemicals for the Oil and Gas Industry*, vol. 72, no. 1–2. 2010.
- [24] J.-A. Östlund, M. Nydén, H. S. Fogler, and K. Holmberg, “Functional groups in fractionated asphaltenes and the adsorption of amphiphilic molecules,” *Colloids Surfaces A Physicochem. Eng. Asp.*, vol. 234, no. 1–3, pp. 95–102, 2004.
- [25] Y. F. Hu and T. M. Guo, “Effect of the structures of ionic liquids and alkylbenzene-derived amphiphiles on the inhibition of asphaltene precipitation from CO₂-injected reservoir oils,” *Langmuir*, vol. 21, no. 18, pp. 8168–8174, 2005.

Chapter 4- Comparison of Experimental Techniques at Ambient and High-Pressure Conditions for Evaluation of Chemistries against Asphaltene Aggregation and Deposition: New Application of HPHT-QCM

4.1 Introduction

Asphaltene precipitation and deposition caused by temperature variation, pressure depletion and oil composition changes can result in formation damage, oil production reduction and increased operating costs. Use of chemical additives is probably the most effective option for preventing or reducing asphaltene problems. Selection of inhibitors for asphaltene deposition is commonly based upon simple tests conducted on stabilised crude oil samples at ambient conditions. Some of the significant parameters involved in the asphaltene deposition phenomenon are: asphaltene onset pressure (AOP), lower and upper asphaltene envelope, reservoir pressure and bubble point pressure[1]–[3]. Gas injection is one of the most common EOR approaches which increases ultimate oil recovery in many cases because of induced oil viscosity reduction or pushing the oil towards the wellbore[4]. One of the most effective agents in this type of EOR method is natural gas which leads to increase oil production although the natural gas injection into an oil reservoir could change the flow behaviour and the fluids equilibrium properties which cause asphaltene precipitation and deposition problems[5], [6]. Despite several decades of R&D projects, gas induced asphaltene deposition is still a major flow assurance challenge[7], [8]. There are different approaches for asphaltene remediation and inhibition including mechanical techniques (Pigging, mechanical/manual Striping, mechanical Vibration[9], [10]), chemical treatments (dispersants, antifoulants, coagulants, polar co-solvents[11]–[15]) and thermal techniques (steam injection, hot chemical injection, microwave technique, in-situ combustion[9]). Between all these techniques, chemical injection is one of the most widely used strategies to tackle the asphaltene precipitation and deposition barrier[16], [17]. Millions of dollars per year are estimated to be spent each year on installing and servicing asphaltene mitigation equipment and chemicals[18]. In this regard, development of a new reliable technique for evaluation of asphaltene inhibitors could help cut the costs and reduce the frequency of treatments. Using classical asphaltene analysis techniques, the

chemical structures of asphaltenes and additives that affect inhibitors performance have been elucidated[19]–[24]. Despite these achievements, studying the effect of inhibitors on asphaltene precipitation and deposition mechanisms under real field conditions remains difficult due to the complex environment in which asphaltenes are destabilised and the lack of a reliable technique. Although all the experimental techniques mentioned in Chapter 3 have provided detailed information about asphaltene formation and interactions with inhibitors, they might not be suitable for evaluation of chemicals with respect to asphaltene precipitation and deposition under realistic field conditions.

Therefore, in this chapter a new high-pressure high-temperature method has been developed in which chemicals are evaluated based on both precipitation and deposition inhibition in order to study their function at relevant conditions. In this study, a technique based on QCM is presented to rank three asphaltene inhibitors based on their efficiency in shifting asphaltene onset point and reducing deposition rate at high pressure. This technique is faster, more reliable and accurate compared to the available tests such as the Asphaltene Inhibitor Screening Test (AIST) and UV-vis-NIR spectrophotometry. Furthermore, we are able to evaluate the effect of inhibitors on the asphaltene deposition rate onto the crystal surface that is obtained by resonance frequency monitoring after precipitation onset point, using dead-oil samples at high pressure-high temperature QCM (HPHT-QCM). The experimental results reveal that the asphaltene inhibitors are able to shift the onset of asphaltene precipitation/aggregation and could reduce the rate of asphaltene deposition, and also the ranking of chemicals could be different from ambient to HPHT condition. In this research work, the influence of chemical additives dosage, ageing time and temperature on the asphaltene precipitation and aggregation phenomena are also investigated.

4.2 Experimental Section

4.2.1 Materials

Experiments were conducted at both ambient and high pressure-high temperature (HPHT) conditions on crude oil “P” from the North Sea. Table 4.1 shows the properties of crude oil “P”.

Table 4. 1. Properties of Crude Oil “P” Used in This Study

Petroleum Fluid	f (g.g ⁻¹)	ρ_o (g.mL ⁻¹)	MW _o (g.mol ⁻¹)	μ_o (cP)
B	0.0397	0.836	181	13.44

The commercial asphaltene inhibitors 6, 10 and 12 were utilised to treat the crude oil samples. These chemicals were selected based on their significant applications and contributions in mitigating asphaltene challenges in industry, which were received from operators. HPLC-grade anhydrous n-heptane (>99%), anhydrous toluene (>99.8%), HPLC grade acetone (≥99.9%) and ethanol (≥99.8%) were purchased from Sigma-Aldrich and used as received.

4.2.2 Asphaltene Inhibitor Screening Test (AIST)

Various dosage of inhibitor 6, 10 and 12 were injected to crude oil “P”. In this regard, 100, 300 and 600 ppm of each inhibitor were provided and analysed. Concentrated solution of each inhibitor in crude oil (2000 ppm), were diluted with n-heptane and inserted in a beaker, then were mixed by magnetic stirrer at 1000 rpm for two hours to obtain a homogeneous solution. 10 mL of n-heptane plus 300 μL of the treated crude oil sample was placed in graduated centrifuge tubes to be centrifuged using a Heraeus Megafuge. The centrifuge tubes were left for a time interval (which is called ageing time hereafter) after which, the quantity of asphaltene aggregates at the bottom of each tube was measured in mL. A blank crude oil with no chemical additive was used as reference.

The applied aging times are 1 hr, 6 hr and 24 hr. The term “clear” is being utilised whenever no asphaltene aggregates were seen at the bottom of the tube and the term “trace” is used for the condition when the quantity of deposit is not high enough to be measured[25], [26]. Comparing the quantity of sediment measured in mL for various injected inhibitors and dosages with reference to the untreated oil, which was the combination of crude oil and n-heptane without any chemical, is done to investigate the efficiency of inhibitors by utilising the AIST.

4.2.3 Detection of asphaltene appearance point using UV-vis-NIR Spectrophotometer

The mixtures of crude oil and precipitant, with and without inhibitor, were provided following the same approach which was described in Section 4.2.2. Mixtures with various proportions of treated or untreated crude oil and n-heptane varying from 0 to 85 vol% of n-heptane were provided. The test tubes were rigorously shaken manually to obtain a homogeneous solution which was then sealed to be preserved from atmosphere. To retain a uniform temperature the test tubes were held in a Stuart Scientific oven which was set at a particular temperature (25 °C and 60 °C were used in these tests). The test tubes were undisturbed for a particular ageing time. The ageing time is the duration between sample preparation and the determination of the NIR light transmittance number. In next step, the NIR transmittance was determined by Hitachi UV-Vis-NIR spectrophotometer Model U-3010. The transmittance numbers were recorded for 1100 and 1300 nm wavelengths. From this measurement it can be concluded that whenever the signal is not saturated, several wavelengths can be utilised to determine the onset point of precipitation. For wavelengths less than 1100 nm, evaluation cannot be done as the signal is saturated. The mass ratio of oil and precipitant exist in every mixture was evaluated and by presuming an ideal mixing and knowing the density of the contents, their volumes were calculated. The light transmittance numbers of each sample were modified by subtracting the n-heptane transmittance and after that the influence of dilution was mathematically omitted [26], [27]. By utilising the transmittance of the crude oil as reference, normalized amount of the corrected transmittance was calculated. These normalized values are often plotted as a function of the volume fraction of n-heptane or crude oil. Another method for illustrating similar results is to use light intensity instead of absorbance, which is more common for presenting results in direct spectroscopy. The normalized light intensity can also be plotted as a function of the volume fraction of crude oil and/or n-heptane. The obtained normalized light intensity was reduced as asphaltene aggregates barricade light rays through the cell, therefore this reduction trend indicates asphaltene aggregation happening, the first deflection from the linear line revealed the precipitation of asphaltenes which called asphaltene appearance point (AAP) hereafter. AAP represents the minimum amount of n-

heptane added to crude oil to cause asphaltene precipitation that is discernible for the utilized technique.

The morphology and architecture of the asphaltene precipitates with and without chemical additives were investigated by Environmental Scanning Electron Microscopy (ESEM) in order to investigate the effect of inhibitors on asphaltene precipitates size and their morphology.

4.2.4 Quartz Crystal Microbalance (QCM)

This technique measures the resonance frequency for a quartz crystal surface inserted into crude oil with and without chemical additive to determine the asphaltene onset point (AOP) at a specific temperature, pressure and composition. Since the asphaltene precipitation is measured independently of deposition using the QCM technique, the effect of inhibitor on asphaltene precipitation and deposition phenomena was independently studied. The crude oil “P” was treated with inhibitors 6, 10 and 12 at various chemical dosages ranging from 119 to 1785 ppm. The blank oil without any inhibitor was considered as reference. Then the treated/blank crude oil samples were loaded into the QCM cell and stabilized at the temperature and pressure of interest. Then, the test fluid is pressurised by injecting natural gas at a constant rate of pressure increase. The composition of injected natural gas is presented in Table 4.2.

Table 4. 2. Natural gas composition

Component	Mole%
N ₂	1.84
C ₁	89.94
CO ₂	0.91
C ₂	5.32
C ₃	1.45
<i>i</i> C ₄	0.20
<i>n</i> C ₄	0.21
<i>i</i> C ₅	0.07
(<i>n</i> C ₅) + C ₆ ⁺	0.06

The QCM technique can provide a robust, reliable method for evaluation of asphaltene inhibitors and deposition risks which has some advantages over other conventional

techniques including; applying more realistic pressure and temperature conditions, small size of the sample, assessment of real time deposition rate, using live oil samples (in addition to dead/stabilised samples). It could be more automated and much cheaper compared to other utilised techniques in industry.

4.3 RESULTS AND DISCUSSION

Three commercial asphaltene inhibitors have been utilised to investigate their effect on asphaltene appearance point, aggregation and deposition phenomena using three different techniques: “AIST”, “UV-vis-NIR spectrophotometry” and “HPHT-QCM”, which have been described in Section 4.2. Natural gas injection was used to induce the asphaltene precipitation at HPHT conditions, which gives the driving force for asphaltene precipitation, instead of the n-heptane titration that is employed in the ambient tests. The results of all these experiments will be presented and discussed in following subsections.

4.3.1 Asphaltene Inhibitor Screening Test (AIST)

Crude oil “P” was treated with inhibitors 6, 10 and 12 at 100, 300 and 600 ppm as described in Section 4.2.2. The results are presented in Figure 4.1 and the volume of asphaltene sediments in the bottom of tubes obtained with/without inhibitors in various ageing times is presented in Table 4.3. With respect to the capability of inhibitors on dispersing the asphaltene aggregates in the mixtures the AIST ranks the inhibitors performance, which also decrease the particles velocity in Brownian motion and, as a result, the amount of deposited asphaltenes[25], [26]. The more effective is the asphaltene inhibitor the less deposition will be seen.

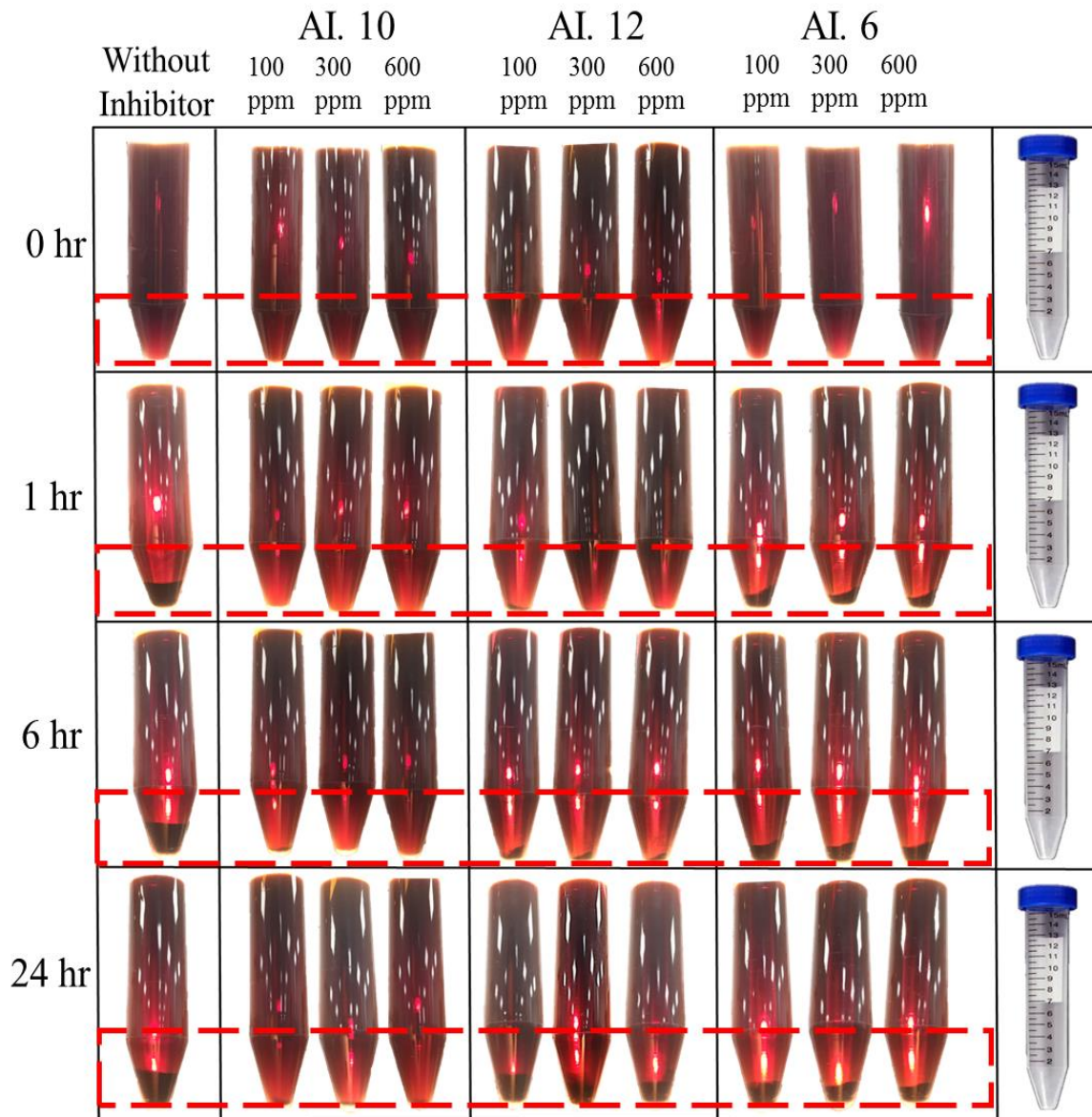


Figure 4. 1. AIST results for crude oil “P” treated with inhibitors 6, 10 and 12 at 100, 300 and 600 ppm for different ageing times of 0 hr, 1 hr, 6 hr and 24 hr.

Table 4. 3. AIST results for crude oil “P” treated with inhibitors 6, 10 and 12 at 100, 300 and 600 ppm for various ageing times

Sample	AI Conc. (ppm)	0 hr (mL)	1 hr (mL)	6 hr (mL)	24 hr (mL)
Crude oil “P”	0	Clear	0.3	0.4	0.5
With AI. 6	100	Clear	0.1	0.2	0.3
	300	Clear	Trace	0.1	0.2
	600	Clear	Trace	0.1	0.1
With AI. 10	100	Clear	Clear	Clear	Trace
	300	Clear	Clear	Clear	Clear
	600	Clear	Clear	Clear	Clear
With AI. 12	100	Clear	Clear	Trace	0.3
	300	Clear	Clear	Trace	0.2
	600	Clear	Clear	Trace	0.2

No asphaltene deposit was observed in sample with inhibitor 10 at 600 ppm after 24 h. Deposits appeared in the reference crude oil (oil without any additive) after 1 h and we had higher amount of asphaltene aggregates as time passed as reported in Table 4.3. However, for samples with all concentrations of asphaltene inhibitor 10 and 12, there is no asphaltene sediment after 1 hr. By conducting UV-vis-NI spectrophotometer tests it was shown that the amount of asphaltene precipitates decreases with higher concentration of inhibitors as shows in Section 4.3.2. Hence the ranking of asphaltene inhibitors based on dispersion of asphaltene aggregates obtained from AIST is as follows: AI. 10 > AI. 12 > AI. 6. In AIST technique, to get a transparent test solution in which asphaltene sediments on the bottom of centrifuge tubes can be detectable, AIST needs a high amount of n-heptane (>97 vol%). Therefore, due to inability of AIST in evaluation of inhibitors at the heptane concentration

in which the highest amount of asphaltene precipitates and/or the largest asphaltene aggregates form, this method cannot be thoroughly reliable. In addition, this highly dilute solution is not a suitable representative of the real field conditions at which asphaltenes precipitate, aggregate and deposit. Hence we employ UV-vis-NI spectrophotometer technique to evaluate asphaltene inhibitors at ambient conditions which could give us more information about inhibitor efficiency.

4.3.2 Evaluation of Asphaltene Inhibitors Using UV-vis-NIR Spectrophotometer

Figure 4.2 shows the results of asphaltene appearance point determination for the crude oil “P” with and without inhibitors 6, 10 and 12 at 100, 300 and 600 ppm at 25 °C and 24 hr ageing time. The crude oil without inhibitor was considered as reference. All plots in Figure 4.2 can be divided to two main trends: the first trend is approximately a horizontal line for low amount of n-heptane (precipitant) and high-volume percentage of crude oil. In this part all systems show the same trend. Next, the second trend which has high amount of n-heptane and low volume of crude oil where the light intensity numbers deflect from the horizontal line. The intersection points between these two trend lines at which this deflection happens illustrates the volume fraction of n-heptane needed for determination of asphaltene appearance point (AAP).

In the second trend line after determination of asphaltene appearance point, Figure 4.2 presents a progressive light intensity decline for the reference fluid. The light intensity reduction reveals an increment in the quantity and size of asphaltene aggregates. For test samples with inhibitors, the light intensity reduced more gently than the reference sample results in slower precipitation and aggregation process rates under the influence of inhibitors. Next, as the heptane concentration reached 60 vol.%, the treated mixture illustrated a second inflexion point at 60 vol.% where the light intensity raised again toward the horizontal base trend line that shows a stable solution with fewer and smaller asphaltene aggregates due to presence of inhibitors.

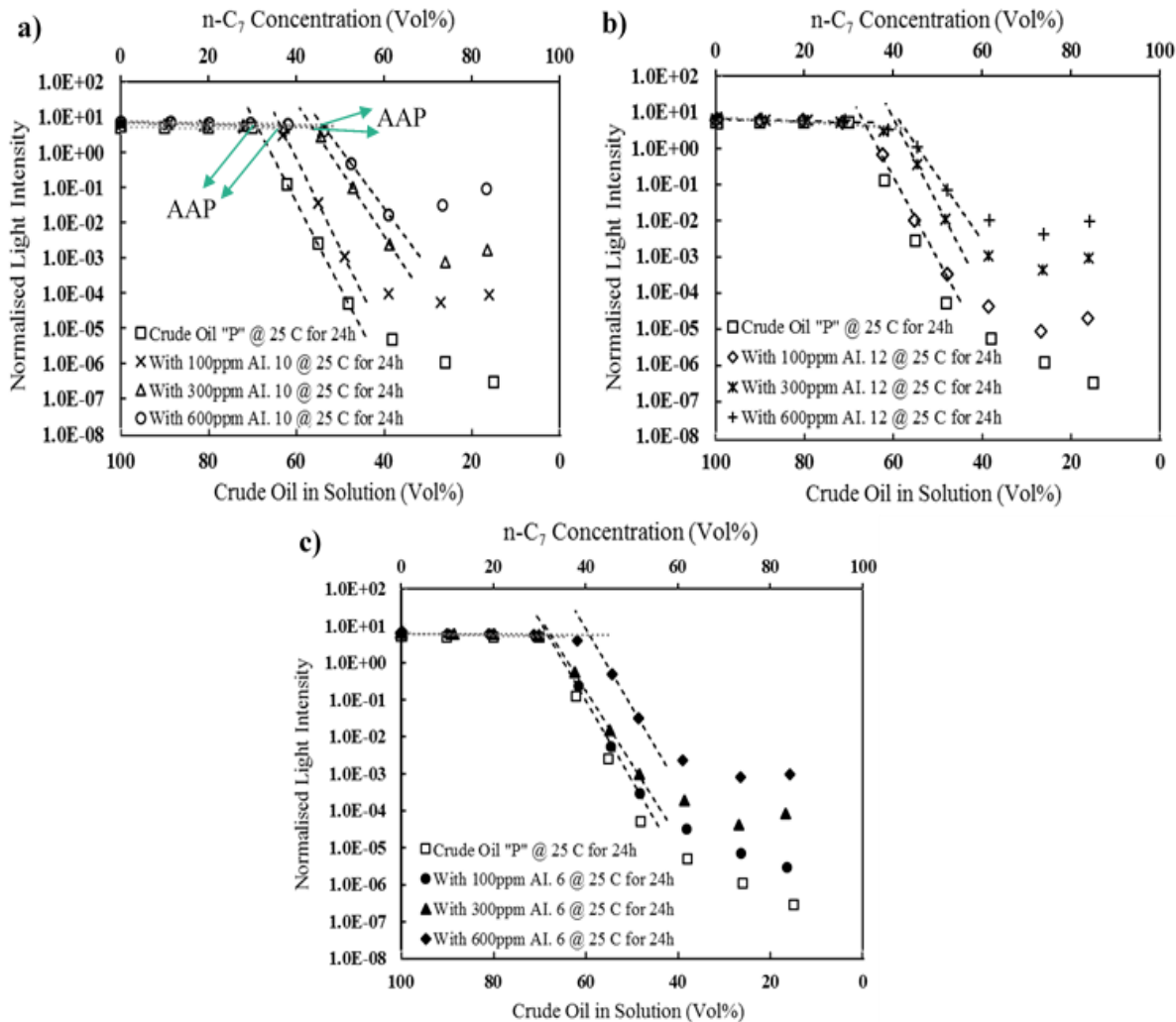


Figure 4. 2. Results of the UV-vis-NIR spectrophotometer technique for the crude oil “P” with, (a) inhibitor 10, (b) inhibitor 12, and (c) inhibitor 6 at 100, 300 and 600 ppm, after mixing with n-heptane and ageing time of 24 hr at 25 °C.

As precipitant increased in the solutions it can influence the asphaltene precipitation mechanism in two ways: first it dilutes asphaltene concentration and in consequence decreases the light intensity, even at below 30 vol.% of n-heptane where there is no precipitation in the solution, second it decelerates the rate of precipitation and aggregation process. If inhibitors exist in the test solution the rate of precipitation and aggregation will slow down more which results in higher light intensity compared to the blank crude oil “P” after 24 hr ageing time.

The inhibitor efficiency on asphaltene precipitation and aggregation inhibition was determined by monitoring the asphaltene appearance point and normalised light intensity

changes due to presence of different inhibitors at various dosages. Regarding to financial aspects low dosage inhibitors are more favourable. Figure 4.2 (a) shows that inhibitor 10 has a profound effect in shifting AAP from ~30.1 to ~38.4 vol% n-heptane at dosage of 100 ppm. While inhibitor 12 could not change the AAP significantly at this concentration (Figure 4.2b). Figure 4.2c illustrates that inhibitor 6 had limited effects at concentrations of 100 and 300 ppm, although at higher inhibitor dosage shifted the AAP from ~32.4 to ~41.6 vol% of n-heptane. As mentioned before in Section 4.3.1, no notable deposition was seen for inhibitor 10 at 300 and 600 ppm after 24 hr ageing time although from direct spectroscopy we observed the occurrence of asphaltene precipitation and aggregation for these systems. The reason of this observation is related to the slow rate of aggregation phenomenon for treated solution with inhibitor 10 at 300 and 600 ppm after 24 hr ageing time compared to the result obtained from the blank crude oil “P”. Unlike inhibitor 6, Figures 4.2a and b present decline trend for asphaltene aggregation and thus higher light transmittance numbers due to dosage increment for inhibitor 10 and 12. They also decreased asphaltene aggregation to a drastically low level at 600 ppm. As can be seen from Figure 4.2, all asphaltene appearance points were shifted for the treated crude oil “P” with inhibitors 6, 10 and 12 at 600 ppm. The inhibitor 10 has better performance compared to inhibitors 6 and 12 at concentration of 100 ppm, thus it can be concluded that at concentration of 100 ppm inhibitor 10 might be the best option. Applying chemical additives at high concentrations in oilfields is not economically favourable and desirable solution. Determination of asphaltene appearance points for crude oil “P” which was blended with 100, 300 and 600 ppm of inhibitors after 24 hr ageing time is presented in Table 4.4.

Table 4. 4. Detection of asphaltene appearance point of crude oil “P” with 100, 300 and 600 ppm dosage of different asphaltene inhibitors, after mixing with n-heptane and aging for 24 hr at 25 °C.

Test Solution	Detection of asphaltene appearance point (n-heptane Vol %)		
	100 ppm	300 ppm	600 ppm
Blank Crude Oil “P”	30.5 ± 1.2	30.5 ± 1.2	30.5 ± 1.2

With inhibitor 6	31.8 ± 2.4	32.4 ± 1.7	41.6 ± 1.5
With inhibitor 10	36.4 ± 1.9	43.3 ± 2.0	45.7 ± 2.1
With inhibitor 12	33.2 ± 1.8	41.1 ± 1.4	42.5 ± 2.2

The control is crude oil P without adding any additives and is utilized as reference for discovering the effect of each inhibitor. A shift in asphaltene appearance point from its number in reference fluid (~30.5 vol% n-heptane) to higher values, stated the influence of utilised asphaltene inhibitor. We believe that there is one main mechanism which explains the change in asphaltene appearance point due to presence of inhibitors. This mechanism is that the inhibitors molecules have interaction with asphaltenes and decrease the asphaltene particle size (before aggregation phenomenon) and also delay the precipitation and aggregation steps, or change the hydrophobicity of asphaltene nanoaggregates by occupying their active sites. In order to investigate this further, the effect of inhibitor on asphaltene precipitates size and its morphology were investigated by ESEM micrographs. Figure 4.3 shows the effect of Inhibitor 6 on asphaltene particle size.

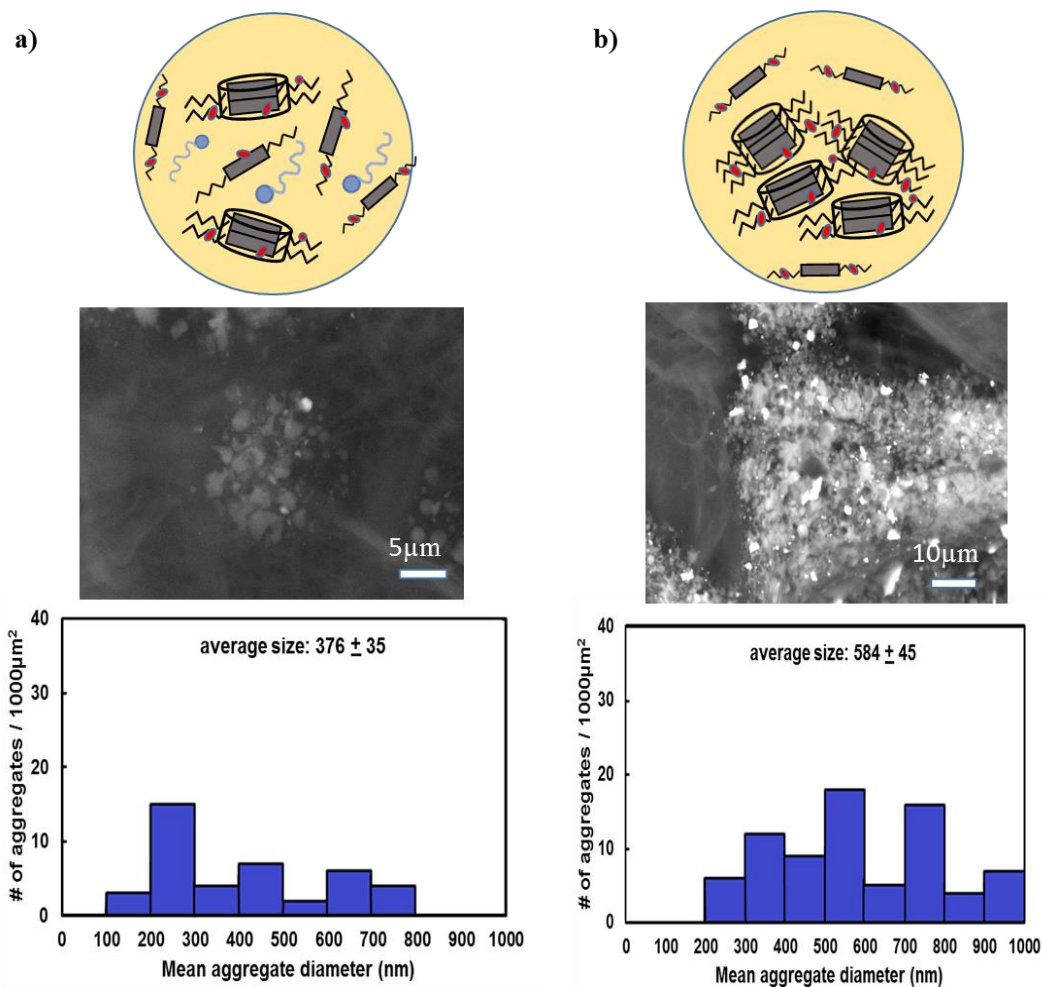


Figure 4. 3. Effect of asphaltene inhibitor on asphaltene particle size obtained by ESEM micrographs: a) with AI. 6, b) without inhibitor. All pictures are analysed using ImageJ.

This figure also presents schematic diagram of possible inhibitors interaction with asphaltenes which curbs the asphaltene-asphaltene nanoaggregate interactions to form larger particles. (zigzag line with red dots): asphaltene monomer, (zigzag line with red dots and squiggly line): asphaltene aggregates, (red dot): heteroatoms, (blue squiggly line): inhibitor.

The micrographs are all analysed using ImageJ and presented in Figure 4.3. Figure 4.3 presents the size distribution of asphaltene precipitates with and without inhibitor. The employed inhibitor reduced the asphaltene particle size. For the samples with inhibitor (Figure 4.3.a), the sizes range from 100 to 800 nm averaging around 376 nm. The measurements without inhibitor have larger asphaltene particle sizes averaging around 584 nm, which is the size of the asphaltene aggregates that can be detected by commercial techniques used for determination of asphaltene precipitation onset. The ranking of

asphaltene inhibitors based on AAP changes obtained from UV-vis-NI spectrophotometer technique is as follows: AI. 10 > AI. 12 > AI. 6 which is in consistent with AIST results in the same conditions. To investigate the influence of temperature on performance of inhibitors, several tests were performed with similar concentrations of inhibitors 6 and 12 at 25 °C and 60 °C and ageing time of 24 hr.

Since some oil properties like density, viscosity and asphaltene solubility depend on temperature. The solubility of asphaltenes in oil usually increases with increasing temperature[28]. In addition, asphaltene contents which precipitate out of the solution at high or low temperatures can be dissimilar with each other since asphaltene is a polydisperse molecule. The influence of temperature on asphaltene behaviour should be considered since each fraction of asphaltene has its own properties like diffusion rate and density. Asphaltene nanoaggregates might precipitate in higher temperatures as they get more unstable.

The results for influence of temperature on mixture of oil and n-heptane with and without inhibitors are presented in Figure 4.4. From Figure 4.4 it seems that the solution without inhibitor has more stable asphaltene nanoaggregates at 60 °C compared to the solution at 25 °C. It is obvious from the test results that the rate of aggregation and precipitation phenomena decreased as the temperature increased. Behaviour of the crude oil at higher temperatures shows that it performs as a more effective solvent for the asphaltene nanoaggregates and the solution requires more n-heptane to detect the asphaltene appearance point. The results for inhibitors 6 and 12 at concentration of 600 ppm at temperatures of 25 °C and 60 °C after 24 hr ageing time are illustrated in Figure 4.4a and b, respectively. As can be seen from Figure 4.4, it is clear that at 600 ppm, inhibitor 12 has the same performance at both 25 °C and 60 °C. So, the increase in temperature has no effect on the inhibitor efficiency.

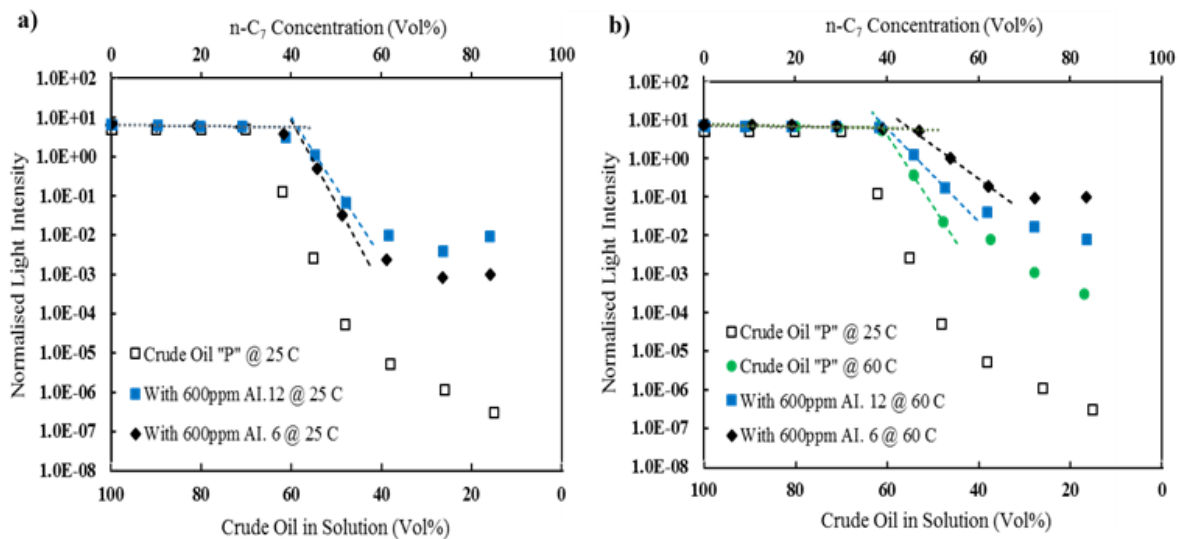


Figure 4. 4. Effect of temperature on performance asphaltene inhibitors for crude oil "P", a) crude oil "P" with and without inhibitors 6 and 12 at 600 ppm at 25 °C, b) Crude oil "P" with and without inhibitors 6 and 12 at 600 ppm at 60 °C, after blending with n-heptane for 24 hr ageing time.

Similar procedure was employed for inhibitor 6 at concentration of 600 ppm, 25 °C and 60 °C for ageing time of 24 hr. The efficiency of inhibitor 6 in shifting AAP is slightly lower than inhibitor 12 at same conditions. However, inhibitor 6 at 60 °C is more effective on asphaltene aggregates dispersion and AAP changes compared to inhibitor 12 and its performance at 25 °C. The ranking of asphaltene inhibitors 6 and 12 based on AAP changes monitoring at higher temperature is: AI. 6 > AI. 12. Therefore, the efficiency and ranking of inhibitors might change at higher temperature. So, we decided to evaluate the inhibitors not only at high temperature but also at high pressure in presence of gas, which is closer to real field conditions, in order to obtain the updated ranking of inhibitor based on operation condition.

4.3.3 Evaluation of Asphaltene Inhibitors Using HPHT-QCM

A QCM has been utilised in this study to evaluate the effectiveness of asphaltene inhibitors on asphaltene precipitation and deposition rate at high pressure-high temperature (HPHT) condition (up to 6000 psia and 60 °C) in presence of gas. The QCM resonance frequency (RF) was measured for one day during continuous natural gas injection to investigate the effect of inhibitors on asphaltene onset point, gas oil ratio (GOR) and deposition rate at

various inhibitors concentrations. The RF is inversely proportional to the mass of quartz crystal surface. If the mass of the QCM surface alters because of the asphaltenes adhered onto the solid surface then a reduction in RF will be observed. The Sauerbrey equation [29] explains how the alteration in RF can be related to the change in mass which is as follows:

$$\Delta f = -f_u^{3/2} \left[\frac{\rho_L \eta_L}{\pi \rho_q \mu_q} \right]^{1/2} \quad (4.1)$$

Where Δf is frequency change (Hz), f_u is frequency of oscillation of unloaded crystal (in air), ρ_l is the density of the liquid in contact with the electrode, η_l is the viscosity of the liquid, ρ_q is density of quartz, and μ_q is shear modulus of quartz for AT-cut crystal. In an ideal condition, the asphaltene deposits with amount of 1 nanogram will give 1 Hz reduction in RF. The initial asphaltene test with no inhibitor was performed on crude oil “P” at 60 °C and various pressures because of continuous natural gas injection. The effects of asphaltene inhibitors on asphaltene onset point (AOP) and gas oil ratio which is required to detect the asphaltene precipitation onsets are presented in Figure 4.5.

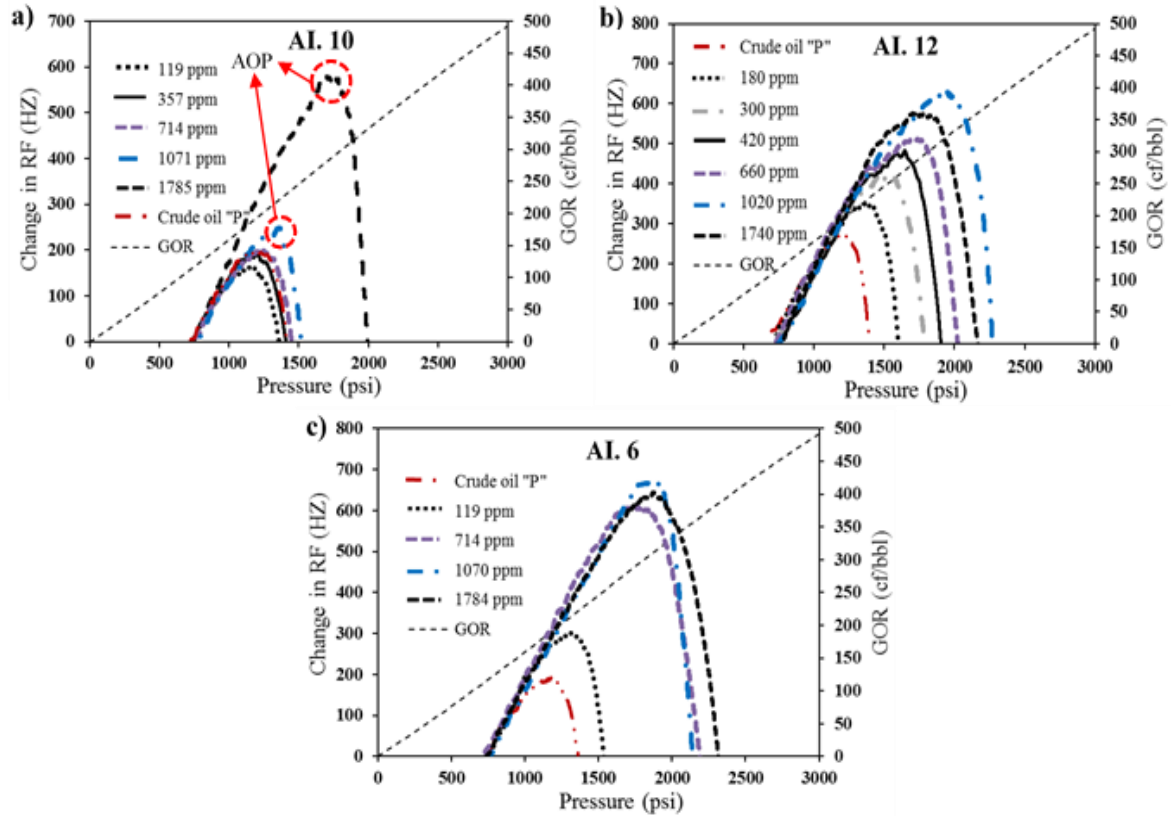


Figure 4. 5. Results of the HPHT-QCM technique for the crude oil “P” with, (a) inhibitor 10, (b) inhibitor 12, and (c) inhibitor 6 at various concentrations, after injecting natural gas at 60 °C.

The RF increases due to the reduction in density and viscosity of the test fluid as pressure increases with injection of gas. The RF declines when asphaltene precipitate out of the solution on the QCM surface. The pressure at which the RF begins to decline represents the asphaltene onset point that is 1195 psi at GOR of 193.04 cf/bbl for blank crude oil “P” without any inhibitor. The AOP/GOR is 1753 psia/290.08 cf/bbl for AI.12, 1790 psi/296.50 cf/bbl for AI. 6 and 1268 psia/205.67cf/bbl for AI.10 with concentrations of 660 and 714 ppm, respectively. Figure 4.6 presents the AOP and GOR obtained by HPHT-QCM versus various concentrations of inhibitors.

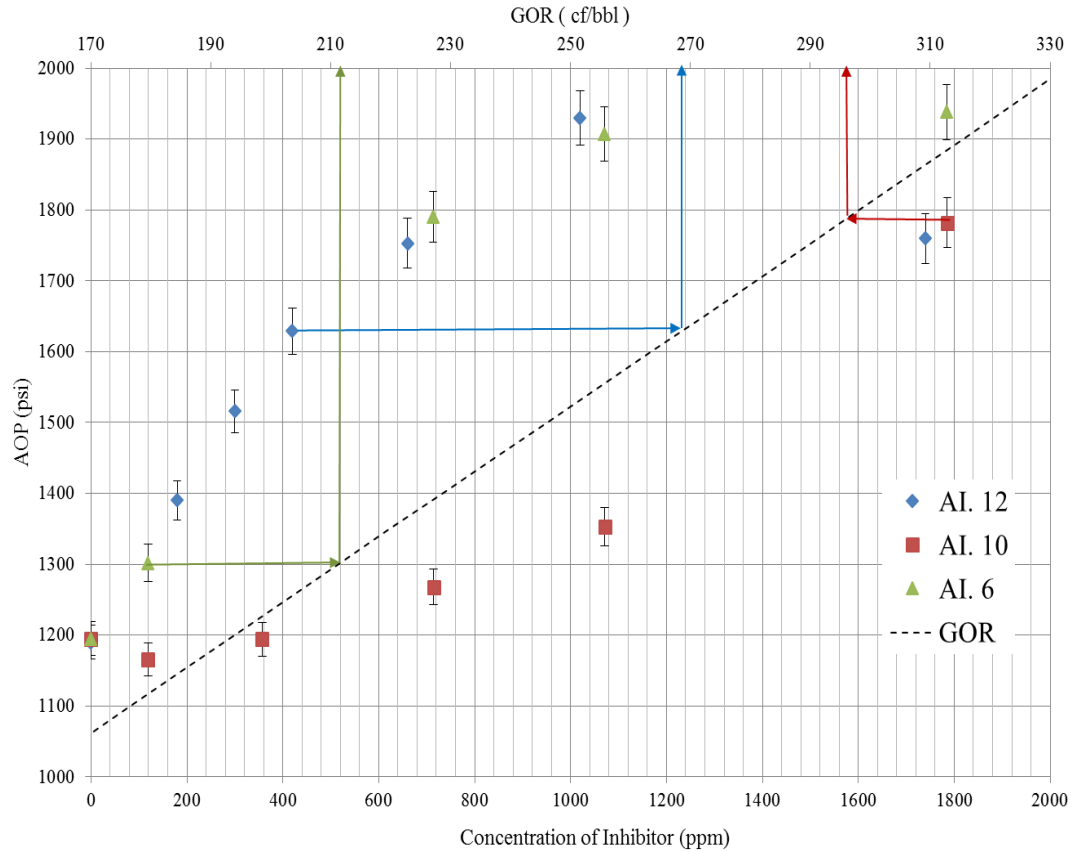


Figure 4. 6. AOP/GOR versus concentration of three inhibitors 6, 10 and 12.

As can be seen inhibitor 6 has better performance compared to the other two inhibitors on AOP shifting and the GOR at which AOP occurs. Inhibitor 10 has a negative effect on asphaltene precipitation at low concentration and has some limited effects at higher concentrations. The results regarding the effect of employed asphaltene inhibitors on deposition rate after the AOP are shown in Figure 4.7, which is RF reduction versus time for crude oil “P” with and without inhibitors at different concentrations. The obtained results show that all utilised inhibitors have a positive impact on reducing the asphaltene deposition rate onto the QCM surface after exceeding the AOP. As can be seen, there is a dramatic difference in the plotted curves between the blank oil “P” without any inhibitor and the same oil with 119 and 180 ppm of inhibitor 6, 10 and 12, respectively.

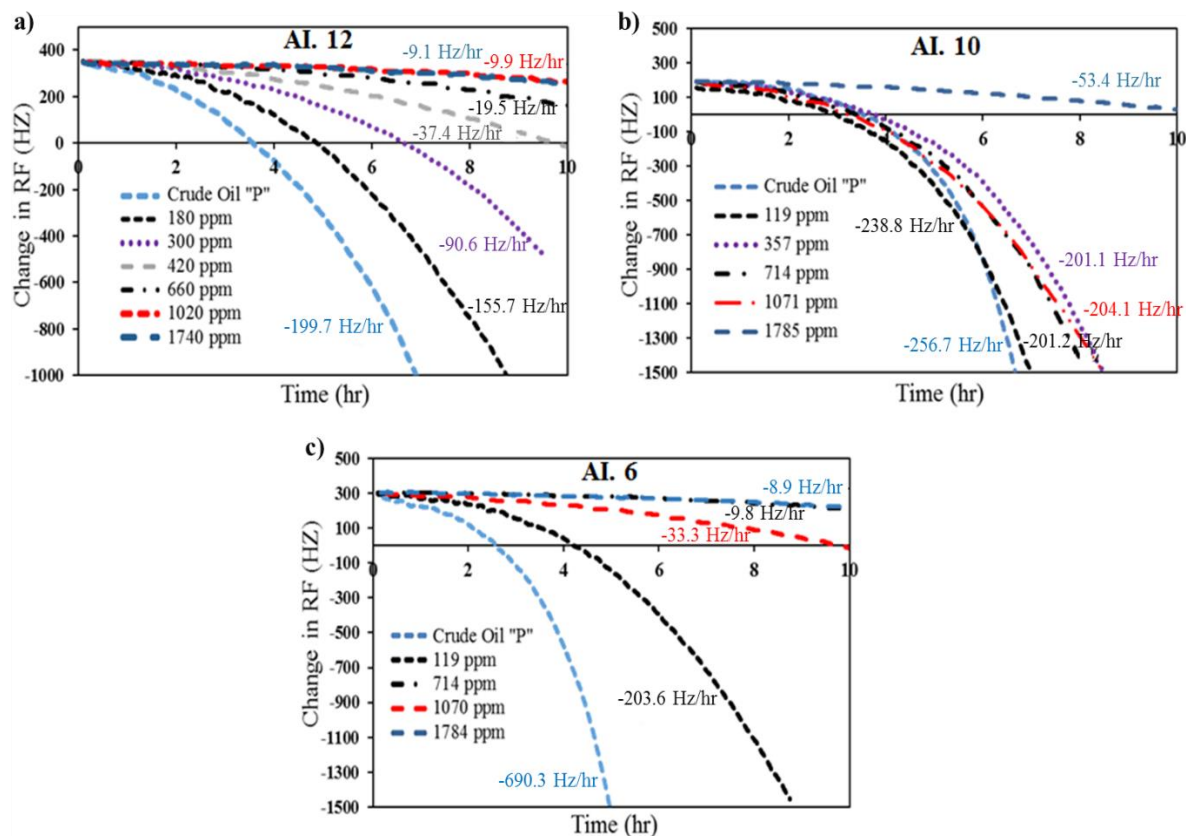


Figure 4. 7. Results of the effect of asphaltene inhibitors on deposition rate at various concentrations, a) AI. 12, b) AI. 10 and c) AI. 6.

The AI. 6 has better efficiency in reducing the deposition rate from -690.3 Hz/hr to -203.6 Hz/hr compared to inhibitors 10 and 12 at the same concentration which decreases the deposition rate from -256.7 Hz/hr to -201.2 Hz/hr and from -199.7 Hz/hr to -155.7 Hz/hr, respectively. A sudden change in RF is observed during the first 4 hrs of the test without inhibitor compared to the test with inhibitors. A significant reduction in the rate of asphaltene deposition could be seen in the tests with inhibitor after beginning of deposition phenomenon. The inhibitors might cover the asphaltene's aromatic cores through π - π interactions between inhibitors aromatic rings and asphaltene's aromatic cores which intercept the stacking of asphaltene molecules into nanoaggregates which causes its better efficiency in AOP shifting and deposition rate reduction. The inhibitors usually can also form H-bonding with active sites of asphaltene nanoaggregates (e.g. carboxylic, sulfoxide groups), the asphaltene aggregates are not able to move toward each other due to the

created steric repulsion between the aliphatic tails of inhibitors that curb the asphaltene growth into larger aggregates. The ranking of asphaltene inhibitors based on AOP/GOR changes and deposition rate reduction using HPHT-QCM technique is as follows: AI. 6 > AI. 12 > AI. 10. Therefore, the ranking of inhibitor obtained at ambient condition (AIST and UV-vis-NIR spectrophotometry) is totally different compared to ranking of inhibitors achieved at HPHT condition in presence of gas. Table 4.5 presents the ranking of utilised asphaltene inhibitors obtained from different techniques.

Table 4. 5. Ranking of asphaltene inhibitors obtained from different techniques

Ranking	AIST	Detection of AAP @ 1 atm and 25 °C (UV-vis-NIR Spectrophotometer)	HPHT-QCM (25 °C)
1	AI. 10	AI. 10	AI. 6
2	AI. 12	AI. 12	AI. 12
3	AI. 6	AI. 6	AI. 10

Based on our study which will be presented in chapter 5, we found that chemical structure of gas induced asphaltene is different from structure of n-alkane induced asphaltene. This could result in having different ranking of inhibitors based on operation conditions. For avoiding EOR induced asphaltene problems, evaluation of chemicals using techniques at ambient condition may not be representative of real performance and efficiency of chemistries which would be found in the field.

4.4 Conclusions

In order to identify appropriate asphaltene inhibitors to avoid or mitigate deferred oil production caused by asphaltene deposition, it is crucial to evaluate the inhibitors by using accurate and reliable techniques which could represent the real or close to real field condition. Based on the obtained results in this research study the commercial asphaltene inhibitors interact with the asphaltene nanoaggregates in the oleic phase to change the asphaltene appearance point which is detected by employed techniques and also decrease the rate of asphaltene aggregation phenomenon accordingly. The HPHT-QCM experiments results presented in this study provide experimental data that do not agree with asphaltene inhibitor evaluation techniques at ambient conditions. The ranking of inhibitors based on

their performance could be significantly affected by pressure and presence of gas at which the tests are performed. On the other hand, the experiments conducted at 25 °C and 60 °C and ambient pressure reveal that the ranking of inhibitors used in this study is different for each temperature condition. This could be as the result of the effect of temperature on the ability of the chemistries to interact with asphaltenes and make them stable in the solution. Therefore, a reliable technique is needed to truly evaluate inhibitor chemistries and their effects on deposition rate based on inhibitor-asphaltene molecules interactions which could be actually differed from n-C₇ to CO₂ injection at high temperature. The HPHT-QCM technique can investigate the effect of inhibitors on the apparent asphaltene deposition rate which is an important indicator of performance. All studied inhibitors could reduce the deposition rate. Additionally, the QCM is ideal for measuring asphaltenes at realistic P/T conditions as they have a high adhesion tendency and it is this property which causes the most problems downhole i.e pipeline restrictions and costly remediation procedures.

4.5 References

- [1] A. Hammami and J. Ratulowski, "Precipitation and Deposition of Asphaltenes in Production Systems: A Flow Assurance Overview," *Asph. Heavy Oils, Pet.*, pp. 617–660, 2007.
- [2] A. H. Youzband, P. Kor, E. Joonaki, V. Taghikhani, R. B. Boozarjomehry, and A. Chapoy, "Development of a New Model for Quantifying of Asphaltene Deposition-Role of Precipitation, Aggregation and Radial Transport," in *79th EAGE Conference and Exhibition 2017*, 2017.
- [3] A. Hassanpouryouzband, E. Joonaki, V. Taghikhani, R. Bozorgmehry Boozarjomehry, A. Chapoy, and B. Tohidi, "A New 2-D Particle-Scale Model to Simulate Asphaltene Deposition in Wellbores and Pipelines," *Energy & Fuels*, Nov. 2017.
- [4] A. Rostami, M. Arabloo, E. Joonaki, S. Ghanaatian, and A. H. Youzband, "Fast Estimation of Supercritical CO₂ Thermal Conductivity by a Supervised Learning Machine-Implications for EOR," in *79th EAGE Conference and Exhibition 2017*, 2017.
- [5] A. K. M. Jamaluddin, J. N. Nighswander, B. F. Kohse, A. El Mahdi, M. A. Binbrek, and P. F. Hogg, "Experimental and theoretical assessment of the asphaltene precipitation characteristics of the Sahil field under a proposed miscible gas

- injection scheme,” in *Abu Dhabi International Petroleum Exhibition and Conference*, 2000.
- [6] M. Parra-Ramirez, B. Peterson, and M. D. Deo, “Comparison of first and multiple contact carbon dioxide induced asphaltene precipitation,” in *SPE International Symposium on Oilfield Chemistry*, 2001.
- [7] A. Ayyaswami, “Innovative In-Situ Remedial Technologies for Petroleum Hydrocarbon Remediation,” in *SPE Middle East Health, Safety, Environment & Sustainable Development Conference and Exhibition*, 2014.
- [8] E. Junaki, S. Ghanaatian, and G. Zargar, “A new approach to simultaneously enhancing heavy oil recovery and hindering asphaltene precipitation,” *Iran. J. Oil Gas Sci. Technol.*, vol. 1, no. 1, pp. 37–42, 2012.
- [9] L. C. Pretorius, “New Application Technology for Internal Pipeline Coatings In-Situ Pipeline Protection using Pigging Techniques,” in *CORROSION 2006*, 2006.
- [10] H. Yarranton, “Asphaltene deposition,” in *Canadian International Petroleum Conference*, 2000.
- [11] S. C. Lightford, E. Pitoni, L. Mauri, and F. Armesi, “Development and Field Use of a Novel Solvent/Water Emulsion for the Removal of Asphaltene Deposits in Fractured Carbonate Formations.”
- [12] A. Khanifar, S. Sheykh Alian, B. Demiral, and N. B. Darman, “Study of asphaltene precipitation and deposition phenomenon during WAG application,” in *SPE Enhanced Oil Recovery Conference*, 2011.
- [13] A. S. Ogunlaja, E. Hosten, and Z. R. Tshentu, “Dispersion of Asphaltenes in Petroleum with Ionic Liquids: Evaluation of Molecular Interactions in the Binary Mixture,” *Ind. Eng. Chem. Res.*, vol. 53, no. 48, pp. 18390–18401, 2014.
- [14] C. Spurell, “Measuring Antifoulant and Corrosion Inhibitor Effectiveness in the Lab,” in *CORROSION 2001*, 2001.
- [15] K. Okamoto and K. Hotta, “Purification Experiments of Ocean Sludge by Activating Microorganisms and Using Coagulants,” in *The Tenth ISOPE Pacific/Asia Offshore Mechanics Symposium*, 2012.
- [16] E. Rogel, “Effect of inhibitors on asphaltene aggregation: a theoretical framework,” *Energy & Fuels*, vol. 25, no. 2, pp. 472–481, 2010.
- [17] M. G. Trbovich and G. E. King, “Asphaltene deposit removal: Long-lasting treatment with a co-solvent,” in *SPE International Symposium on Oilfield Chemistry*, 1991.
- [18] L. Cenegy, “Survey Of Successful World-wide Asphaltene Inhibitor Treatments In Oil Production Fields,” *Proc. SPE Annu. Tech. Conf. Exhib.*, 2001.

- [19] H. H. Ibrahim and R. O. Idem, "Interrelationships between asphaltene precipitation inhibitor effectiveness, asphaltene characteristics, and precipitation behavior during n-heptane (light paraffin hydrocarbon)-induced asphaltene precipitation," *Energy and Fuels*, vol. 18, no. 4, pp. 1038–1048, 2004.
- [20] E. F. Ghouloum, M. Al-Qahtani, and A. Al-Rashid, "Effect of inhibitors on asphaltene precipitation for Marrat Kuwaiti reservoirs," *J. Pet. Sci. Eng.*, vol. 70, no. 1–2, pp. 99–106, 2010.
- [21] G. González and A. Middea, "Peptization of asphaltene by various oil soluble amphiphiles," *Colloids and Surfaces*, vol. 52, pp. 207–217, 1991.
- [22] J. Wang, C. Li, L. Zhang, G. Que, and Z. Li, "The properties of asphaltene and their interaction with amphiphiles," *Energy and Fuels*, vol. 23, no. 7, pp. 3625–3631, 2009.
- [23] A. Yen, Y. R. Yin, and S. Asomaning, "Evaluating Asphaltene Inhibitors: Laboratory Tests and Field Studies." Society of Petroleum Engineers.
- [24] M. Barcenas, P. Orea, E. Buenrostro-González, L. S. Zamudio-Rivera, and Y. Duda, "Study of medium effect on asphaltene agglomeration inhibitor efficiency," *Energy & Fuels*, vol. 22, no. 3, pp. 1917–1922, 2008.
- [25] P. Juyal, V. Ho, A. Yen, and S. J. Allenson, "Reversibility of Asphaltene Flocculation with Chemicals," *Energy & Fuels*, vol. 26, no. 5, pp. 2631–2640, May 2012.
- [26] A. A. Melendez-Alvarez, M. Garcia-Bermudes, M. Tavakkoli, R. H. Doherty, S. Meng, D. S. Abdallah, and F. M. Vargas, "On the evaluation of the performance of asphaltene dispersants," *Fuel*, vol. 179, pp. 210–220, 2016.
- [27] M. Tavakkoli, M. R. Grimes, X. Liu, C. K. Garcia, S. C. Correa, Q. J. Cox, and F. M. Vargas, "Indirect Method: A Novel Technique for Experimental Determination of Asphaltene Precipitation," *Energy & Fuels*, vol. 29, no. 5, pp. 2890–2900, 2015.
- [28] F. M. Vargas, D. L. Gonzalez, G. J. Hirasaki, and W. G. Chapman, "Modeling asphaltene phase behavior in crude oil systems using the perturbed chain form of the statistical associating fluid theory (PC-SAFT) equation of state," *Energy & Fuels*, vol. 23, no. 3, pp. 1140–1146, 2009.
- [29] G. Sauerbrey, "Verwendung von Schwingquarzen zur Wägung dünner Schichten und zur Mikrowägung," *Zeitschrift für Phys.*, vol. 155, no. 2, pp. 206–222, 1959.

Chapter 5- Exploration of the Difference in Molecular Structure of n-C₇ and CO₂ Induced Asphaltenes

5.1 Introduction

Asphaltene–asphaltene interactions play a critical role in flow assurance problems. Supramolecular assemblies of asphaltene molecules through cooperative and noncovalent binding such as Brønsted acid–base interactions between carboxylic acids and pyridine groups, hydrogen bonding, metal coordination complexes because of presence of nickel and vanadium, van der Waals interactions between naphthenic, cycloalkyl and alkyl groups to form hydrophobic pockets, and dipole interactions and π – π stacking between the parallel polycondensed aromatic sheets are the dominant drivers of asphaltene precipitation and aggregation phenomena [1]–[3]. The lengths of asphaltene alkyl chains affect their stability in crude oil, since longer alkyl chains cause a reduction in precipitation and aggregation rate [4]. Thus, a better knowledge of asphaltene molecular architectures is imperative for researchers and operators to develop improved technologies for addressing asphaltene deposition problems and designing new class of inhibitors/dispersants.

Recent developments in the key analytical techniques, i.e. X-ray diffractometry (XRD) [5], [6], NMR spectroscopy [7], [8] and electron microscopy [9], have continuously pushed the limits for studying challenging carbonaceous and high molecular weight assemblies such as asphaltenes. X-ray crystallography remains the primary tool for determination of interlayer spacing, crystallite size, and crystallite diameter of asphaltenes and major accomplishments have been reported in recent years [5], [6]. Particularly remarkable advances have been achieved in understanding asphaltene morphologies using scanning electron microscopy (SEM) and high resolution transmission electron microscopy techniques (HRTEM) [9]. The last decade has also witnessed major achievements by NMR [7], [8], [10], [11] and FTIR [12] spectroscopy. These techniques have been used to determine the structure and composition of petroleum fractions including asphaltenes. Two recent reviews, one on analytical techniques for the characterization of hydrocarbon mixtures by Herod et al.[13] and a second the application of various state of the art

analytical methods for petroleum analysis in oil & gas industry by Ryan P. Rodgers et al.[14] cover most of the important works up to 2012.

In previous chapter, a high pressure-high temperature quartz crystal microbalance (HPHT-QCM) rig has been utilised to illustrate asphaltene deposition under real field conditions. HPHT-QCM is a facility which is able to simulate the oil production conditions and form asphaltene deposits under different PT conditions. HPHT-QCM can also simulate gas injection conditions. In this regard, identification of compositional and structural variations between HPHT-QCM and n-C₇ asphaltenes is significant since a new molecular level information of asphaltenes has become crucial to increase the ability to make the right decisions to tackle asphaltene challenges in the field. In this chapter, we present the first characterization study on the HPHT-QCM asphaltene deposits under gas injection conditions and examine compositional, structural and morphological changes with n-C₇ asphaltenes from the same parent crude oil achieved in the laboratory; utilising NMR spectroscopy, FTIR and ESEM/EDX analysis. We elucidate that the n-C₇ induced asphaltenes displayed greater aromaticity and a higher degree of condensation than CO₂ asphaltenes extracted from the parent crude oil. Our results also reveal that HPHT-QCM asphaltenes are richer in oxygen containing polar species compared to the parent crude oil. The obtained results are consistent with field asphaltene deposits and asphaltenes induced due to depressurization[15] emulsion rag layer[16], [17], and steam assisted gravity drainage (SAGD) asphaltene deposits[18].

5.2 Experimental Section

5.2.1 Chemicals

The n-heptane (n-C₇) (>99%), anhydrous toluene (Tol) (>99.8%), and ethanol (≥99.8%) were purchased from Sigma-Aldrich and used in this study as received for experiments and washing purposes. The natural gas composition which was used for HPHT-QCM test is as follows (*Mole%*): N₂ (1.84%), C₁ (89.94%), CO₂ (0.91%), C₂ (5.32%), C₃ (1.45%), iC₄ (0.20%), nC₄ (0.21%), iC₅ (0.07%), (nC₅) + C₆⁺ (0.06%).

5.2.2 n-C₇ Induced Asphaltenes and HPHT-QCM Deposits

Asphaltenes and a parent heavy crude oil (API = 12) were used in this study. Table A1.1 in Appendix 1 presents the SARA analysis of the crude oil used in this work. Asphaltenes were extracted by utilising the ASTM standard method D6560-12 with slight changes [19], [20]. As a brief description, 400 mL of n-C₇ was mixed with 10 gr of crude oil in an ultrasonic bath. The crude oil + n-C₇ solution was then heated at 90 °C under reflux for 1 hr. The solution was then allowed to rest overnight. Precipitated asphaltenes were collected by filtration using Whatman grade 42 filter paper and placed in a Soxhlet apparatus with n-C₇ to remove non-asphaltenic fractions until no colour was observed in the washing solvent after ~72 hr. The deposited asphaltenes were dissolved in hot toluene (~98 °C), which was finally withdrawn to generate solid asphaltenes for analytical experiments. The HPHT-QCM tests can be conducted under different ranges of crude oil composition at various operating conditions.

The set-up comprises high pressure cells, water jacket, temperature-controlled circulator, a magnetic mixer system as an agitator, quizix pump, high-pressure vessels, valves and lines, pressure and temperature sensors, and various gauges and indicators. The pressure can be increased up to 6000 psi, and the test fluid can be heated up to 150 °C. The mixing cell, as the crude oil container in the experimental system, had a volume of 120 mL. The principal of the measurement is based on monitoring of the variations in the Resonant Frequency (RF) for a QCM inserted into the crude oil due to changes in mass of the QCM surface. For the gas injection HPHT-QCM experiments, first half of the 120 mL cell was filled with crude oil and then the QCM carefully immersed inside the oil. Temperature of the system was set at 60 °C for conducting the tests. The crude oil was charged by stepped injection of natural gas and CO₂ into the mixing cell at a constant pressure rate (~1.1 psi/min) from ~600 psi. The gas at room temperature was injected into the system and timed to reach equilibrium. The magnetic stirrer was also started, rotating at 500 rpm to mix the injected gas and crude oil. The onset pressure of asphaltene precipitation was noted, as was the deposition rate onto the QCM surface. After deposition test, the CO₂ induced asphaltene deposits from the QCM surface was extracted and dried for characterisation. Deposits onto the QCM set up after CO₂ injection and its schematic figure are presented in Figure 5.1.

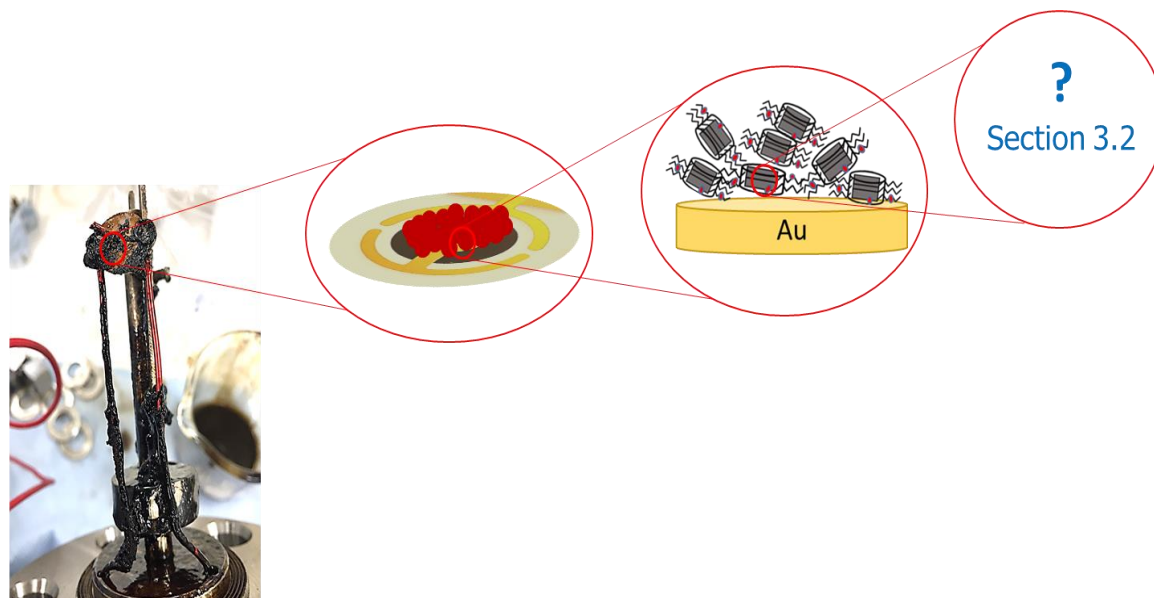


Figure 5.1. Picture and schematic illustration of asphaltene deposits onto the gold crystal surface of QCM after CO₂ injection.

More details about the QCM setup and the principal behind its measurements have been presented by Edris Joonaki et al [21].

5.2.3 ESEM/EDX Analysis

ESEM micrographs/EDX map have been used innovatively in petroleum industry such as identification of chemical wettability treatments[22], [23]. In this research work, the study of morphology and elemental analysis of asphaltenes were performed by SEM- EDX. An FEI Quanta 650 FEG SEM, with a backscattered electron (BSE) imaging detector, equipped with an Oxford Instruments X-Max^N 150 mm energy dispersive x-ray (EDX) detector, was used for the present study. For both imaging and elemental analysis, the microscope was operated in low-vacuum mode (0.83 Torr) at 20 kV, spot size of 4.5, dwell of 10 μ s and a working distance of 10 mm.

5.2.4 Characterisation by FTIR Spectroscopy

The FTIR spectra were recorded using FTIR-4000 Series (JASCO Edition) spectrometer including a Peltier stabilized DLaTGS detector and a high output ceramic source coupled

with an attenuated total reflectance (ATR) mode with high throughput monolithic diamond and ZnSe. The spectral domain is 650–4000 cm^{-1} with a resolution of 0.7 cm^{-1} .

5.2.5 ^1H and ^{13}C NMR Experiments

The proton ^1H and carbon ^{13}C NMR spectroscopy analyses were performed using a Bruker AVI400 spectrometer operating at 400.1 MHz and 100.6 MHz for proton and carbon, respectively. Toluene- d_8 (99.96 atom% D) was used as received from Sigma-Aldrich as solvent for NMR tests. The proton data were acquired using a 3.96 s acquisition time, a 8278 Hz sweep width and a relaxation time of 1.0s. The carbon spectra were collected with a 1.30 s acquisition time, a 25125 Hz sweep width, and a relaxation time of 2.0 s. The carbon spectra resulted from 1024 scans. Chemical shifts (δ) presented here are reported relative to tetramethyl silane (TMS) used as internal standard.

5.2.5.1 NMR Analysis procedure

The approaches proposed by Speight[24], [25] and Gillet[26] were employed in this study to analyse the band area and interpret both the ^1H and ^{13}C NMR spectra which were used to determine the percentage of each type of proton and carbon. The structural parameters of the asphaltenes i.e. n , average number of carbons per chain, number of aliphatic chain by aromatic hexagon, aromatic size ratio C_p/C_{ar} (C_p and C_{ar} are aromatic peripheral and aromatic carbon atoms, respectively), and aromaticity were obtained using NMR spectra analysis.

5.3 Results and Discussion

5.3.1 HPHT-QCM Results

The QCM resonant frequency (RF) was monitored during the natural gas and CO_2 injection to determine the asphaltene precipitation onset point (AOP) and respective gas oil ratio (GOR). The AOP and related GOR can be changed depending on the type of injected gas which is mixed with crude oil inside the QCM cell. The obtained results for AOP determination and the effect of injected CO_2 and natural gas on asphaltene deposition rate onto the QCM surface are presented in Figure 5.2.

As can be seen in Figure 5.2a, the asphaltene onset point was detected at ~1009 psia and ~156 scf/bbl GOR and ~1964 psia and ~324 scf/bbl GOR due to injection of CO₂ and natural gas, respectively, at 60 °C and 500 rpm in-situ mixing. Therefore, the AOP/GOR is lower for the utilised crude oil with injected CO₂ compared to natural gas.

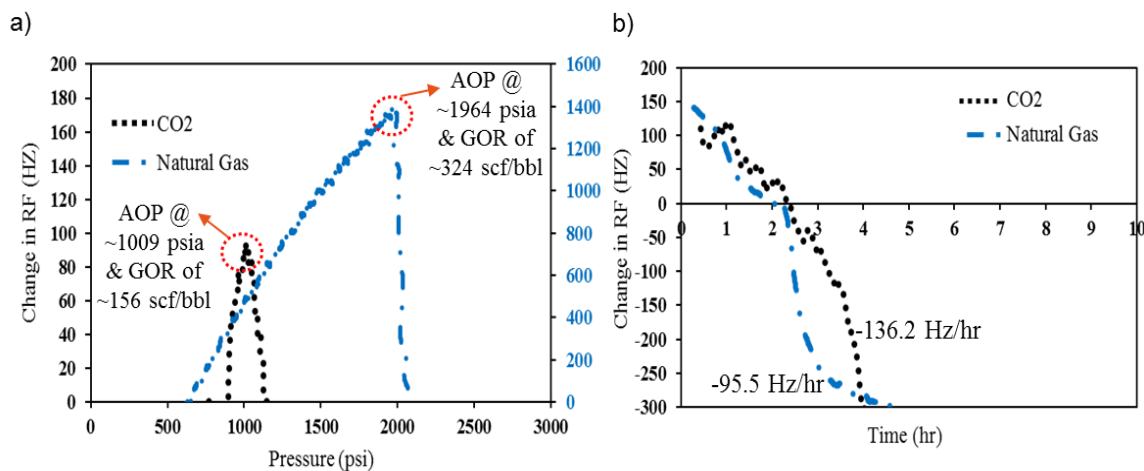


Figure 5. 1. HPHT-QCM results at 60 °C for a) measurement of AOP and respective GOR and b) determination of asphaltene deposition rate, due to natural gas and CO₂ injection.

The results regarding RF reduction versus time for two tests with different injected gases are plotted in Figure 5.2b, which represents the influence of gas type on asphaltene deposition rate after the AOP. The results reveal that the CO₂ worsened the deposition rate after detection of AOP. The deposition rates for different injected gases are -95.5 Hz/hr for natural gas and -136.2 Hz/hr for CO₂. The CO₂ solubility in the resins could increase with an increase in pressure and decrease with an increase in temperature. The solubility of CO₂ in some resins is lower compared to some other resins which is mainly owing to smaller accessible free volume as a result of higher molecular weight of those particular resins.

5.3.2 Characterisation of CO₂ and n-C₇ Asphaltenes

The elementary analysis data for both n-C₇ and CO₂ induced asphaltenes is presented in Table 5.1.

Table 5. 1. Chemical Composition of Asphaltenes (w/w%)

Asphaltenes	C	H	S	O	N _H /N _C *
-------------	---	---	---	---	----------------------------------

n-C ₇	83.19	6.63	7.12	3.06	0.96
CO ₂	85.17	7.19	2.85	4.55	1.01

* H/C is the atomic ratio of hydrogen and carbon.

The value of the atomic ratio $N_H/N_C=1.01$ for CO₂-asphaltenes indicates a lower aromaticity compared to 0.96 obtained with n-C₇ asphaltenes from the same parent crude oil used in this study. Moreover, the significant differences were found with the oxygen and sulphur contents being 3.06 wt% (O) and 7.12 wt% (S) for n-C₇ asphaltene and 4.55 wt% (O) and 2.85 wt% (S) for CO₂-asphaltene. The high polarity of the CO₂-asphaltene reveals that some of its oxygen contents are contributed in structure of acids and/or ketone fractions.

5.3.2.1 ESEM/EDX analysis

Figures 5.3 and 5.4 present the ESEM/EDX analysis results of the two different asphaltenes (n-C₇ and CO₂-asphaltenes respectively). The ESEM micrographs were analysed by ImageJ software. Figure 5.3a shows smooth surfaces with irregular shape of asphaltenes on them and also indicates the presence of agglomerate asphaltene particles. It should be noted that these agglomerate particles could be formed due to higher aromaticity of n-C₇ asphaltene. Asphaltene particles in Figure 5.3a have two different sizes: small sized particles with an average length of $\sim 3.3 \mu\text{m}$, and large sized particles of $\sim 11.2 \mu\text{m}$.

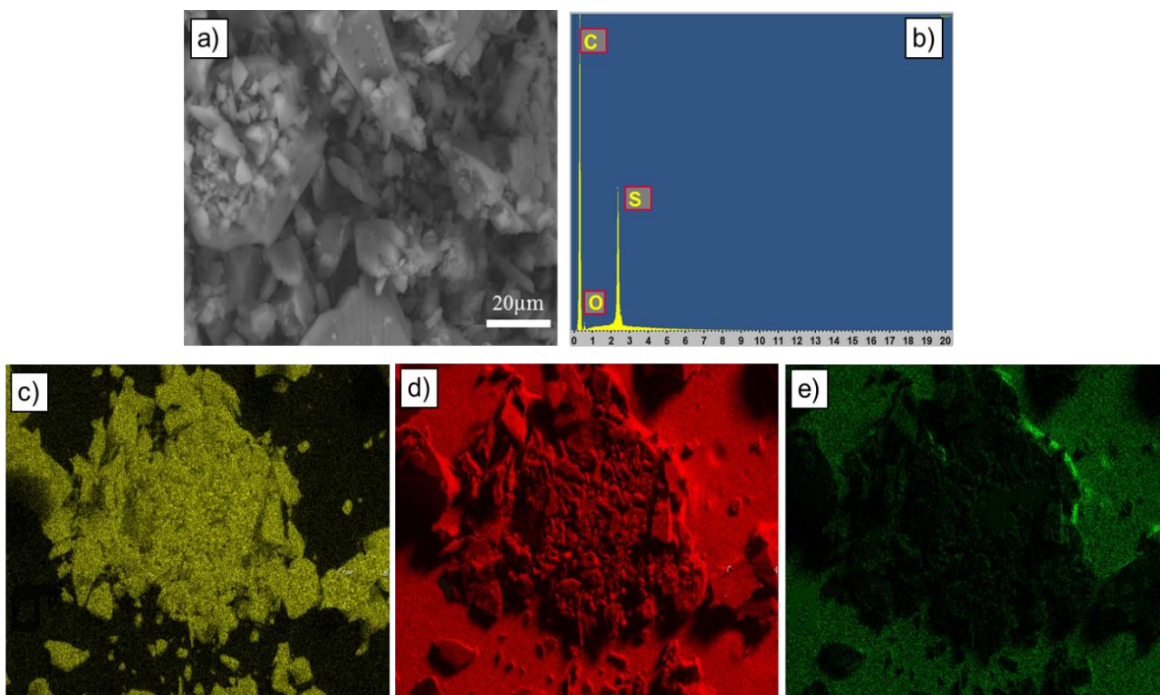


Figure 5. 2. ESEM/EDX elemental mapping of n-C₇-asphaltenes by ESEM: (a) micrograph of asphaltene, (b) elemental analysis, (c) S *k* mapping, (d) C *k* mapping, (e) O *k* mapping

As can be seen in Figure 5.4a, CO₂-asphaltenes have a porous structure with cavities having two different size categories: one category is a small sized group (~3.7 μm) and the second one is big sized group (~10.4 μm). The porous structure of CO₂-asphaltene could be formed during separation of adsorbed resins moiety from asphaltene surfaces. The asphaltenes tend to adsorb resin microparticles, which would be removed from asphaltene surface after washing with solvents, causing the occurrence of cavities. Cavities in n-C₇ asphaltenes are not as evident as in the aforementioned asphaltenes induced by CO₂ injection.

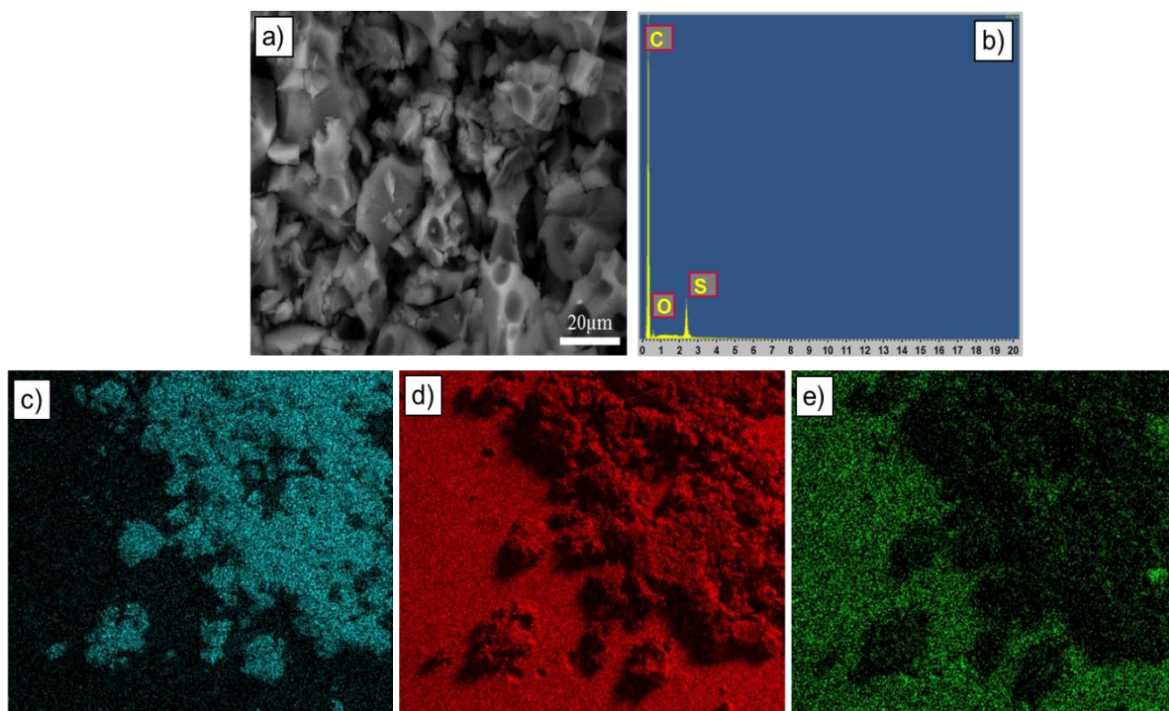


Figure 5. 3. ESEM/EDX elemental mapping of CO₂-asphaltenes by ESEM: (a) micrograph of asphaltene, (b) elemental analysis, (c) S k mapping, (d) C k mapping, (e) O k mapping

This alteration in morphology of studied asphaltenes is mainly because of i) the temperature at which the asphaltene was precipitated out of the solution, ii) type of precipitants which are n-C₇ and CO₂ in this work, and consequent reaction intensity, and iii) the rate of asphaltene precipitation and aggregation phenomena. Qualitative analysis of the composition and elemental mapping of the n-C₇ and CO₂-asphaltenes are presented in Figure 5.3 (b, c, d, e) and Figure 5.4 (b, c, d, e), respectively. For the two asphaltene types, carbon (C), sulphur (S), and oxygen (O) are the constructor elements (as given in Table 5.1) and evenly distributed throughout the samples. The oxygen content in CO₂-asphaltenes was increased from 3.06 to 4.55 wt% respect to n-C₇ asphaltenes. The interactions between CO₂ and asphaltene nanoaggregates during gas injection process could result in higher quantity of oxygen in CO₂ induced asphaltenes. In the case of n-C₇ asphaltenes, the sulphur content was increased compared to CO₂-asphaltenes. More ESEM micrographs of n-C₇ and CO₂-asphaltenes with different magnifications are presented in the Appendix 1 (Figures A1.1 and A1.2).

5.3.2.2. FTIR Spectroscopy

The full FTIR spectra of two n-C₇ and CO₂ asphaltene samples are shown in Figure 5.5a. The corresponding major spectral bands are similar to typical asphaltene spectra reported in the literature[27], [28]. In the full spectra, Figure 5.5a, there is a distinct difference between the n-C₇ and CO₂ asphaltenes in the range of 700-3700 cm⁻¹. The corresponding major vibrational assignments are given in Table A1.2 (Appendix 1).

The related structures are also given in Figure 5.5b. These major bands are seen in all spectra except that three adjacent hydrogens at 760 cm⁻¹ poses to be incorporated into the 4H peak at 745 cm⁻¹ for n-C₇ asphaltene. The clear peaks at ~1030 cm⁻¹ indicates the contribution of S=O and C-S bonds in two asphaltene structures. As can be seen in Figure 5.5b, there is a peak related to alkyl chains with more than four carbons at 700–720 cm⁻¹ for both asphaltenes. This reveals that asphaltenes have low content of long alkyl chains attached to their structures. As seen in Figure 5.5c, the C=C aromatic stretching peaks at ~1600 cm⁻¹ and ~1650 cm⁻¹ are observed for n-C₇ asphaltene and CO₂-asphaltene, respectively. The peak of C=O in carboxylic acids appears for CO₂-asphaltene at 1760 cm⁻¹, which cannot be seen for n-C₇ asphaltene. The X-H stretch region, where X is N, O, and S, between 3150 and 3700 cm⁻¹ is presented in Figure 5.5d.

A broad envelope is observed for CO₂-asphaltene which indicates presence of hydrogen bonding dominated by O-H. The CH₃/CH₂ stretch region from 2600 to 3200 cm⁻¹ is shown in Figure 5.5e. With zooming in on this region, it can be found that some C_{aro}-CH₃ at ~2730 cm⁻¹ is attached to condensed aromatic structure of n-C₇ asphaltene.

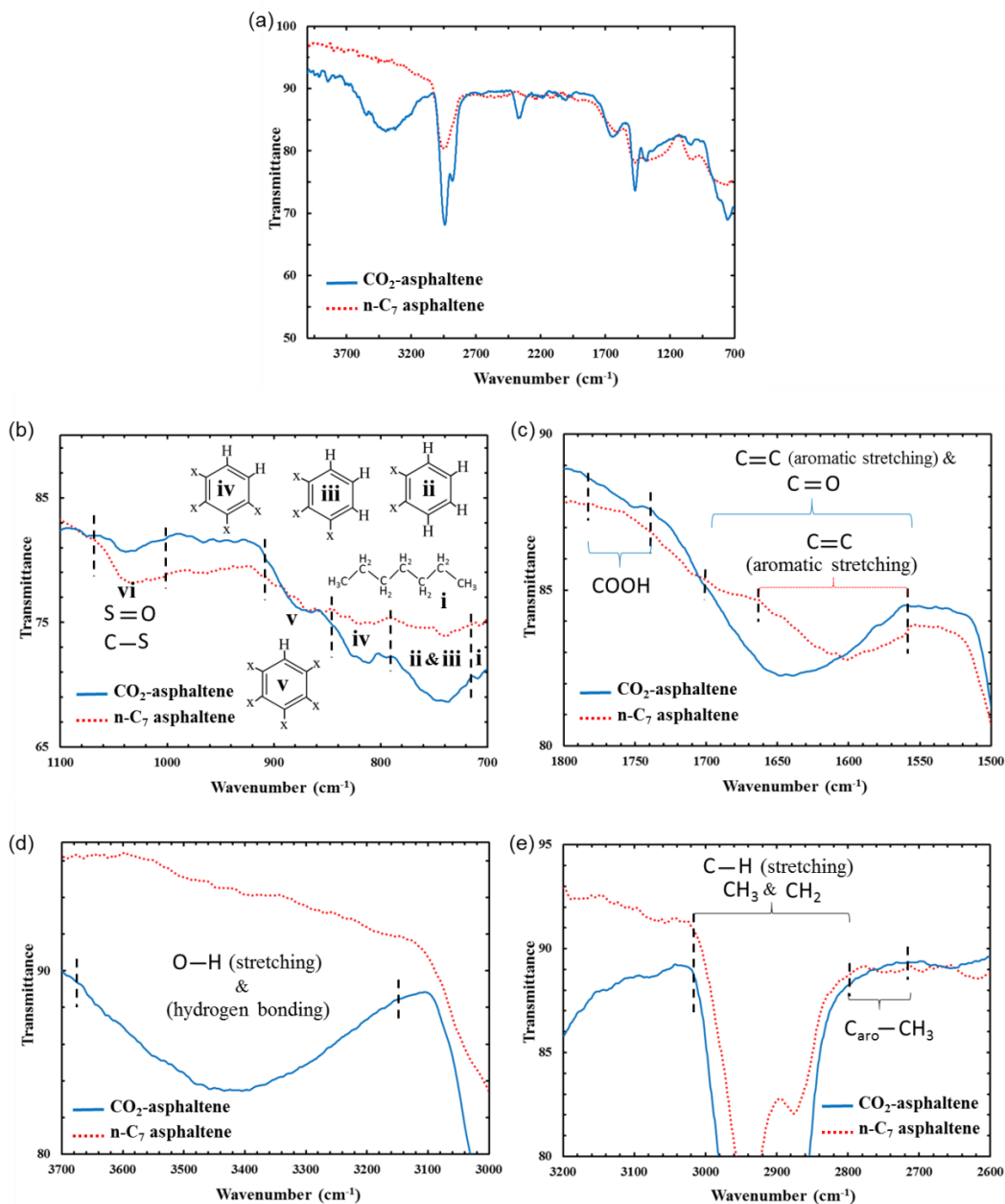


Figure 5.4. a) Full FTIR spectra of n-C₇ and CO₂-asphaltenes. b) Zoomed in plot of the aromatic C-H region. Sulfoxide can be observed for both asphaltenes. Presence of C-S and long alkyl chains are intense for n-C₇ and CO₂-asphaltene, respectively. c) Comparison of spectra of two studied asphaltenes in the range of 1500-1800 cm⁻¹. It is found that the n-C₇ asphaltene is dominated thoroughly by aromatic C=C stretch vibrations at ~1600 cm⁻¹. (R-COOH) functional group can be detected in CO₂ induced asphaltene. d) The spectra of free and hydrogen bonded O-H group. The CO₂-asphaltenes shows a distinct content of O-H at ~3440 cm⁻¹ which cannot be observed as an accountable moiety in the n-C₇ asphaltene. e) The C-H stretch region for CH₂/CH₃ in alkyl features. The C-H vibrations in methyl groups attached to aromatic cores is seen in n-C₇ asphaltene structure.

Apart from the mentioned distinct differences, there are small differences related to branching of alkyl chains, such as in peak positions at $\sim 1380\text{ cm}^{-1}$, as well as in the merged peak for the CH_3/CH_2 deformation at $\sim 1460\text{ cm}^{-1}$. These data reveal that the CO_2 -asphaltene obtained from HPHT-QCM test has less condensed aromatic structure (not very significant) and contain a higher concentration of oxygen contained functional groups attached to its aliphatic chains compared to studied n- C_7 asphaltenes.

5.3.2.3. ^1H and ^{13}C NMR Analysis

In this study, ^1H and ^{13}C NMR spectra are used to show the complex structure of n- C_7 and CO_2 - asphaltenes. The ^1H NMR spectral peak shifts can recognise various types of hydrogens in the asphaltene molecules[8], [11]. The assignments of hydrogens, which are named as H_{ar} , H_{α} , H_{β} , and H_{γ} , in respective parts per million ranges and integral intensities are given in Table A1.3 (Appendix 1). The ^1H NMR spectra of n- C_7 and CO_2 -asphaltenes are shown in figures 5.6a and b, respectively.

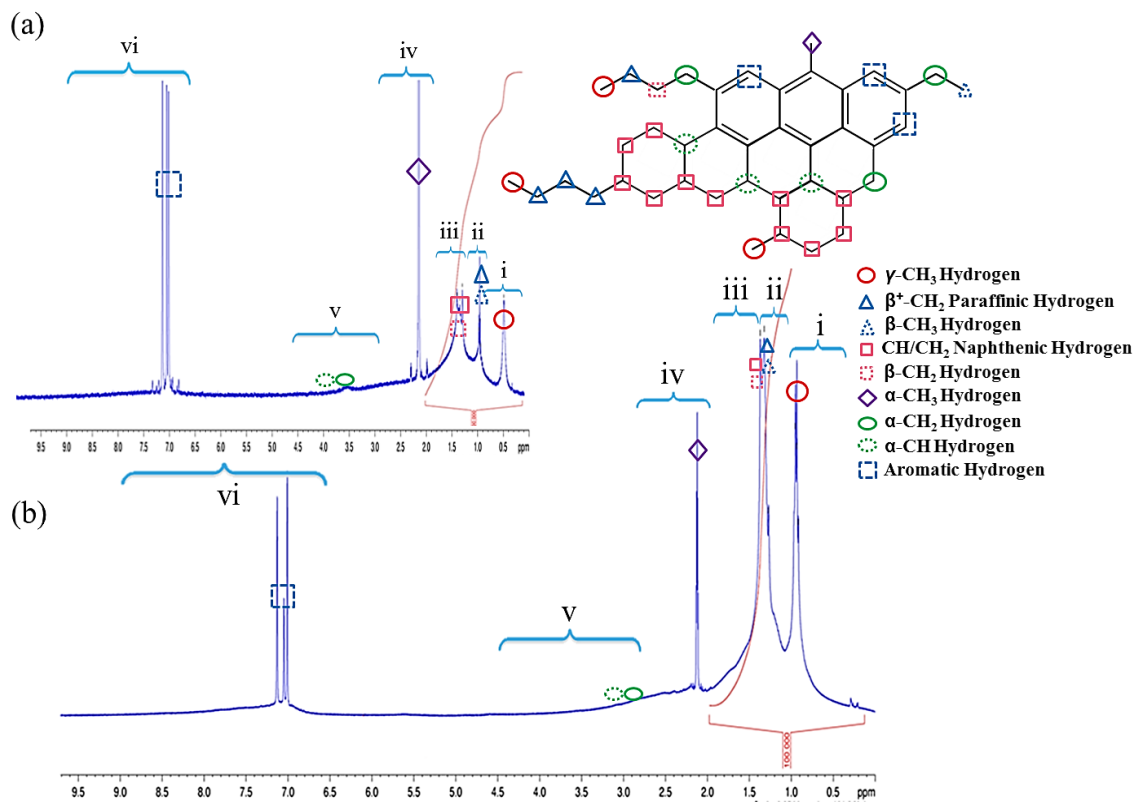


Figure 5. 5. Representative proton 400.1 MHz NMR spectrum of a) n- C_7 asphaltene, b) CO_2 -asphaltene

The peaks related to hydrogens on β -position (CH/CH₂) to aromatic rings and hydrogens of naphthenic –CH/CH₂ are observed at 2.00–1.40 ppm (integral region iii), β -CH₃ and β^+ -CH₃ paraffinic hydrogens appeared at 1.40–1.00 ppm (integral region ii), and γ -CH₃ hydrogens to aromatic rings appeared at 0.95-0.30 (integral region i). In Figure 5.6, the integral regions iv and v have been assigned to α -CH₃ and α -CH/CH₂ hydrogens at 2.90-2.00 and 4.50-2.90 ppm, respectively. The strong peaks at 9.00-6.50 ppm are attributed to aromatic hydrogens (integral region vi).

Figure 5.7 shows ¹³C NMR spectra of studied n-C₇ and CO₂ asphaltenes. The spectra obtained from ¹³C NMR experiments is divided into two main regions. The first one in the range 0-70 ppm is assigned to the aliphatic carbons while the second ranging from 90 to 180 ppm assigns to the aromatic carbon resonance. The assignments of ¹³C chemical shifts in asphaltenes NMR spectra and related integral intensities are presented in Table A1.4 (Appendix 1).

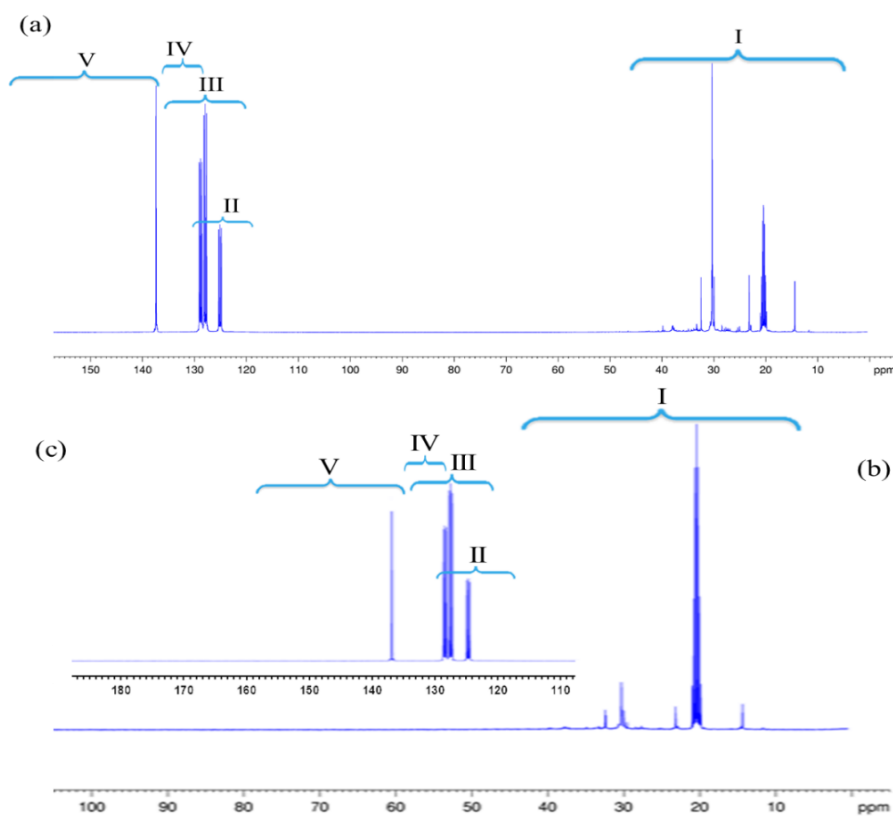


Figure 5. 6. Representative carbon 100.6 MHz NMR spectrum for a) n-C₇ asphaltene, b) aliphatic domain of CO₂-asphaltene, and c) aromatic domain of CO₂-asphaltene.

An integration of ¹H and ¹³C NMR spectra at different chemical shifts ranges enable us to determine some average structural parameters, such as f_a the aromaticity factor, n the average number of carbons per alkyl side chain, A_s the percentage of peripheral aromatic carbon substitution, Φ shape factor of aromatic sheet and r the number of substituent rings based on procedures described by Speight[24] and others[25], [26].

The obtained results presented in Table 5.2 reveal that the n-C₇ and CO₂ asphaltene molecules have aromaticity factor of 0.62 and 0.54, respectively, which is described as the ratio of aromatic carbons (C_{ar}) to sum of aliphatic and aromatic carbons ($C_{ar} + C_{al}$). The average number of carbon atoms in alkyl side chains are 3.8 carbons for n-C₇ asphaltenes and 4.1 carbons for CO₂ induced ones. The values of A_s (~33.6 and ~36.4 %) and of Φ (0.49 and 0.55) for n-C₇ and CO₂ asphaltenes show presence of high ratio condensation of aromatic rings in their molecular structures. Therefore, the n-C₇ asphaltenes are determined

to be relatively more aromatic compared to CO₂ induced asphaltenes which are obtained from HPHT-QCM tests.

Table 5. 2. Average molecular parameters of n-C₇ and CO₂-asphaltene molecules derived from the integrated ¹H and ¹³C NMR analysis

Parameter	n-C ₇ asphaltene	CO ₂ -asphaltene
C _{ar}	26.1	23.5
C _{al}	16.2	19.2
C _p	12.8	12.9
<i>f</i> _a	0.62	0.54
Φ	0.49	0.55
<i>n</i>	3.8	4.1
C _{sub}	4.3	4.7
C _{us}	8.5	8.2
A _s	33.6	36.4
<i>r</i>	0.22	0.16
R _{na}	0.96	0.77
C _{na}	3.36	2.69
H _{ar} (%)	21.1	19.9
H _α (%)	20.9	19.5

H_{β} (%)	38.3	46.6
H_{γ} (%)	19.8	14.1

C_{ar} , number of aromatic carbons; C_{al} , number of aliphatic carbons; C_p , number of peripheral aromatic carbons; f_a , aromaticity factor; Φ (C_p/C_{ar}), shape factor of aromatic sheet n , average number of carbons per alkyl side chain; C_{sub} , number of substituted aromatic carbons; C_{us} , number of unsubstituted aromatic carbons; A_s , percent of substitution of peripheral aromatic carbons; r , number of substituent rings; R_{na} , total number of naphthenic rings per molecule; C_{na} , total number of naphthenic carbons per molecule.

C_p/C_{ar} value is related to the total number of rings and the condensation degree of aromatic systems. The aromatic structures for different C_p/C_{ar} ratios presented in Figure 5.8 are ones proposed by Ruiz-Morales[29] for asphaltene molecules which were obtained using fluorescence and quantum determinations. As can be seen in Figure 5.8, the reduced C_p/C_{ar} value shows the presence of larger aromatic core; i.e. it is more condensed.

The obtained values of $C_p/C_{ar} = 0.49$ and 0.55 for n-C₇ and CO₂-asphaltenes reveal that the numbers of aromatic rings are 7–9 and 6–7 per sheet for n-C₇ and CO₂-asphaltenes, respectively, in case of one fragment molecule. By utilising fluorescence tests [30], [31] and quantum calculation [29], Ruiz-Morales [29] indicated that some aromatic cores could not possibly be included in asphaltene molecular structures. It was also inferred that there are 5–10 benzoic rings in each aromatic core region in asphaltene molecules. Based on these investigations, we are able to suggest the most probable aromatic structures for both n-C₇ and CO₂-asphaltenes which are presented in figures 5.9 and 5.10, respectively.

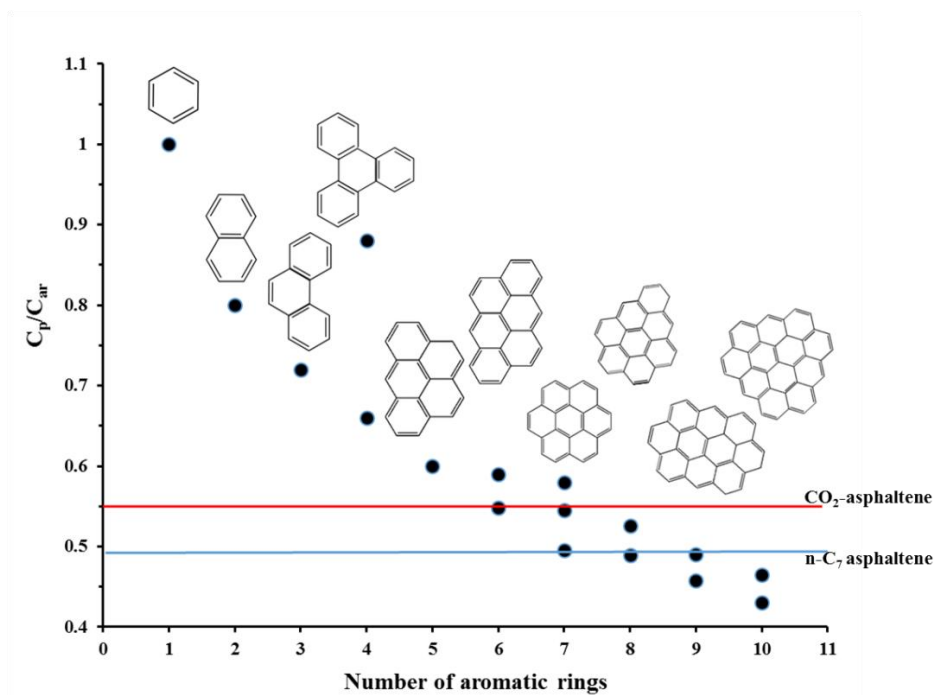


Figure 5. 7. The determined C_p/C_{ar} ratio as a function of total number of aromatic rings in n-C₇ and CO₂-asphaltenes molecular structures.

The circular structures, coronene 7 fused aromatic rings, and benzo-perylene/anthanthrene 6 aromatic rings might be the best structural candidates of the aromatic core regions for n-C₇ and CO₂-asphaltenes. On the other hand, based on FTIR and EDX analysis results, on average there are 1 and 2 sulphur atoms in aromatic structures of n-C₇ and CO₂-asphaltene molecules, respectively.

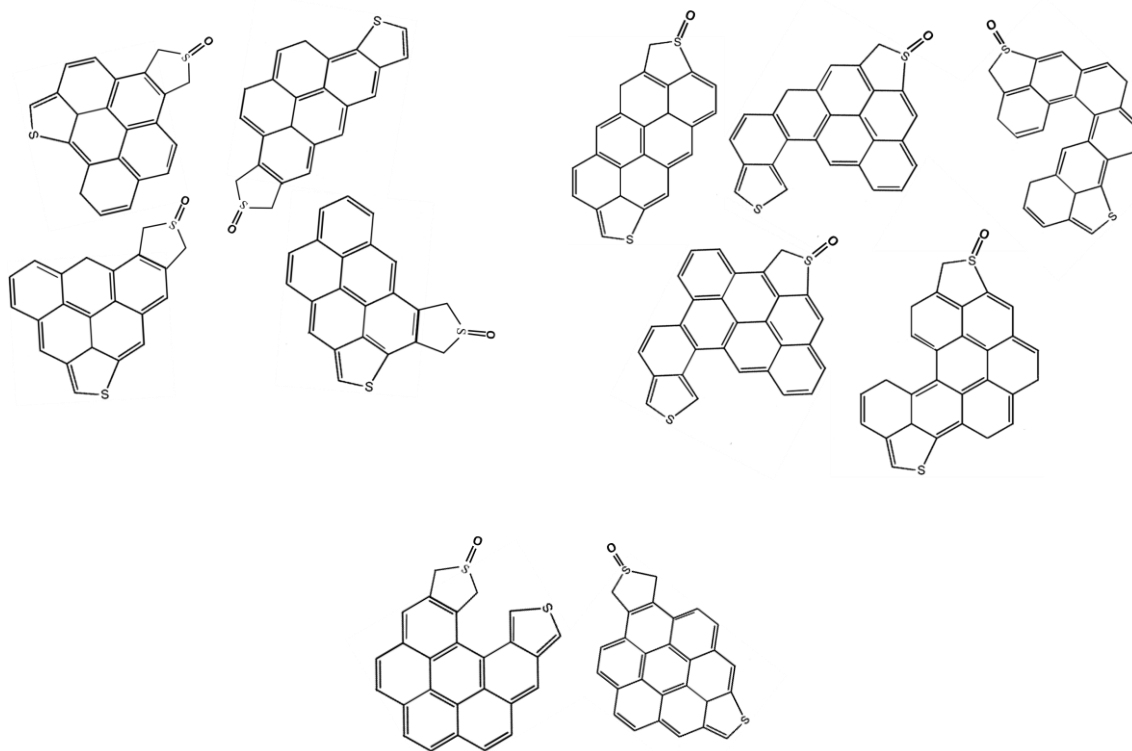


Figure 5. 8. Proposed aromatic structures for studied n-C₇ asphaltenes based on integrated ¹H and ¹³C NMR results.

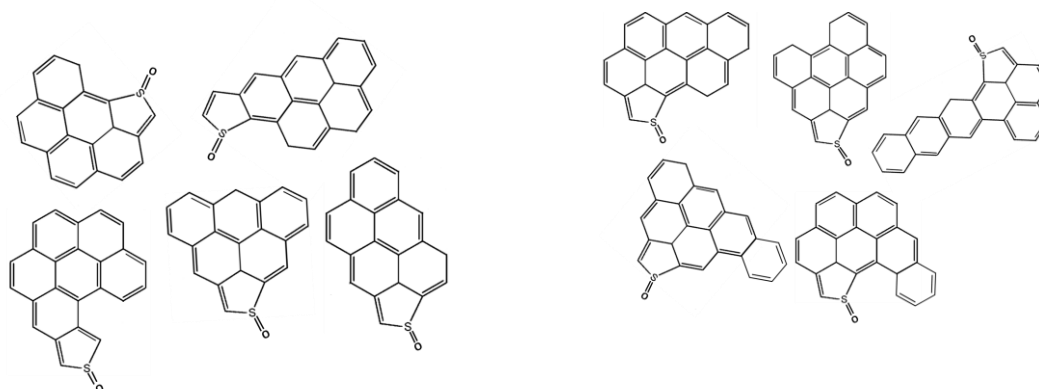


Figure 5. 9. Proposed aromatic structures for studied CO₂-asphaltenes based on integrated ¹H and ¹³C NMR results.

Both of two studied asphaltenes have sulfoxide functional group in their fused ring regions. All average molecular parameters, aromaticity factors, addressed functional groups and proposed aromatic structures of studied asphaltenes obtained from utilised analytical techniques are in agreement and in the same order with ones determined from solid state cross polarization, variable cross polarization in the literature[32]–[35].

5.4 Conclusions

In this chapter, we explore the differences between the molecular structures of n-C₇ and CO₂-asphaltenes obtained under HPHT-QCM conditions. Based on the results, it has been observed that the HPHT-QCM asphaltene deposits are structurally, morphologically and compositionally different from n-C₇ precipitated asphaltenes. Two morphologies were observed by ESEM micrographs: (1) porous structures with cavities (CO₂-asphaltenes), and (2) smooth surfaces with variously sized asphaltene particles on them (n-C₇ asphaltenes). The recognised differences in morphology are because of the type of precipitant, n-C₇ and CO₂, and test conditions utilised for asphaltene separation, which results in precipitation/aggregation kinetics changes and removal of resins from the asphaltenes. It was also observed that the CO₂-asphaltenes are richer in oxygen containing moieties which play a critical role in asphaltene-inhibitor and asphaltene-solid surface interactions during the deposition process. The studied n-C₇ asphaltene has a relatively larger aromatic core which results in larger stacking compared to CO₂ induced asphaltene from HPHT-QCM test. On the other hand, the π–π stacking between aromatic cores and

hydrogen bonding between functional groups are the main drivers of asphaltene precipitation and aggregation phenomena and also the inhibition interactions between asphaltene and inhibitor/dispersant molecules. Therefore, this work shows that the differences in composition and molecular structure of various asphaltenes obtained under HPHT and ambient conditions would need specific types of chemistries which can appropriately contribute to the deposition tendency of that particular asphaltene at specified operating condition. Some inhibitors are more effective with the least aromatic structure of asphaltene in terms of kinetics, whereas they can be more effective with more aromatic asphaltenes in terms of thermodynamic equilibrium. On the other hand, some chemicals have the highest efficiency in terms of asphaltene instability onset point with the lowest metal contents and the highest average number of carbons per alkyl side chain in asphaltenes molecular structures.

We infer that a reliable technique is required for oilfield chemical industry to truly evaluate inhibitor chemistries and their effects on deposition rate based on respective interactions which could be actually differed from n-C₇ to CO₂ injection.

5.5 References

- [1] E. Buenrostro-Gonzalez, H. Groenzin, C. Lira-Galeana, and O. C. Mullins, "The overriding chemical principles that define asphaltenes," *Energy & Fuels*, vol. 15, no. 4, pp. 972–978, 2001.
- [2] A. M. McKenna, A. G. Marshall, and R. P. Rodgers, "Heavy petroleum composition. 4. Asphaltene compositional space," *Energy & fuels*, vol. 27, no. 3, pp. 1257–1267, 2013.
- [3] M. Sedghi, L. Goual, W. Welch, and J. Kubelka, "Effect of asphaltene structure on association and aggregation using molecular dynamics," *J. Phys. Chem. B*, vol. 117, no. 18, pp. 5765–5776, 2013.
- [4] H. H. Ibrahim and R. O. Idem, "Interrelationships between Asphaltene Precipitation Hydrocarbon) -Induced Asphaltene Precipitation," *Energy*, no. 9, pp. 1038–1048, 2004.
- [5] J. Christopher, A. S. Sarpal, G. S. Kapur, A. Krishna, B. R. Tyagi, M. C. Jain, S. K. Jain, and A. K. Bhatnagar, "Chemical structure of bitumen-derived asphaltenes by nuclear magnetic resonance spectroscopy and X-ray diffractometry," *Fuel*, vol. 75, no. 8, pp. 999–1008, 1996.

- [6] F. Trejo, J. Ancheyta, T. J. Morgan, A. A. Herod, and R. Kandiyoti, "Characterization of asphaltenes from hydrotreated products by SEC, LDMS, MALDI, NMR, and XRD," *Energy & Fuels*, vol. 21, no. 4, pp. 2121–2128, 2007.
- [7] F. Betancourt Cardozo, E. Avella Moreno, and C. A. Trujillo, "Structural Characterization of Unfractionated Asphalts by ¹H NMR and ¹³C NMR," *Energy & Fuels*, vol. 30, no. 4, pp. 2729–2740, 2016.
- [8] W. Qing, J. Chunxia, G. Jianxin, and G. Wenxue, "¹H NMR and ¹³C NMR Studies of Oil from Pyrolysis of Indonesian Oil Sands," *Energy & Fuels*, vol. 30, no. 3, pp. 2478–2491, 2016.
- [9] F. Trejo, J. Ancheyta, and M. S. Rana, "Structural characterization of asphaltenes obtained from hydroprocessed crude oils by SEM and TEM," *Energy & Fuels*, vol. 23, no. 1, pp. 429–439, 2009.
- [10] J. C. Poveda and D. R. Molina, "Average molecular parameters of heavy crude oils and their fractions using NMR spectroscopy," *J. Pet. Sci. Eng.*, vol. 84, pp. 1–7, 2012.
- [11] A. Hauser, F. AlHumaidan, and H. Al-Rabiah, "NMR investigations on products from thermal decomposition of Kuwaiti vacuum residues," *Fuel*, vol. 113, pp. 506–515, 2013.
- [12] D. Liu, Z. Li, Y. Fu, Y. Zhang, P. Gao, C. Dai, and K. Zheng, "Investigation on asphaltene structures during Venezuela heavy oil hydrocracking under various hydrogen pressures," *Energy & Fuels*, vol. 27, no. 7, pp. 3692–3698, 2013.
- [13] A. A. Herod, K. D. Bartle, T. J. Morgan, and R. Kandiyoti, "Analytical methods for characterizing high-mass complex polydisperse hydrocarbon mixtures: an overview," *Chem. Rev.*, vol. 112, no. 7, pp. 3892–3923, 2012.
- [14] R. P. Rodgers and A. M. McKenna, "Petroleum analysis," *Anal. Chem.*, vol. 83, no. 12, pp. 4665–4687, 2011.
- [15] G. C. Klein, S. Kim, R. P. Rodgers, A. G. Marshall, and A. Yen, "Mass spectral analysis of asphaltenes. II. Detailed compositional comparison of asphaltenes deposit to its crude oil counterpart for two geographically different crude oils by ESI FT-ICR MS," *Energy & fuels*, vol. 20, no. 5, pp. 1973–1979, 2006.
- [16] L. A. Stanford, R. P. Rodgers, A. G. Marshall, J. Czarnecki, and X. A. Wu, "Compositional characterization of bitumen/water emulsion films by negative-and positive-ion electrospray ionization and field desorption/ionization Fourier transform ion cyclotron resonance mass spectrometry," *Energy & fuels*, vol. 21, no. 2, pp. 963–972, 2007.
- [17] L. A. Stanford, R. P. Rodgers, A. G. Marshall, J. Czarnecki, X. A. Wu, and S. Taylor, "Detailed elemental compositions of emulsion interfacial material versus

- parent oil for nine geographically distinct light, medium, and heavy crude oils, detected by negative-and positive-ion electrospray ionization Fourier transform ion cyclotron resonanc,” *Energy & fuels*, vol. 21, no. 2, pp. 973–981, 2007.
- [18] T. M. Schaub, D. W. Jennings, S. Kim, R. P. Rodgers, and A. G. Marshall, “Heat-exchanger deposits in an inverted steam-assisted gravity drainage operation. Part 2. Organic acid analysis by electrospray ionization Fourier transform ion cyclotron resonance mass spectrometry,” *Energy & fuels*, vol. 21, no. 1, pp. 185–194, 2007.
- [19] A. Standard, “D6560-12,” *Test Method Determ. Asph. (Heptane Insolubles) Crude Pet. Pet. Prod. ASTM Int. West Conshohocken, PA*, 2012.
- [20] M. L. Chacon-Patino, S. J. Vesga-Martinez, C. Blanco-Tirado, J. A. Orrego-Ruiz, A. Gomez-Escudero, and M. Y. Combariza, “Exploring occluded compounds and their interactions with asphaltene networks using high-resolution mass spectrometry,” *Energy & Fuels*, vol. 30, no. 6, pp. 4550–4561, 2016.
- [21] E. Joonaki, R. Burgass, A. Hassanpouryouzband, and B. Tohidi, “Comparison of Experimental Techniques for Evaluation of Chemistries against Asphaltene Aggregation and Deposition: New Application of High-Pressure and High-Temperature Quartz Crystal Microbalance,” *Energy & Fuels*, 2017.
- [22] H. R. Erfani Gahrooei, M. H. Ghazanfari, and F. Karimi Malekabadi, “Wettability alteration of reservoir rocks to gas wetting condition: A comparative study,” *Can. J. Chem. Eng.*, vol. 96, no. 4, pp. 997–1004, 2018.
- [23] H. R. E. Gahrooei and M. H. Ghazanfari, “Toward a hydrocarbon-based chemical for wettability alteration of reservoir rocks to gas wetting condition: Implications to gas condensate reservoirs,” *J. Mol. Liq.*, vol. 248, pp. 100–111, 2017.
- [24] J. G. Speight, “A structural investigation of the constituents of Athabasca bitumen by proton magnetic resonance spectroscopy,” *Fuel*, vol. 49, no. 1, pp. 76–90, 1970.
- [25] J. G. Speight, *The desulfurization of heavy oils and residua*. CRC Press, 1999.
- [26] S. Gillet, P. Rubini, J.-J. Delpuech, J.-C. Escalier, and P. Valentin, “Quantitative carbon-13 and proton nuclear magnetic resonance spectroscopy of crude oil and petroleum products. I. Some rules for obtaining a set of reliable structural parameters,” *Fuel*, vol. 60, no. 3, pp. 221–225, 1981.
- [27] M. Daaou, A. Modarressi, D. Bendedouch, Y. Bouhadda, G. Krier, and M. Rogalski, “Characterization of the nonstable fraction of Hassi– Messaoud Asphaltenes,” *Energy & Fuels*, vol. 22, no. 5, pp. 3134–3142, 2008.
- [28] V. Calemma, P. Iwanski, M. Nali, R. Scotti, and L. Montanari, “Structural characterization of asphaltenes of different origins,” *Energy & Fuels*, vol. 9, no. 2, pp. 225–230, 1995.

- [29] Y. Ruiz-Morales, "Molecular orbital calculations and optical transitions of PAHs and asphaltenes," *Asph. Heavy Oils, Pet.*, pp. 95–137, 2007.
- [30] E. Y. Sheu and D. A. S. Asphaltenes, *Fundamentals and Applications*. Springer, 1995.
- [31] O. C. Mullins, E. Y. Sheu, A. Hammami, and A. G. Marshall, *Asphaltenes, heavy oils, and petroleomics*. Springer Science & Business Media, 2007.
- [32] T. Fergoug and Y. Bouhadda, "Determination of Hassi Messaoud asphaltene aromatic structure from 1 H & 13 C NMR analysis," *Fuel*, vol. 115, pp. 521–526, 2014.
- [33] Y. Bouhadda, P. Florian, D. Bendedouch, T. Fergoug, and D. Bormann, "Determination of Algerian Hassi-Messaoud asphaltene aromaticity with different solid-state NMR sequences," *Fuel*, vol. 89, no. 2, pp. 522–526, 2010.
- [34] B. Schuler, S. Fatayer, G. Meyer, E. Rogel, M. Moir, Y. Zhang, M. R. Harper, A. E. Pomerantz, K. D. Bake, M. Witt, D. Peña, J. D. Kushnerick, O. C. Mullins, C. Ovalles, F. G. A. van den Berg, and L. Gross, "Heavy Oil Based Mixtures of Different Origins and Treatments Studied by Atomic Force Microscopy," *Energy & Fuels*, vol. 31, no. 7, pp. 6856–6861, Jul. 2017.
- [35] B. Schuler, G. Meyer, D. Peña, O. C. Mullins, and L. Gross, "Unraveling the Molecular Structures of Asphaltenes by Atomic Force Microscopy," *J. Am. Chem. Soc.*, vol. 137, no. 31, pp. 9870–9876, Aug. 2015.

Chapter 6- Effects of Waxes and Respective Chemistries on Asphaltene Aggregation and Deposition Phenomena: Experimental and Modelling Studies

6.1 Introduction

Organic solid deposition is a serious challenge in oil industry from production to oil transportation and storage operations[1]. The paraffin wax can affect rheological properties and asphaltene phase behaviour in oleic phase through using wax components in asphalt industry (asphalt binder) and blending of different crude oils, or oil with light or heavy paraffinic compounds[2], [3]. From a chemical composition viewpoint, although the high molecular weight normal paraffins are the major moieties in wax deposits, long iso and cycloalkanes and high molecular weight polyaromates named asphaltenes are got existed as well[4]. On the other hand the asphaltenes, which are extracted from the oil tank deposits, encompass a large amount of waxes[5].

Paraffin wax is one of the main components of crude oil, that is well known as straight, ring formed, and/or branched alkanes with high carbon atom numbers, e.g. more than 18[6], [7]. Wax can cause serious challenges such as adhering to the pipeline surfaces and restricting flow. Additionally, it can lead to increasing viscosity, reducing flow, and finally increment of operation costs. The major concern is the formation/appearance of wax at the highest temperature at which the crystallization of wax can be occurred that is called wax appearance temperature (WAT)[8]. There are different experimental techniques that are utilised to determine the WAT such as light scattering (Near infra-red (NIR) and Ultraviolet (UV) spectroscopy), cross polarization microscopy (CPM), differential scanning calorimetry (DSC), viscosity measurement using rheometer, and Quartz Crystal Microbalance (QCM)[9]–[12]. Pour point is defined by ASTM D97 as the lowest temperature, considerably lower than WAT, at which a liquid loses its flow characteristics due to an increase in the amount of precipitated wax[13]. Various chemistries can be employed as wax inhibitors, such as ethylene vinyl acetate copolymers, vinyl acetate olefin copolymers, alkylesters, polyalkylacrylates, alkyl phenols and alpha olefin copolymers, to

address related flow assurance issues through pour point depression and/or wax precipitates despersancy[14], [15].

The role of asphaltenes during the wax crystallization has not yet been well understood. The influence of asphaltenes has been explained contradictorily. Some researchers noted no significant interactions between wax and asphaltenes but asphaltenes may result in smaller interspersed wax crystals[16], [17], and others claimed that asphaltenes worsening the paraffin wax associated flow assurance problems[4], [18]. On the other hand, the data of asphaltene solubility in various light n-paraffins solvents, which was obtained from optical microscopy[19], light scattering[20], refractive index[21], and UV-vis spectrophotometry[22], has been widely available in the literature. Some asphaltenes properties like molecular mass distribution, density and solubility parameters are fitted and adjusted using aforementioned experimental data of asphaltene precipitation yield curves[23], [24]. Fitted curves can be utilised to estimate the asphaltene phase behaviour in other chemical compositions (changing precipitant agents) or different pressure and temperature conditions[25], [26]. Although the effect of different light n-paraffin solvents on the asphaltene phase behaviour has been greatly investigated, the potential effects of heavy paraffins and respective chemistries on asphaltene precipitation and deposition have not yet been unveiled. The aim of this study is to shed some light on the effect of waxes and related chemicals on asphaltene solubility and stability in crude oil. Firstly, the performance of various wax inhibitors in pour point reduction and WAT changes was evaluated using a rheometer for viscosity measurement. Then a long chain paraffin, as the main constituent of paraffinic crudes, and wax inhibitors were separately blended with crude oil at various concentrations, and their effects on the precipitation and deposition of asphaltenes of the treated oils were studied using our in-house QCM. A modelling investigation was also conducted for mechanistic understanding of observations from experiments. Asphaltenes precipitation from intact crude oil and paraffin wax added oils was thermodynamically modelled using perturbed chain statistical associating fluid theory (PC-SAFT) equation of state and a good agreement between experimental and modelling results was achieved.

6.2 Experimental Section

6.2.1 Materials

Experiments were conducted with an additive free crude oil from North Sea. Table 6.1 presents the properties of crude oil at 1 atm and 20 °C.

Table 6. 1. Properties of crude oil used in this study at 1 atm and 20 °C

f (g g ⁻¹) (n-C ₇ induced asphaltene)	ρ_o (g mL ⁻¹)	MW _o (g mol ⁻¹)	μ_o (cP)
0.0315	0.824	177	12.2

Four different wax inhibitors, which were commercially sourced and are denoted as INH.3, INH.4, INH.6, and INH.9 were utilised to treat the crude oil sample and investigate their effects on WAT, pour point, and asphaltene precipitation and deposition phenomena. Table 6.2 shows the composition and application of each inhibitor in oilfield chemical industry.

Table 6. 2. The composition suggested optimum dosage by supplier and application of each wax inhibitor

Wax Inhibitor	Chemistry	Characteristics	Proposed optimum dosage (ppm)
INH-3	Naphtalene, 1,2,4, Trimethylbenzene	Paraffin inhibitor	400
INH-4	Ethylene Vinyl Acetate polymer in aromatic solvent	Pour point depressant	400
INH-6	Mixture of surfactants and high molecular weight copolymers in aromatic solvent	Paraffin and asphaltene inhibitor	350
INH-9	propriety mixture of detergents and surfactants	Wax inhibitor	400

These chemistries were chosen based on their applications and contributions in mitigating wax challenges in industry and used as received from suppliers. For each chemical, the suppliers suggested dosage rate as the effective optimum concentration (as mentioned in Table 6.2) has been employed in this study. A commercial paraffin wax with melting temperature range of 54-56 °C supplied by Meade-King Robinson & Co Ltd was used in the recombination procedure, which is addition of a certain amount of wax to the crude oil, without any additional purification. Based on the distribution of representative paraffin waxes from generic paraffinic oils, the paraffin carbon number was chosen. For crude oil modification with paraffin waxes or chemicals, ~140 g of oil and the calculated mass of each paraffin wax/chemical were heated up to 60°C. Then, the paraffin was gently appended to the crude oil sample and homogenized for at least 1 hr, to eschew local concentration of the paraffin waxes or respective chemicals. The n-heptane (n-C₇; >99%), anhydrous toluene (Tol; >99.8%), and ethanol (≥99.8%) were acquired from Sigma-Aldrich and utilised in this study as received for washing purposes. For asphaltene deposition tests, the natural gas composition, which was injected to QCM cell for precipitating asphaltenes, was given in chapter 5.

6.2.2 Determination Rheological Properties, WAT and Wax Pour Point

Determination rheological properties of studied crude oil were conducted with temperature sweeps utilising a stress controlled rotational-type rheometer acquired from Anton Paar Ltd (Physica MCR 301). Almost all the measurements presented were carried out with the aid of 25mm diameter and 1° angle cone and plate geometry (Cones CP50-1). It comprises two circular plates with a space in between at which the reservoir fluid is placed. The bottom plate is fixed in rotational terms while the top is fitted to a shaft, floated on a sophisticated air bearing to keep friction to a very low level. It is then fitted to a sensitive electric motor to control the torque of the system while rotating/oscillating according to pre-set experimental parameters. The gap between the lower and upper test plates is set to be 0.1mm length to reach optimum measurement precision. The main reason to select this geometry was because of its capability to make uniform shear rate on the thorough measuring surface area. Hence, it could generate a homogeneous flow and eliminated particle migration alongside the measuring system. The sample size required to fill the

geometry was 22cc which would lead to reach thermal equilibrium easily due to having small amount of sample. The base plate temperature was accurately controlled within 0.1°C in the range of -40 °C to +200 °C with a Peltier system. An external temperature-regulated bath (Grant, GP200) was also connected to the rheometer, set at 20 °C to cover the routine testing regime range of -30 °C to 60 °C of the measuring system. After performing primary experiments, it was illustrated that shear rate of 10s⁻¹ would give us reproducible curves for the tested fluid. The capability of the Anton Paar, Physica MCR 301 rheometer using oscillatory mode at atmospheric conditions, enables us to determine the pour point with different applied stresses. Preliminary measurements proved that a frequency of 1.59 Hz with an amplitude of 25 μNm results in getting data close to the pour point obtained from ASTM procedure, at least for the studied oil sample. The rheometer software recorded all necessary oscillation data including deflection angle, loss modulus and storage modulus which were utilised to determine the pour point in a temperature sweep. The starting temperature and cooling rate for both WAT and pour point determination experiments are 50 °C and 1 °C/min, respectively. The destination temperature and shear rate for all WAT experiments are 5 °C and 10 s⁻¹, respectively. The accuracy of using rheometer for pour point measurement was found to be ±0.2 °C which is thoroughly acceptable in comparison with the ASTM D-97 method[27], [28].

6.2.3 QCM Tests

The deposition experiments should be conducted at natural gas contents above the asphaltene precipitation onset pressure. Herein the asphaltene onset pressure of precipitation was defined as the lowest natural gas content at which asphaltene precipitation/inclination in change in resonance frequency of QCM is first observed after a stepwise pressure increase process. High pressure-high temperature QCM (HPHT-QCM) technique was employed to determine the onsets and monitor the comparative deposition rate. The QCM technology has been used at Heriot-Watt Institute of Petroleum Engineering for over twenty years. Initial studies showed potential uses in some measurements relevant to the oil industry including wax, hydrates, asphaltenes, saturation pressure and scale. Further details are given in a paper by Burgass et al[12] and Joonaki et al[29], [30]. The principal of the measurement is to monitor changes in the Resonance

Frequency (RF), and electrical properties at RF, for a QCM surface submersed in the test fluid as a result of variations in the mass of the QCM or changes in the viscosity and density of the fluids brought about by changes in temperature and/or pressure. In this study, the capability of the QCM has been used for investigation of the effect of additional paraffin wax and respective inhibitors on asphaltene onset pressure (AOP) and deposition rate of tested crude oil under real field representative conditions (HPHT along with applied shear stress). The natural gas with a composition as presented in section 2.1, was injected at a constant rate of ~1.1 psi/min from 600 psi. The gas at room temperature was injected into the QCM cell at 60 °C and timed to reach equilibrium. The magnetic stirrer was also switched on, rotating at 500 rpm to mix the injected gas and crude oil and apply the shear stress.

6.2.4 PC-SAFT Equation of State

The PC-SAFT EoS is formulated as one of the most reliable tools to predict the phase behaviour of complex fluids[31]–[33]. Dispersive interactions are defined in this model by extension of the perturbation theory of Baker and Henderson[34]. In this EoS molecules are considered as chains composed of spherical segments, dividing the total intermolecular forces into reference and perturbation terms. To model bulk properties of the hydrocarbon mixtures and phase equilibria three parameters that are the segment number in the chain (m), the spherical segment diameter (σ), and the dispersion interaction energy between the segments (ϵ/k) are required for each non-associating and nonpolar components. These parameters are derived by simultaneously fitting the PC-SAFT EoS to thermo-physical experiments as function of the average molecular weight of the component. For associating compounds, however, two additional parameters are required, the association energy (ϵ^{AB}) and the association volume (κ^{AB}). Within the PC-SAFT EoS, an improved square well potential for the segment of a chain is been used, describing the residual Helmholtz free energy. In this work we used our in-house thermodynamic software to predict the asphaltene phase behaviour which is based on the framework of the PC-SAFT proposed by Gross and Sadowski[35]. Here, the residual Helmholtz free energy is split into two terms, the hard-chain reference fluid and the dispersion contribution.

$$\tilde{a} = \tilde{a}^{hc} + \tilde{a}^{disp} \quad (6.1)$$

The compressibility factor is expressed through the following equation

$$Z = 1 + \eta_p \left(\frac{\partial \tilde{a}^{res}}{\partial \eta_p} \right)_{T, x_i} \quad (6.2)$$

The pressure in units of Pa = N/m² can be calculated through the following relation

$$P = Z k_B T \rho_n \left(10^{10} \frac{\text{\AA}}{m} \right)^3 \quad (6.3)$$

According to Equations (6.1) and (6.3), it is

$$Z = 1 + Z^{hc} + Z^{disp} \quad (6.4)$$

The fugacity coefficient and the chemical potentials for different components are expressed through Equations (6.5) and (6.6), respectively

$$\ln \varphi_k = \mu_k^{res}(T, v_v) / kT - \ln Z \quad (6.5)$$

$$\mu_k^{res}(T, v_v) / kT = \tilde{a}^{res} + (Z - 1) + \left(\frac{\partial \tilde{a}^{res}}{\partial x_k} \right)_{T, v, x_i \neq x_k} - \sum_{j=1}^N x_j \left[\left(\frac{\partial \tilde{a}^{res}}{\partial x_j} \right)_{T, v, x_i \neq x_j} \right] \quad (6.6)$$

Further detailed information about the thermodynamic phase behaviour modelling using PC-SAFT EoS can be found elsewhere [32].

6.3 Results and Discussion

6.3.1 Performance of Different Wax Inhibitors: WAT and Pour Point Determination

Four commercial wax inhibitors have been employed to investigate their effect on WAT, pour point, asphaltene precipitation and deposition phenomena using two different techniques: ‘‘Rheometer’’, and ‘‘HPHT-QCM’’, which have been explained in previous section. The efficiency of an additive was evaluated based on the reduction of non-

Newtonian viscosity when it was added to the system. In all cases, the viscosity obtained at the lowest temperature is the “maximum viscosity” which was aimed for the evaluation of the inhibitor performance. Figure 6.1 illustrates the viscosity changes (cP) with temperature reduction (°C) for the blank crude oil and with various inhibitors at specified concentrations which were proposed as optimum ones by suppliers.

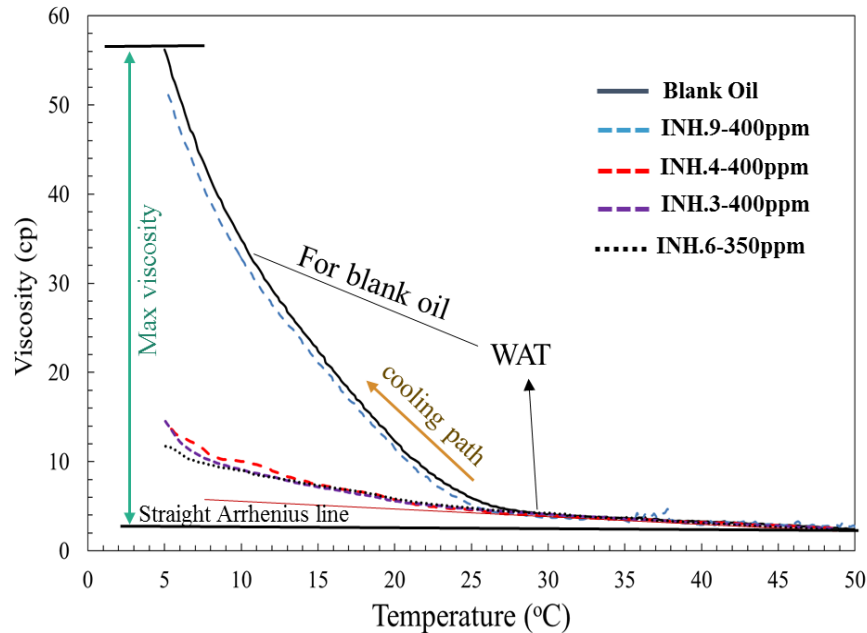


Figure 6. 1. The viscosity changes due to temperature reduction for the blank crude oil and in presence of various inhibitors at specified concentrations.

As the cooling process started well above the wax appearance temperature, the viscosity gradually increased. This behaviour continued following the Arrhenius temperature dependence of Newtonian fluids until wax started to precipitate out from the crude oil. Equation 6.7 below explains a linear Arrhenius relationship for Newtonian range [36]:

$$\mu = Ae^{-E_a/RT} \quad (6.7)$$

Where μ is the Newtonian dynamic viscosity, E_a is activation energy of viscous flow in joules, R is universal gas constant, T is the temperature, and A is Pre-exponential factor largely dependent on the entropy of activation of flow. A sudden deviation in viscosity was then observed owing to formation of wax crystals. The point at which non-Arrhenius behaviour began, is considered as the WAT. As the temperature decreased further below

the WAT, wax crystals grew which leads the oil sample to become more non-Newtonian, and therefore the viscosity increased at a higher rate. The viscosity variations in the mixtures of oil + wax inhibitors, were noticeable. It was also observed that the viscosity in non-Newtonian region decreased in presence of all inhibitors particularly the polymeric ones. Table 6.3 presents a summary of the results and the test conditions using the rheometer with atmospheric geometry.

Table 6. 3. The experiment conditions and results of rheometer tests with atmospheric geometry and shear rate of 10 s^{-1} , using blank crude oil and blended with various wax inhibitors

Fluid	WAT (°C)	Minimum Viscosity (cP)	Maximum Viscosity (cP)	Maximum viscosity reduction compared to blank (%)
Blank Oil	29.1	2.4	56.2	0.0
INH-9, 400ppm	29.2	2.7	51.9	7.7
INH-4, 400ppm	24.2	2.4	17.5	68.9
INH-3, 400ppm	21.2	2.4	16.2	71.2
INH-6, 350ppm	22.5	2.3	12.3	78.1

Typically, wax inhibitors performance can be categorised in three classes: 1- high viscosity reduction, 2- moderate reduction, and 3- no significant change or slightly increasing. As can be seen from Figure 6.1 and Table 6.3, inhibitors INH-3, 4 and 6 are placed in Class1, and INH-9 is put in Class3. As an overall ranking, INH-3 and 6 were found to be better viscosity modifiers compared to the other tested inhibitors.

The efficiency of wax inhibitors can also be evaluated based on their capability to reduce the pour point. The pour point reduction may lead to higher production rates and lower production costs for the operators consequently. The experiment conditions and pour point results from rheometer on oscillation mode using different wax inhibitors at optimum concentration are shown in Table 6.4.

Table 6. 4. The test conditions and results of rheometer experiments on oscillation mode with Angular frequency= 10 rad/s, Frequency= 1.6 Hz, and Amplitude Torque=25 μ Nm, using blank crude oil and dosed with different wax inhibitors

Fluid	Destination T (°C)	Pour point (°C)
Blank Oil	-20.0	-5.3
INH-9, 400ppm	-20.0	-8.9
INH-3, 400ppm	-25.0	-22.5
INH-6, 350ppm	-25.0	-23.6
INH-4, 400ppm	-25.0	-25.0

The liquid-like behaviour of the reservoir fluid is identified by the loss modulus (viscous response) while the solid-like behaviour is identified by the storage modulus (elastic response). When the wax-oil mixture was at a temperature above the pour point, loss modulus was at a higher value compared to the storage modulus. When temperature decreased, both moduli values increased till the test fluid reached to the pour point. At pour point, storage modulus is equal to the loss modulus. Storage modulus increased if the mixture was subjected to a further cooling. Figure 6.2 also presents the effect of wax inhibitors on pour point reduction for the treated oil sample.

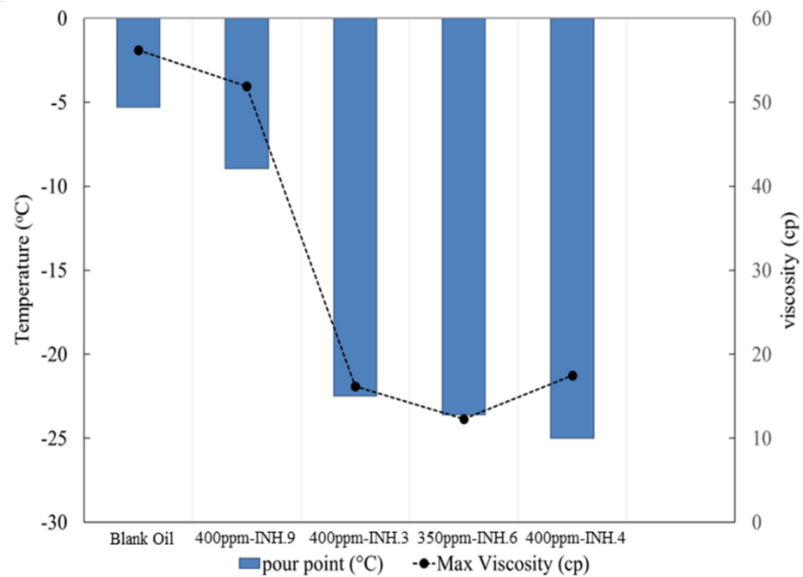


Figure 6. 2. The effect of wax inhibitors on pour point reduction for the modified crude oil sample.

All the chemicals decreased the pour point with almost keeping the same efficiency as they had for viscosity reduction. The INH-4 and 6 could reduce the pour point as better depressants from $-5.29\text{ }^{\circ}\text{C}$ to $-25\text{ }^{\circ}\text{C}$ and $-23.6\text{ }^{\circ}\text{C}$, respectively.

6.3.2 Effect of Wax and Related Inhibitors on Asphaltene Instability

The asphaltene aggregation and deposition experiments should be conducted at and above the natural gas contents of precipitation onset. Herein, the asphaltene onset point (AOP) is defined as the pressure with lowest gas-oil ratio at which asphaltene precipitation is occurred. A HPHT-QCM has been utilised in this study to investigate the effectiveness of paraffin wax and different wax inhibitors on the asphaltene precipitation and deposition rate at elevated pressure and temperature condition in the presence of natural gas. The change in resonant frequency (RF) was monitored during the natural gas injection to determine the asphaltene precipitation onset point and respective gas mole percentage (gas-oil ratio, GOR) which is mixed with crude oil within the QCM cell. The obtained results for AOP determination and the effect of various wax inhibitors on asphaltene aggregation and deposition rate onto the QCM surface are given in Figure 6.3. The change in RF increases as a result of a decrease in viscosity of density of the fluid due to gas injection and declines when asphaltenes start precipitating out of the crude oil.

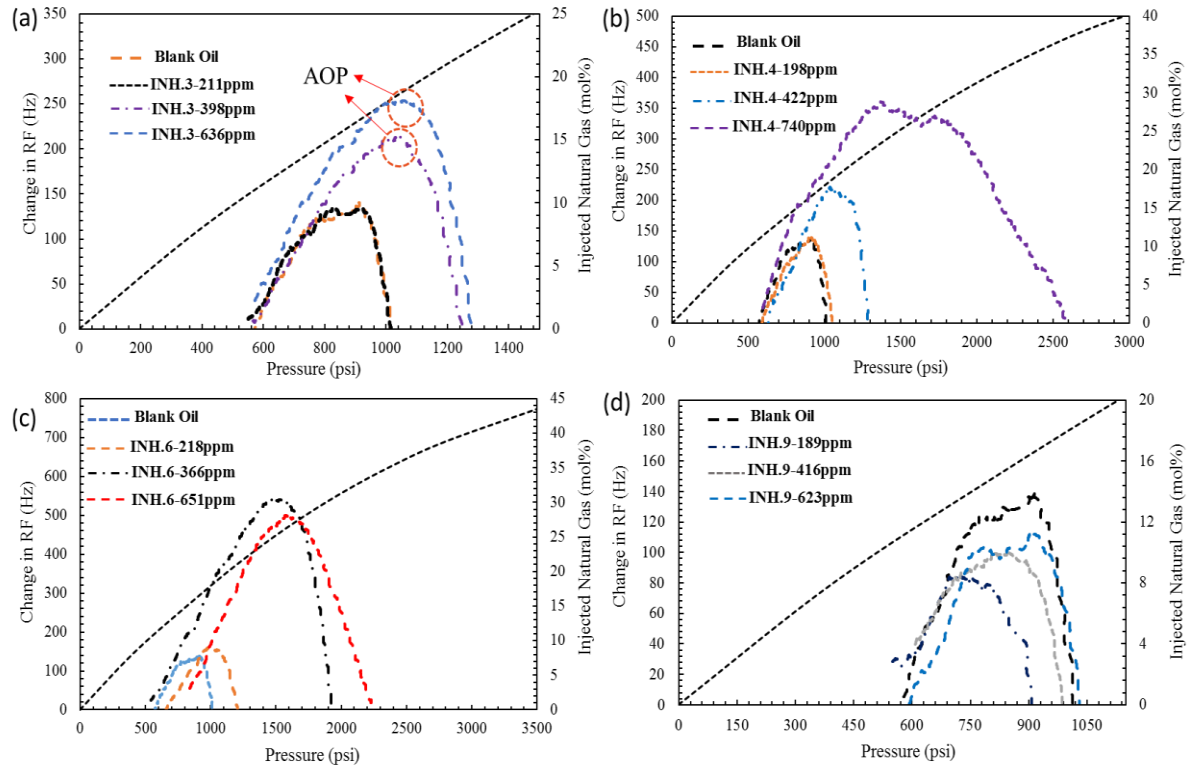


Figure 6. 3. Results of the HPHT-QCM experiments for the examined crude oil with wax inhibitors: a) INH-3, b) INH-4, c) INH-6, and d) INH-9 at different concentrations.

The pressure at which the RF starts to reduce represents the AOP that is ~844 psi at ~15.21 mol% injected gas for blank crude oil without any wax inhibitor. The AOP/GOR is ~1561 psia/26.11 mol% for INH-6, ~1082 psia/19.35 mol% for INH-4, ~1047 psia/18.71 mol% for INH-3, and ~847 psia/15.11 mol% for INH-9 with concentrations of 366, 422, 398, and 416 ppm, respectively, all close to the optimum concentrations which have been used for WAT and pour point depression tests.

Figure 6.4 shows the AOP and GOR obtained by HPHT-QCM versus different concentrations of wax inhibitors. The black dash line curve in Figure 6.4 is the respective injection natural gas (GOR, mol %) for each AOP. Therefore, the representative AOP and GOR for each inhibitor at given dosage rate can be identified. As can be observed, INH-6 has better performance in comparison with three other wax inhibitors on changing AOP and respective GOR (mol%). INH-9 actually aggravated asphaltene precipitation at concentrations of 189 and 416 ppm and became neutral at higher concentrations started from 623 ppm.

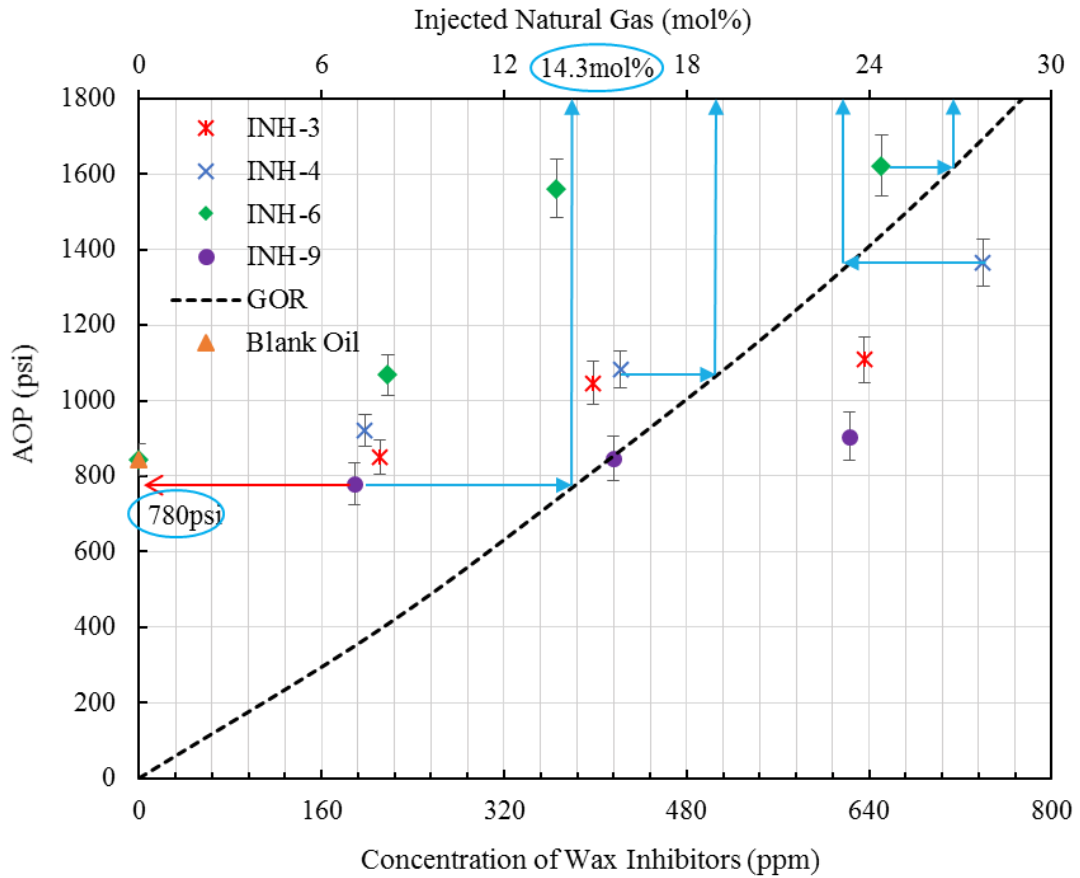


Figure 6. 4. AOP/GOR versus concentration of four wax inhibitors; INH-3, 4, 6, and 9.

The effect of each wax inhibitor with different concentration on the comparative deposition rate, which is RF reduction versus time, after the AOP are presented in Figure 6.5. The achieved results clearly show that all employed wax inhibitors except INH-9 have a positive effect on the asphaltene rate reduction onto the QCM surface after exceeding the AOP. As can be seen, INH-9 at concentrations of 189 and 416 ppm increases the deposition rate from -316.4 Hz/hr to -369.1 Hz/hr and -327.8 Hz/hr, respectively.

As can be observed, there is a drastic change in deposition rate curves between the blank oil and with 366, 398, and 422 ppm of inhibitors 6, 3, and 4, respectively. INH-6 has much better performance in decreasing the asphaltene deposition rate from -316.43 to -55.3 Hz/hr compared to wax inhibitors 3 and 4 at the optimum concentration, which reduces the deposition rate down to -192.1 Hz/hr and -219.6 Hz/h, respectively. A dramatic alteration in RF can be seen during the first 2 hrs of the experiment without inhibitor compared to the

test with wax inhibitors. The ranking of wax inhibitors based on AOP/GOR alterations and deposition rate reduction obtained using HPHT-QCM method is as follows: INH-6 > INH-4 > INH-3 > INH-9.

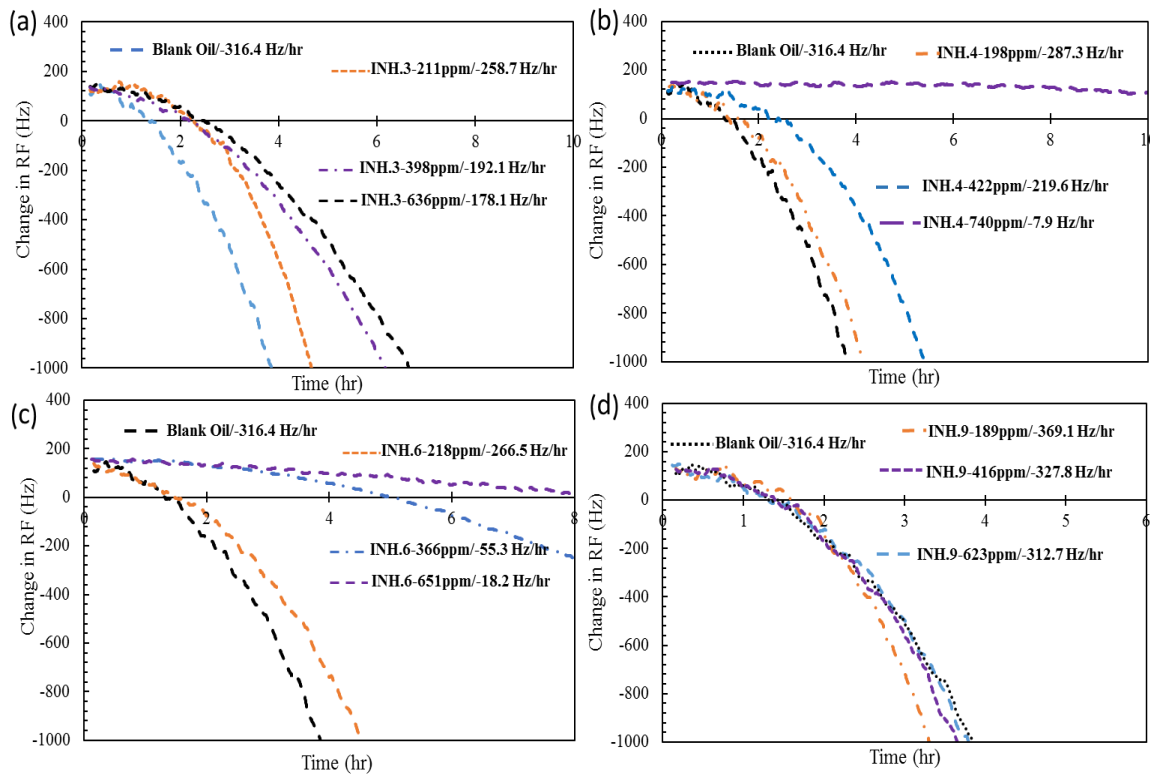


Figure 6. 5. Results of the effect of different wax inhibitors: a) INH-3, b) INH-4, c) INH-6, d) INH-9 on the asphaltene deposition rate at various concentrations.

INH-3 contains Naphtalene, 1,2,4, Trimethylbenzene which can interact with asphaltene nanoaggregates through π stacking interaction with asphaltenes aromatic cores. However, it cannot curb further interactions between nanoaggregates since it does not have any strong surface-active functional group to interact with asphaltene molecules through hydrogen bonding, acid-base or van der Waals interactions.

On the other hand, INH-6 and 9 have polymeric structures in aromatic solvents (e.g. Ethylene Vinyl Acetate (EVA) polymer), and in addition to π - π interactions they also can disturb self-association interactions of asphaltene through creating steric repulsion between the aliphatic tails of polymers and asphaltene nanoaggregates that cause significant effect on AOP shifting and decreasing the deposition rate. The effect of wax at different dosage

rates on asphaltene precipitation and deposition was tested using HPHT-QCM at 60 °C. The AOP and QCM based deposition rate were considered as representative performance criteria for capability of waxes to act as inhibitor or promoter. Figure 6.6a shows an increase in AOP/GOR with the addition of paraffin wax. Hence, the addition of whole waxes appears to improve the solubility of asphaltene nanoaggregates in crude oil and stability of asphaltenes increases with increasing wax concentration used in this study.

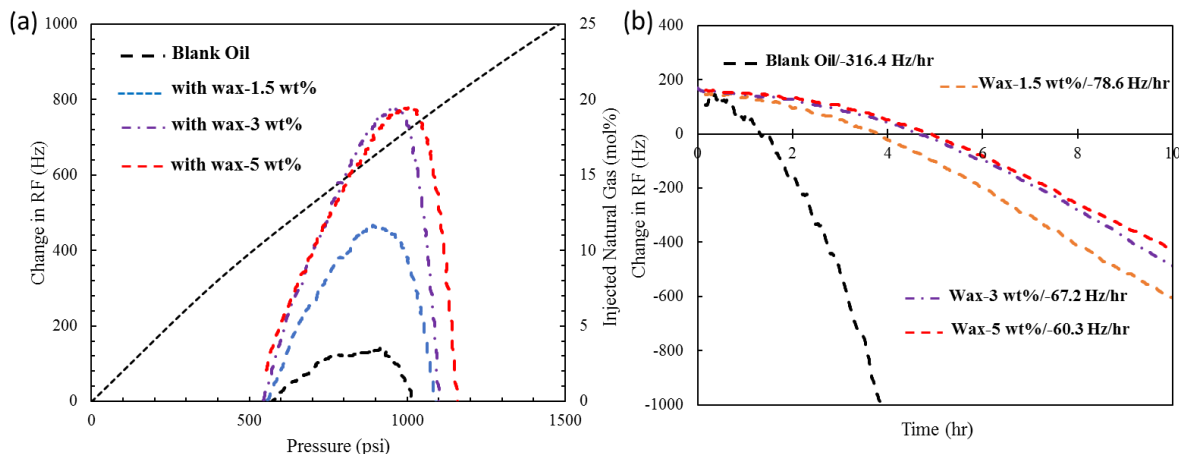


Figure 6. 6. The effect of addition of wax at various concentrations to the crude oil on a) AOP/GOR, b) representative asphaltene deposition rate.

Figure 6.6b indicates that the addition of whole waxes could decrease the asphaltene deposition rate on the QCM surface for all samples tested. As can be observed, 5wt% addition of wax to the crude oil can result in the deposition rate reduction from -316.4 Hz/hr to -60.3 Hz/hr. Asphaltene precipitation is therefore affected by an ensemble of waxes with long aliphatic chains. It is proposed that waxes with various aliphatic chains might form synergies when acting on asphaltene precipitation and aggregation. Large aliphatic chain containing waxes interact with asphaltene and inflict steric interferences during asphaltene nucleation. This could cause formation of more contorted asphaltene aggregates with less tendency to interact and do self-association phenomenon.

6.3.3 Thermodynamic Modelling

The PC-SAFT EoS was employed to predict the asphaltene phase behaviour when the various wax contents were added to the system. The influence of paraffin wax on asphaltene stability zones in the crude oil at different system compositions (i.e. different

gas/oil ratios) is illustrated in Figure 6.7a-b. The relative errors (REs) between experimental and modelling results are also provided in Figure 6.7c. It can be seen that for all modified crudes with different wax contents the model predictions are in good agreement with the experimental results. In general, the relative error was in reasonable range of less than 6% for all the experiments. However, for modified crudes with lower wax contents more satisfactory predictions have been achieved (RE = 1.52%). A distinct deviation was occurred once the model underestimates the AOP changes and does not well match with the asphaltene precipitation onset in the higher paraffin wax region (RE = 5.67%). A probable elucidation to variations between the model prediction and QCM experimental data at high wax content might be ascribed to the generalisations in the crude oil fraction properties utilised, in addition to the uncertainties in the asphaltene structure and onset point determination in high paraffin wax modified crude oil samples.

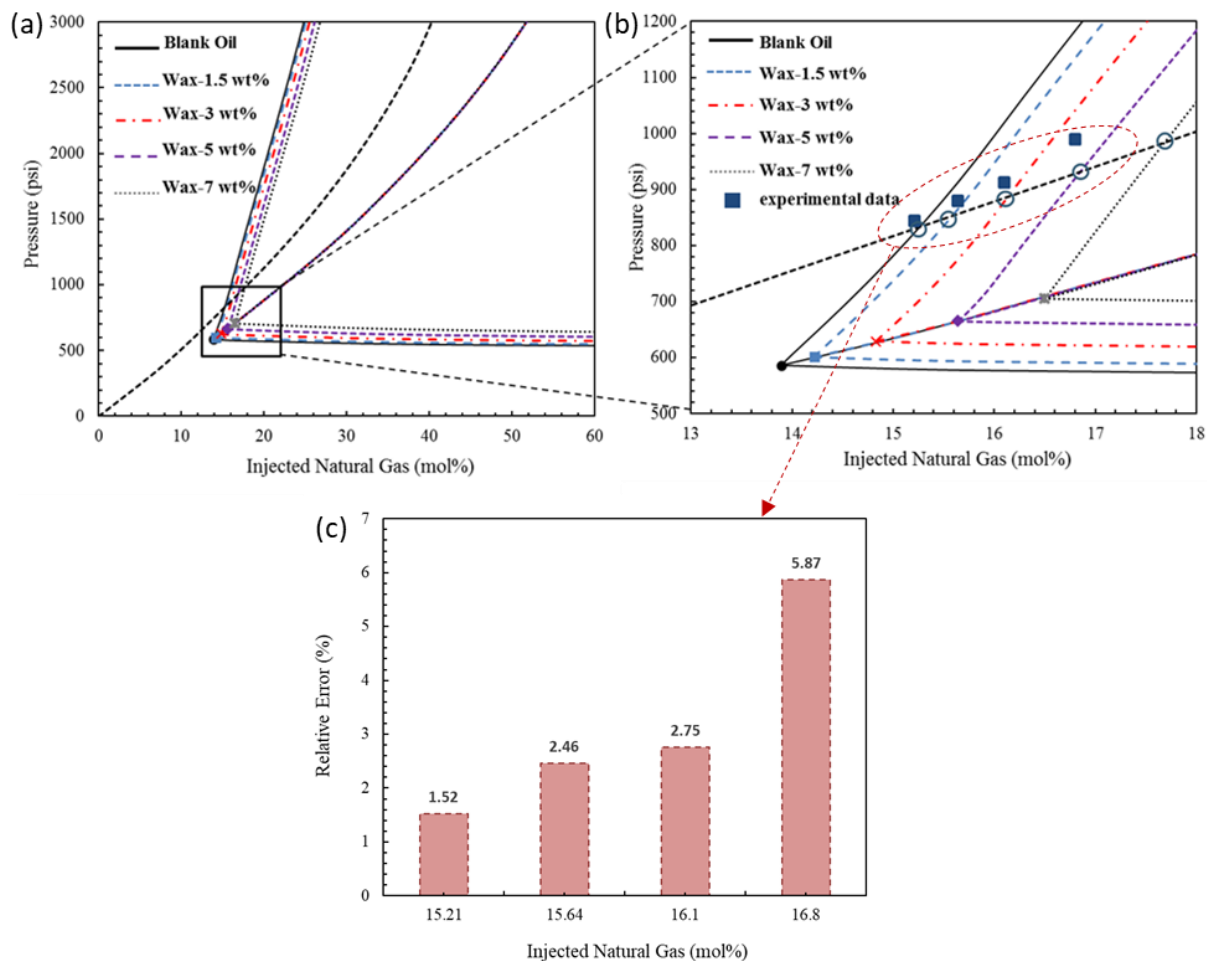


Figure 6. 7. PC-SAFT modelling results of the effect of wax addition to the crude oil on asphaltene stability at various concentrations of 1.5wt%, 3wt%, 5wt%, and 7wt%: a) modelling results, b) zoomed-in plot of modelling results with experimental data, c) relative error of PC-SAFT predictions compared to experimental data.

A comparison between the graphs for lower wax contents with those of higher wax contents in Figures 6.7a-b reveal that the model results present the same trend as experimental results in shifting the asphaltene onset point and increasing respective gas-oil ratio: AOP/GOR increases with increase of paraffin wax content. This could be explained by the presence of heavier hydrocarbons in the crude oil and significantly higher solubility of asphaltene in hydrocarbons with higher carbon number than those with lower ones, widening the asphaltene stability range.

Another hypothesis for the positive effect of wax in reducing asphaltene deposition could be that, upon increasing the molar percentage of heavy fraction of the oil, liquid

hydrocarbon phase split into different phases, liquid number 1 (lighter hydrocarbons as the main fraction) and liquid number two (heavy hydrocarbons as the main fraction), consequently, significant fraction of asphaltene was dissolved in liquid#2, which in turn, reduces the asphaltene fraction in liquid#1, causing the changes in asphaltene onset points and deposition rates. Further research studies on this hypothesis through attaining more experimental data and/or molecular dynamic simulations will result the confirmation of the proposed mechanisms and propositions throughout this work.

6.4 Conclusions

The effects of different wax inhibitors on WAT and pour point depression were evaluated first. Then the crude oil compositional modifications by addition of examined wax inhibitors and various paraffin wax contents in crudes and their influences on the asphaltene stability were investigated by monitoring of asphaltene precipitation onset point changes and deposition behaviour asphaltene nanoaggregates. The results indicate that it may be possible to find an optimum dosage at which the wax inhibitor can reduce both wax and asphaltene deposition problems. A wax inhibitor which is highly efficient in viscosity reduction might not be an appropriate chemical solution in addressing organic deposition challenge. Some wax inhibitors can hinder asphaltene aggregation and deposition and some of them aggravate those phenomena. The HPHT-QCM results showed that, as predicted using the thermodynamic model, wax content can reduce the asphaltene deposition rate and shifting AOP. This occurs might be owing to higher solubility of asphaltenes in hydrocarbons with higher carbon number compared to those with lower ones. Asphaltene phase behaviour in the paraffinic modified oils was also modelled using PC-SAFT EoS. The predictions were compared with the experimental results. It was observed that the relative error was in rational range (less than 6%) for all the tests. However, for modified crudes with lower paraffin wax concentrations more satisfactory predictions have been attained.

6.5 References

- [1] H. Mehrabian, M. A. Bellucci, M. R. Walsh, and B. L. Trout, “Effect of Salt on Antiagglomerant Surface Adsorption in Natural Gas Hydrates,” *J. Phys. Chem. C*, vol. 122, no. 24, pp. 12839–12849, 2018.
- [2] P. Redelius, “Bitumen solubility model using Hansen solubility parameter,” *Energy & fuels*, vol. 18, no. 4, pp. 1087–1092, 2004.
- [3] B. J. Musser and P. K. Kilpatrick, “Molecular characterization of wax isolated from a variety of crude oils,” *Energy & Fuels*, vol. 12, no. 4, pp. 715–725, 1998.
- [4] M. del C. García, “Crude oil wax crystallization. The effect of heavy n-paraffins and flocculated asphaltenes,” *Energy & fuels*, vol. 14, no. 5, pp. 1043–1048, 2000.
- [5] L. Carbognani, L. DeLima, M. Orea, and U. Ehrmann, “Studies on large crude oil alkanes. II. Isolation and characterization of aromatic waxes and waxy asphaltenes.,” *Pet. Sci. Technol.*, vol. 18, no. 5–6, pp. 607–634, 2000.
- [6] M. A. Kelland, *Production chemicals for the oil and gas industry*. CRC press, 2014.
- [7] J. Ruwoldt, S. Subramanian, S. Simon, H. Oschmann, and J. Sjöblom, “Asphaltene fractionation based on adsorption onto calcium carbonate: Part 3. Effect of asphaltenes on wax crystallization,” *Colloids Surfaces A Physicochem. Eng. Asp.*, 2018.
- [8] M. Ameri Mahabadian, A. Chapoy, and B. Tohidi, “A New Thermodynamic Model for Paraffin Precipitation in Highly Asymmetric Systems at High Pressure Conditions,” *Ind. Eng. Chem. Res.*, vol. 55, no. 38, pp. 10208–10217, 2016.
- [9] K. Paso, H. Kallevik, and J. Sjöblom, “Measurement of wax appearance temperature using near-infrared (NIR) scattering,” *Energy & Fuels*, vol. 23, no. 10, pp. 4988–4994, 2009.
- [10] F. H. Marchesini, A. A. Aliche, P. R. de Souza Mendes, and C. M. Ziglio, “Rheological characterization of waxy crude oils: Sample preparation,” *Energy & Fuels*, vol. 26, no. 5, pp. 2566–2577, 2012.
- [11] J. J. Espada, J. A. P. Coutinho, and J. L. Pena, “Evaluation of methods for the extraction and characterization of waxes from crude oils,” *Energy & Fuels*, vol. 24, no. 3, pp. 1837–1843, 2010.
- [12] R. W. Burgass and B. Tohidi, “Development and Validation of Small Volume Multi-Tasking Flow Assurance Tool,” in *SPE Asia Pacific Oil and Gas Conference and Exhibition*, 2011, vol. M.
- [13] A. D97, “Standard test method for pour point of petroleum products,” *Annu. B. Stand.*, 2005.

- [14] A. L. C. Machado and E. F. Lucas, "Influence of ethylene-co-vinyl acetate copolymers on the flow properties of wax synthetic systems," *J. Appl. Polym. Sci.*, vol. 85, no. 6, pp. 1337–1348, 2002.
- [15] B. Wei, "Recent advances on mitigating wax problem using polymeric wax crystal modifier," *J. Pet. Explor. Prod. Technol.*, vol. 5, no. 4, pp. 391–401, 2015.
- [16] X. Yang and P. Kilpatrick, "Asphaltenes and waxes do not interact synergistically and coprecipitate in solid organic deposits," *Energy & Fuels*, vol. 19, no. 4, pp. 1360–1375, 2005.
- [17] R. Venkatesan, J.-A. Östlund, H. Chawla, P. Wattana, M. Nydén, and H. S. Fogler, "The effect of asphaltenes on the gelation of waxy oils," *Energy & fuels*, vol. 17, no. 6, pp. 1630–1640, 2003.
- [18] M. del C. García and L. Carbognani, "Andersen, S. I," *Energy & Fuels*, vol. 15, no. 5, pp. 1021–1027, 2001.
- [19] T. Maqbool, A. T. Balgoa, and H. S. Fogler, "Revisiting asphaltene precipitation from crude oils: A case of neglected kinetic effects," *Energy & Fuels*, vol. 23, no. 7, pp. 3681–3686, 2009.
- [20] K. Kraiwattanawong, H. S. Fogler, S. G. Gharfeh, P. Singh, W. H. Thomason, and S. Chavadej, "Effect of asphaltene dispersants on aggregate size distribution and growth," *Energy & Fuels*, vol. 23, no. 3, pp. 1575–1582, 2009.
- [21] J. Castillo, H. Gutierrez, M. Ranaudo, and O. Villarroel, "Measurement of the refractive index of crude oil and asphaltene solutions: onset flocculation determination," *Energy & fuels*, vol. 24, no. 1, pp. 492–495, 2009.
- [22] Z. Yang, S. Chen, H. Peng, M. Li, M. Lin, Z. Dong, J. Zhang, and Y. Ji, "Effect of precipitating environment on asphaltene precipitation: Precipitant, concentration, and temperature," *Colloids Surfaces A Physicochem. Eng. Asp.*, vol. 497, pp. 327–335, 2016.
- [23] D. P. Powers, H. Sadeghi, H. W. Yarranton, and F. G. A. Van Den Berg, "Regular solution based approach to modeling asphaltene precipitation from native and reacted oils: Part 1, molecular weight, density, and solubility parameter distributions of asphaltenes," *Fuel*, vol. 178, pp. 218–233, 2016.
- [24] D. M. Barrera, D. P. Ortiz, and H. W. Yarranton, "Molecular weight and density distributions of asphaltenes from crude oils," *Energy & fuels*, vol. 27, no. 5, pp. 2474–2487, 2013.
- [25] A. K. Tharanivasan, H. W. Yarranton, and S. D. Taylor, "Application of a regular solution-based model to asphaltene precipitation from live oils," *Energy & Fuels*, vol. 25, no. 2, pp. 528–538, 2010.

- [26] O. C. Díaz, J. Modaresghazani, M. A. Satyro, and H. W. Yarranton, "Modeling the phase behavior of heavy oil and solvent mixtures," *Fluid Phase Equilib.*, vol. 304, no. 1–2, pp. 74–85, 2011.
- [27] R. F. G. Visintin, R. Lapasin, E. Vignati, P. D'Antona, and T. P. Lockhart, "Rheological behavior and structural interpretation of waxy crude oil gels," *Langmuir*, vol. 21, no. 14, pp. 6240–6249, 2005.
- [28] M. Kane, M. Djabourov, and J.-L. Volle, "Rheology and structure of waxy crude oils in quiescent and under shearing conditions," *Fuel*, vol. 83, no. 11–12, pp. 1591–1605, 2004.
- [29] E. Joonaki, J. Buckman, R. Burgass, and B. Tohidi, "Exploration of the Difference in Molecular Structure of n-C₇ and CO₂ Induced Asphaltenes," *Ind. Eng. Chem. Res.*, 2018.
- [30] E. Joonaki, R. Burgass, A. Hassanpouryouzband, and B. Tohidi, "Comparison of Experimental Techniques for Evaluation of Chemistries against Asphaltene Aggregation and Deposition: New Application of High-Pressure and High-Temperature Quartz Crystal Microbalance," *Energy & Fuels*, 2017.
- [31] A. Hassanpouryouzband, M. V. Farahani, J. Yang, B. Tohidi, E. Chuvilin, V. Istomin, and B. Bukhanov, "Solubility of Flue Gas or Carbon Dioxide-Nitrogen Gas Mixtures in Water and Aqueous Solutions of Salts: Experimental Measurement and Thermodynamic Modeling," *Ind. Eng. Chem. Res.*, vol. 58, no. 8, pp. 3377–3394, Feb. 2019.
- [32] A. Hassanpouryouzband, E. Joonaki, V. Taghikhani, R. Bozorgmehry Boozarjomehry, A. Chapoy, and B. Tohidi, "New Two-Dimensional Particle-Scale Model to Simulate Asphaltene Deposition in Wellbores and Pipelines," *Energy and Fuels*, vol. 32, no. 3, pp. 2661–2672, Nov. 2018.
- [33] M. Fathinasab, M. Salehzadeh, M. Amiri, M. Montazer, and M. Z. Hasanvand, "A literature review of asphaltene entity, precipitation, and deposition, introducing recently models of deposition in the well column," *J. Oil, Gas Petrochemical Sci.*, vol. 1, no. 2, pp. 83–89, 2018.
- [34] J. A. Barker and D. Henderson, "Perturbation theory and equation of state for fluids. II. A successful theory of liquids," *J. Chem. Phys.*, vol. 47, no. 11, pp. 4714–4721, 1967.
- [35] J. Gross and G. Sadowski, "Perturbed-Chain SAFT: An Equation of State Based on a Perturbation Theory for Chain Molecules," *Ind. Eng. Chem. Res.*, vol. 40, no. 4, pp. 1244–1260, 2001.
- [36] H. P. Roenningsen, B. Bjoerndal, A. Baltzer Hansen, and W. Batsberg Pedersen, "Wax precipitation from North Sea crude oils: 1. Crystallization and dissolution

temperatures, and Newtonian and non-Newtonian flow properties,” *Energy & Fuels*, vol. 5, no. 6, pp. 895–908, 1991.

Chapter 7-A New 2-D Particle Scale Model to Simulate Asphaltene Deposition in Wellbores and Pipelines

7.1 Introduction

It is extremely important to identify the flow of precipitated and aggregated asphaltene particles and determine their disposition for deposition. However, because of the complexity of the asphaltenes molecular structure and lack of proper knowledge of the asphaltene aggregates deposition process, modelling studies of this undesirable phenomena are scarce. Recent advances in asphaltenes science enable us to have a new look at how a reliable asphaltene deposition model can sufficiently predict asphaltene deposition tendencies onto the surfaces and cause a significant positive effect on fluid flow assurance in pipelines and porous media[1].

Here, a few articles and some of the obtained results from previous asphaltene deposition model studies will be briefly described. The first was authored by Escobedo and Mansoori[2] who developed an asphaltene deposition model based on models for aerosol (microscopic liquid or solid particles dispersed on air currents) deposition. The model was developed by accounting for both diffusive and convective mechanisms for transport of asphaltene particle to the pipe wall[3]. Jamialahmadi, et al.[4] developed a mechanistic asphaltene deposition model based on three parameters of oil velocity, bulk and surface temperature, and concentration of flocculated asphaltenes. They conducted flow loop experiments to determine the rate of asphaltene deposition by measurement of the thermal resistivity of asphaltene deposit. They proposed an Arrhenius type equation for adhesion force between flocculated asphaltenes and the metal surface, ignoring the effect of particle size distribution of precipitated asphaltenes. The model developed by Jamialahmadi was then utilized by Soulgani et al.[5] for predicting asphaltene deposition in an oil reservoir. They matched the experimental asphaltene deposition rate with a correlation based on the aforementioned Arrhenius exponential term with an assumption of chemical reaction mechanism controlled the asphaltene deposition onto the tubing surface. There is no validation for the proposed deposition mechanism. Ramirez-Jaramillo et al.[6] proposed

the application of a molecular diffusion model to describe the transportation of asphaltene aggregates to the wall. They claimed that the net rate of asphaltene deposition is the difference between the rate of deposition and removal of asphaltene. These researchers employed Fick's law for molecular diffusion accounting for the rate of deposition and Kern and Seaton[7] model for expressing the removal of asphaltene deposition. They also considered that the asphaltene aggregates concentration gradient was due to the wall temperature gradient. This modelling methodology inspired from a well-developed hypothesis for wax deposition by Burger et al[8] which is unfortunately not in agreement with laboratory data obtained by Greaves et al.[9]. Their experimental data on asphaltene deposition using a Couette device revealed that the wall temperature gradient did not cause a significant effect on the asphaltene deposition rate. Eskin, et al.[10] developed an asphaltene deposition model based on particle flux mass transfer expressions in turbulent flows. They assumed a population balance model for asphaltene particle size distribution over pipe cross section and Brownian diffusion for transport of aggregated asphaltenes to the wall surface. The model had three tuning parameters which were obtained by conducting laboratory tests with a Couette device, while thermodynamics of asphaltene precipitation from bulk solution was not addressed. The asphaltene deposition model of Vargas, et al.[11] consists of several sub-models explaining the asphaltene precipitation, aggregation, transport, and deposition onto the wall surface. The pseudo-first-order reactions were utilized to model the asphaltene aggregation and deposition steps. The particle transport was defined by the convection-diffusion equation. The diffusivity of asphaltene aggregates in fluid flow through a pipe was considered to be fixed and approximately equal to the determined diffusivity of asphaltene particles in toluene. The model included different tuning parameters that had to be identified based on experimental data. Hashmi, et al.[12] introduced a new asphaltene deposition model with proposing that asphaltene deposition onto the metal surface is governed by a diffusion driven mechanism. Asphaltene deposition and clogging were assessed by injecting precipitating petroleum fluid mixtures into a capillary tube. The agreement was found between model predictions and experimental data. However, the model was only developed for laminar flow, and further investigation is required to verify the model in the more real condition of fluid flow along a pipe or wellbore. Vilas Boas Favero, et al.[13] proposed new device to investigate

asphaltene deposition phenomenon. The apparatus was made of a packed bed of stainless steel beads over which a solution of crude oil-alkane is flown and the asphaltene deposit well monitored. The experimental results prove the use of the advection-diffusion equation to model asphaltene deposition. They matched the obtained asphaltene deposition profile along the packed bed with theoretical behaviour predicted by the diffusion-limited correlations for mass-transfer deposition.

A review of the existing literature reveals that there is a lack of comprehensive deposition simulator which fully considers all effective parameters. These parameters such as thermodynamics of asphaltene precipitation, aggregation of precipitated nano-scale particles and finally the transport of particles to the surface and deposition of particles.

In this chapter, a novel framework was developed to predict the deposition profile of asphaltenes along the flow of a multiphase fluid from the wellbore to the wellhead. In this model, the PC-SAFT equation of state was used to study the stability of oil/asphaltene mixtures. A new classification for the asphaltene particle size of precipitated asphaltenes was also presented to describe the Newton's second law related. The Smoluchowsky[14] aggregation kinetic model was used to account for the self-association of asphaltenes. A modified sub-model was also developed for asphaltene deposition term. Advection - Diffusion (ADE) equation in cylindrical coordinate was used to track the transport of asphaltene particles in both axial and radial directions. A numerical scheme was applied to solve all governing PDEs simultaneously. The results obtained from the new model was compared and validated against experimental data of asphaltene deposition in the capillary tube to show the robustness of the model.

7.2 Model Development

7.2.1 Thermodynamic Modelling

The PC-SAFT EoS has been one of the most reliable equations of state which was proposed for non-associating fluids by applying the perturbation theory of Barker and Henderson[15] for dispersive interactions within PC-SAFT model. A simple approximate solution for a given molecular model is typically described by using perturbation theories. Originally, the PC-SAFT assumed the hard sphere fluid as a reference fluid and was

developed for spherical molecules. In this methodology, the total intermolecular forces are divided into reference and perturbation term. The hard chain fluid with high attractive intermolecular forces is assumed as the reference fluid in the model. This model needs three parameters of each non-associating and non-polar components which are the segment number in the molecule (m), the segment diameter (σ), and the interaction energy between each molecular segment ε/k to model both phase equilibria and bulk properties of the hydrocarbon mixtures. These parameters are related to the average molecular weight of the component and are determined commonly by simultaneously fitting the PC-SAFT EoS to the measured saturated liquid density, speed of sound, heat capacity, and vapor-pressure data of the components. A modified squared-well potential for the segment of a chain is assumed within the PC-SAFT EoS which describes the residual Helmholtz free energy of a mixture of non-associating fluids. In the framework of the PC-SAFT proposed by Gross and Sadowski[16], the residual Helmholtz free energy is separated into hard-chain reference fluid and the dispersion contribution. The respective equations have been presented in Chapter 6.

In order to perform the stability analysis and flash calculations, the fugacity coefficients are needed. The stability/flash calculation is then utilized for modelling of PVT experiments to get thermodynamic results from the equation of state. This was schematically represented in Figure 7.1. Different asphaltene compositions in mixtures were tested using the stability analysis based on the Tangent Plane Distance concept[17] to study the thermodynamics of asphaltene particles in the oil phase corresponding to the global minimum of the Gibbs energy of the mixture. It should be stated that if the asphaltene phase was stable in the oil, the result of stability analysis would be used as the initial guess composition to conduct the flash calculation. More details on the stability analysis applied here can be found elsewhere.[18]–[20]

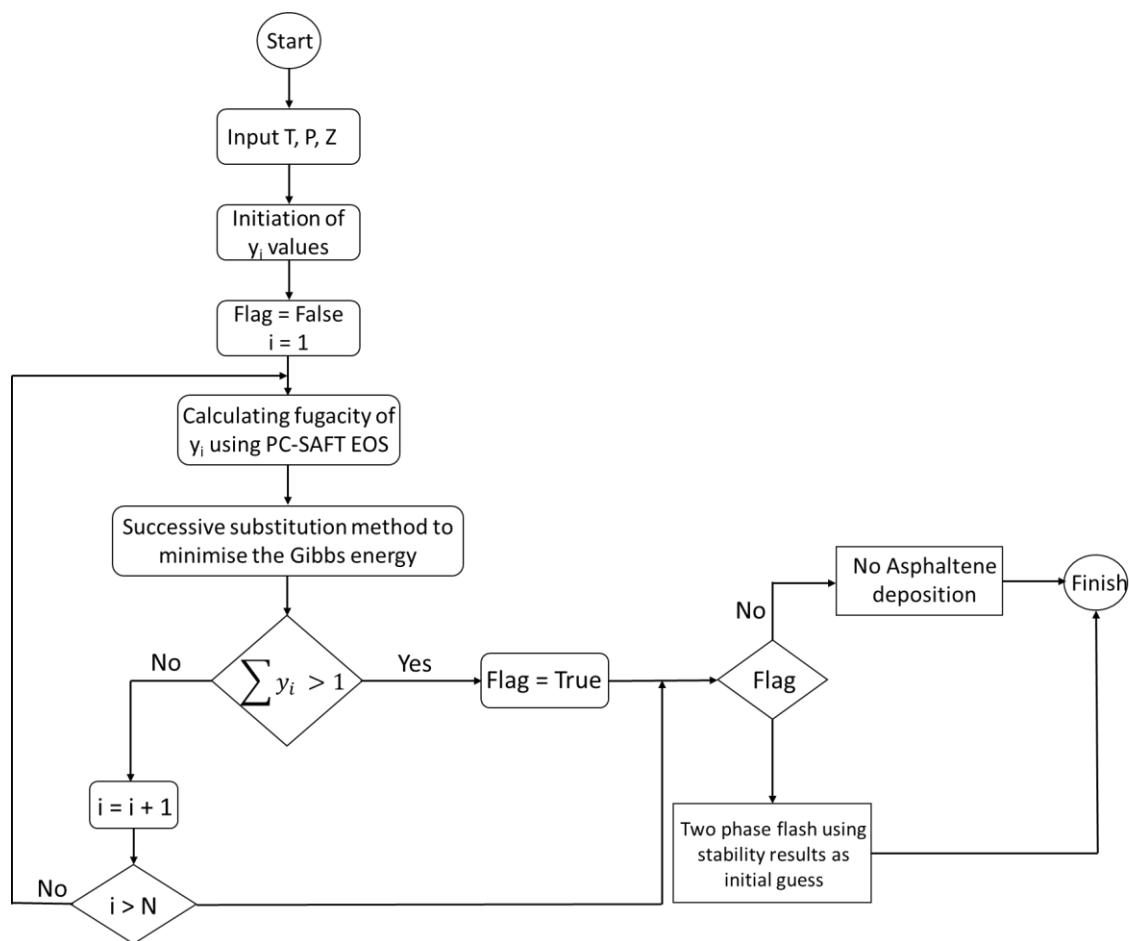


Figure 7. 1. Flow chart of the flash algorithm used to study the stability of asphaltene- oil mixtures.

Figure 7.1 shows the details of thermodynamic calculations of the oil-asphaltene system studied in this work. As explained, for each non-associating species the PC-SAFT equation of state requires three parameters. In order to characterize the oil, these three parameters should be determined for each pseudo-component. The parameters were found based on the SARA (saturates, aromatics, resins, and asphaltenes) analysis of the oil, density of stock tank oil, bubble point and live oil composition of the mixture. Correlations for the three PC-SAFT parameters were previously reported as a function of the molecular weight for paraffins, benzene derivatives, and aromatics. These results were directly used to fit parameters for each component, except for the asphaltene component. The PC-SAFT parameters for asphaltene were fit by matching the measurements of asphaltene onset point with model predictions[21].

7.2.2 Viscosity

A viscosity model based on the correlation developed by Jossi et al. [22] was used to determine the viscosity of the flowing oil containing suspended asphaltene particles. Lohrenz et al. [23] extended the correlation developed by Jossi for computation of the viscosity of hydrocarbons referring as Lohrenz-Bray-Clark or LBC correlation in the oil and gas industry. The LBC correlation is a fourth-degree polynomial equation in terms of the reduced density as follows:

$$\left[(\eta - \eta^*) \xi + 10^{-4} \right]^{1/4} = a_1 + a_2 \rho_r + a_3 \rho_r^2 + a_4 \rho_r^3 + a_5 \rho_r^4 \quad (7.1)$$

where η^* , ξ , and ρ_r are the viscosity of the dilute gas, the viscosity reducing parameter the reduced density respectively. Constants a_1 to a_5 were reported by Jossi et al [22]. In this work, the Lohrenz et al. [23] mixing rules were used for hydrocarbons. Also, the Brinkman [24] viscosity model was used to calculate the viscosity of a fluid containing a dilute suspension of asphaltene particles given by :

$$\mu = \frac{\eta}{(1 - \phi)^{2.5}} \quad (7.2)$$

where ϕ refers to the volume fraction of the asphaltene particles.

7.2.3 Kinetics of Asphaltene Precipitation

Once the asphaltene nano-aggregates become unstable in the oil phase, they start precipitating out of the solution at a specific rate. The rate depends on the difference between the actual concentration of asphaltene in the bulk of oil phase and the equilibrium concentration at the system temperature and pressure. This time-dependent process can be explained by following first-order reaction equation:

$$R_{per} = -k_p (C - C_{eq}) \quad (7.3)$$

where the C is the actual concentration of asphaltene in the oil phase and C_{eq} is the asphaltene concentration at equilibrium condition. The factor k_p was considered to be

constant in most previously published work on the development of asphaltene deposition model, however, in this work an Arrhenius equation type was proposed for k_p as follows:

$$k_p = -k_0 e^{\alpha_p (C - C_{eq})} \quad (7.10)$$

Thus, the final equation for the rate of precipitation of unstable asphaltene particles takes the following form:

$$R_{per} = k_0 e^{\alpha_p (C - C_{eq})} (C - C_{eq}) \quad (7.11)$$

7.2.4 Aggregation of Precipitated Asphaltenes

After precipitation of the asphaltene particles from the bulk of oil phase, the nano-aggregates tend to stick to each other and form larger aggregates due to asphaltene natural self-associating characteristic. The change in the concentration of particles with size k can be modelled using the Smoluchowski[25], [26] equation as follows:

$$\frac{dC_k}{dt} = \frac{1}{2} \sum_{i+j=k} K_{ij} C_i C_j - C_k \sum_{i \geq k} K_{ik} C_i \quad (7.6)$$

where C_k is the concentration of particles with size k , in number of particles per cubic meters and K_{ij} is the collision kernel between i and j particles. For the collision of particles with approximately equal size during the diffusion-limited regime, the collision kernel, K_{ij} , can be estimated according to the following equation[25], [26]:

$$K_{ij} = \frac{8k_B T}{3\mu} \beta \quad (7.7)$$

where T is the temperature in Kelvin, k_B is the Boltzmann constant in $m^2 \cdot kg/s^2$. K , μ is the viscosity in Pa.s, and β is the collision efficiency.

As experimentally shown, while asphaltene particles smaller than $0.01 \mu m$ were considered as nano-aggregates suspended in the oil phase, asphaltene particles larger than $0.01 \mu m$ can be precipitated when asphaltenes become unstable in the liquid phase [11].

7.2.5 Kinetics of Asphaltene Deposition

The precipitated asphaltenes start getting aggregated and the asphaltene aggregates smaller than 10 μm move towards the tubing wall due to the diffusional forces. In this work, a new equation was proposed to model the asphaltene deposition expressed as:

$$R_d = -k_d C^{n\mu} \quad (7.8)$$

where the R_d is the rate of as asphaltene deposition, C is the actual concentration of asphaltene, μ is the viscosity of the oil and the k_d and n are two adjustable parameters.

7.2.6 Modelling the Mass and Heat Transfer Process

In this study, the cylindrical coordinates were used to simulate the distribution of asphaltene aggregates along an oil well column. A two-dimensional axial-radial flow mass transfer equation was used for the simulation purposes. This type of coordinates was able to track the transport of asphaltenes in both radial and axial directions by considering asphaltene deposition, kinetics of asphaltene precipitation, molecular and eddy diffusion and also the kinetics of deposition rate on the surface. The Advection-Diffusion equation in the cylindrical coordinate is[27]:

$$\frac{\partial C}{\partial t} + V_r \frac{\partial C}{\partial r} + V_z \frac{\partial C}{\partial z} + \frac{V_\theta}{r} \frac{\partial C}{\partial \theta} = (D_{wo} + \varepsilon_m) \left[\frac{1}{r} \frac{\partial}{\partial r} \left(r \frac{\partial C}{\partial r} \right) + \frac{1}{r^2} \frac{\partial^2 C}{\partial \theta^2} + \frac{\partial^2 C}{\partial z^2} \right] + R \quad (7.9)$$

where R is the rate of production and consumption of precipitated asphaltenes which can be obtained from Eq. (7.3), and D_{wo} is the asphaltene diffusivity coefficient in the oil phase. In the present work, the Stokes-Einstein equation with additional tuning parameter for asphaltene particles has been used to calculate diffusivity coefficient[28]. This value is given by:

$$D_{wo} = f_d \frac{k_B T}{6\pi\mu r_k} \quad (7.10)$$

where r_k is the radius of particle size k and f_d is the diffusivity tuning parameter. Compared to advection, transport caused by diffusion in z -direction is very small. Accordingly, diffusion in this direction is neglected. Considering that the precipitated particles only diffuse in the radial direction and assuming the symmetricity in the z direction, the equation above can be rewritten as:

$$\frac{\partial C}{\partial t} = -V_z \frac{\partial C}{\partial z} + (D_{wo} + \varepsilon_m) \left[\frac{\partial^2 C}{\partial r^2} + \frac{1}{r} \frac{\partial C}{\partial r} + \frac{\partial^2 C}{\partial Z^2} \right] - k_p (C - C_{eq}) \quad (7.11)$$

where the relation for R was replaced with that in Eq. (7.3). The Finite Difference Method (FDM) was used to solve the above partial differential equation (PDE) subject to the following boundary conditions:

Concentration of Asphaltene at initial time along the wellbore is known and constant:

$$C \text{ at } (t = 0, z, r) = C_0 \quad (7.12)$$

Concentration of Asphaltene in the fluid while entering to the wellbore is constant:

$$C \text{ at } (t, z = 0, r) = C_r \quad (7.13)$$

Asphaltene concentration change during production at $r=0$ is zero:

$$\frac{\partial C}{\partial r} \text{ at } (t, z, r = 0) = 0 \quad (7.14)$$

Deposition occurs at $r = r_w$ according to deposition kinetics:

$$\frac{\partial C}{\partial r} @ (t, z, r = r_w) = -k_d C_d^{n\mu} \quad (7.15)$$

C_d is the concentration of those asphaltene aggregates which can deposit on the surface. Equation 7.15 is the key part for modelling the deposit layer formation, where r_w reduces after deposition occurs,

Similarly, for the heat transfer in the cylindrical geometry described in this work, the following equation can be used as[29]:

$$\frac{\partial T}{\partial t} + v_r \frac{\partial T}{\partial r} + v_z \frac{\partial T}{\partial z} + \frac{v_\theta}{r} \frac{\partial T}{\partial \theta} = (\alpha_T + \varepsilon_h) \left[\frac{1}{r} \frac{\partial}{\partial r} \left(r \frac{\partial T}{\partial r} \right) + \frac{1}{r^2} \frac{\partial^2 T}{\partial \theta^2} + \frac{\partial^2 T}{\partial Z^2} \right] + R \quad (7.16)$$

where, α_T is the thermal diffusivity. The heat generation due to change in the asphaltene phase behavior was reported negligible in the literature[30]. In addition, assuming symmetricity along the z axis, Eq. (7.16) can be simplified as:

$$\frac{\partial T}{\partial t} = -V_z \frac{\partial T}{\partial z} + (\alpha_T + \varepsilon_h) \left[\frac{\partial^2 T}{\partial r^2} + \frac{1}{r} \frac{\partial T}{\partial r} + \frac{\partial^2 T}{\partial z^2} \right] \quad (7.17)$$

Likewise, the mass transfer boundary conditions, the following conditions can be utilized to solve the PDE's:

Fluid temperature is equal to the reservoir temperature while entering the wellbore:

$$T \text{ at } (t, z = 0, r) = T_{res} \quad (7.18)$$

Fluid Temperature is equal to the well head temperature while getting out of the wellbore:

$$T \text{ at } (t, z = L, r) = T_{WH} \quad (7.19)$$

Temperature gradient at centre of the wellbore is zero:

$$\frac{\partial T}{\partial r} \text{ at } (t, z, r = 0) = 0 \quad (7.20)$$

Temperature gradient at $r=r_w$ is equal to convective heat transfer from surrounding material:

$$\frac{\partial T}{\partial r} \text{ at } (t, z, r = r_w) = \frac{h_c}{k_{ho}} (T_w - T_o) \quad (7.21)$$

where, h_c is convective heat transfer coefficient of casing material. It should be mentioned that while the asphaltene layer covers the metal surface, the heat transfer can be affected by the deposition layer and Eq. (7.21) would change to:

$$\frac{\partial T}{\partial r} \text{ at } (t, z, r = r_w) = \frac{h_{As}}{k_{ho}} (T_w - T_o) \quad (7.22)$$

7.2.7 Size Classification of Precipitated Asphaltene Particles

As discussed in Section 2.3, it was assumed that asphaltene nano-aggregates start precipitating out of the liquid phase at the size greater than 0.01 μm . After formation of asphaltene precipitates, the aggregation due to diffusional force between the particles starts which make the distribution asphaltene particles size. In order to solve the aforementioned heat and mass transfer PDEs, it is required to characterize and classify this distribution to solve the equations. In this regard, the asphaltene particles were classified in 12 groups presented in Table 7.1.

Table 7. 1. Classification of asphaltene based on sizes of the aggregates

i (Group)	1	2	3	4	5	6	7	8	9	10	11	12
Size (μm)	0.01	0.02	0.04	0.08	0.16	0.32	0.64	1.28	2.56	5.12	10.24	20.48=<

Using the Smoluchowski[14] equation and considering the generation and consumption of asphaltene particle size, the rate of change in concentration of each asphaltene aggregate size can be modelled as:

$$\text{For } i = 1; \quad \frac{\partial C_i}{\partial t} = \left[\frac{\partial C}{\partial t} + k_p (C - C_{eq}) \right] \frac{C_i}{C} - KC_i^2 - k_p (C - C_{eq}) \quad (7.23)$$

For $i=1$, the term of particle generation due to smaller asphaltene aggregates is zero.

$$\text{For } i=2:11; \quad \frac{\partial C_i}{\partial t} = \left[\frac{\partial C}{\partial t} + k_p (C - C_{eq}) \right] \frac{C_i}{C} + \frac{1}{2} KC_{i-1}^2 - KC_i^2 \quad (7.24)$$

$$\text{For } i=12; \quad \frac{\partial C_i}{\partial t} = \left[\frac{\partial C}{\partial t} + k_p (C - C_{eq}) \right] \frac{C_i}{C} + \frac{1}{2} KC_{i-1}^2 \quad (7.25)$$

In contrary to particle size $i=1$, the term KC^2 is zero for $i=12$ since there is no larger asphaltene aggregate than the aggregates in the aggregate group with $i=12$ in our classification.

And for C in the Eq. (7.9), we have;

$$C = \sum_{i=1}^{12} C_i \quad (7.26)$$

It should be noted that it was assumed that asphaltene particles just aggregate in a step-by-step process. It means that the aggregates with size number i further flocculate to reach the aggregate size $i+1$ or may break and become the aggregate with size $i-1$.

The asphaltene nano-aggregates are stable and soluble in crude oil at reservoir conditions. However, as shown in Figure 7.2, when the crude oil moves up from the reservoir to the well head along the wellbore, the pressure, temperature, and viscosity of the oil change. Due to alterations in these conditions, the asphaltene nano-aggregates which are dissolved in the solution, become unstable and separate out of the crude oil.

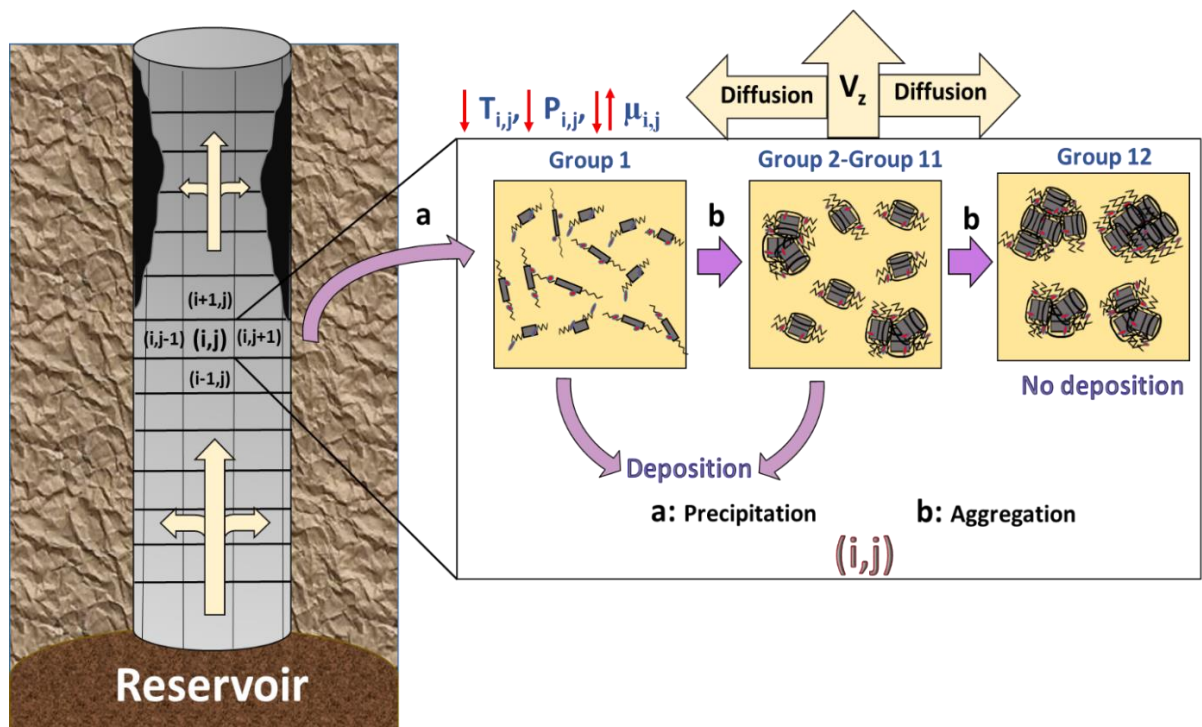


Figure 7. 2. Schematic of precipitation, aggregation, and deposition of asphaltene during the production from the reservoir to well head.

This step of generation of primary aggregates is called asphaltene precipitation (Group 1). Then, some of the precipitated asphaltene particles are moved along the well bore with the oil flow and some of them might be deposited onto the surface. These primary asphaltene aggregates can also interact with each other and form larger particles through the aggregation process (Group 2-11). Again, some of these secondary asphaltene aggregates

may deposit and some of them continue aggregation process and make bigger aggregates (Group 12) which are carried along with the oil flow and cannot deposit onto the walls.

7.2.8 Change in Pressure and Fluid Velocity along the Flow

As the fluid flows along the tubing, its pressure changes resulting from friction, gravity and also velocity variation. In this study, the Darcy-Weisbach [31] equation was utilized to predict the pressure loss during flow in the pipeline as expressed below:

$$\Delta P = g\rho\Delta z + \frac{\rho}{2}\Delta v^2 + \frac{2f_F\rho v^2 L}{D} \quad (7.27)$$

where the friction factors in the pressure loss due to friction in both laminar and turbulent flow can be calculated as:

For laminar flow
$$f_F = \frac{16}{N_{Re}} \quad (7.28)$$

For turbulent flow
$$\frac{1}{\sqrt{f_F}} = -4 \log \left\{ \frac{\varepsilon}{3.7065} - \frac{5.0452}{N_{Re}} \log \left[\frac{\varepsilon^{1.1098}}{2.8257} + \left(\frac{7.149}{N_{Re}} \right)^{0.8981} \right] \right\} \quad (7.29)$$

where ε is the relative roughness. The velocity distribution of the fluid flow inside the pipeline for laminar flow can be related the pressure difference across the pipe and with incorporating the Poiseuille equation inside the tube, the following equation can be obtained [32]:

$$V_z = \frac{\Delta P R^2}{4\mu L} \left[1 - \left(\frac{r}{r_w} \right)^2 \right] \quad (7.30)$$

where r_w is the capillary/wellbore radius, which will be reduced after asphaltene deposition. For turbulent flow, the modified law of the wall can efficiently predict the radial velocity profile [33] and can be expressed as follows:

$$V_z = V_z^+ \sqrt{\frac{\tau_w}{\rho}} \quad (7.31)$$

where V_z^+ and τ_w refer to dimensionless velocity and shear stress at the wall, respectively, and calculated by:

$$V_z^+ = \begin{cases} r^+ & r^+ \leq 5 \\ 5 \ln r^+ - 3.05 & 5 \leq r^+ \leq 30 \\ 2.5 \ln r^+ + 5.5 & 30 \leq r^+ \end{cases} \quad (7.32)$$

$$\tau_w = f_F \frac{\rho v^2}{8} \quad (7.33)$$

where r^+ is the dimensionless distance and is given by:

$$r^+ = \frac{r_w - r}{\nu_\mu} \sqrt{\frac{\tau_w}{\rho}} \quad (7.34)$$

where ν_μ is the kinematic viscosity. The most important basic processes occurring in an asphaltene deposition simulation for a defined well were schematically illustrated in Figure 7.3.

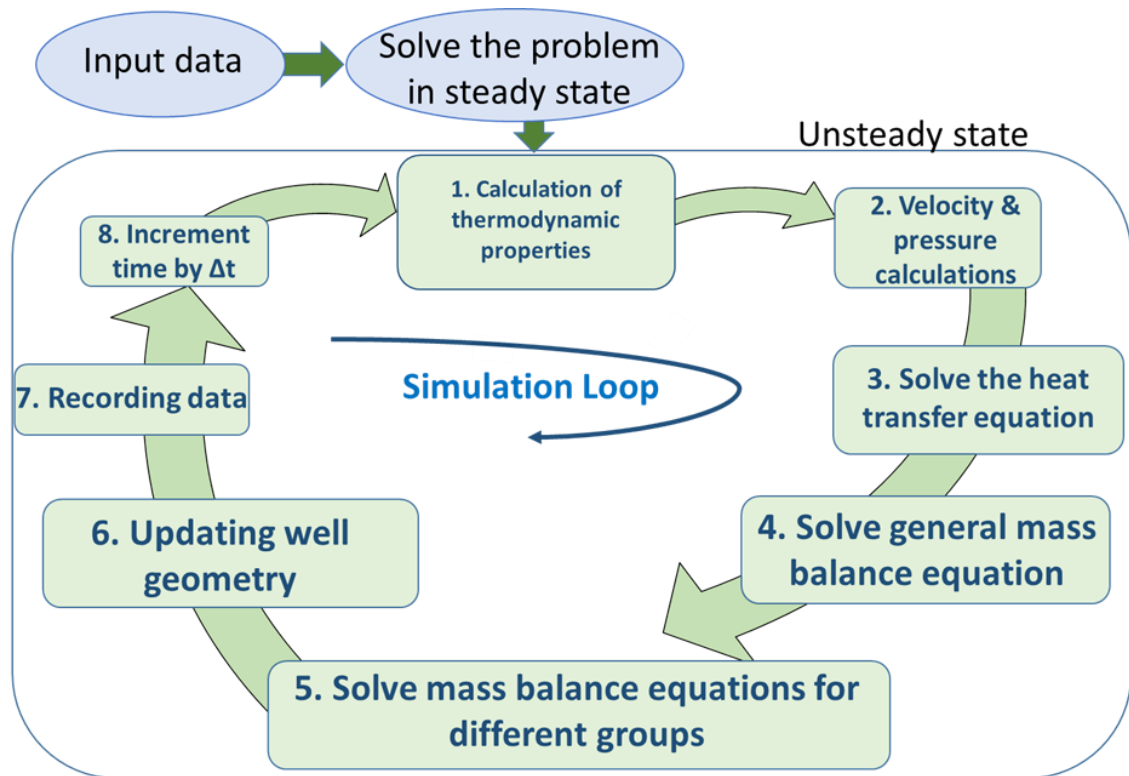


Figure 7. 3. Typical simulation loop; each step begins with thermodynamic calculation part, continues with mass and heat transfer calculations, geometry section, data recording and ends with time update

It should be noted that Figure 7.3 gives a simplified picture as in practice many more detailed processes came into play. The simulation loop was sustained by a combination of three main parts, i.e., thermodynamic packages, dynamic packages, and data analysis as expounded in Figure 7.1. In addition, as can be seen from Figure 7.3, the geometry of the flow area changes once the amount of asphaltene deposition changes with time. This will, in turn, change fluid flow dynamics in the wellbore, causing change in the amount of precipitated asphaltene along the wellbore during the production time. The numerical method for solving Equations 7.11 and 7.17 was provided in the Appendix 2.

7.3 Results and Discussion

7.3.1 Example of an Asphaltene deposition Simulation

The following parameters set and used to model the asphaltene deposition in a well column. The sample well data and all other parameters required for modelling were listed in Table 7.2.

Table 7. 2. Parameters used in the modeling of asphaltene deposition.

Parameter	Value
Well Depth	4572 m
Production String Diameter	3.492 cm
Earth Temperature Gradient	0.0271 K/m
P_{res}	35.594 MPa
P_{WH}	10.466 MPa
T_{res}	427.594 K
T_{WH}	307.95 K
h_c	50 W/m ² .K
α_T	9.8×10^{-7} m ² /s
f_d	1.81×10^2
β	0.68
k_0	3.14×10^{-2} s ⁻¹
α_p	8.19×10^2 cm ³ /gr
k_d	6.18×10^{-4} s ⁻¹

As mentioned before in the structure of the new asphaltene deposition model, the thermodynamic characterization of the crude oil was one of the very first steps in order to achieve an accurate and reliable thermodynamic model at various temperature and pressure. The results of the thermodynamic model were used then as input data for the asphaltene deposition model developed in this study. The crude oil composition was obtained from elsewhere[21]. The crude oil thermodynamic properties such as saturation pressure and asphaltene onset pressures for various temperatures and the dead oil SARA analysis data were obtained from Panuganti, et al.[21]. A detailed explanation of the characterization procedure and the PC-SAFT parameters used in this work are available in the literature (Ting et al. and Gonzalez et al.[34], [35]). The oil density was reported to be about 36-40°API. The oil characterization was conducted to match the given density range, and the PC-SAFT prediction result was 38°API. The effect of temperature on the saturation pressure of the crude oil is shown in Figure 7.4.

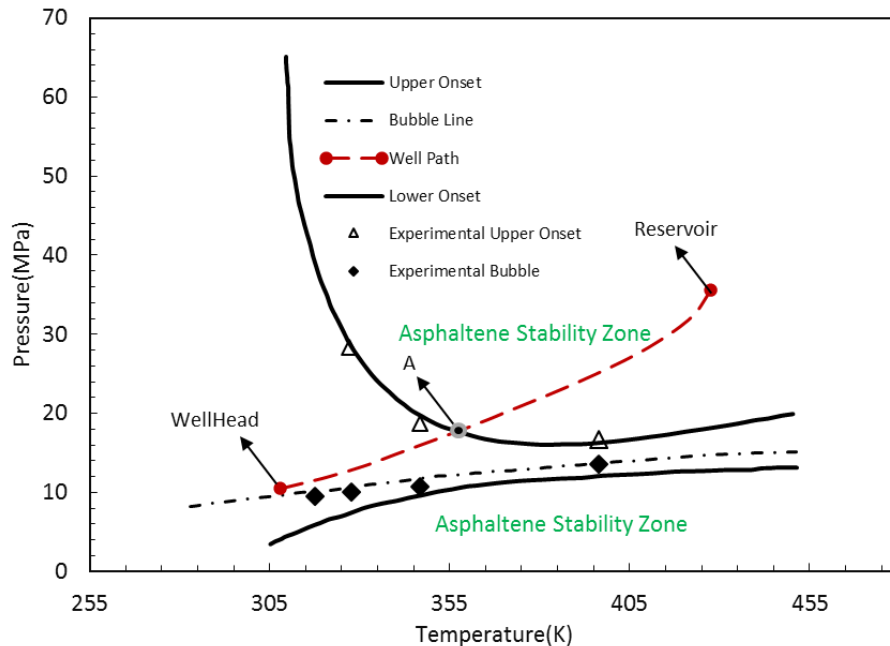


Figure 7. 4. Asphaltene phase behaviour at different pressure and temperature for the crude oil investigated in this study

The black solid diamond data points in Figure 7.4 are the experimentally determined bubble points pressure data from Panuganti, et al.[21]. The black dash dot line in Figure 7.4 is the PC-SAFT prediction of the bubble pressure for various temperatures, and as can be observed the PC-SAFT predictions match very well with the experimental measurements. The triangle data points with represent the experimentally determined asphaltene upper onset pressure for different temperatures. The black solid line represents the PC-SAFT predictions. It should be noted that the PC-SAFT predictions match the experimental data very well when the reported onset values compared to the simulation results. The wellbore operating conditions are shown from reservoir to the wellhead by the long dash line. The black round dot line represents the PC-SAFT prediction of the lower asphaltene precipitation onset pressure curve. The region between the upper asphaltene onset pressure and the lower onset pressure curves makes the asphaltene precipitation region. The crude oil is stable in terms of asphaltene precipitation above this region. As the crude oil flows upward along the wellbore, the pressure and temperature decreased, as observed from long dash line, and the crude oil goes into the asphaltene precipitation region, where the asphaltene particles start coming out of the solution (Point A). This phenomenon continuously takes place until the bubble line, after which the light components of the crude oil begin separating out of the solution. Because of the removal of these light components from the crude oil, which are themselves appropriate precipitating agents for asphaltene particles, the crude oil becomes a more suitable solvent for asphaltenes, and therefore the asphaltene particles again become stable in crude oil below the lower asphaltene onset pressure curve. The obtained pressure and temperature data were matched to the well bore depth, and this information was utilized to determine the thermodynamic stability of asphaltenes in crude oil along the well bore depth. This was a significant input data for the modelling of asphaltene deposition.

Temperature and pressure information is crucial for modelling and is fundamentally related to asphaltene deposition, forward predictions, and reservoir and borehole stability analysis. Figure 7.5 shows temperature and pressure profiles along the well bore. Temperature and pressure effects were basically identified as a major cause of changes in asphaltene precipitation and deposition. Figure 7.5 presents a typical temperature profile for the

borehole wall which is different from the formation temperature. This difference depends on the heat transfer properties of casing material in presence of asphaltene deposition. A pressure-depth profile in a well drilled in a field under production is also presented in Figure 7.5.

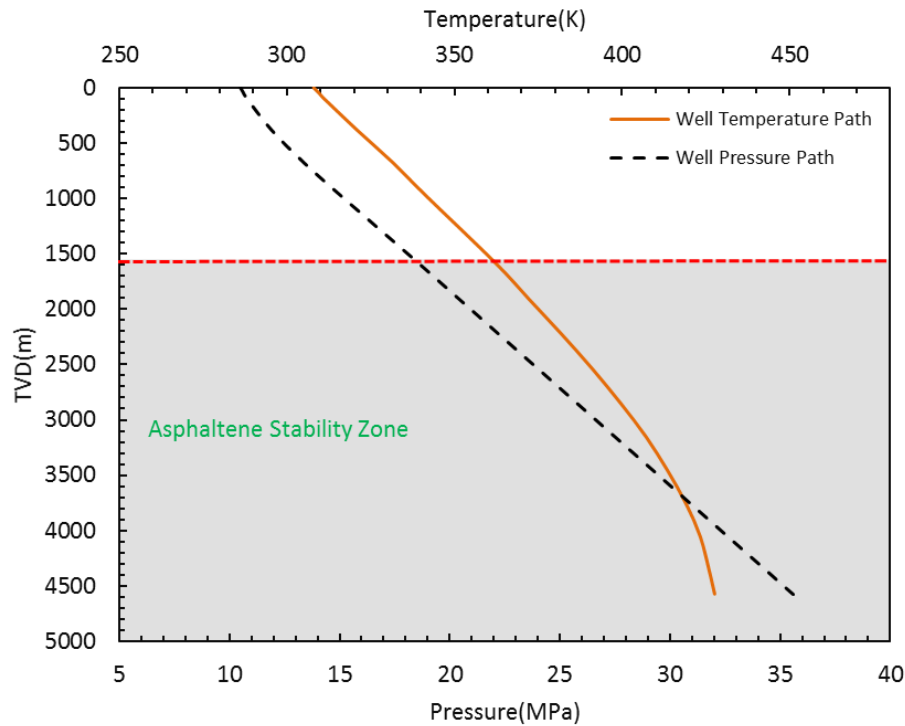


Figure 7. 5. Well temperature and pressure profiles along the true vertical depth in two asphaltene stable and asphaltene unstable regions.

The pressures in and out of asphaltene stability zone, have been affected by vertical flow through the reservoir and also asphaltene precipitation and deposition. The measured gradients reflect the pressure drop created by the vertical flow.

Higher asphaltene content in crude oil causes additional problems related to oil transportation and processing because of an increase in oil viscosity due to the presence of more asphaltenes. Our modelling results on oil viscosity and true vertical depth in well bore affecting the crude oil viscosity are plotted in Figure 7.6.

The viscosity of the crude oil increases due to the presence of precipitated asphaltene aggregates. This increase became significant at and after the asphaltene flocculation onset

and therefore could be utilized to determine the asphaltene precipitation onset points. Oil compositional grading due to asphaltene precipitation along the well bore was an undeniable phenomenon and with asphaltene compositional changes, the crude oil viscosity varied considerably with true vertical depth.

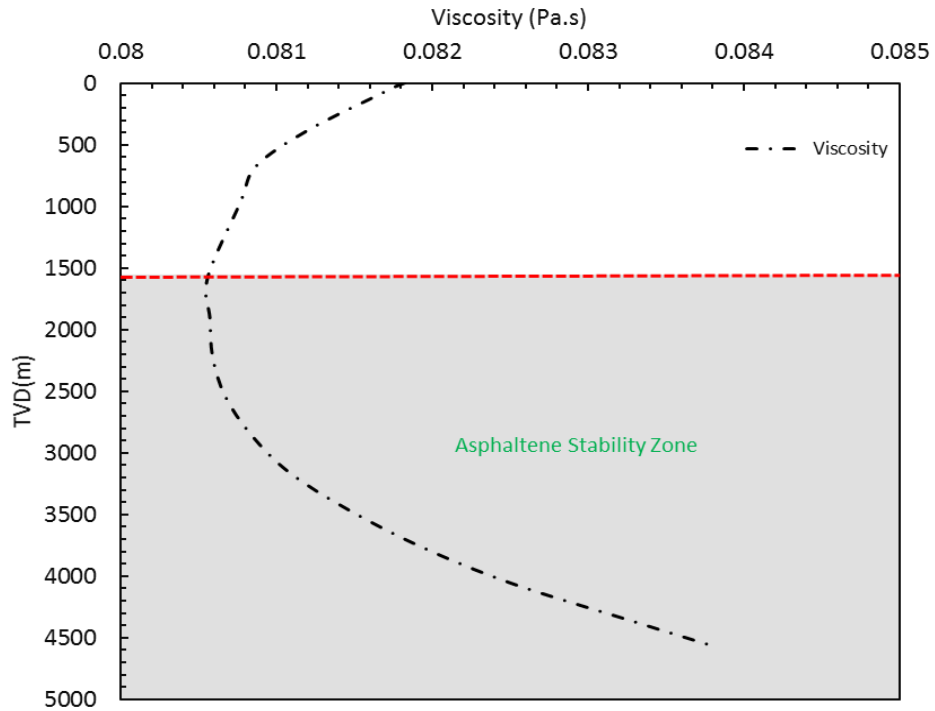


Figure 7. 6. Viscosity variation with the true vertical depth in two asphaltene stable and asphaltene unstable regions.

The asphaltene deposition could be reliably predicted, characterized as a highly oil viscous zone with high asphaltene content, by using modelling study of the crude oil viscosity changes with depth because of asphaltene compositional grading.

Utilizing appropriate kinetic parameters presented in Table 7.2 and also by employing the thermodynamic model explained in the previous sections, the asphaltene deposition model was developed. Figure 7.7 shows the variation of asphaltene deposition thickness in different true vertical depths (TVD) at various time periods. As seen from this figure, the time dependent deposition thickness increases over time in the studied well column. After nine months, a larger segment of the well column will be exposed to the asphaltene deposition. Also, it can be observed that at the depth of nearly 1600 meters the asphaltene

in the system started depositing, where the pressure of the system fell below the upper asphaltene onset pressure, and the thickness reached a maximum amount at the depth of nearly 800 meters. The reduction in the distance between the graphs with respect to time, as given in Figure 7.7, indicate that the asphaltene deposition rate decreases over time.

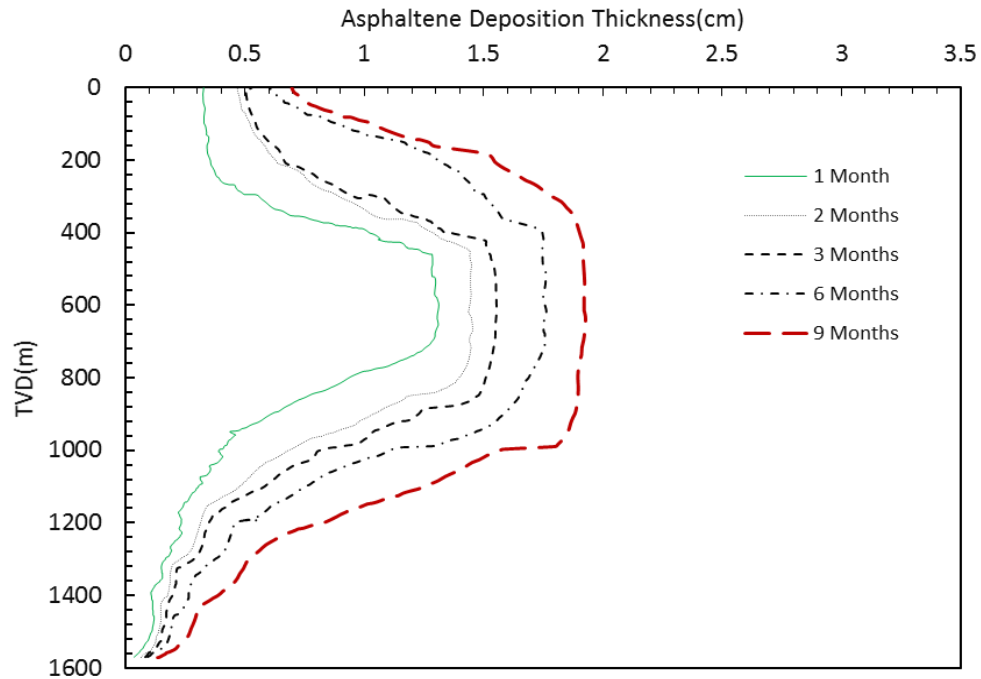


Figure 7. 7. Asphaltene deposit layer thickness distribution along the depth of the well bore for different production times.

This could be plausibly justified by the fact that upon depositing more asphaltene on tubing wall at constant bottom hole and wellhead pressures, a reduction in the flow area and consequently a reduction in the flow rate (Equation 7.27) can happen which, in turn, can lead to a less asphaltene flow causing a decrease in the asphaltene deposition rate. In addition, change in the wellbore radius and flow rate of the fluid can change the pressure-temperature conditions of the fluid altering the thermodynamic properties of the fluid along the wellbore. This effect can be clearly observed from Figure 7.8 which will be discussed.

Figure 7.8 shows the amount of destabilized and suspended asphaltene particles in the bulk of flow throughout the well column at various time periods. As can be seen from this figure, the asphaltene particles dissolved in the oil phase could start getting destabilized at the depth of nearly 1600 meters. The concentration changes displayed two distinct

transitions (d_1 , d_2) as a function of well depth for this system which was the result of variation in the amount of stable asphaltene at different P, T conditions following kinetic equations. This transition was observed during all production times at various depths with different slopes, but the initial concentration change (d_0-d_1) was more equally pronounced at all times which was reasonable according to the low amount of asphaltene deposition near upper onset line.

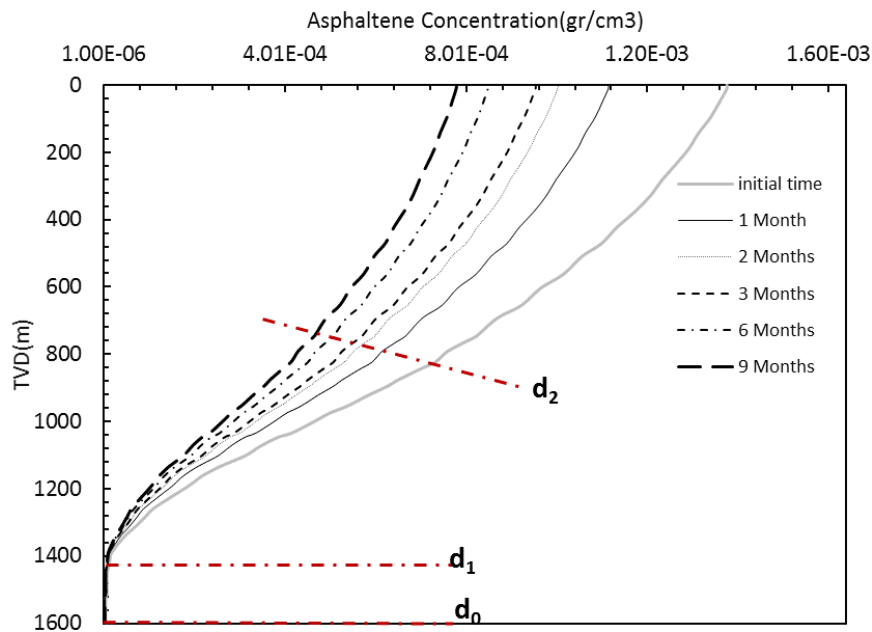


Figure 7. 8. Asphaltene concentration change along the depth of the well bore for different production times.

After the depth of around 1400(d_1), at the outset, the destabilization of asphaltene was fast and steep which was due to fast change in temperature and pressure of the flow. It is worth noting that the results given in Figure 7.8 were consistent with those reported as Figure 7.4 for the temperature and pressure profiles of the vertical flow from the reservoir to the wellhead. Starting from depth around 800(d_2) meters, the trend of destabilized asphaltene slowed down which showed a possible increase in the deposition of asphaltene already destabilized but suspended in the bulk of flow. Additionally, more deposition could result in less difference in concentration from equilibrium state could also explain the lower destabilization rate. The situation was exacerbated over the production life and it showed

that the system was more susceptible to asphaltene deposition at the wellhead and near the wellhead region. Also, decrease in the amount of the precipitated asphaltene over time could be explained by the change in the pressure-temperature conditions of the wellbore reducing the asphaltene phase fraction at equilibrium state. What's more, the previously discussed reduction in the asphaltene deposition rate can be explained by the reduction in the precipitated asphaltene amount after 9 months reducing the deposition rate according to Equation 7.15.

Figures 7.9 and 7.10 show the weight percent of destabilized and suspended asphaltene particles precipitated out of the bulk of flow in each group with different particle size as described in Table 7.1 at the initial flow rate and after nine months of production respectively.

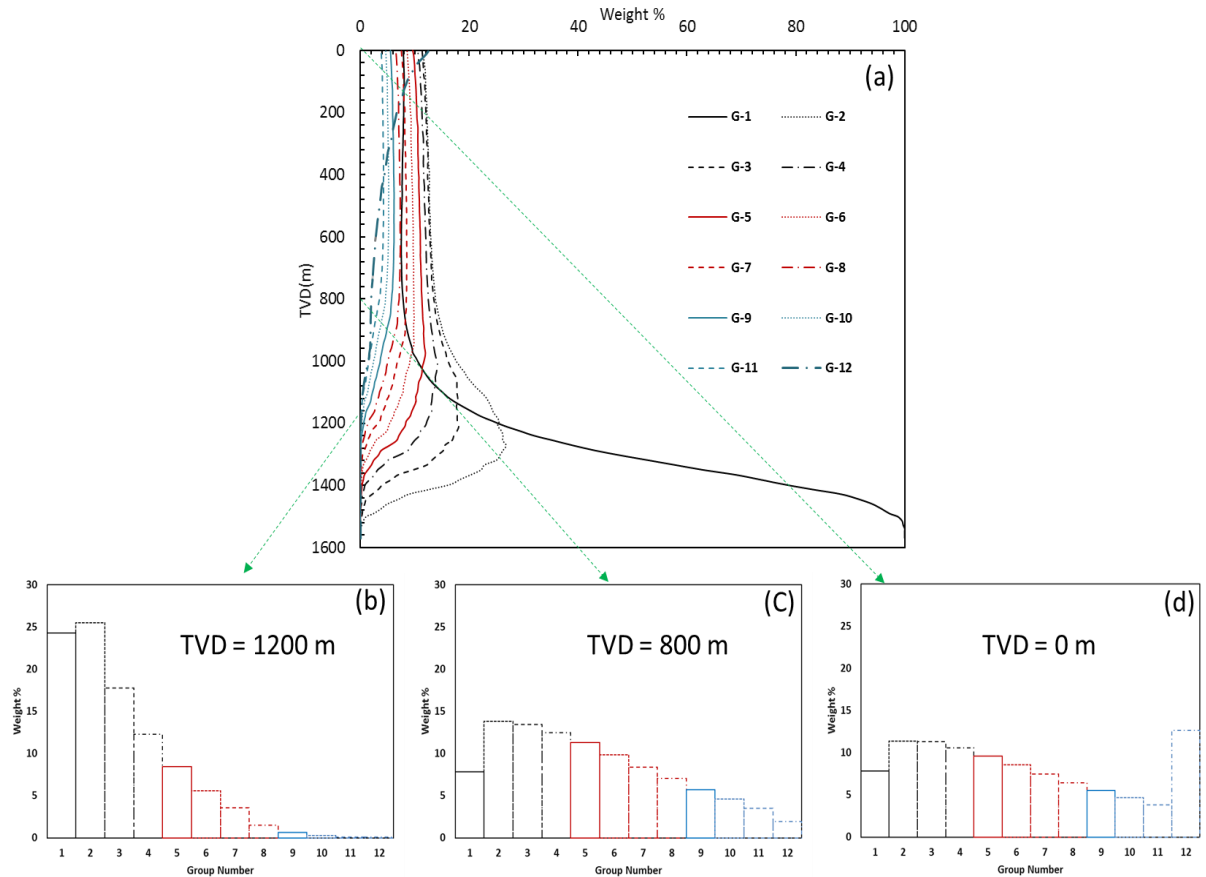


Figure 7. 9. Asphaltene particles size classification along the depth of the well bore at the initial flow of the production.

As it can be seen from Figures 7.9a and 7.10a, the percentage of nano-aggregates (Group 1) decreases along the well column. In fact, these particles significantly tended to get aggregated and formed larger aggregates. Some of the nano-aggregates can also deposit on the well column wall. Larger aggregates started increasing at the depth of nearly 1600 meters and reached a plateau at approximately 800 meters depth of the well column (see particle size distribution at this depth at Figure 7.9c and 7.10c). In particular, it was possible to recognize three main regimes for Groups 2-11 along the wellbore, i.e., an initial rapid increase of mass percent followed by a slow decrease which eventually evolved into a final plateau. Largest aggregates, formed as Group 12, could not deposit on the well column wall while smaller aggregates had higher potential to get deposited on the production tubing wall. In general, the same trend, as observed in the initial flow rate, can be seen after 9 months of production. However, it should be mentioned that, as expected, after nine months, the aggregate sizes decreased along the well column. It is also worth noting that the minimum amount of Group 1 along the wellbore after 9 months is substantially higher than that for the initial time, whereas, for the Group 12, graphs showed the opposite pattern.

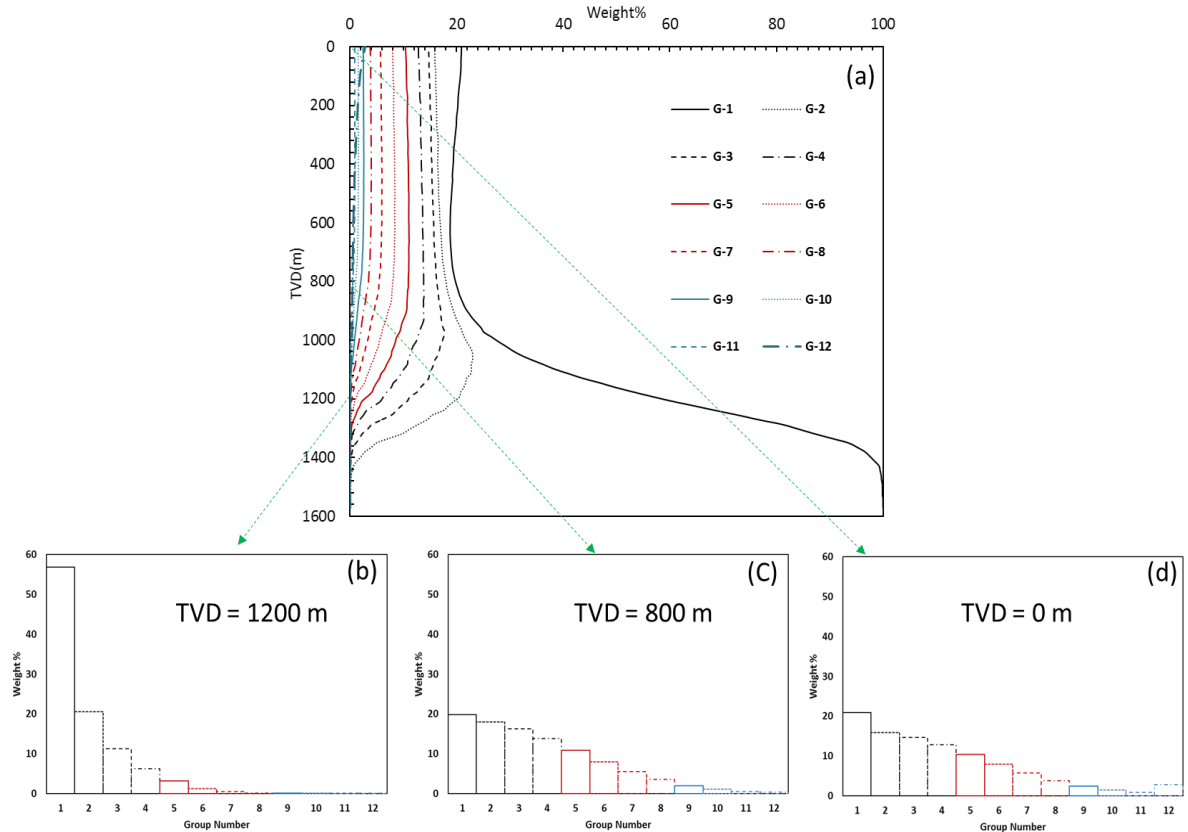


Figure 7. 10. Asphaltene particles size classification along the depth of the well bore after 9 months of production.

The possible reason for this behaviour is that owing to lower precipitated asphaltene concentration after 9 months (Figure 7.8), the asphaltene aggregation rate reduces according to Equation 7.6, which will keep the fraction of Group 1 at higher state and that of Group 12 at lower one.

Figure 7.11 shows the variation and distribution of asphaltene particles with different sizes along the well column at various time periods in depositing (Group 1-11) and overall (Group 1-12) forms. As seen, more deposition could occur with the asphaltene particles with smaller sizes. This can be justified by the fact that the smaller aggregates have larger diffusion coefficients and, therefore, move towards the pipeline wall more quickly and could get deposited on the surface.

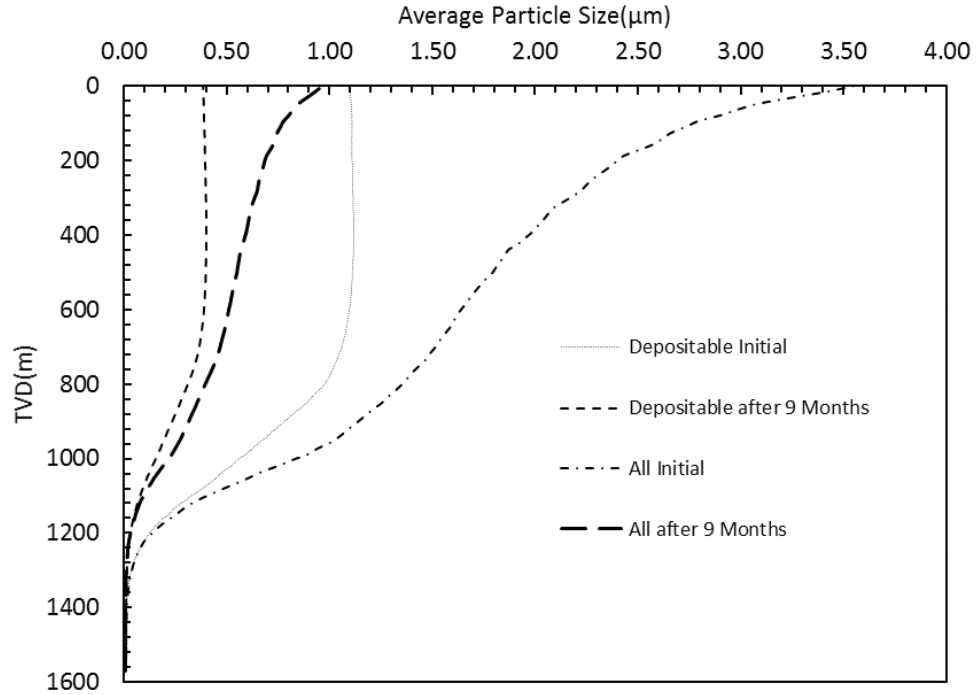


Figure 7. 11. Average asphaltene particles size distribution along the depth of the well bore for different production times.

It can be observed that the graphs for depositing particles reached a plateau after an initial increase, indicating the equality between precipitation and consumption of these particles both at deposition and forming Group12. Here, the beginning of the plateau depth was reasonably the same as those reported in Figures 7.9 and 7.10. Since average particle size depends on both number of particles and particles size, these results indicated that Group 12 had a major role in increasing overall particle size above the depth of 1200 (Figures 7.9b-d and 7.10b-d). Finally, it can be seen that the average size at the initial time was higher compared to that after 9 months. These results highlight the previously deduced effect of the aggregation rate change corresponding to the amount of precipitated asphaltenes.

7.3.2 Capillary Tube Experiments

The developed model for the prediction of asphaltene deposition rate on a steel surface was validated with the experimental data reported in the literature[36], [37]. The asphaltene deposition test, performed at the New Mexico Institute of Mining and Technology, was

used to assess the prediction capability of the new model. All the parameters including the saturates, aromatics, resins and asphaltene data, crude oil density, diameter, length of the capillary tube and the flow rate of crude oil and pentadecane solution were reported [36], [37]. The asphaltene deposition profile along the capillary length of the pipe was obtained and presented as Figure 7.12a. The deposition flux profile revealed that the amount of asphaltene deposition was maximum at the beginning of the capillary tube as a result of the maximum concentration driving force at these areas. The asphaltene deposition was reduced along the axial length of the capillary tube as the amount of asphaltene aggregates in the flowing crude oil/precipitant solution decreased. The comparison of the results from the developed model with the experimental data found in the experiments of Wang and Buckley[36] and Kurup et al.[37] is shown in Figure 7.12a.

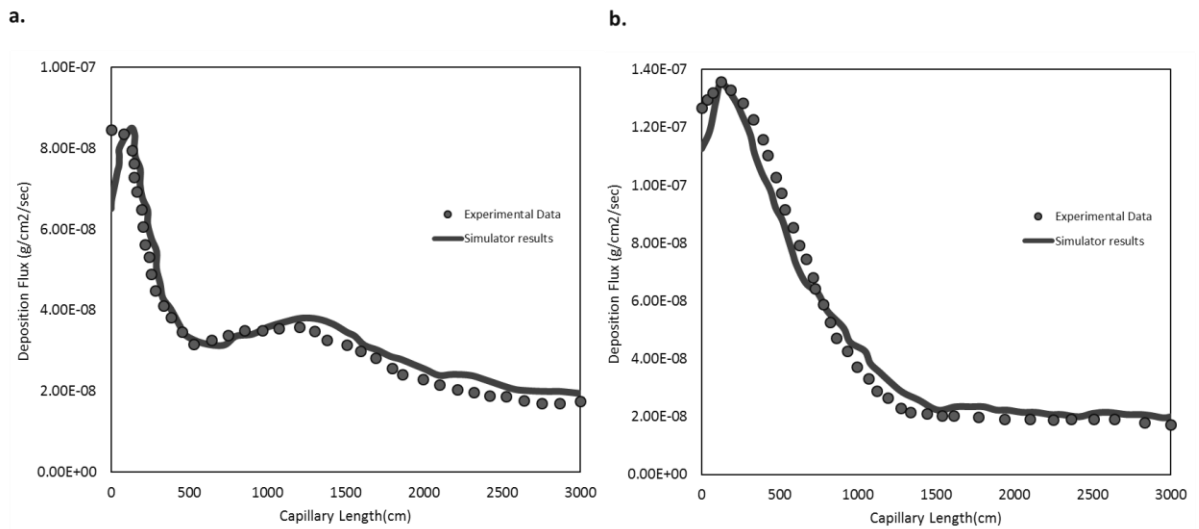


Figure 7. 12. The comparison of the results obtained from the model with the asphaltene deposition experimental data in a capillary tube for a) Test#1 and b) Test#2.

It should be stated that the kinetic parameters were determined by matching the data for the peak of the asphaltene deposition flux obtained by simulations with the experimental data. In this set of experiments, the temperature of the system was kept constant and the pressure change was not noticeable along the axial length of the tube. As can be seen, the results obtained from the new model were thoroughly consistent with the experimental results. Another capillary tube deposition experiment was conducted with different operating conditions using the same crude oil/pentadecane solution as explained for the previous test.

The aim of the second test was to investigate the effect of a change in operating conditions on the asphaltene deposition flux in the capillary test tube. The tube used in this set of experiments had a larger diameter, and the experiment was performed at a higher flow rate of the oil/precipitant solution. The asphaltene deposition flux profile along the capillary length of the pipe was presented in Figure 7.12b (solid black data points). It can be observed that for larger diameter capillary tube and higher flow rate, a relatively higher magnitude of asphaltene deposition can be seen as compared to the deposition flux in a thinner tube and at lower flow rates (Figure 7.12a). A larger diameter tube and higher flow rate resulted in a higher amount of asphaltene mass flux into the pipe, allowing more asphaltene particles to be unstable and precipitated out of the solution and ready to be deposited onto the pipe surface, and therefore made an increase in the asphaltene deposition accordingly. The results of the new model were compared with this set of experimental data. Since the same oil/precipitant solution was used in the second set and the temperature and the other conditions were all remained constant, hence, the same kinetic parameters were used for the asphaltene prediction as explained in the case of the first comparison. Once again, it can be seen from this comparison that the new model can accurately predict the experimental data.

7.4 Conclusions

A new dynamic and two-dimensional particle scale model was developed in this work to simulate the asphaltene deposition in a synthetic oil well. The model could explain the effect of asphaltene particle size in the aggregation and deposition of asphaltene on the well tubing wall. It was shown that the asphaltene aggregates tended to interact with each other due to the Brownian motion and formed larger particles and, therefore, this fact was taken into account in the asphaltene deposition model by considering the variation of asphaltene particle size during the oil flow along the flowline. It was also concluded that smaller aggregates had higher tendency to deposit on the tubing wall due to the large radial diffusivity of the particles. The results showed that the amount of asphaltene deposition along with the rate of asphaltene deposition strongly depended on the production time and it was concluded that both the amount and the rate of asphaltene deposition reduced over time. The results obtained from the new model were compared with those reported in the

literature and good agreement between the results was observed. In the modeling of the crude oil phase behavior, an accurate and reliable equation of state was employed in order to characterize the phase behavior of oil/asphaltene/gas systems. It should be stated that all thermodynamic parameters, used in the model, were directly emanated from the published literature. The capability in predicting the experimental results associated with the numerical features including the computation time could be considered as the clearest advantages of the new model developed in this work.

7.5 References

- [1] D. Eskin, O. Mohammadzadeh, K. Akbarzadeh, S. D. Taylor, and J. Ratulowski, "Reservoir impairment by asphaltenes: A critical review," *Can. J. Chem. Eng.*, vol. 94, no. 6, pp. 1202–1217, 2016.
- [2] J. Escobedo and G. Mansoori, "Asphaltene and Other Heavy-Organic Particle Deposition During Transfer and Production Operations," in *Proceedings of SPE Annual Technical Conference and Exhibition*, 1995, pp. 343–358.
- [3] D. M. Paes, P. R. Ribeiro, M. Shirdel, and K. Sepehrnoori, "Study of asphaltene deposition in wellbores during turbulent flow," *J. Pet. Sci. Eng.*, vol. 129, pp. 77–87, 2015.
- [4] M. Jamialahmadi, B. Soltani, H. Müller-Steinhagen, and D. Rashtchian, "Measurement and prediction of the rate of deposition of flocculated asphaltene particles from oil," *Int. J. Heat Mass Transf.*, vol. 52, no. 19, pp. 4624–4634, 2009.
- [5] B. Soltani Soulgani, D. Rashtchian, B. Tohidi, and M. Jamialahmadi, "Integrated Modelling Methods for Asphaltene Deposition in Wellstring," *J. Japan Pet. Inst.*, vol. 52, no. 6, pp. 322–331, 2009.
- [6] E. Ramirez-Jaramillo, C. Lira-Galeana, and O. Manero, "Modeling asphaltene deposition in production pipelines," *Energy & fuels*, vol. 20, no. 3, pp. 1184–1196, 2006.
- [7] D. Q. Kern and R. E. Seaton, "A theoretical analysis of thermal surface fouling," *Br. Chem. Eng.*, vol. 4, no. 5, pp. 258–262, 1959.
- [8] E. D. Burger, T. K. Perkins, and J. H. Striegler, "Studies of wax deposition in the trans Alaska pipeline," *J. Pet. Technol.*, vol. 33, no. 06, pp. 1–75, 1981.
- [9] M. Greaves, S. Ayatollahi, M. Moshfeghian, H. Alboudwarej, and H. W. Yarranton, "Estimation of SARA fraction properties with the SRK EOS," *J. Can. Pet. Technol.*, vol. 43, no. 09, 2004.

- [10] D. Eskin, J. Ratulowski, K. Akbarzadeh, and S. Andersen, "Modeling of asphaltene deposition in a production tubing," *AIChE J.*, vol. 58, no. 9, pp. 2936–2948, 2012.
- [11] F. M. Vargas, J. L. Creek, and W. G. Chapman, "On the Development of an Asphaltene Deposition Simulator," *Energy & Fuels*, vol. 24, no. 4, pp. 2294–2299, Apr. 2010.
- [12] S. M. Hashmi, M. Loewenberg, and A. Firoozabadi, "Colloidal asphaltene deposition in laminar pipe flow: Flow rate and parametric effects," *Phys. Fluids*, vol. 27, no. 8, p. 83302, 2015.
- [13] C. Vilas Bôas Fávero, A. Hanpan, P. Phichphimok, K. Binabdullah, and H. S. Fogler, "Mechanistic Investigation of Asphaltene Deposition," *Energy & Fuels*, vol. 30, no. 11, pp. 8915–8921, Nov. 2016.
- [14] M. Elimelech, J. Gregory, X. Jia, R. A. Williams, M. Elimelech, J. Gregory, X. Jia, and R. A. Williams, "Chapter 6 – Modelling of aggregation processes," in *Particle Deposition & Aggregation*, 1995, pp. 157–202.
- [15] J. A. Barker and D. Henderson, "Perturbation theory and equation of state for fluids. II. A successful theory of liquids," *J. Chem. Phys.*, vol. 47, no. 11, pp. 4714–4721, 1967.
- [16] J. Gross and G. Sadowski, "Perturbed-Chain SAFT: An Equation of State Based on a Perturbation Theory for Chain Molecules," *Ind. Eng. Chem. Res.*, vol. 40, no. 4, pp. 1244–1260, 2001.
- [17] M. L. Michelsen, "The isothermal flash problem. Part I. Stability," *Fluid Phase Equilib.*, vol. 9, no. 1, pp. 1–19, 1982.
- [18] M. L. Michelsen, "The isothermal flash problem. Part II. Phase-split calculation," *Fluid Phase Equilib.*, vol. 9, no. 1, pp. 21–40, 1982.
- [19] M. L. Michelsen, "Calculation of multiphase equilibrium," *Comput. Chem. Eng.*, vol. 18, no. 7, pp. 545–550, 1994.
- [20] A. K. Gupta, P. Raj Bishnoi, N. Kalogerakis, and R. Bishnoi, "A Method for the Simultaneous Phase Equilibria and Stability Calculations for Multiphase Reacting and Non-Reacting Systems," *Fluid Phase Equilib.*, vol. 63, pp. 65–89, 1991.
- [21] S. R. Panuganti, M. Tavakkoli, F. M. Vargas, D. L. Gonzalez, and W. G. Chapman, "SAFT model for upstream asphaltene applications," *Fluid Phase Equilib.*, vol. 359, pp. 2–16, 2013.
- [22] J. A. Jossi, L. I. Stiel, and G. Thodos, "The viscosity of pure substances in the dense gaseous and liquid phases," *AIChE J.*, vol. 8, no. 1, pp. 59–63, 1962.
- [23] J. Lohrenz, B. G. Bray, and C. R. Clark, "Calculating viscosities of reservoir fluids from their compositions," *J. Pet. Technol.*, vol. 16, no. 10, pp. 1–171, 1964.

- [24] H. C. Brinkman, "The viscosity of concentrated suspensions and solutions," *J. Chem. Phys.*, vol. 20, no. 4, p. 571, 1952.
- [25] T. Maqbool, S. Raha, M. P. Hoepfner, and H. S. Fogler, "Modeling the aggregation of asphaltene nanoaggregates in crude oil- precipitant systems," *Energy & Fuels*, vol. 25, no. 4, pp. 1585–1596, 2011.
- [26] C. V. B. Fávero, T. Maqbool, M. Hoepfner, N. Haji-Akbari, and H. S. Fogler, "Revisiting the flocculation kinetics of destabilized asphaltenes," *Adv. Colloid Interface Sci.*, vol. 244, pp. 267–280, 2017.
- [27] Y. A. Cengel and J. M. Cimbala, "Fluid Dynamics: Fundamentals and Applications," *Seoul, Korea: McGraw-Hill Korea*, 2006.
- [28] J. T. Edward, "Molecular volumes and the Stokes-Einstein equation," *J. chem. Educ.*, vol. 47, no. 4, p. 261, 1970.
- [29] A. K. Datta, *Biological and bioenvironmental heat and mass transfer*. CRC Press, 2002.
- [30] P. Singh, R. Venkatesan, H. S. Fogler, and N. Nagarajan, "Formation and aging of incipient thin film wax-oil gels," *AIChE J.*, vol. 46, no. 5, pp. 1059–1074, 2000.
- [31] S. Whitaker, "Flow in porous media I: A theoretical derivation of Darcy's law," *Transp. porous media*, vol. 1, no. 1, pp. 3–25, 1986.
- [32] N. H. Chen, "An explicit equation for friction factor in pipe," *Ind. Eng. Chem. Fundam.*, vol. 18, no. 3, pp. 296–297, 1979.
- [33] S. Zheng, M. Saidoun, T. Palermo, K. Mateen, and H. S. Fogler, "Wax Deposition Modeling with Considerations of Non-Newtonian Characteristics: Application on Field-Scale Pipeline," *Energy & Fuels*, 2017.
- [34] D. L. Gonzalez, P. D. Ting, G. J. Hirasaki, and W. G. Chapman, "Prediction of asphaltene instability under gas injection with the PC-SAFT equation of state," *Energy & fuels*, vol. 19, no. 4, pp. 1230–1234, 2005.
- [35] P. David Ting, G. J. Hirasaki, and W. G. Chapman, "Modeling of Asphaltene Phase Behavior with the SAFT Equation of State," *Pet. Sci. Technol.*, vol. 21, no. 3–4, pp. 647–661, Jan. 2003.
- [36] J. Wang, J. S. Buckley, and J. L. Creek, "Asphaltene deposition on metallic surfaces," *J. Dispers. Sci. Technol.*, vol. 25, no. 3, pp. 287–298, 2004.
- [37] A. S. Kurup, F. M. Vargas, J. Wang, J. Buckley, J. L. Creek, H. Subramani J, and W. G. Chapman, "Development and application of an asphaltene deposition tool (ADEPT) for well bores," *Energy & Fuels*, vol. 25, no. 10, pp. 4506–4516, 2011.

Chapter 8-Effect of Different Gas Injection Scenarios on Asphaltene Precipitation and Deposition Using Quartz Crystal Microbalance

8.1 Introduction

Asphaltene precipitation and deposition is a common issue with which operators are faced in oilfields worldwide while miscible gas is injected to reservoirs for enhanced oil recovery (EOR) purposes. Gas injection is an effective tool for EOR and can increase oil recovery in many cases due to a reduction in oil viscosity or pushing the oil towards the well, whether it is miscible or not. Two of the most effective agents in this type of EOR technique are carbon dioxide and natural gas which are observed to increase oil production although CO₂ or natural gas injection into an oil reservoir usually alters the flow behaviour and the fluids equilibrium properties which can result asphaltene precipitation and deposition [1-4]. N₂ has also been used for gas injection in deep, high pressure light oil reservoirs since it can function as an inert and non-corrosive gas. N₂ gas flooding can achieve miscible conditions for such reservoirs. The applications of immiscible N₂ gas injection can be mentioned as reservoir pressure preservation, cycling of condensate reservoirs and as a drive gas for immiscible slugs [5-8]. As the composition of reservoir fluid is changed due to gas injection process, the asphaltene nanoaggregates might precipitate out of the crude oil and deposition occurs onto solid surfaces [3-7]. Asphaltene deposition can plug the formation, wellbores, and production facilities, isolate oil from the flowing section of the reservoir, significantly alter the wettability properties of the reservoir, and therefore may cause a reduction in the efficiency of the EOR processes. Therefore, a comprehensive investigation on asphaltenes should be conducted as a section of gas-injection studies. Researchers often use n-C₇ at ambient conditions for laboratory tests, whilst asphaltene precipitation happens in the field as a result of changes in pressure, temperature and composition. One of the key parameters for identifying asphaltene precipitating process is the asphaltene onset pressure (AOP). A common and widespread approach which has been utilised in the literature for determination of AOP is solid detection system (SDS) based on near-infrared (NIR) light-scattering method [9-13]. The ordinary procedures for detecting AOP are commonly

performed by using a mixture of reservoir fluid sample and injection gas, and different gas-combination volumes are usually examined [1, 2, 14]. The advantage of employing different experimental parameters of gas-combination volume is better understanding of asphaltene risks in a gas injection process. This kind of study however can demonstrate only a static asphaltene behaviour for a specific type of gas, and it may cause incorrect evaluation of asphaltene risks. Limited experimental data can be found in literature, focusing on the potential influence of gas flooding on asphaltene induced flow assurance problems.

One of the main objectives of this study is to provide novel insights into the effect of different gases on asphaltene instability in crude oil under real conditions. This report presents a novel technique, high pressure high temperature quartz crystal microbalance (HPHT-QCM), for determination of asphaltene onset pressure and asphaltene deposition rate in presence of various gases. The effect of four widely used injection gases for EOR purposes; nitrogen (N₂), carbon dioxide (CO₂), methane (CH₄) and natural gas on asphaltenes were investigated using HPHT-QCM. The effects of two different mixtures of gases which are named Mix.A and flue gas on asphaltene precipitation and deposition rate have also been investigated in order to determine the influence of gas impurities on asphaltene phase behaviour.

8.2 Experimental Sections

8.2.1 Materials

The crude oil under this study was a light separated oil with an API° 33.7. Table 8.1 shows its chemical compositions and PVT properties at both atmospheric and reservoir conditions.

Table 8. 1. Oil Composition at atmospheric and reservoir conditions and respective Thermodynamic Data*

Component	Atmospheric Liquid	Reservoir Fluid
(Symbol)	(Mole %)	(Mole %)

N₂	0.000	0.707
CO₂	0.000	0.349
H₂S	0.000	0.000
C₁	0.085	48.920
C₂	0.172	5.376
C₃	0.830	5.348
i-C₄	0.433	1.097
n-C₄	1.753	2.828
i-C₅	1.418	1.172
n-C₅	2.757	1.672
i-C₆	2.591	1.149
n-C₆	2.637	1.059
Mc-C₅	1.317	0.515
Benzene	0.220	0.076
c-C₆	0.845	0.314
C₇	5.202	1.876
Mc-C₆	1.782	0.634
Toluene	0.733	0.254
i-C₈	0.097	0.044
C₈	6.499	2.259
Ethyl Benzene	0.546	0.189
m&p-Xylene	0.792	0.274
o-Xylene	0.944	0.325
C₉	5.241	1.811
C₁₀	7.170	2.474
C₁₁	5.501	1.896
C₁₂	4.481	1.544
C₁₃	4.271	1.472
C₁₄	3.717	1.281
C₁₅	3.305	1.139

C₁₆	2.849	0.982
C₁₇	2.442	0.842
C₁₈	2.334	0.804
C₁₉	2.148	0.740
C₂₀	1.895	0.653
C₂₁	1.597	0.550
C₂₂	1.398	0.482
C₂₃	1.306	0.450
C₂₄	1.198	0.413
C₂₅	1.077	0.371
C₂₆	0.948	0.327
C₂₇	0.918	0.316
C₂₈	0.878	0.303
C₂₉	0.824	0.284
C₃₀₊	12.849	4.428

* API Gravity: 33.7°API @ 60°F (Water Free), Vapor Gravity: 0.817 (Air = 1.00), MW: 228.92 g.mol⁻¹, wt% of C₇₊ fractions content: 80.486, wt% of C₁₀₊ fractions content: 70.646, wt% of C₂₀₊fractions content: 45.120, wt% of C₃₀₊ fractions content: 30.688.

In this work, dead crude oil was mixed with different gases, N₂, CO₂ and CH₄, Mix. A, natural and flue gases to investigate the effect of these gases on asphaltene instability in crude oil. The composition of Mix. A, natural and flue gas are shown in Tables 8.2, 8.3 and 8.4, respectively.

Table 8. 2. Injected Mix. A gas composition

Component	Mole%
N ₂	20.05
C ₁	41.30
CO ₂	38.65

Table 8. 3. Injected natural gas composition

Component	Mole%
N ₂	1.84
C ₁	89.94
CO ₂	0.91
C ₂	5.32
C ₃	1.45
<i>i</i> C ₄	0.20
<i>n</i> C ₄	0.21
<i>i</i> C ₅	0.07
(<i>n</i> C ₅) + C ₆ ⁺	0.06

Table 8. 4. Injected flue gas composition

Component	Mole%
N ₂	84.51
CO ₂	15.49

8.2.2 High Pressure-High Temperature Quartz Crystal Microbalance (HPHT-QCM)

One of our main goals for this study was the design and development of a HPHT-QCM system for investigation of asphaltene instability in crude oil in presence of various gases. The system is required to work under different ranges of reservoir pressure and temperatures and also crude oil composition. Figure 8.1 presents both the picture and schematic diagram of the HPHT-QCM system. It consists of the high-pressure cells, water jacket, temperature controlled circulator, a magnetic mixer system as an agitator, quizix pump, high-pressure vessels, valves and lines, pressure and temperature sensors, and different gauges and indicators. The maximum working pressure of this set up is 6000 psi, and the system can be heated up to 150 °C. The mixing cell had a volume of 120 mL. The HPHT-QCM system has the capability to conduct tests under wide ranges of pressure, temperature, and composition. The principal of the measurement is to monitor changes in the Resonant Frequency (RF), and electrical properties at RF, for a QCM submersed in the test fluid (as a result of variations in the mass of the QCM or changes in the viscosity and density of the fluids brought about by changes in temperature and/or pressure). In this

work, the capability of the QCM has been tested for monitoring asphaltene onset pressure (AOP) changes in real fluids in presence of different gases. Before the measurement, first the crude oil was heated for 2hrs at 60 °C and then vigorously shaken to dissolve any solid materials such as wax and asphaltenes in the oil and maintain them in liquid phase. Then 70 mL of crude oil was inserted into the high-pressure mixing cell and QCM immersed inside the oil. The solution was mixed at constant rate of 500 rpm during all gas injection processes. Temperature was set at 60 °C for conducting the experiments. Gas was then injected to give a starting pressure at which the system was stable with no asphaltene deposition occurring. The pressure was then increased step-wise. Each step was 10 psi for 9 mins. During the injection process, the resonance frequency was measured through the reservoir fluid every 15 sec.



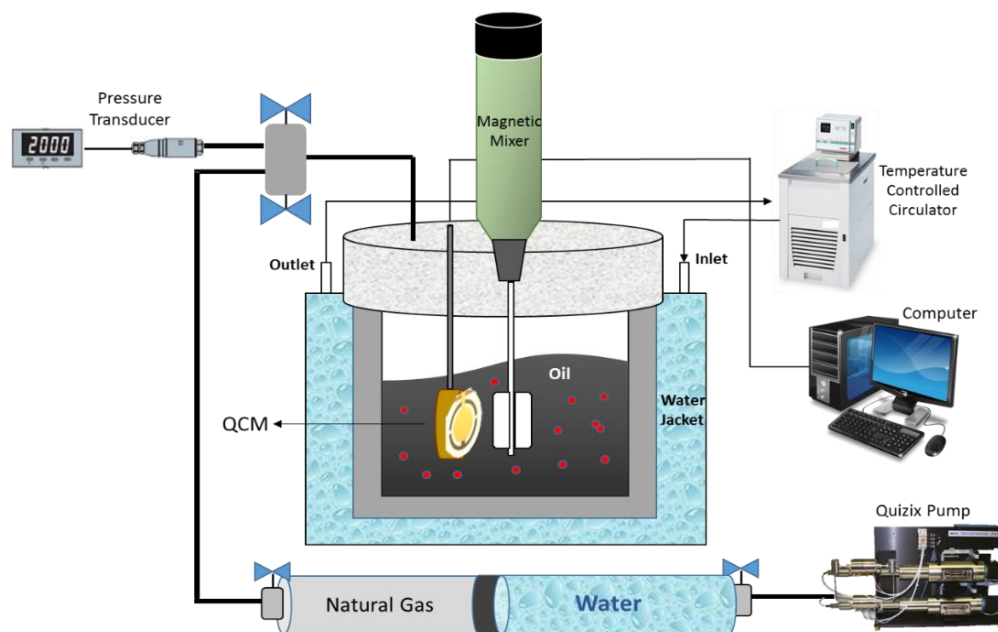


Figure 8. 1. Picture and schematic diagram of HPHT-QCM set up

8.3 Results and Discussion

The QCM resonant frequency (RF) was monitored during the gas injection process to detect the asphaltene onset pressure. The RF is inversely proportional to the mass of QCM crystal surface. The RF is very sensitive to mass change meaning that levels down to hundreds of nanograms of asphaltene can be Hz. The initial asphaltene test was conducted on at 60 °C with continuous natural gas injection. The obtained result for onset pressure (AOP) is presented in Figure 8.2 which shows ΔRF (HZ) versus pressure.

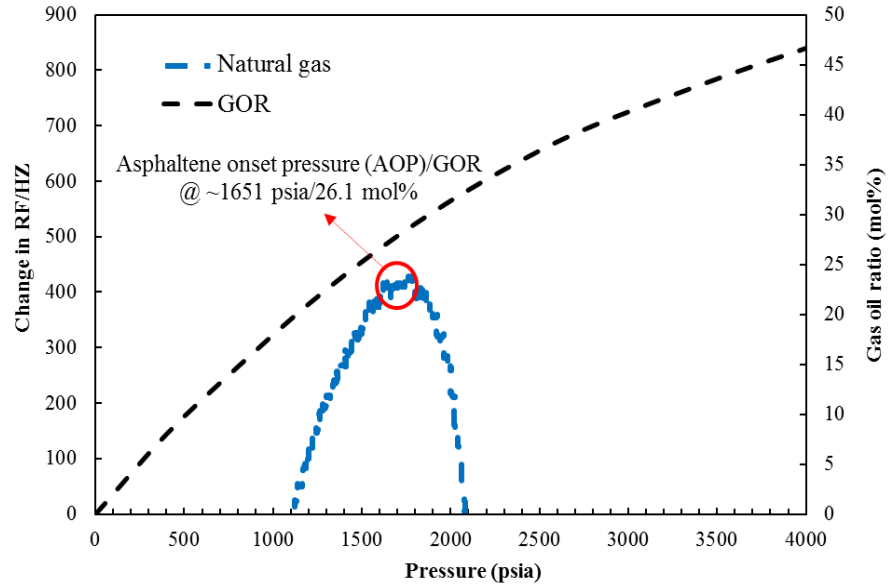


Figure 8. 2. Results of the HPHT-QCM method for the crude oil mixed with natural gas at 60 °C

Based on the data presented in Figure 8.2, the asphaltene onset pressure was detected ~1780 psia due to injection of natural gas at 60 °C and 500 rpm mixing for 24 h. The experimental data obtained by the HPHT-QCM technique are quite repeatable. Figure 8.3 shows three different data sets obtained by the QCM for the crude oil used in this study mixed with natural gas for 24 h. Figure 8.3 shows that both the trend of data and the detection of asphaltene onset pressure are similar in the three tests. For all of the experimental data obtained in this study, each single experiment has been repeated at least 2 times.

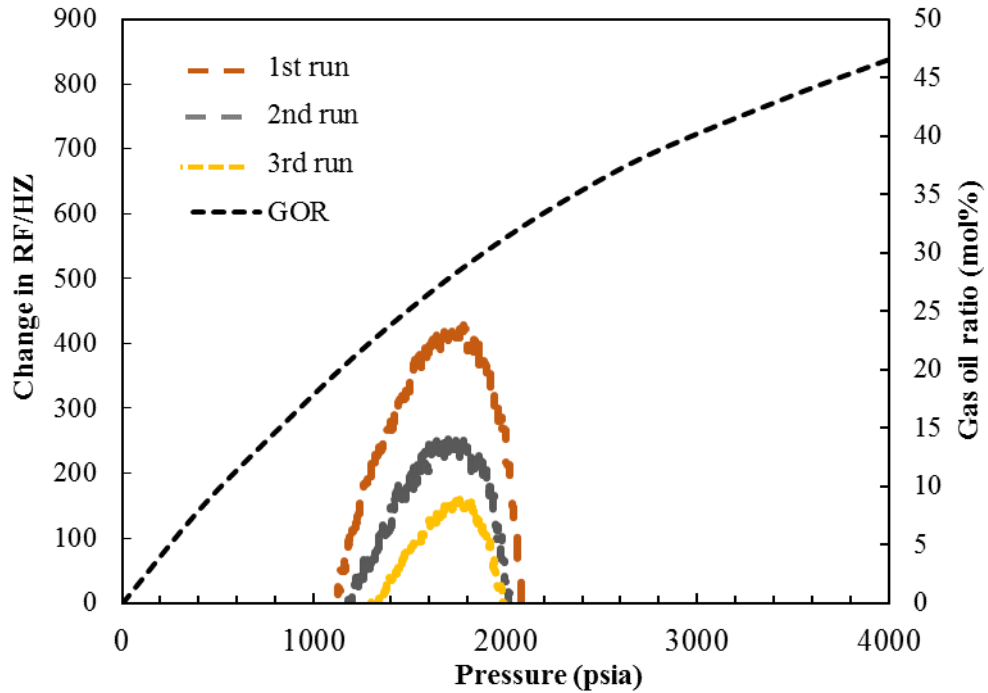


Figure 8. 3. Results of 3 repetitions for the crude oil mixed with natural gas at 60 °C

The AOP is dependent upon the type of injected gas which is mixed with crude oil inside the QCM cell. The AOP are much lower for the crude oil with injected CO₂ compared to other injected gases. The effects of added gases on reducing asphaltene stability in the crude oil used in this work are found in the following order: CO₂ > Natural gas > CH₄ > Mix. A > N₂ & Flue gas. The effect of gas type on the AOP shifting for four injected fluids, CO₂, CH₄, Mix. A and Natural gas is presented in Figure 8.4.

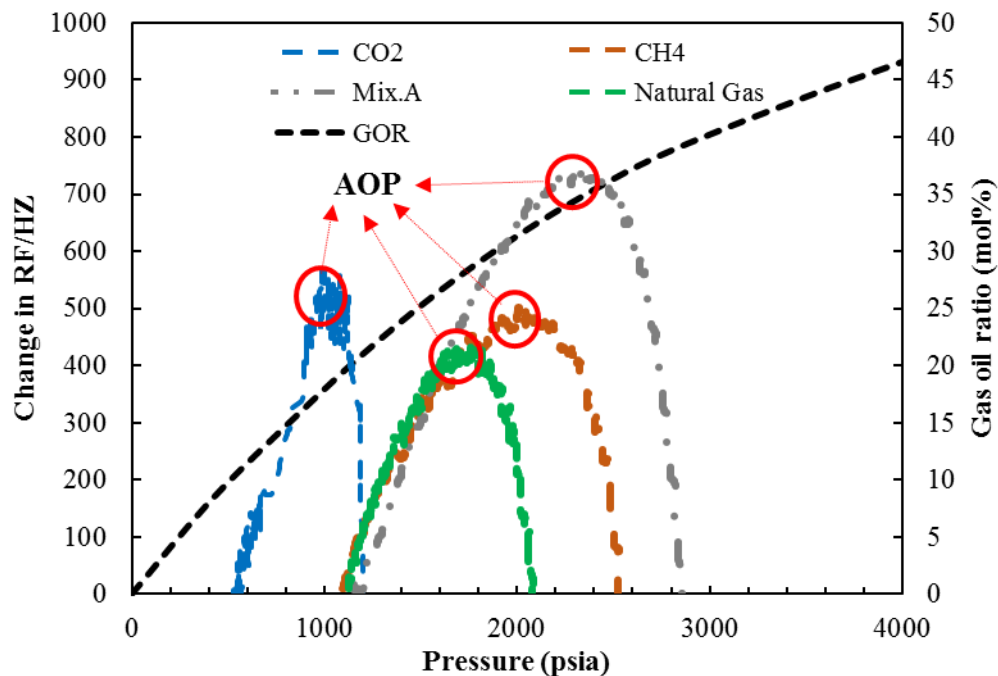


Figure 8. 4. The effect of injected gas type on asphaltene onset pressure obtained by HPHT-QCM technique

In all cases, a new sample from the same crude oil was used. The small variation in the temperature of the system did not have any strong effect on the obtained results. The AOPs/GOR were detected by HPHT-QCM at around 1040 psia/17.9 mol%, 1651 psia/26.1 mol%, 2082 psia/32.2 mol%, and 2360 psia/34.9 mol% for the injected CO₂, natural gas, CH₄, and Mix. A gases, respectively. For the other two injected gases N₂ and flue gas, no asphaltene precipitation was observed up to 6000 psia at the same temperature and agitating conditions. The results of these tests and experimental conditions are shown in Table 8.5.

Table 8. 5. Experimental conditions and asphaltene phase behaviour for different gas injection scenarios

Gas type	Step	Pressure (psia)	Temperature (°C)	Mixing time @ 500 rpm (h)	Phase(s)*	Asphaltene behaviour status
Natural Gas						
	1	1120	60	24	L+G	no precipitation
	25	1360	60	24	L+G	no precipitation
	43	1540	60	24	L+G	no precipitation
	67	1780	60	24	L+G+S	precipitation

	79	1900	60	24	L+G+S	deposition
	109	2200	60	24	L+G+S	deposition
CO₂						
	1	520	60	24	L+G	no precipitation
	25	760	60	24	L+G	no precipitation
	41	920	60	24	L+G	no precipitation
	53	1040	60	24	L+G+S	precipitation
	61	1120	60	24	L+G+S	deposition
	69	1200	60	24	L+G+S	deposition
Mix. A						
	1	1140	60	24	L+G	no precipitation
	67	1800	60	24	L+G	no precipitation
	123	2360	60	24	L+G+S	precipitation
	145	2580	60	24	L+G+S	deposition
	149	2620	60	24	L+G+S	deposition
	155	2680	60	24	L+G+S	deposition
N₂						
	1	1200	60	72	L+G	no precipitation
	75	1940	60	72	L+G	no precipitation
	117	2360	60	72	L+G	no precipitation
	249	3680	60	72	L+G	no precipitation
	365	4860	60	72	L+G	no precipitation
	455	5740	60	72	L+G	no precipitation
CH₄						
	1	1080	60	24	L+G	no precipitation
	15	1220	60	24	L+G	no precipitation
	57	1640	60	24	L+G	no precipitation
	79	1860	60	24	L+G	no precipitation
	103	2100	60	24	L+G+S	precipitation
	141	2480	60	24	L+G+S	deposition
Flue Gas						
	1	1200	60	72	L+G	no precipitation
	69	1880	60	72	L+G	no precipitation
	127	2460	60	72	L+G	no precipitation
	253	3720	60	72	L+G	no precipitation

379	4980	60	72	L+G	no precipitation
455	5740	60	72	L+G	no precipitation

* L: liquid, G: gas, S: solid (asphaltene aggregates)

All data sets obtained from HPHT-QCM indicate an increase in the amount of the asphaltene deposits adhering onto the QCM surface with increasing pressure. Additionally, at higher pressures, the tendency toward asphaltene precipitation phenomena is stronger than at lower pressures. The gas influence on the asphaltene precipitation can be explained in terms of the solubility behaviour and the associated polarizability. For non-polar components mixtures, the mixture solubility parameter is a function of density and the electronic polarizabilities of the mixture components. If a high amount of low-molecular weight species is dissolved into the oil phase, the solubility parameter is reduced and asphaltene precipitation might occur. The presence of components in crude oil with lower polarizabilities reduces the oil's solubility parameter and increases the probability of asphaltene precipitation. Natural gas, CH₄, CO₂ and Mix. A show low polarizability values that make them strong asphaltene precipitants for the crude oil. Participation of components which are high in polarizability keeps asphaltenes stable in the solution. As an example, toluene, benzene, xylene and high molecular weight aromatic molecules are well-known asphaltene solvents with high polarizability. Composition variations due to gas injection which increase density might increase asphaltene solubility, and composition changes due to pressure depletion that reduce the density might have the opposite influence on asphaltene stability in solution. Because both density and component polarizability influence the solubility parameter of the solution, contradictory effects could be seen.

The results regarding RF reduction versus time for six tests with various injected gases are plotted in Figure 8.5 which represents the effect of gas type on deposition rate after the AOP.

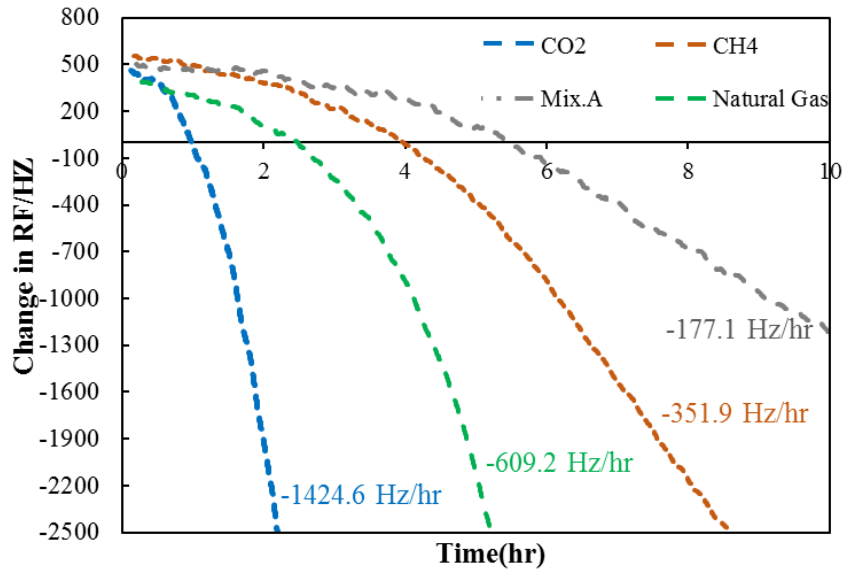


Figure 8. 5. Plot showing changes in RF vs. time represents asphaltene deposition rate affected by different injected gas types.

The results indicate that all gases, except N₂ and flue gas, increase the asphaltene deposition rate after exceeding the AOP. This phenomenon is attributed to the change in the adsorption behaviour of the asphaltene aggregates onto the QCM gold surface, from different gas molecular structure which can interrupt the asphaltene's functional groups-gold surface interactions. As can be seen, there is a significant difference in the plotted curves between the crude oil with CO₂ gas injection and the same oil mixing with Mix. A. Mix. A which contains 28.65 mole% CO₂ has a significant performance in reducing the deposition rate from -1424 Hz/hr to -177 Hz/hr compared to the pure CO₂ injection. The effects of injected gas type on increasing asphaltene deposition rate onto the QCM surface after AOP for the crude oil utilised in this research study are found in the following order: CO₂ (-1424.6 HZ/hr) > Natural gas (-609.2 HZ/hr) > CH₄ (-351.9 HZ/hr) > Mix. A (-177.1 HZ/hr) > N₂ & Flue gas which is the same order as for asphaltene instability in crude oil.

These tests were carried out using HPHT-QCM technology in the absence of a porous medium (real reservoir core plug) with no fluid flow. However, heavy asphaltene deposition is occurs in the well tubings of reservoirs during both natural pressure depletion and different EOR gas injection operations. These facts show extremely high importance of the asphaltene precipitation of during the oil flow in the reservoir or in the well's tubing

and the respective streaming potential and their interactions with the surface-active sites of the asphaltene aggregates. A careful study of this should be conducted in the future in order to quantify the effect of various fluid flow conditions and the characteristics of asphaltene precipitation, aggregation and deposition phenomena for different gas injection scenarios in core plugs.

8.4 Conclusions

In this paper, a novel experimental technique called HPHT-QCM technique has been proposed to detect asphaltene onset pressure for real oil samples in presence of gas and monitor the effect of different gas injection scenarios on asphaltene precipitation and deposition phenomena. The injection of Natural gas, CH₄, Mix. A and CO₂ promotes asphaltene precipitation and deposition in live oil fluids. The effects of injected gases on increasing both asphaltene precipitation and deposition rate in the crude oil used in this study are found in the following order: CO₂ > Natural gas > CH₄ > Mix. A > N₂ & Flue gas. The presence of light components with lower polarizabilities decreases the oil's solubility parameter and increases the probability of asphaltene precipitation and deposition accordingly.

8.5 References

- [1] Jamaluddin, A.K.M., Nighswander, J.N., Kohse, B.F., El Mahdi, A., Binbrek, M.A., and Hogg, P.F. 2000. Experimental and Theoretical Assessment of the Asphaltene Precipitation Characteristics of the Sahil Field under a Proposed Miscible Gas Injection Scheme. Paper SPE 87292 presented at the Abu Dhabi International Petroleum Exhibition and Conference, 15–18 October. <http://dx.doi.org/10.2118/87292-MS>.
- [2] Parra-Ramirez, M., Peterson, B., and Deo, M.D. 2001. Comparison of First and Multiple Contact Carbon Dioxide Induced Asphaltene Precipitation. Paper SPE 65019 presented at the SPE International Symposium on Oilfield Chemistry, Houston, 13–16 February. <http://dx.doi.org/10.2118/65019-MS>.

- [3] Srivastava, R.K., Huang, S.S., and Dong, M. 1999. Asphaltene Deposition during CO₂ Flooding. SPE Prod & Fac14 (4): 235–245. SPE-59092-PA. <http://dx.doi.org/10.2118/59092-PA>.
- [4] Yin, R.Y., Yen, A.T., and Asomaning, S. 2000. Asphaltene Inhibitor Evaluation in CO₂ Floods: Laboratory Study and Field Testing. Paper SPE 59706 presented at the SPE Permian Basin Oil and Gas Recovery Conference, Midland, Texas, USA, 21–23 March. <http://dx.doi.org/10.2118/59706-MS>.
- [5] Kokal, S., Al-Ghamadi, A., and Krinis, D. 2003. Asphaltene Precipitation in High Gas-Oil Ratio Wells. Paper SPE 81567 presented at the Middle East Oil Show, Bahrain, 9–12 June. <http://dx.doi.org/10.2118/81567-MS>.
- [6] Kokal, S., Al-Dokhi, M., Al-Zubail, M., and Al-Saeed, S. 2004. Asphaltene Precipitation in a Saturated Gas-Cap Reservoir. Paper SPE 89967 presented at the SPE Annual Technical Conference and Exhibition, Houston, 26–29 September. <http://dx.doi.org/10.2118/89967-MS>.
- [7] Sarma, H.K. 2003. Can We Ignore Asphaltene in a Gas Injection Project for Light-Oils? Paper SPE 84877 presented at the SPE International Improved Oil Recovery Conference in Asia Pacific, Kuala Lumpur, 20–21 October. <http://dx.doi.org/10.2118/84877-MS>.
- [8] Uchiyama, R., Yamada, Y., Ishii, H., and Salameh, L.A. 2008. Sweet and Sour Gas Injection as an Enhanced Oil Recovery Method in Abu Dhabi Offshore Oil Fields. Paper SPE 118096 presented at the Abu Dhabi International Petroleum Exhibition and Conference, Abu Dhabi, UAE, 3–6 November. <http://dx.doi.org/10.2118/118096-MS>.
- [9] Garcia, M.C., Chiaravalle, N., Sulbaran, A., El Chiriti, K., and Chirinos, A. 2001. Production Restarting on Asphaltene-Plugged Oil Wells in a Lake Maracaibo Reservoir. Paper SPE 69513 presented at the SPE Latin American and Caribbean Petroleum Engineering Conference, Buenos Aires, 25–28 March. <http://dx.doi.org/10.2118/69513-MS>.

- [10] Gholoum, E.F., Oskui, G.P., and Salman, M. 2003. Investigation of Asphaltene Precipitation Onset Conditions for Kuwaiti Reservoirs. Paper SPE Paper 81571 presented at the Middle East Oil Show, Bahrain, 9–12 June 2003. <http://dx.doi.org/10.2118/81571-MS>.
- [11] Gonzalez, D.L., Jamaluddin, A.K.M., Solbakken, T., Hirasaki G.J., and Chapman, W.G. 2007. Impact of Flow Assurance in the Development of a Deepwater Prospect. Paper SPE 110833 presented at the SPE Annual Technical Conference and Exhibition, Anaheim, California, USA, 11–14 November. <http://dx.doi.org/10.2118/110833-MS>.
- [12] Negahban, S., Bahamaish, J.N.M., Joshi, N., Nighswander, J., and Jamaluddin, A.K.M. 2005. An Experimental Study at an Abu Dhabi Reservoir of Asphaltene Precipitation Caused By Gas Injection. SPE Prod & Fac 20 (2): 115–125. SPE-80261-PA. <http://dx.doi.org/10.2118/80261-PA>.
- [13] Oskui, G.P., Salman, M., Gholoum, E.F., Rashed, A., Al Matar, B.S., Al-Bahar, M., and Kahali, K. 2006. Laboratory Technique for Screening Asphaltene Inhibitors for Kuwaiti Reservoirs. Paper SPE 106361 presented at the SPE Technical Symposium of Saudi Arabia Section, Dhahran, Saudi Arabia, 21–23 May. <http://dx.doi.org/10.2118/106361-MS>.
- [14] Yin, Y.R. and Yen, A.T. 2000. Asphaltene Deposition and Chemical Control in CO₂ Floods. Paper SPE 59293 presented at the SPE/DOE Improved Oil Recovery Symposium, Tulsa, 3–5 April. <http://dx.doi.org/10.2118/59293-MS>.

Chapter 9- Water versus Asphaltenes; Liquid–Liquid and Solid–Liquid Molecular Interactions Unravel the Mechanisms behind an Improved Oil Recovery Methodology

9.1 Introduction

Understanding of possible molecular interactions at liquid-liquid and solid-liquid interfaces can shed lights onto the nature's design and authorise fine manipulation aptitude in biological, manufacturing, microfluidic and oil recovery applications. Of particular interest is the capability to control the aggregation of organic and biological macromolecules, which typically poses significant challenges for oil industry and human life, respectively.

The liquid–liquid and solid–liquid interfaces play critical roles in many physical, chemical and biological processes, from phase transfer catalysis to liquid chromatography, lubrication, colloidal stabilisation , liquid-liquid extraction to pharmaceutical drug delivery, remediation of environmental contamination and enhanced oil recovery (EOR)[1]–[6]. Particularly, the water-oil and oil-solid interfaces are becoming increasingly illustrated within the scientific community.

Growth in oil and energy demand and aging reservoirs are few sakes why companies have been looking at various techniques to increase oil recovery rates which are referred to enhanced oil recovery methods including gas injection, water flooding, and water alternating gas (WAG) injection scenarios[7], [8]. It was explored that the oil production efficiency could also be increased by decreasing the salinity of the flooded water, i.e. without using costly and possibly detrimental chemistries, which is named low salinity water flooding (LSWF)[9]–[12]. Still, the microscopic drivers of the oil recovery enhancement owing to LSWF are under intense debate. Competitive wetting of oil and water on solid surfaces and respective wettability transitions are advocated as keys to increase recovery during water injection process. A solid is often referred to as thoroughly water-wet (hydrophilic), oil-wet (lipophilic), or mixed wet. A number of researchers have also investigated crude oil–water interfacial rheology regarding the stability of water-in-oil (W/O) microemulsions as one of the mechanisms of water flooding induced recovery

increment[13], [14]. These researchers inferred that the elasticity of the liquid–liquid interface to stability of microemulsions is owing to formation of interfacial thin layers from surface active species in the oil respect to the ion concentrations in the aqueous phase. These surface-active polar species, which play important roles in wettability alterations and formation of W/O microemulsions, are asphaltenes in crude oil. During water/gas injection scenarios, asphaltene may accumulate at the liquid–liquid and solid–liquid interfaces and form microemulsions (due to interfacial tension reduction) and alter the wettability of solid surfaces, respectively. Yet, the mechanisms of these two phenomena through asphaltene polar compounds is not completely understood because of the complexity of asphaltenes molecular structures and their behaviour under realistic conditions.

Polycyclic aromatic hydrocarbons (PAHs), which are organic compounds constructed by carbon aromatic rings and hydrogen, are ubiquitous in society[15]. PAHs are regularly utilised in a wide range of scientific and technological fields such as fundamental chemistry, the chemical and petrochemical industry, amidst a multitude of others[16]–[18]. Asphaltenes are PAHs which have mighty sheet-like structures of interlocked heterocyclic aromatic rings and contain both polar and nonpolar species. Additionally, they constituted by $11 \pm 4\%$ heteroatoms like O atoms (exist in carboxylic acid, hydroxyl, carbonyl groups, phenol, etc.), S atoms (in sulfoxide, thiophene), and N atoms (in pyrrole, pyridine) along with trace amount of coordinated heavy metals such as V, Ni, Fe. The surface active functional groups like carboxylic acids ($-\text{COOH}$) in asphaltenes are well-known to be adsorbed at the oil–water and oil–solid interfaces and can construct organized thin film sections[19]–[21]. Asphaltenes tend to precipitate out of the solution (2-10 nm), aggregate (>10 nm), and deposit onto the solid surfaces during the production/transportation of crude oil owing to the alterations in equilibrium conditions, e.g., composition, temperature, and pressure. Crude oil is co-produced with water during the water flooding processes which contains dissolved salts of sodium, potassium, calcium, and magnesium, particularly in the case of LSWF. In this regard, systematic investigation of asphaltene-brine interactions is of interest to build fundamental understanding of the role of brine in asphaltene deposition. Such indispensable investigations are still in their infancy. In the past decade, a limited number of controversial research studies have been undertaken to understand the effect of

water emulsions on asphaltene precipitation and deposition. From a review of available literature[22]–[25], it appears that opinion differs significantly as to which experimental methods should be utilised to determine the asphaltene stability and deposition tendency, which conditions should be applied and how data should be interpreted. Several workers have claimed that the presence of emulsified water had no remarkable influence on the asphaltene precipitation[22], [25], while others concluded that water increases the solubility of the asphaltenes in the system and delays the asphaltene aggregation and deposition phenomena[23], [24]. All the aforementioned research studies have been conducted with the use of deionized water in the absence of any salts. They also used n-alkanes as precipitants which could not emulate the real field conditions. This makes the outcome of the investigation not appropriately precise, since our own recent work proved that asphaltene molecular structure can be varied based on the operating conditions which is a key to asphaltene behaviour at liquid-liquid and solid-liquid interfaces[26]. There are no reports of the effect of brine with varying ionic strengths on asphaltene aggregation and deposition phenomena at elevated pressure and temperature systems. No authentic model material has been developed that can imitate asphaltene behaviour, and this commands the use of genuine samples in any scientific illustration. Herein, we utilised real oil sample and asphaltenes obtained from that parent sample during the experiments. Understanding the behaviour of asphaltenes at interfaces lies on the interactions between asphaltene nanoaggregates/brine in original crude oil. Therefore, it is vital to meticulously investigate these interactions under different salinity conditions which has remained a gap in the literature. The aim of the present work is to study the interactions between water and asphaltene molecules in presence of different ions using newly measured high-pressure high temperature quartz crystal microbalance (HPHT-QCM) data along with various analytical techniques with particular focus on low salinity water/gas injection for increment of oil production. This work documents an extensive set of HPHT-QCM experiments to inquire the impact of brine with variety of ionic strength on asphaltene aggregate size, deposition and micro scale wettability transition of QCM surface. Furthermore, our study sheds light on the mechanisms underpinning LSWF and elucidates how large a role water molecules act at fluid-solid interfaces.

9.2 Materials and Methods

We utilised a petroleum fluid, that we call BR, and determined its asphaltene content as well as its molecular weight, density and viscosity. The QCM experiments were conducted using AT-cut (optimized for 90 °C) 5 MHz quartz crystal coated with gold purchased from Testbourne Ltd. The diameter of the crystal is 25.4 mm, while the front electrode diameter is 12.7 mm, the crystal thickness is 333 μm , and the crystal surface roughness is 50 \AA . The sensors were cleaned using anhydrous heptane and toluene (>99%) from Sigma-Aldrich (used as received) followed by rinsing with deionised water and blow-drying with nitrogen to remove all surface-active impurities. To be more realistic for mechanistic studies we precipitated asphaltenes by adding natural gas in our QCM test set-up. The utilised natural gas composition is as follows (*Mole %*): N_2 (1.84%), C_1 (89.94%), CO_2 (0.91%), C_2 (5.32%), C_3 (1.45%), $i\text{C}_4$ (0.20%), $n\text{C}_4$ (0.21%), $i\text{C}_5$ (0.07%), ($n\text{C}_5$) + C_6^+ (0.06%). After the deposition test, the gas induced asphaltene deposit from the QCM surface was extracted and dried for characterisation. The detailed procedure has been presented in our previous articles[26], [27]. The asphaltene content of BR is determined by adding HPLC-grade anhydrous *n*-heptane (>99%, Sigma Aldrich) and define X ($\text{mL}\cdot\text{g}^{-1}$) as the *n*-heptane ratio, showing the volume of *n*-heptane added to 1gr of petroleum fluid. After mixing of 4gr crude oil with 160 mL *n*-heptane, $X=40$ $\text{mL}\cdot\text{g}^{-1}$, for 10min in a sonicator bath and allowed to be equilibrated for 24hr before separation of asphaltene fraction, the solution was filtered through a 0.2mm pore-size cellulose nitrate whatman filter followed by washing with excess *n*-heptane until shiny black asphaltenes were appeared. The filtrate is then collected, dried and weighed to give the *n*-heptane asphaltene content as presented in Table 9.1. The density of the crude oil BR, ρ_o , is measured using a densitometer (Anton Paar). The density of the asphaltene, ρ_a , is determined by preparation of a solution of 0.05 g asphaltene in 20 mL toluene and measuring the density of the solution. The viscosity measurements are conducted using a stress controlled rotational-type rheometer (Anton Paar, Physica MCR 301) with the aid of 25mm diameter and 1° angle cone-plate geometry (Cones CP50-1). The water content results in ppm, are measured by a coulometer (Karl Fischer 331 coulometer). Deionized (DI) water was produced using an ELGA DV 25 Integral Water Purification System. For all the brine phases, we utilised freshly DI water in which different combinations of the following salts were dissolved: NaCl, KCl, CaCl_2 , and

MgCl₂, which were purchased from Sigma-Aldrich and used as received (Analytical grade, purity >99.5%). Single and multi-salts solutions are within the range of 100 mM to 1 M ionic strengths to mimic low salinity water and sea water which are injected into the reservoirs for secondary/tertiary oil recovery. The ionic strength, defined as

$$I = \frac{1}{2} \sum_{i=1}^n z_i^2 c_i \quad (9.1)$$

Where c_i , z_i , and n are the concentration, the valence of the i th ionic species, and the number of different species, respectively. All the solutions were adjusted to pH 6 with HCl/NaHCO₃ and NaOH (purchased from Sigma Aldrich). The amount of acid or base augmented was meagre respect to the ionic strength of the solutions. The crude oil BR was placed on top of the salt solutions thick film to increase the oil/brine contact surface area followed by inverting andante to facilitate molecular interactions at oleic-aqueous interface and obtain suitable mixing but to avoid emulsification. Some water remained at the bottom of the vials and oils were intently separated for the pursuant tests. An FEI Quanta 650 FEG SEM, with a backscattered electron (BSE) imaging detector, equipped with an Oxford Instruments X-MaxN150 mm energy dispersive X-ray (EDX) detector, was used in this work. For both imaging and elemental analysis, the microscope was operated in low-vacuum mode (0.83 Torr) at 20 kV, spot size of 4.5, dwell of 10 μ s, and a working distance of 10 mm. The FTIR spectra were recorded using an FTIR-4000 Series (JASCO Edition) spectrometer including a Peltier stabilized DLaTGS detector and a high output ceramic source coupled with an attenuated total reflectance (ATR) mode with high through put monolithic diamond and ZnSe. The spectral domain is 650–4000 cm⁻¹ with a resolution of 0.7 cm⁻¹. The proton ¹H and carbon ¹³C NMR spectroscopic analyses were conducted using a Bruker AVI400 spectrometer operating at 400.1 and 100.6MHz for proton and carbon, respectively. Toluene-d₈ (99.96atom % D) was utilised as received from Sigma-Aldrich as a solvent for the NMR experiments. The proton data were obtained employing a 3.96s acquisition time, 8278 Hz sweep width, and 1.0s relaxation time. The carbon spectra were achieved with a 1.30 s acquisition time, a 25 125 Hz sweep width, and 2.0s relaxation time. The carbon spectra resulted from 1024 scans. Herein the given chemical shifts (δ) are reported respect to tetramethylsilane (TMS) utilised as internal standard. All stable microemulsions and asphaltene aggregates were imaged using state of art petrographic

microscope using a 50× objective with 0.25µm resolution, and asphaltene aggregate sizes were counted by ImageJ to analyse the number of aggregates of various sizes per area of 1500 µm².

9.3 Results and Discussion

9.3.1 Characterisation of asphaltene and the parent oil

Material properties of the crude oil BR including its density ρ_o , its viscosity μ_o , asphaltene content f , asphaltene density ρ_a , and water content (ppm) are provided in Table 9.1. The elementary analysis data for the asphaltene fraction in w/w % are shown in Table 9.2.

Table 9. 1. Material properties of the petroleum fluid, BR: oil density ρ_o , viscosity μ_o , asphaltene content f , asphaltene density ρ_a , water content (ppm)

Petroleum Fluid	ρ_o (g.mL ⁻¹)	μ_o (cP)	f (g.g ⁻¹)	ρ_a (g.mL ⁻¹)	water content (ppm)
BR	0.828	12.15	0.0312	1.05 ± 0.07	845

Table 9. 2. Elemental contents of the asphaltenes isolated from petroleum fluid BR (w/w%)

Asphaltenes	C	H	S	O	N _H /N _C *
BR	84.38	7.79	2.96	4.87	1.03

* H/C is the atomic ratio of hydrogen and carbon.

Figures 9.1e–h show the ESEM/EDX analysis results of the asphaltenes. Figure 9.1e shows agglomeration of irregular shape asphaltene particles (with an average length of ~3.7µm) owing to high aromaticity in presence of smooth surface asphaltenes (large-sized particles of ~12.4µm). Qualitative analysis of the asphaltene composition and its elemental mappings are given in Figure 9.1f–h. Both S and O are the constructor heteroatoms and evenly distributed throughout the asphaltene deposits.

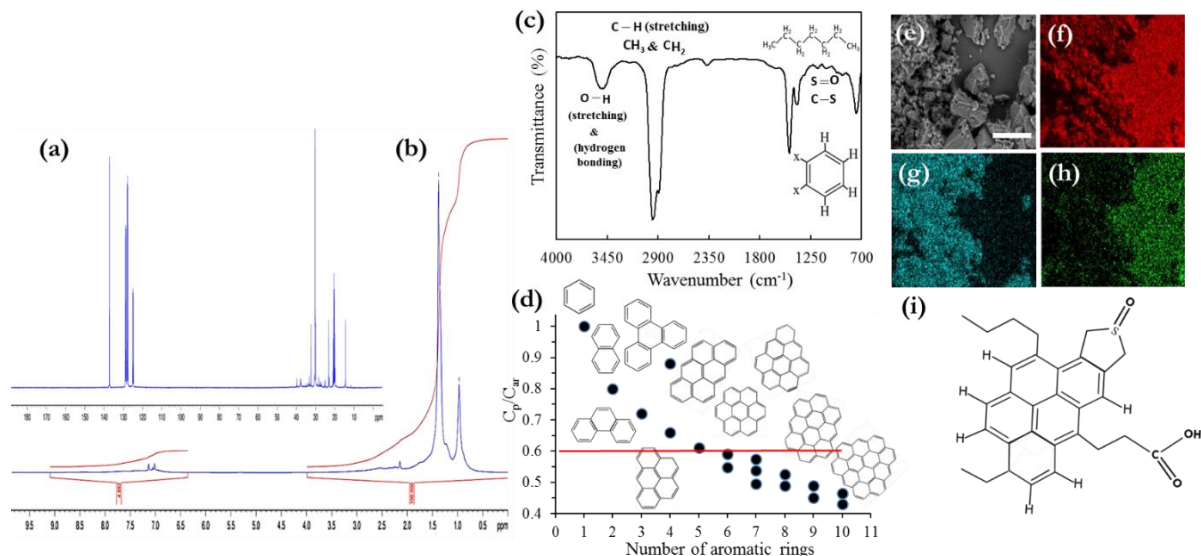


Figure 9. 1. Characterisation of asphaltene isolated from crude oil BR, (a) representative ^{13}C 100.6 MHz NMR spectra, (b) representative ^1H 400.1 MHz NMR spectra, (c) FTIR spectra of asphaltene with representative structures assigned to related spectra range, (d) Determined C_p/C_{ar} ratio as a function of total number of aromatic rings in studied asphaltene molecular structure, (e) ESEM micrograph of asphaltene with white scale bar of 20 μm , EDX elemental mapping of (f) C k mapping, (g) S k mapping, and (h) O k mapping, (i) hypothetical asphaltene molecular structure derived based on the attained advanced spectroscopy data. No effort was accomplished to fit the structure to the molecular weight, solubility, or further physical circumscriptions.

FTIR spectra of the asphaltene moiety was measured and indicated in Figure 9.1c. Three characteristic peaks at 1670, 1417, and 1372 cm^{-1} were caused by the C=C stretching, the stretching vibration of aromatic rings, and CH_3/CH_2 deformation in the asphaltene. The characteristic peaks at 3490, 1760, and 1027-130 cm^{-1} were attributed to three oxygen and sulfur-containing groups on the asphaltenes of $-\text{O}-\text{H}$, $-\text{C}=\text{O}$ of carboxylic acid, $-\text{S}=\text{O}/-\text{C}-\text{S}$ and $-\text{C}-\text{O}$ of sulfoxide and secondary alcohols/ethers, respectively. Three adjacent hydrogens at 760 cm^{-1} seemed to be agglutinated into the 4H peak at 745 cm^{-1} . There is a small peak ascribed to the long alkyl chains at 700–720 cm^{-1} , which denotes that the asphaltene molecule has trace amount of alkyl chains attached to its structure. The presence of a $\text{C}_{\text{aro}}-\text{CH}_3$ attached to the condensed asphaltene aromatic structure can be observed at $\sim 2730 \text{ cm}^{-1}$. The related bonding in the asphaltene molecular structure are also depicted in Figure 9.1c. The liaising major vibrational assignments are presented in Table A1.2

(Appendix A1). For further detailed structural characterisation, ^{13}C and ^1H NMR spectra are utilised and presented in Figures 9.1a and 1b, respectively. The chemical shifts δ (in ppm) for ^1H NMR corresponding to the characteristic signal intensities are 0.30–0.95 (γ - CH_3 hydrogens to aromatic rings), 1.00–1.40 (β - CH_3 , β^+ - CH_3 paraffinic hydrogens), 1.40–2.00 (β -position CH/CH_2 to aromatic rings, naphthenic $-\text{CH}/\text{CH}_2$), 2.00–2.90 and 2.90–4.50 (α - CH_3 , α - CH/CH_2), 6.50–9.00 (aromatic hydrogens). The related chemical shifts for ^{13}C NMR corresponding to the characteristic signal intensities are 0–70 ppm (aliphatic carbon, C_{al}), and 90–180 ppm (aromatic carbon, C_{ar}). The assignments of ^1H and ^{13}C chemical shifts in asphaltene NMR spectra discussed above are listed in Table A1.3 and A.4, respectively. An integration of ^1H and ^{13}C NMR spectra at various chemical shifts can succour us to determine some average structural parameters like the shape factor of asphaltene aromatic sheet, Φ ($\text{C}_{\text{p}}/\text{C}_{\text{ar}}$), which is the ratio of number of peripheral aromatic carbons C_{p} to aromatic carbons based on the procedures demonstrated by Joonaki et al.[26] and others[28], [29]. Figure 9.1d shows the aromatic structures for various $\text{C}_{\text{p}}/\text{C}_{\text{ar}}$ ratios which are acquired using fluorescence and quantum determinations[30]. The Φ value is related to the total number of rings and the condensation degree of asphaltene aromatic cores. Herein, the achieved value of $\Phi = 0.59$ reveals that the possible number of aromatic rings is 6 per sheet for one fragment asphaltene molecule. Based on all analytical findings, we can signify the most probable asphaltene molecular structure which is observed in Figure 9.1i.

9.3.2 Formation of water in oil micro-emulsions: the roles of asphaltenic compounds at water/oil interface, ionic strength, and ion valency

The IR Spectroscopy analysis is very significant to identify the hydrogen bonding networks in water, water-asphaltene and hydrated cations in brine solutions. This type of analysis will enable us to identify the hydrogen bonds between the $-\text{COOH}/-\text{C}-\text{S}/-\text{S}=\text{O}$ groups of the asphaltene and the water molecules, and also to grab the alterations of O–H stretch vibration that are known for their sensitivity to the strength of the hydrogen bond network. To recognise the influences of ionic strength and ion valency on hydrogen bonding between the water and asphaltene molecules at water-oil interface, we obtained the IR vibrational spectrum for the crude oil BR in contact with various brine solutions which are

shown in Figure 9.2a. From the IR spectra, we denote that there is roughly one realm of 3200 and 3750 cm^{-1} (broad envelope, dominated hydroxyl $-\text{O}-\text{H}\cdots\text{O}$ bonding) which undergoes pronounced changes in their intensities owing to alterations in ionic strength of water from DI to HS brine and monovalent $[\text{Na}^+]$ to divalent $[\text{Ca}^{2+}]$ cations leading to multiplicity variations of h-bonding species. The intensity of the characteristic peak at $\sim 3495 \text{ cm}^{-1}$ for four brines is clearly increasing owing to reducing the salinity and ion valency which result in accumulation of asphaltene nanoaggregates at water-oil interface and construction of stronger H-bonding network between carboxylic acid functional group of asphaltenes and water molecules. The lack of significant changes in intensity of aromatic $\text{C}=\text{C}$ in presence of water droplets can explicitly impeach the recent assertions of potent asphaltene adsorption at the interface owing to the π -electron interactions between the vast PAHs and the water molecules[31]. The $-\text{COOH}$ and/or $-\text{OH}$ containing moieties like asphaltene molecules have attitude to be adsorbed at the interface and decrease the interfacial tension strikingly. However, the density of delicate formed film relies on their innate size and shape, moreover, on their amphiphilicity. Therefore, the interface can spontaneously bend to incorporate more asphaltene molecules. An asphaltenic-laden water-oil interface might spontaneously bend toward either the brine or the oleic phase, and this signifies the rivalry between the interaction district of the polar aromatic group and the aliphatic chains. In the existing occasion, the asphaltene molecules comprise various surface-active functional groups and short hydrophobic tails (Figure 9.1i) which lead to formation of W/O micro-emulsions.

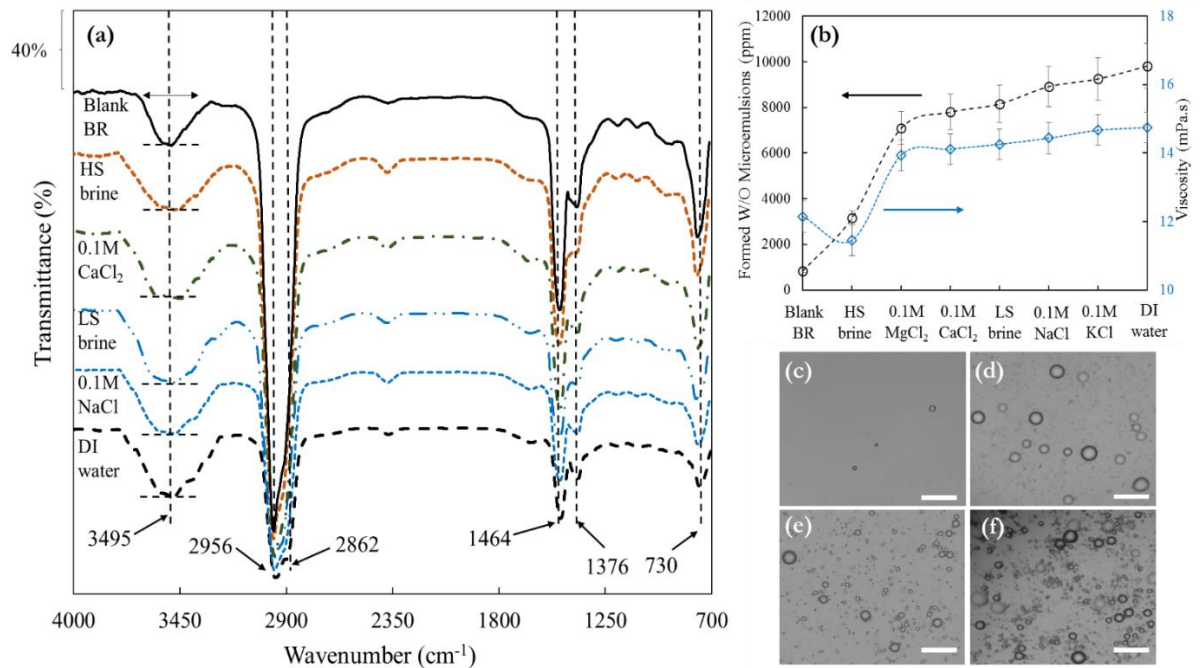


Figure 9. 2. Formation of spontaneous asphaltene stabilised water in oil micro-emulsions and its effect on the fluid viscosity. (a) FTIR spectra of blank petroleum fluid and after contact with DI water, 1M HS and 0.1M LS brines, and CaCl₂ and NaCl brines with ionic strength of 0.1M. (b) Water in oil (W/O) micro-emulsions contents for blank oil and after contact with DI water and various brines with different ionic strengths and respective viscosity data. Microscopic images of the W/O micro-emulsions for (c) blank crude oil BR, (d) large 1M HS brine droplets, (e) smaller 0.1M LS brine droplets compared to HS brine, and (f) tiny DI water droplets. The white scale bar in microscopic images is 100 μm.

As can be seen from Figure 9.2b, we found that the formation of spontaneous water in oil micro-emulsions and asphaltene nanoclusters at water-oil interface is a potent function of ionic strength of brine solutions. Reducing the salinity of the aqueous phase and utilisation of monovalent ions instead of divalent ones would result in delaying the coalescence phenomenon and augmenting the emulsions stability accordingly. The microscopic images reported in Figures 9.2c-f illustrate that the spontaneous emulsification phenomenon was enhanced as the concentration of salts and divalent ions decreased and presence of these water micro-droplets in oil might affect the asphaltene aggregation and deposition drivers which will be discussed later herein. We daresay that the variations in droplet size and concentration of water droplets for the LS and HS brine, solutions with ionic strength of 0.1M [NaCl, KCl] and 0.1M [CaCl₂, MgCl₂] are pertinent to the arrangement of asphaltene

molecules at the water-oil interface[32] and the ensuing interface interactions (Figures 9.2b-f). We denote that Mg^{2+} , Ca^{2+} with higher valence than K^+ , Na^+ had less stable brine micro-emulsions. It is postulated that the presence of salts may promote the asphaltenic species desorption from the water-oil interface and reduce the hydration of the polar functional groups. In the case of DI water, the droplets stayed discrete, while increasing the ionic strength and valency would tend to brine droplet weight and sizes increment leading to prevail repulsive interactions and attain early onset of coalescence. The charge inversion may play a critical role on the adsorption behaviour of the asphaltenes at the fluid-fluid interface. In Figure 9.2b, we show the viscosity of crude oil in contact with DI water and brine with different ionic strengths. Bulk rheology measurements ascertain that BR oil to be a Newtonian fluid with viscosity of $\mu=12.15$ mPa·s at the shear rate of between 10 s⁻¹. Up to 3160 ppm HS brine concentration, the viscosity decreases ~6% in comparison with the sample without water augmentation. Above 4000 ppm, with reducing the salinity and valence of the cations the viscosity increased ~21% and 22% for KCl brine with ionic strength of 0.1M and DI water, respectively. The initial decrease in the viscosity could be declarative of the presence of smaller asphaltene aggregates[33] owing to addition of HS brine compared to blank BR oil. Then the viscosity increment might be depicted as the structural alterations caused by the abundance of water molecules.

9.3.3 The effect of water with/out various ionic strengths on asphaltene aggregation

We determine the size of asphaltene aggregates using petrographic micrographs in order to demonstrate the influence of brine solutions with various ionic strengths. Figures 9.3a-d indicate microscopic imaging results for blank BR, DI water, LS, and HS brines. No significant discrepancy can be observed in the average size of asphaltene aggregates when comparing the images from the influence of ionic strength. The average size of the aggregates augmented with salinity of brine. We also determined the quantity of asphaltene aggregates and their size distribution at each image with/out brine solutions by ImageJ and depict them in Figures 9.3e-h. For the sample without presence of any aqueous phase in the system, albeit the size range is between 1 and 12 μ m the average size of aggregates is ~5 μ m and the asphaltene aggregates are chiefly concentrated ~4 μ m (Figures 9.3a and e). In

the presence of DI water, the size range is from 1 to 9 μm with an average of $\sim 3 \mu\text{m}$ (Figures 9.3b and f).

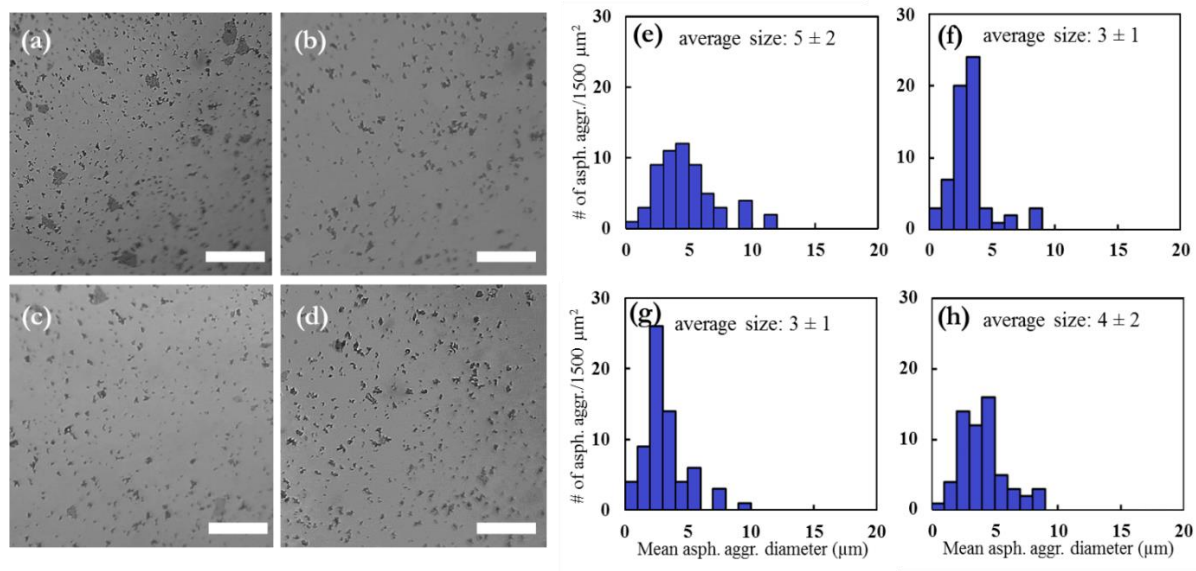


Figure 9. 3. Images of asphaltene aggregates for (a) blank oil, and in presence of (b) DI water, (c) 0.1M LS brine, (d) 1M HS brine. Here the white scale bar in micrographs is 10 μm . The particle size distribution of asphaltene aggregates for (e) blank oil BR, and with (f) DI water, (g) LS brine, and (h) HS brine. The particle sizes are counted with ImageJ.

As can be observed from Figures 9.3c and g, after addition of LS brine although the size distribution of asphaltene aggregates was different (with larger aggregates), the average aggregates size was $\sim 3 \mu\text{m}$ the same as DI water. We also conducted the measurements in presence of HS brine and perceived some larger aggregates compared to LS and DI water with the average aggregates size of $\sim 4 \mu\text{m}$ as shown in Figures 9.3d and h. The literature illustrated the impact of water on the asphaltene particles size in solvents, particularly in toluene[34], [35]. The presented micrographs, for the first time, attain new data on the influence of brines with various ionic strengths on the size of asphaltene aggregates. Asphaltenes can form a networking soft structure at liquid-liquid interface. This deformable structure could not be packed and tight owing to the steric hindrance between asphaltene aggregates. The electrostatic interactions at the fluid-fluid interface can elucidate the impact of low salinity brine on the viscoelasticity and asphaltene structure of the interface. Therefore, the electrical double-layer expansion[36], [37] might be the symptom for vast content of crude oil surface active species (e.g. asphaltenes, resins) at the

liquid–Liquid interface. A diffuse ionic stratum can be constructed due to adsorption of the ions to the electrically negatively charged water-oil interface which can spotlight all the interactions with the bulk solution. The Debye length, κ^{-1} , which the stoutness of the effectual layer is pertinent to, defined as:

$$\kappa^{-1} = \sqrt{\frac{k_B T \epsilon_r \epsilon_0}{2 N_A e^2 I}} \quad (9.2)$$

Where k_B is the Boltzmann constant, T is the temperature, ϵ_r the dielectric constant of brine, ϵ_0 the permittivity of free space, N_A the Avogadro number, e the electron charge, and I the ionic strength (eq. 9.1). The κ^{-1} is reversely related to the brine ionic strength. The polar surface active moieties like asphaltenes adsorb onto the water-oil interface without ions owing to their polar functional groups formed hydrogen bonding network at the interface (as depicted in Figure 9.2a) which can cause prevention of competing self-assembly contacts and aggregates growth. The diffuse stratum is flattened at low ionic strength leading to the potent screening and the asphaltenes are adsorbed and organized at the fluid-fluid interface by electrostatic interactions. The κ^{-1} is tenuous at high ionic strength; the opposing ions decrease the charge screening and also disturb the hydrogen bonding structure at periphery of $-\text{COOH}/-\text{OH}$ containing groups at the oil-water interface which results in reduction of asphaltene-water interactions at the interface and facilitation of multiple asphaltene intermolecular π -stacking/H-bonding interactions and particle size increment accordingly.

9.3.4 The role of brine solutions with different salinities on asphaltene deposition and respective micro-scale wettability transition of solid surface

Herein we provide the results from extensive sets of HPHT-QCM measurements to illustrate the influence of water with/out different ion concentrations on asphaltene deposition. To the best of our knowledge, there is no report of such data in the literature. The schematic of the HPHT-QCM setup is given in Chapter 8. The mass alteration of the QCM owing to the interactions respect to its surface can lead to resonance frequency (RF) changes. For liquids, the change in RF is also related to the viscosity and density of the surrounding medium, according to the following equation[38], [39]:

$$\Delta f = -f_0^{3/2} \left[\frac{\mu_l \rho_l}{\pi \rho_q \mu_q} \right]^{1/2} \quad (9.3)$$

Where Δf is the frequency change (Hz), f_0 is the frequency of oscillation of unloaded crystal, ρ_l is the density of the liquid in contact with the electrode, μ_l is the viscosity of the liquid, ρ_q is density of quartz ($\rho_q = 2.648 \text{ g.cm}^{-3}$), and μ_q is shear modulus of quartz for AT-cut crystal ($\mu_q = 2.947 \times 10^{11} \text{ g.cm}^{-1}.\text{s}^{-2}$). When the QCM is in contact with the crude oil, the vibration amplitude and also the acceleration decay exponentially from the crystal surface into the crude oil as shown in Figure 9.4. It is mathematically illustrated by the equation below[40]:

$$A(y) = A_0 \exp\left(-\frac{y}{\delta}\right) \quad (9.4)$$

Where δ is the penetration depth which is equal to $(\mu_l/\pi f_0 \rho_l)^{1/2}$ defined as the effective thickness of the crude oil that is driven to move by the vibrating crystal with a displacement decaying exponentially, and A_0 is maximum vibration amplitude at the centre of the crystal.

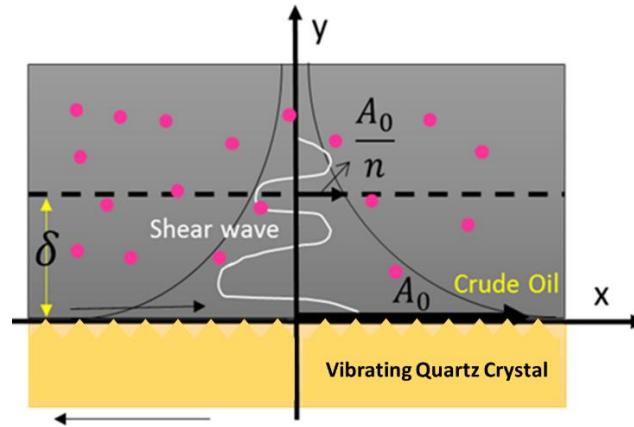


Figure 9. 4. Amplitude and acceleration decay at the quartz crystal-oil interface

Lower the vibration amplitude and acceleration are obtained owing to larger distance (y) from the QCM-oil interface. A certain small volume of crude oil placed at distance δ from the QCM-oil interface will generate a frequency alteration n times smaller than that generated by the same volume of crude oil placed in direct contact with the quartz crystal surface. The significant fact is that by measuring small changes in RF, tiny amount of

asphaltene deposits in nano-gram range can be detected. Under the real field situation, the asphaltene deposition challenge happens due to gas injection scenarios or depressurisation process. We conducted the tests with injection of gas and oil in various gas/oil ratios (GORs) in presence of water micro-emulsions for imitating the WAG-EOR conditions and measured the asphaltene onset point (AOP) and deposition rate onto the QCM surface. In Figure 9.5a, the diagram indicates ΔRF versus pressure for natural gas and BR oil at different GORs in presence of DI water with/out various salt concentrations and ion valences to monitor the AOP changes. The pressure at which the RF starts declining signifies the AOP[26], [27] which is ~ 954 psi at GOR of ~ 15.6 mol% for the blank BR crude oil. As can be seen in Figure 9.5a, a distinct AOP shift is detected in presence of HS brine for which the AOP/GOR is ~ 1221 psia/21.8 mol%. The AOP/GOR is ~ 1360 psia/23.9 mol% for 0.1M $MgCl_2$, ~ 1706 psia/27.7 mol% for 0.1M $CaCl_2$, ~ 1820 psia/28.9 mol% for LS brine, ~ 1914 psia/30.1 mol% for 0.1M $NaCl$, ~ 1990 psia/31.2 mol% for 0.1M KCl , and ~ 2554 psia/36.4 mol% for DI water. Figure 9.5b depicts the results of the impact of brine solutions with different ionic strengths on the asphaltene deposition rate after the AOP which is RF decline versus time ($\Delta RF \cdot \Delta t^{-1}$, deposition rate representative[26], [27]) for BR oil with/out brine micro-emulsions at different salts concentrations. There is a drastic discrepancy in the plotted curves between the blank BR oil without any water micro-emulsion and with presence of DI water, HS and LS brines. DI water reduced the deposition rate from -708.7 to -99.8 Hz/hr. HS and LS brines decreased the rate of asphaltene deposition down to -286.5 Hz/hr and -229.6 Hz/hr, respectively.

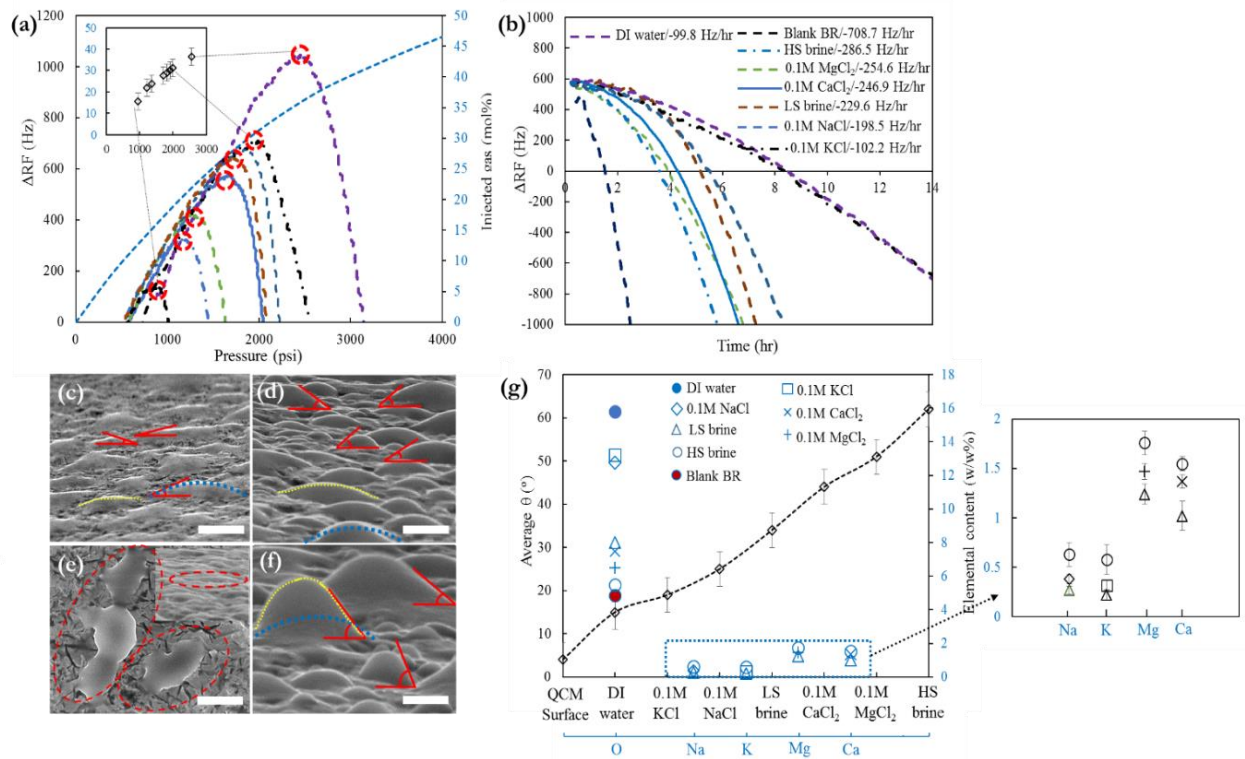


Figure 9. 5. The effect of water with/without various ionic strengths and ion types on (a) AOP shifting and related GOR changes, and (b) asphaltene deposition rate onto the QCM surface. ESEM micrographs of micro-droplets of water on gold plate of QCM surface in presence of (c) DI water, (d) 0.1M LS brine, (e) no water, plain surface, and (f) 1M HS brine illustrating water contact angle variability owing to ionic strength changes. The white scale bar depicted in images is 20 μm . (g) the average contact angle values of water micro-droplets on the surface with/without presence of brines with different salinities and ion types and respective elemental analysis of trapped brine sandwiched between asphaltene deposits and the QCM surface.

The influence of water/brines in preventing and/or delaying the asphaltene precipitation and deposition phenomena is perceived for the BR oil; we elucidate that the influence is not particular for specific ionic strength and ion valency. Based on the attained results, plainly the delay in asphaltene precipitation and deposition rate decrement are potently relied on the concentration of salts in brine solutions. Lower ionic strengths and ion valency resulted in higher effect on preferable AOP shifting and deposition rate reduction. It is worth noting that a distinguished fluctuation is noted at high concentration of water in oil micro-emulsions (DI water) possibly owing to structural alterations caused by water molecules in asphaltene nanoaggregates. There are two conceivable elucidations for this

dramatic influence of water/brines on QCM asphaltene experiments. The first hypothesis is that the water molecules interact with asphaltene molecules, curb further intermolecular interactions and reduce the size of asphaltene aggregates which has been demonstrated in previous section. The second possible driver is that the water/brines construct a thin film layer at periphery of the QCM surface and prevent asphaltenes from depositing. In order to elucidate if the second driver is dominant, we monitored the micro-wettability alterations of gold surface of the QCM due to ion valency/concentration changes. Figures 9.5c-g present the images of water droplets onto the solid surface in presence of various ions and corresponding contact angle values. In order to analyse the competitive wetting of organic species and water on the QCM surface, we measured the contact angle of water micro-droplets. The microscopic contact angles of water are depicted in mainly side view micrographs (Figures 9.5c-f). We measured different contact angles under each condition in various regions of the solid surface to accurately determine the influence of brine salinity and ion valency on the wettability transition of the surface. Then average values of these local contact angles at micro-scale were determined which denoted as θ_{av} and represent the general wettability of the solid surface. To the best of our knowledge, this is the first report of such a data in the literature. Figures 9.5c-g illustrate the impacts of the concentrations of the combined mono and divalent cations on the micro-droplets contact angle changes. If the DI water serves as a reference with θ_{av} of $\approx 15^\circ$, the θ_{av} increased with increasing salinity of the water. The θ_{av} in presence of LS brine showed an increment from 15° to $\approx 34^\circ$. The only remarkable district was noticed between LS and HS brines that is $\approx 28^\circ$, from 34° to $\approx 62^\circ$. The representative extracted water micro-droplet dimensions in average for LS and HS brines are $15.8 \mu\text{m}$ (height) $\times 51.6 \mu\text{m}$ (width) and $20.4 \mu\text{m}$ (height) $\times 46.7 \mu\text{m}$ (width), respectively. We also demonstrated the effects of the valence of the cations in the brine solutions on the contact angle transitions. Increasing the concentration of $[\text{K}^+]$ from 0 to 0.1M was resulting in θ_{av} increment from 15° to $\approx 19^\circ$. Due to replacement of $[\text{K}^+]$ with $[\text{Na}^+]$ at same concentration, the θ_{av} increased up to $\approx 25^\circ$ which reveals the importance of cation type in addition to ionic strength. However, when $[\text{Ca}^{2+}]$ is added instead of $[\text{Na}^+]$, the θ_{av} raised to $\approx 44^\circ$, and 33 mM $[\text{Mg}^{2+}]$ leads to a θ_{av} of 51° . This evidently underlines how significant the roles of ion type and valency are in wettability

alteration phenomenon. To unravel the mechanisms behind this observation, we require to consider the interactions between the cations and the charged QCM surface.

Figure 9.5g indicates the elemental analysis of the asphaltene deposits onto the surface and related concentrations (w/w %) of [O], [Na⁺], [K⁺], [Ca²⁺], and [Mg²⁺] to reveal the effects of water with/out various salts on the deposition rate reduction and micro-wettability changes. The [O] content increased with reducing the salinity of the brine and substitution of divalent cations with monovalent ones. It elucidates that more water molecules trapped in asphaltene deposits on the solid surface in presence of monovalent cations containing water and lower ionic strength brine. The concentrations of divalent cations are more than monovalent cations due to their sizes and hydration states leading to high strength ion-surface interactions and more potently cation adsorption onto the gold surface. The bare ion radii and hydrated ion radii for different cations utilised in this study have been presented in Table A3.1 (Appendix 3). The activity coefficients for the cations in the chloride solutions are determined using the Debye-Huckel equation[41]:

$$\log \gamma_i = -\frac{Az_i^2\sqrt{I}}{1+Ba_i\sqrt{I}} + b_i I \quad (9.5)$$

where A and B are the temperature dependant coefficients, I is ionic strength (eq. 9.1) and a_i and b_i are individual cation activity coefficient parameters which are given in Table A3.1. The size of the divalent cations and respective number of water molecules surrounding the cations are greater compared to the monovalent cations. The hydration happens readily for metal cations at the QCM-fluid interfaces. Water molecules can benefit a substantial portion of coordination for the metal cations. The binding energy, E_{bw} , of the water molecules to the divalent cations in vacuum is defined as[42]:

$$E_{bw} = E(\text{cation} + 6\text{water}) - E(\text{Cation}) - 6E(\text{water}) \quad (9.6)$$

This expression illustrates that the more negative the binding energy, the more potently the water molecules append to the cation. The free energy of hydration and the binding energy for first hydration shell (6 water molecules) are -1821 and -1395 kJ.mol⁻¹ for [Mg²⁺], while they are -1500 and -1063 kJ.mol⁻¹ for [Ca²⁺] cation[43]. Based on the obtained results (Figure 9.5g), it can be inferred that the divalent cations adsorbed more strongly onto the

surface owing to their higher concentrations in deposits and ruptured the ordered structure of water molecules and their H-bonding network at the solid-liquid interface that lead to direct molecular contact of asphaltenes and providing of free surface active sites accessible to readily interact with asphaltene nanoaggregates. This proposition is consistent with the higher concentrations of trapped divalent cations compared to monovalent cations. On the other hand, the hydration number of metal cations reduced with decrease in ion valency, and in presence of monovalent cations, more water molecules from the hydrated cations are released which increases the amount of free water molecules into the oil-water interface and oleic phase that results in further mobility of the cations. The contact angle for three phases (QCM surface-oil-water) system can be deduced from the Young's equation[44]:

$$\Delta(\cos\theta) = \frac{(\Delta\gamma_{os} - \Delta\gamma_{ws})}{\Delta\gamma_{ow}} \quad (9.7)$$

and,

$$(\Delta\gamma_{os} - \Delta\gamma_{ws}) \propto \Delta\Delta E_{ads}(\text{asphaltene, mono v di - valent cation})$$

where γ_{ow} , γ_{os} , and γ_{ws} are interfacial tensions between oil and water, oil-solid, and water-solid surfaces, respectively. The $\Delta\Delta E_{ads}(\text{asphaltene, mono v di - valent cation})$ is the alteration of the discrepancy in adsorption energy for the asphaltene molecule, relative to water molecule. It can elucidate how the surface tendency for asphaltene molecules compared to its tendency for water molecules in presence of mono/di valent cations. If $\Delta\Delta E_{ads}(\text{asphaltene, mono v di - valent cation})$ is negative the preference of asphaltene to be adsorbed onto the solid surface is higher than water molecules in presence of specific cation. Herein, for the studied case of solid-liquid-vapour phase using ESEM micrographs, the Eq. 9.7 can be expressed in terms of work of adhesion:

$$W_{SL} = \gamma_{LV}(1 + \cos\theta) \quad (9.8)$$

where $W_{SL} = \gamma_{LV} + \gamma_{SV} - \gamma_{SL}$, and S, L, and V stand for solid, liquid, and vapour phases. The Eq. 9.8 can be rewritten in terms of binding energy per unit area as follows:

$$1 + \cos\theta = \frac{E_{b-asph}}{A\gamma_{LV}} \quad (9.9)$$

where A is surface area, and E_{b-asph} is the binding energy of the asphaltene molecules to the QCM surface and can be defined as:

$$E_{b-asph} = E_{surf} + E_{asph} - E_{surf.asph} \quad (9.10)$$

where $E_{surf.asph}$ is the total energy of the adsorbed asphaltene molecule on the gold surface of the QCM, E_{surf} is the total energy of the gold surface alone and E_{asph} is the total energy of the asphaltene molecule in a vacuum. Taking into account E_{b-asph} and $\Delta\Delta E_{ads}(asphaltene, mono\ v\ di - valent\ cation)$, previously discussed preference of cations for adsorption, and achieved contact angles presented in Figure 9.5g could explain why monovalent cations are more effectual in suppressing the asphaltene adsorption on the gold surface and reducing the corresponding contact angles of water micro-droplets. Through similar drivers, Ca^{2+} and K^{+} are more efficient in inhibiting the adsorption of asphaltene nanoaggregates onto the QCM surface compared to Mg^{2+} and Na^{+} , respectively. Generally, the binding affinity of alkali and earth alkaline cations in our thin film systems both at solid-liquid and liquid-liquid interfaces is presumably to be a plural influence pertinent to the ion valency, the hydration of the surfaces and ions and the interacting surfaces charges. Our results concur with some reports in the literature on the effect of cations on adsorption of proteins[45] and stearic acid[46] onto the mica surface.

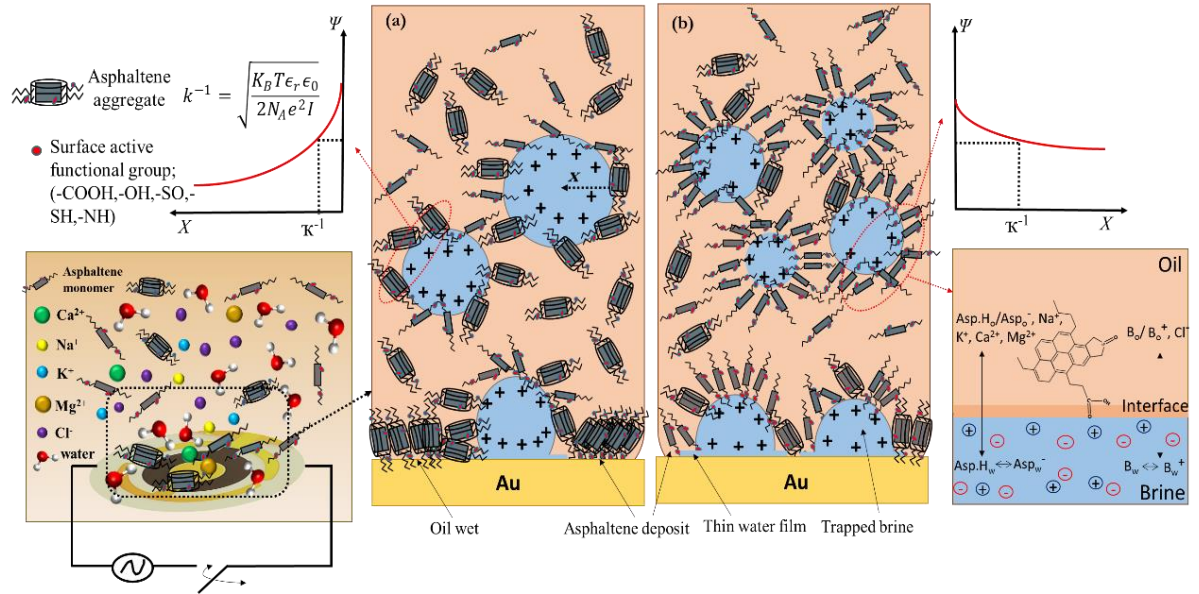


Figure 9.6. Model representation of the molecular scale phenomena that elucidate the effect of ionic strength on asphaltene aggregation, deposition, formation and stability of W/O micro-emulsions, asphaltene interactions at water-oil interface and microscopic wettability transition for (a) high ionic strength, and (b) low ionic strength brines with respective Debye length (κ^{-1}). Ions can alter the electrostatic potential (ψ). Micro-brine droplets and thin water film sandwiched between oil-asphaltene deposits and the QCM solid surface, owing to cations (mainly multivalent ones) induced rupture of protective water films the asphaltene aggregates are allowed to adhere and trapped patches of brine are left on the surface. The ions water shielding and anions (in (a) & (b)) are not depicted for the sake of lucidity.

Figure 9.6 illustrates all the proposed derived mechanisms of asphaltene deposition in presence of brines with variety of ionic strengths, formation of water in oil micro-emulsions, and micro-wettability transitions all observed in this study. We caution that our results require further investigations down to molecular scales and have set the stage for density functional theory (DFT) calculations and molecular dynamic simulations with consideration of all the equations (5)-(10) to build a better understanding of the proposed mechanisms which is currently under investigation from the current authors.

This is the first study to illustrate the effect of water in oil micro-emulsions in presence of different ionic strengths and dissolved chloride salts of a variety of alkali and earth alkaline cations on asphaltene aggregation and deposition phenomena under realistic conditions. It also opens a door to a better understanding of the key low salinity EOR drivers. Additionally, the results demonstrate the first experimental evidence backed by analytical results on the role of ion valency on micro-wettability transition in presence of asphaltenes.

Although the thickness of the Debye layer κ^{-1} (eq. 9.2) increases with decreasing the ionic strength, it stays in a domain where the prevailing forces are controlled by stunted range of interactions that are not thoroughly captured by Derjaguin–Landau–Verwey–Overbeek (DLVO)[47] theory. Without requirement to invoke any model, our present study clearly implies that the ion type in addition to ion concentration has drastic influences on wettability and asphaltene interactions at liquid-liquid and solid-liquid interfaces.

Our results have potential applications in other systems as well. Mechanisms involving interface interactions are of significant relevance for the understanding and control of biological systems. We have acquired no debates against the mechanisms being expandable to the biological macromolecules interactions. The conformation of tiny and mighty organic species, proteins as biological macromolecules, as well as the specificity of molecular recognition are governed by the identical types of intermolecular forces including attractive and repulsive forces as asphaltenes. Therefore, it could be conceivable to elucidate the three-dimensional (3D) structures of these species and their recognition specificities based on the mutual principles. The hydrogen bonds play a pivotal role in every field of biochemistry[48], [49]. The reiterated occurrence of interactions between aliphatic chains, π -stacking and H-bonding in biological macromolecules such as proteins[50], [51] alludes a functional role for them in describing the structures stability, in vast molecular recognition events as well as the folding drivers of macromolecules. This denotes that the same interactions as asphaltenes are presumably to happen on the cell surface. In summary, our treatise outlines testable mechanisms for protein adsorption, protein-protein and protein-water interactions, and protein aggregation inhibition through progress of nanomedicine design. Further work on this topic through quantum mechanical simulations will address confirmation of hypothesis and propositions throughout this study with hitherto unaccessed molecular level resolution.

9.4 References

- [1] R. Dias, A. A. Martins, R. Lima, and T. M. Mata, *Single and two-phase flows on Chemical and Biomedical Engineering*. Bentham Science Publishers, 2012.
- [2] J. N. Israelachvili, “Intermolecular and Surface Forces, (Academic Press, London, 1991).”

- [3] I. Benjamin, "Molecular structure and dynamics at liquid-liquid interfaces," *Annu. Rev. Phys. Chem.*, vol. 48, no. 1, pp. 407–451, 1997.
- [4] Y. Li, "Oil recovery by low salinity water injection into a reservoir: A new study of tertiary oil recovery mechanism," *Transp. porous media*, vol. 90, no. 2, pp. 333–362, 2011.
- [5] K. A. Terrón-Mejía, R. López-Rendón, and A. G. Goicochea, "Desorption of hydrocarbon chains by association with ionic and nonionic surfactants under flow as a mechanism for enhanced oil recovery," *Sci. Rep.*, vol. 7, no. 1, p. 9586, 2017.
- [6] M. A. Ahmadi and S. R. Shadizadeh, "Spotlight on the new natural surfactant flooding in carbonate rock samples in low salinity condition," *Sci. Rep.*, vol. 8, no. 1, p. 10985, 2018.
- [7] X. Zhao, M. J. Blunt, and J. Yao, "Pore-scale modeling: Effects of wettability on waterflood oil recovery," *J. Pet. Sci. Eng.*, vol. 71, no. 3–4, pp. 169–178, 2010.
- [8] J. Sheng, *Modern chemical enhanced oil recovery: theory and practice*. Gulf Professional Publishing, 2010.
- [9] G.-Q. Tang and N. R. Morrow, "Influence of brine composition and fines migration on crude oil/brine/rock interactions and oil recovery," *J. Pet. Sci. Eng.*, vol. 24, no. 2, pp. 99–111, 1999.
- [10] N. Morrow and J. Buckley, "Improved oil recovery by low-salinity waterflooding," *J. Pet. Technol.*, vol. 63, no. 05, pp. 106–112, 2011.
- [11] M. D. Jackson, D. Al-Mahrouqi, and J. Vinogradov, "Zeta potential in oil-water-carbonate systems and its impact on oil recovery during controlled salinity waterflooding," *Sci. Rep.*, vol. 6, p. 37363, 2016.
- [12] S. Prabhakar and R. Melnik, "Wettability alteration of calcite oil wells: Influence of smart water ions," *Sci. Rep.*, vol. 7, no. 1, p. 17365, 2017.
- [13] P. M. Spiecker and P. K. Kilpatrick, "Interfacial rheology of petroleum asphaltenes at the oil– water interface," *Langmuir*, vol. 20, no. 10, pp. 4022–4032, 2004.
- [14] C. G. Quintero, C. Noik, C. Dalmazzone, and J. L. Grossiord, "Formation kinetics and viscoelastic properties of water/crude oil interfacial films," *Oil Gas Sci. Technol. l'IFP*, vol. 64, no. 5, pp. 607–616, 2009.
- [15] M. Blumer, "Polycyclic aromatic compounds in nature," *Sci. Am.*, vol. 234, no. 3, pp. 34–45, 1976.
- [16] J. C. Gentry, "Benzene production and economics: a review," *Asia-Pacific J. Chem. Eng.*, vol. 2, no. 4, pp. 272–277, 2007.

- [17] A. K. Haritash and C. P. Kaushik, "Biodegradation aspects of polycyclic aromatic hydrocarbons (PAHs): a review," *J. Hazard. Mater.*, vol. 169, no. 1–3, pp. 1–15, 2009.
- [18] D. J. Cook, S. Schlemmer, N. Balucani, D. R. Wagner, B. Steiner, and R. J. Saykally, "Infrared emission spectra of candidate interstellar aromatic molecules," *Nature*, vol. 380, no. 6571, p. 227, 1996.
- [19] P. Tchoukov, F. Yang, Z. Xu, T. Dabros, J. Czarnecki, and J. Sjöblom, "Role of asphaltenes in stabilizing thin liquid emulsion films," *Langmuir*, vol. 30, no. 11, pp. 3024–3033, 2014.
- [20] J. Bi, F. Yang, D. Harbottle, E. Pensini, P. Tchoukov, S. Simon, J. Sjöblom, T. Dabros, J. Czarnecki, and Q. Liu, "Interfacial layer properties of a polyaromatic compound and its role in stabilizing water-in-oil emulsions," *Langmuir*, vol. 31, no. 38, pp. 10382–10391, 2015.
- [21] H. W. Yarranton, H. Hussein, and J. H. Masliyah, "Water-in-hydrocarbon emulsions stabilized by asphaltenes at low concentrations," *J. Colloid Interface Sci.*, vol. 228, no. 1, pp. 52–63, 2000.
- [22] A. K. Tharanivasan, H. W. Yarranton, and S. D. Taylor, "Asphaltene precipitation from crude oils in the presence of emulsified water," in *Energy and Fuels*, 2012, vol. 26, no. 11, pp. 6869–6875.
- [23] S. Aslan and A. Firoozabadi, "Effect of water on deposition, aggregate size, and viscosity of asphaltenes," *Langmuir*, vol. 30, no. 13, pp. 3658–3664, 2014.
- [24] C. Hu, J. C. Sabio, A. Yen, N. Joshi, and R. L. Hartman, "Role of water on the precipitation and deposition of asphaltenes in packed-bed microreactors," *Ind. Eng. Chem. Res.*, vol. 54, no. 16, pp. 4103–4112, 2015.
- [25] M. Tavakkoli, A. Chen, C.-A. Sung, K. M. Kidder, J. J. Lee, S. M. Alhassan, and F. M. Vargas, "Effect of emulsified water on asphaltene instability in crude oils," *Energy & Fuels*, vol. 30, no. 5, pp. 3676–3686, 2016.
- [26] E. Joonaki, J. Buckman, R. Burgass, and B. Tohidi, "Exploration of the Difference in Molecular Structure of n-C₇ and CO₂ Induced Asphaltenes," *Ind. Eng. Chem. Res.*, 2018.
- [27] E. Joonaki, R. Burgass, A. Hassanpouryouzband, and B. Tohidi, "Comparison of Experimental Techniques for Evaluation of Chemistries against Asphaltene Aggregation and Deposition: New Application of High-Pressure and High-Temperature Quartz Crystal Microbalance," *Energy & Fuels*, 2017.
- [28] J. G. Speight, *The desulfurization of heavy oils and residua*. CRC Press, 1999.

- [29] M. Daaou, A. Modarressi, D. Bendedouch, Y. Bouhadda, G. Krier, and M. Rogalski, "Characterization of the nonstable fraction of Hassi- Messaoud Asphaltenes," *Energy & Fuels*, vol. 22, no. 5, pp. 3134–3142, 2008.
- [30] Y. Ruiz-Morales, "Molecular orbital calculations and optical transitions of PAHs and asphaltenes," *Asph. Heavy Oils, Pet.*, pp. 95–137, 2007.
- [31] V. Pauchard, J. P. Rane, and S. Banerjee, "Asphaltene-laden interfaces form soft glassy layers in contraction experiments: A mechanism for coalescence blocking," *Langmuir*, vol. 30, no. 43, pp. 12795–12803, 2014.
- [32] A. B. Andrews, A. McClelland, O. Korkeila, A. Demidov, A. Krummel, O. C. Mullins, and Z. Chen, "Molecular orientation of asphaltenes and PAH model compounds in Langmuir- Blodgett films using sum frequency generation spectroscopy," *Langmuir*, vol. 27, no. 10, pp. 6049–6058, 2011.
- [33] T. E. Chávez-Miyauchi, L. S. Zamudio-Rivera, and V. Barba-López, "Aromatic polyisobutylene succinimides as viscosity reducers with asphaltene dispersion capability for heavy and extra-heavy crude oils," *Energy & Fuels*, vol. 27, no. 4, pp. 1994–2001, 2013.
- [34] S. I. Andersen, J. M. Del Rio, D. Khvostichenko, S. Shakir, and C. Lira-Galeana, "Interaction and solubilization of water by petroleum asphaltenes in organic solution," *Langmuir*, vol. 17, no. 2, pp. 307–313, 2001.
- [35] D. S. Khvostichenko, S. I. Andersen, and A. I. Viktorov, "Solubility and binding of water in toluene solutions of asphaltenes," *Russ. J. Appl. Chem.*, vol. 77, no. 6, pp. 1013–1018, 2004.
- [36] R. A. Nasralla and H. A. Nasr-El-Din, "Double-layer expansion: is it a primary mechanism of improved oil recovery by low-salinity waterflooding?," *SPE Reserv. Eval. Eng.*, vol. 17, no. 01, pp. 49–59, 2014.
- [37] A. P. Gast and A. W. Adamson, *Physical chemistry of surfaces*. Wiley New York, 1997.
- [38] L. Goual, G. Horváth-Szabó, J. H. Masliyah, and Z. Xu, "Adsorption of bituminous components at oil/water interfaces investigated by quartz crystal microbalance: Implications to the stability of water-in-oil emulsions," *Langmuir*, vol. 21, no. 18, pp. 8278–8289, 2005.
- [39] Y.-T. Wu, P.-J. Akoto-Ampaw, M. Elbaccouch, M. L. Hurrey, S. L. Wallen, and C. S. Grant, "Quartz crystal microbalance (QCM) in high-pressure carbon dioxide (CO₂): experimental aspects of QCM theory and CO₂ adsorption.," *Langmuir*, vol. 20, no. 9, pp. 3665–73, 2004.
- [40] V. M. Mecea, "From quartz crystal microbalance to fundamental principles of mass measurements," *Anal. Lett.*, vol. 38, no. 5, pp. 753–767, 2005.

- [41] H. C. Helgeson, "Thermodynamics of hydrothermal systems at elevated temperatures and pressures," *Am. J. Sci.*, vol. 267, no. 7, pp. 729–804, 1969.
- [42] Y. Marcus, "Thermodynamics of solvation of ions. Part 5.—Gibbs free energy of hydration at 298.15 K," *J. Chem. Soc. Faraday Trans.*, vol. 87, no. 18, pp. 2995–2999, 1991.
- [43] H. Sakuma, M. P. Andersson, K. Bechgaard, and S. L. S. Stipp, "Surface tension alteration on calcite, induced by ion substitution," *J. Phys. Chem. C*, vol. 118, no. 6, pp. 3078–3087, 2014.
- [44] T. Young, "III. An essay on the cohesion of fluids," *Philos. Trans. R. Soc. London*, no. 95, pp. 65–87, 1805.
- [45] D. M. Czajkowsky and Z. Shao, "Inhibition of protein adsorption to muscovite mica by monovalent cations," *J. Microsc.*, vol. 211, no. 1, pp. 1–7, 2003.
- [46] M. E. J. Haagh, I. Siretanu, M. H. G. Duits, and F. Mugele, "Salinity-dependent contact angle alteration in oil/brine/silicate systems: the critical role of divalent cations," *Langmuir*, vol. 33, no. 14, pp. 3349–3357, 2017.
- [47] B. V Deryaguin, "BV Deryaguin and L. Landau, *Acta Phys. Chem.* 14, 633 (1941).," *Acta Phys. Chem.*, vol. 14, p. 633, 1941.
- [48] G. A. Jeffrey and G. A. Jeffrey, *An introduction to hydrogen bonding*, vol. 32. Oxford university press New York, 1997.
- [49] S. Scheiner, *Hydrogen bonding: a theoretical perspective*. Oxford University Press on Demand, 1997.
- [50] M. Nishio, "The CH/ π hydrogen bond in chemistry. Conformation, supramolecules, optical resolution and interactions involving carbohydrates," *Phys. Chem. Chem. Phys.*, vol. 13, no. 31, pp. 13873–13900, 2011.
- [51] M. Nishio, M. Hirota, and Y. Umezawa, *The CH/ π interaction: evidence, nature, and consequences*, vol. 21. John Wiley & Sons, 1998.

Chapter 10- Conclusions and Recommendations

The main concern of this thesis was to propose and develop new practical solutions in surface chemistry and computational sciences such as new experimental techniques for evaluation of different additives, new asphaltene deposition simulator, and new screening techniques for monitoring of asphaltene-surface active moieties molecular interactions in the context of mitigating asphaltene associated flow assurance barriers. This chapter summarizes the contributions of this thesis, its key findings and recommendations for the future research directions.

10.1 Major Contributions

The research conducted throughout this study mainly investigated the application of quartz crystal microbalance under realistic conditions for reliable evaluation of various chemistries, identifying the effects of different gas injection scenarios on asphaltene destabilisation, and understanding of possible drivers of asphaltene aggregation and deposition phenomena. In this context, the major contributions of current work can be summarized as:

- i. Design and development of a hybrid technique for determination of asphaltene onset points and evaluation of inhibitors at ambient conditions.
- ii. Determination of asphaltene onset pressure (AOP) and evaluation of asphaltene/wax inhibitors with appropriate carrier solvents using high pressure-high temperature quartz crystal microbalance as a novel technique.
- iii. Development of new two-dimensional dynamic asphaltene deposition simulator for prediction of precipitation and deposition along the wellbore.
- iv. Understanding of the drivers of asphaltene aggregation and deposition and testing the chemistries against those mechanisms.
- v. Studying the effect of waxes and respective chemistries on asphaltene aggregation and deposition phenomena.

- vi. Investigation of possible interactions of asphaltene nanoaggregates at solid/liquid and oil/water interfaces using state of the art imaging facilities and analytical techniques.
- vii. Exploration of the difference in molecular structure of $n\text{-C}_7$ and CO_2 induced asphaltenes using FTIR, NMR, ESEM/EDX analysis and QCM.
- viii. Investigation of the effect of different gases and water with different salinities/presence of various ion types on asphaltene aggregation and deposition.

10.2 Key Findings

Based on the work conducted in this project, the following points can be considered as conclusions of the research:

In this treatise, the hybrid technique has been developed and examined for the determination of asphaltene appearance point and evaluation of asphaltene inhibitors. The effectiveness of two commercial inhibitors, phthalic acid and the alkylbenzene-derived amphiphiles including nonylphenol and dodecylbenzene sulfonic acid as asphaltene inhibitors were studied. The effects of the structures of these chemicals on their capabilities to hinder the asphaltene precipitation were also investigated and possible mechanisms of asphaltene precipitation inhibition were proposed. Our findings reveal that the H-bonding with -N/O-H groups of asphaltenes is the main mechanism of asphaltene precipitation inhibition caused by n -nonylphenol and Phthalic acid at the periphery of asphaltene nanoaggregates. It has been found that the DDBSA amphiphilic molecules can curb the asphaltene particles growth to form flocs through both ion-pair and H-bonding interactions.

In chapter 4 a comparison between the results of the QCM technique at elevated pressure and temperature condition and dead crude oil testing at ambient condition is presented. The results of this chapter indicate that the change in temperature, pressure and presence of gas could alter the ranking of chemistries for mitigating asphaltene challenges. Through chapter 5, we were seeking for find a reason for having different rankings of chemicals based on their deposition inhibition performance between QCM and other utilised techniques. It has been depicted that the HPHT-QCM asphaltene deposits from parent crude oil are richer in oxygen species, such as the O_x and R-OH polar groups, relative to

the n-C₇ asphaltenes. The results of chapter 5 provide High-Pressure information that leads to better understanding of asphaltene precipitation and deposition phenomena and could be taken into account when designing prevention strategies to avoid asphaltene problems throughout the oil production process.

The chapter 6 explains the role of waxes during the asphaltene aggregation and deposition phenomena. This study confirms that changes in the chemistry of the wax inhibitors could result in significant differences in pour point reduction and viscosity profiles in crude oil. These structural changes along with dosage rate also led to differences in the effect of wax inhibitors on handling or aggravating asphaltene deposition. The chapter 6 results showed that waxes can reduce the asphaltene deposition rate and shift the AOP.

A newly developed dynamic and two-dimensional particle scale model was presented in chapter 7 to simulate the asphaltene deposition in a synthetic oil well. It was concluded that the rate of asphaltene deposition increases while the concentration of nano-aggregates increases in the well column. The tendency of smaller aggregates to deposit on the surface could be explained due to the increase in the diffusion coefficient of asphaltene aggregates. It was also shown that the results of the new simulation were in good agreement with the experimental data.

The experimental results in chapter 8 reveal that injection of CO₂, CH₄, Mix. A and natural gases can lead asphaltenes to become unstable in crude oil and tend to precipitate out of the solution and deposit onto the QCM surface. It has also been depicted that the asphaltene precipitation condition is strongly dependent upon gas composition. A comparison between the six gases showed that, when added in the same pressure condition, CO₂ was the strongest precipitant followed by natural gas, CH₄ and Mix. A. In initial tests at pressures up to the maximum of the equipment no onset was been observed in presence of pure N₂ and a flue gas which is really promising for the EOR purposes.

The first study to investigate the impacts of water in oil micro-emulsions in presence of different ionic strengths and dissolved chloride salts of a variety of alkali and earth alkaline cations on asphaltene aggregation and deposition phenomena under realistic conditions was presented in chapter 9. The results depict that owing to the substitution of divalent cations

with monovalent ones, asphaltene deposition is repelled and the solid surface becomes more hydrophilic, proposing a generalizable strategy to control wettability and an elucidation for the profitability of so-called low salinity water flooding, an enhanced oil recovery methodology. For biological application, this treatise provides insights into the potential roles of ions and hydrogen bonds in the protein deposition in tissues and self-assembly interactions and efficiency of drugs against protein aggregation drivers.

10.3 Recommendations and Prospects

Considering the discussions through the different chapters of this dissertation, the following ideas can be considered as research topics for future work:

1. It is believed asphaltene related problems could change with the age/pressure of the reservoir. Current industrial practice is to use an oil sample from the initial sampling campaign and evaluate the asphaltene risks for the whole life of the reservoir within the reservoir and production conduit. However, with the reservoir depletion significant amounts of gas could leave the oil at reservoir conditions. This could result in a different condition with respect to asphaltene deposition in the system (i.e., reservoir, downhole and pipeline). It is proposed to investigate the effect of depletion on the asphaltene risk with and without chemical additives.

It is proposed to simulate the effect of reservoir depletion on the reservoir fluids samples, as suggested below:

- a) For each fluid sample obtained at each pressure-step (in Differential Liberation test) simulate wellbore and pipeline conditions.
- b) Analyse and evaluate potential asphaltene problem for the resulting oil, including effect of shear rate.
- c) Find a suitable solution/chemical to avoid asphaltene problem in the original sample.
- d) Investigate the effectiveness of the mitigation option found for the original oil for subsequent oil samples.

e) Measure the viscosity of oil resulting from each pressure step. Check the reliability of the originally tuned viscosity model in predicting the viscosity of the oil obtained at each pressure step under reservoir, wellbore and pipeline conditions.

Finally, later in the life of a reservoir lift gas may be used to help with low reservoir pressure. It is proposed to extend the investigation to the effect of lift gas on the asphaltene problems as well as mechanical effects.

2. Due to a reduction in the reservoir pressure production rates are lower, resulting in a lower shear stress in the pipeline which could change the nature of asphaltene problem. It is proposed to conduct a comprehensive study of rheological properties of oil resulting from reservoir depletion with and without addition of inhibitors/carrier solvents.
3. Modelling is an integrated and important part of all of the above activities. It is proposed to build on recent achievements in asphaltene modelling presented in chapter 7 and develop computational fluid dynamics (CFD) as a new module addition to it in order to predict the occurrence and calculate the magnitude and profile of asphaltene deposition in the wellbore particularly for turbulent flow conditions.
4. Later in the life of a reservoir production rate declines resulting in lower fluid velocity and shear rates. These factors, combined with reduced GOR and increased fluid viscosity could contribute to asphaltene problems, as the asphaltene aggregates may settle in the pipeline and/or the shear stress from fluid flow may not be high enough to reduce/eliminate asphaltene induced blockage in the pipeline/wellbore. It is proposed to conduct a comprehensive study on the rheological properties of oil as a function of pressure (i.e., oils resulting from aforementioned DL tests), temperature and shear rates at conditions above and below AOP. The objective is to evaluate the associated risks and factors affecting asphaltene deposition with the aim of minimising such risks. The data generated in this suggested work could be used for further development of asphaltene deposition model as mentioned above.

5. We caution that our results in chapter 9 require further investigations down to molecular scales and have set the stage for density functional theory (DFT) calculations and molecular dynamic simulations with consideration of all the equations (9.5) - (9.10) to build a better understanding of the proposed mechanisms and also address confirmation of hypothesis and propositions throughout this study with hitherto unaccessed molecular level resolution.

Appendix 1

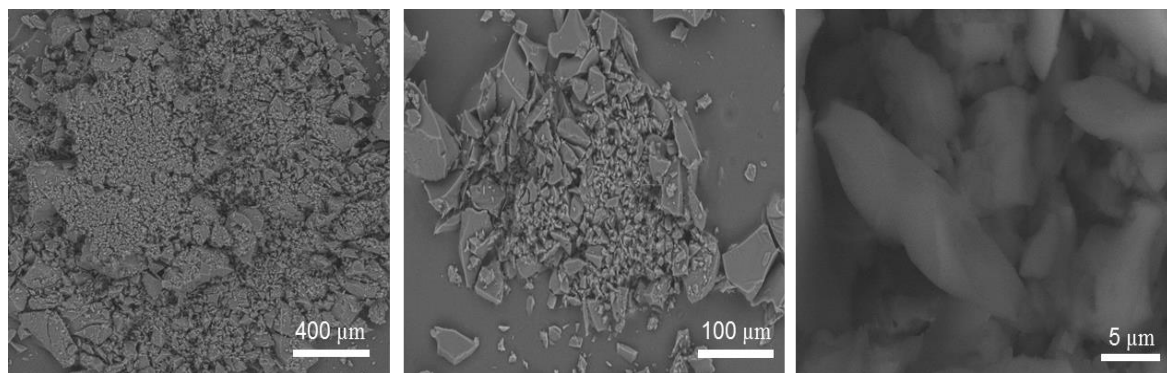


Figure A1. 1 More ESEM micrographs of n-C₇-asphaltenes with different magnifications

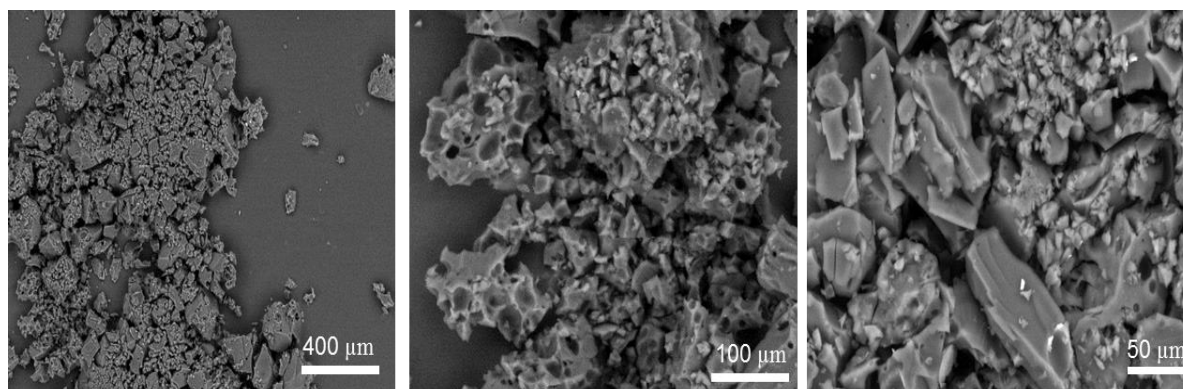


Figure A1. 2 More ESEM micrographs of CO₂-asphaltenes with different magnifications

Table A1. 1 SARA analysis of the crude oil used in chapter 5

Property	Value
Saturates (wt %)	44.2
Aromatics (wt %)	36.1
Resin (wt %)	11.7
n-C ₇ asphaltenes (wt %)	8

Table A1. 2 Infrared spectral range assignments of the main bands observed in n-C₇ and CO₂ asphaltenes characterised in this study

Absorption bands (cm ⁻¹)	Functional groups
3700–3200	Stretching vibration of the O–H bonds (the bands are broadened due to hydrogen bonding)
3000–2800	Stretching vibration of the C–H bonds in CH ₃ /CH ₂
2730	C _{aro} –CH ₃
1800–1660	Stretching of the carbonyl groups C=O bonds (COOH)
1590–1620	Stretching of the C=C bonds of aromatic

moieties	
1370–1460	C–H deformation in CH ₃ /CH ₂
~1030	S=O, C–S
865	C _{aro} –H(1) (v)
805	C _{aro} –H(2) (iv)
760	C _{aro} –H(3) (iii)
745	C _{aro} –H(3) (ii)
715	–(CH ₂) _n – [n≥4]

Table A1. 3 Proton chemical shift correlation chart for studied asphaltenes

Chemical shift ranges (ppm)	Integral intensity	Type of proton	assignment
9.00 – 6.50	vi	H _{ar}	aromatic hydrogens
4.50 – 2.90	v	H _α (methylene/methyne)	α-CH, α-CH ₂
2.90 – 2.00	iv	H _α (methyl protons)	α-CH ₃
2.00 – 1.40	iii	H _β (naphthenic protons)	β-CH ₂ , CH/CH ₂ naphthenic

1.40 – 1.00	ii	H_{β}, H_{β^+}	$\beta\text{-CH}_3, \beta^+\text{-CH}_2$, paraffinic CH_2
0.95 – 0.30	i	H_{γ}	methyl hydrogen in γ position attached to aromatic ring; methyl hydrogen in alkane

Table A1. 4 Carbon chemical shift correlation chart for studied asphaltenes

Chemical shift ranges (ppm)	Integral intensity	Type of carbon	assignment
160.0 – 137.0	V	$C_{\text{ar-alk}}$	alkyl-substituted aromatic carbon except CH_3
137.0 – 129.0	IV	$C_{\text{ar-CH}_3}, C_{\text{ar-n}}$	methyl-substituted aromatic carbons, carbon at junction of an aromatic and naphthenic rings
136.0 – 123.0	III	$C_{\text{aa}}, C_{\text{aaa}}$	carbon at junction of two and three aromatic rings
130.0 – 118.0	II	$C_{\text{ar-H}}$	aromatic protonated carbons
45.00 – 5.00	I	$C_{\text{al}}, C_{\text{n}}$	Saturated carbons, naphthenic carbons

Appendix 2

Numerical Method

In this research study, the finite centered difference method is used to discretize and also build the matrix for solving the Eqs. (7.11), (7.23), (7.24) and (7.25) simultaneously. Replacing the central finite-divided-difference formula for each term of Eq. (7.11), the following relation is achieved for steady state condition:

$$C_{i,j}A + C_{i,j-1}B + C_{i,j+1}D + C_{i+1,j}E + C_{i-1,j}F = 0 \quad (\text{A2.1})$$

Where the relations for A, B, D, E and F can be found in Table A2.1.

Table A2. 1 Definition of parameters used in equation 3

Term	A	B	D	E	F	a
	$1 - \frac{a}{r \times \Delta r} + \frac{2a}{\Delta r^2} + \frac{2a}{\Delta z^2}$	$B = \frac{a}{r \times \Delta r} - \frac{2a}{\Delta r^2}$	$-\frac{a}{\Delta r^2}$	$-\frac{a}{\Delta z^2}$	$-1 - \frac{a}{\Delta z^2}$	$-\frac{\Delta z(D_{wo} + \epsilon_m)}{v_z}$

Then, the matrix of unknowns is made as follows:

$$\begin{bmatrix}
 1 & 0 & \dots & \dots & \dots & \dots & \dots & \dots & \dots & 0 \\
 0 & 1 & \dots & \dots & \dots & \dots & \dots & \dots & \dots & \dots \\
 \vdots & \vdots & \vdots & \vdots & \vdots & \vdots & \vdots & \vdots & \vdots & \vdots \\
 \dots & F & \dots & B & A & D & \dots & E & \dots & \dots \\
 \vdots & \vdots & \vdots & \vdots & \vdots & \ddots & \vdots & \vdots & \vdots & \vdots \\
 \vdots & \vdots & \vdots & \vdots & \vdots & \ddots & \vdots & \vdots & \vdots & \vdots \\
 \vdots & \vdots & \vdots & \vdots & \vdots & \ddots & \vdots & \vdots & \vdots & \vdots \\
 \vdots & \vdots & \vdots & \vdots & \vdots & \ddots & \vdots & \vdots & \vdots & \vdots \\
 0 & 0 & \dots & \dots & \dots & \dots & \dots & 0 & 1 & \dots
 \end{bmatrix}
 \begin{bmatrix}
 C_{0,0} \\
 C_{0,1} \\
 \vdots \\
 C_{0,rN-1} \\
 C_{1,0} \\
 \vdots \\
 C_{1,rN-1} \\
 \vdots \\
 C_{zN-1,rN-1}
 \end{bmatrix}
 =
 \begin{bmatrix}
 C_{BH} \\
 C_{BH} \\
 \vdots \\
 C_{BH} \\
 0 \\
 \vdots \\
 0 \\
 \vdots \\
 C_{WH}
 \end{bmatrix} \quad (\text{A2.2})$$

Where the C_{BH} stands for concentration at the depth of bottom hole and C_{WH} represents the concentration at the wellhead.

The implicit method is used to solve Eq. (7.11) at steady state condition. After solving at the stable condition, the explicit method is utilized to find the concentration (C) at unstable condition as follows:

$$C_{i,j,t+1} = C_{i,j,t} + \left[\begin{array}{l} -v_z \frac{C_{i+1,j,t} - C_{i,j,t}}{\Delta z} + \\ (D_{wo} + \varepsilon_m) \left[\frac{C_{i,j+1,t} - 2C_{i,j,t} + C_{i,j-1,t}}{\Delta r^2} + \frac{1}{r} \frac{C_{i,j+1,t} - C_{i,j,t}}{\Delta r} + \right. \\ \left. \frac{C_{i+1,j,t} - 2C_{i,j,t} + C_{i-1,j,t}}{\Delta z^2} \right] - \\ k_0 e^{\alpha(C_{i,j,t} - C_{eq})} \end{array} \right] \quad (A2.3)$$

The same method is employed to solve the PDEs and also respective matrix to find the temperature at each grid.

Appendix 3

Table A3. 1 Bare ion radii, hydrated ion radii, ion size parameter \AA , and the individual ion activity coefficient parameters in eq. 4 for various cations used in this study

Ion	Bare Ion Radii (nm)	Hydrated Ion Radii (nm)	$\text{\AA}/(10^{-10} \text{ m})^{[1]}$	$a (10^{-10} \text{ m})^{[2]}$	$b^{[2]}$
K ⁺	0.149	0.331	3.0	3.5	0.015
Na ⁺	0.117	0.358	4.0-4.5	4.0	0.075
Ca ²⁺	0.100	0.412	6	5.0	0.165
Mg ²⁺	0.072	0.428	8	5.5	0.20

References

[1] Garrels, R. M., & Christ, C. L. Solutions, minerals, and equilibria. New York: Harper & Row (1965).

[2] Plummer, L. N., Jones, B. F., & Truesdell, A. H. WATEQF: a Fortran IV version of WATEQ, a computer program for calculating chemical equilibrium of natural waters (1976).